Decomposition Kinetics of Polymer-Nanocomposite Materials

By

Wael Alsaedi

A Thesis

Submitted to the Graduate Faculty

In Partial Fulfillment of the Requirements

For the Degree of

MASTER OF SCIENCE

Department of Chemistry

Faculty of Science

University of Prince Edward Island

(Charlottetown)

Abstract:

The synthesis of polythiophenes functionalized with an alkyl group such as coumarin and naphthol were performed successfully. A previously - described technique of WS_2 synthesis from thiourea and tungstic acid was utilized to synthesize exfoliated WS_2, which was employed to synthesize nanocomposite materials. Also, novel exfoliated polythiophene and poly(3-alkylthiophene) with naphthol nanocomposites using various percentages of tungsten disulfide were prepared using *in-situ* polymerization of the monomer with iron (III) chloride in the presence of exfoliated WS_2. Additionally, the exfoliated nanocomposites of polyaniline were synthesized by an *in-situ* polymerization reaction of aniline with ammonium peroxydisulfate in the presence of exfoliated WS_2.

The poly(3-alkylthiophene) decorated with naphthol was characterized by using techniques such as NMR, FTIR, and TGA. These techniques were utilized to determine the difference between the monomers and their polymers. Both polymers displayed a noticeable improvement in thermal stability. The exfoliated nanocomposites of PThN-WS_2 were also characterized using techniques such as FT-IR and XRD.The results obtained suggest that there is an interaction between the polymer and the WS_2 due to the vibrational change in the IR spectrum.

Ozawa's method was applied to determine the decomposition kinetics of these exfoliated nanocomposites using the Thermogravimetric Analysis (TGA). The activation energies for PTh and their six different compositions of WS_2 were measured under air. Each sample was studied using four selected heating rates: 5, 10, 20 and 40 ^{o}C/min. The

similar procedures were followed to compute Ea for PThN-WS_2 nanocomposites. The results demonstrated that the incorporation of nanofillers has improved the Ea value for PTh-WS_2 and PThN-WS_2 nanocomposites.

It was found that the presence of alkyl group (naphthol) on the thiophene ring has enhanced the Ea by approximately 65 kJ/mol compared to pure PTh with around 79.9 kJ/mol. Furthermore, the values of the Ea for exfoliated PT-WS_2 and PThN-WS_2 compositions were increased by incorporating higher percents of WS_2 in comparison to that of pure PT or PThN.

Ozawa's method was also applied to determine the activation energies for the pure polyaniline and their nanocomposites with WS_2. All experiments were carried out in a TGA at four different heating rates under a nitrogen atmosphere. It was demonstrated that the incorporation of exfoliated WS_2 in polyaniline showed an enhancement in the Ea values. Also, 12.5% of WS_2-PANI composition recorded the highest Ea with 165 kJ/mol compared to that of Ea of pristine PANI with 129.8 kJ/mol.

Table of Contents

List of Table

Table Page

List of Figure

Figure Page

1. Chapter 1:

2. Chapter 2:

List of Schemes:

Scheme page

List of Symbols and Abbreviations

APS	Ammonium persulfate
CPs	Conducting polymers
CVD	Chemical vapour deposition
^{13}C	NMR Carbon 13 nuclear magnetic resonance spectroscopy
^{o}C	Degrees Celsius
DSC	Differential Scanning Calorimetry
$CDCl_3$	Deuterated chloroform
DCC	Dicyclohexylcarbodiimide
DCM	Dichloromethane
DCU	Dicyclohexylurea
DMAP	N,N'-dimethylaminopyridine
DMF	N,N'-dimethylformamide
2D	Two- dimensional
Ea	Activation Energy
Eg	Band gap
FT-IR	Fourier Transform Infrared Spectroscopy
GRIM	Grigrard metathesis method
^{1}H	NMR Proton nuclear magnetic resonance spectroscopy
kJ/mol	kilos joule per mole
LED	Light-emitting diodes
LDA	Lithium diisopropylamide
MHz	Mega hertz

mL	Millilitre
mM	Millimolar
mmol	Millimoles
M	Molar
MO	Molecular orbital
mol	Moles
m	Multiplet
NMR	Nuclear magnetic resonance spectroscopy
PANI	Polyaniline PANI
PDI	Polydispersity index
PMT	Polymethylthiophene
P3AT	Poly(3-alkylthiophene)
PPE	Poly(para-phenylene ethylene)
PINCs	Polymer – inorganic nanocomposites
PPP	Poly(para-phenylene)
PT	Polythiophene
PThC	Polymer of 2-(3-Thienyl)ethanol with Coumarin-3-carboxylic acid
PThN	Polymer of 3-Thiophenecarboxylic acid with 2-Naphthol
PPV	Poly(para-phenylene vinylene)
PPY	Polypyrrole
q	Quartet
rr-P3ATs	Regioregular- Poly(3-alkylthiophene
s	Singlet

TEM	Transmission Electron Microscopy
TGA	Thermogravimetric analysis
Th	Thiophene
ThC	2-(3-Thienyl)ethanol with Coumarin-3-carboxylic acid
THF	Tetrahydrofuran
TMDs	Transition Metal Dichalcogenides
ThN	3-Thiophenecarboxylic acid with 2-Naphthol
XRD	X-ray powder diffraction

Acknowledgments

First of all, I would love to express my deepest sense of appreciation to my supervisor Professor Alaa Abd-El-Aziz for motivation, inspiration, continued assistance, advice and critical review of several perspectives of this research. I strangely express my sincere appreciation to Professor Rabin for his guidance and suggestions throughout the course of study and proofreading of my thesis. Also, I would like to take this opportunity to thank Professor Nola for her proofreading and her useful suggestions of my thesis.

I would like to thank Michael Cowper for his valuable suggestions and proofreading of some chapters, and Inan for his assistance in the laboratory work, Stephen Scully for his training on some the instruments in the chemistry department. I express my gratitude to Alaa's group and Rabin's groups for their useful help in the experimental work. I would also like to express my appreciation to Tabiha Universty for the scholarship awarded and the financial supports.

Special appreciation is due to my wife Reem Aloufi for enduring so patiently the division of my attention during this research and for the continued help, support and encouragement she always provides me.

I am also deeply indebted to my sister and brothers for their love, morale, encouragement and support throughout the years I lived far from them.

Finally, I dedicate my thesis to the most patient, innocent heart of my little beautiful angel mother whose inspiring brief note of "I love you Mum" was always standing like the Goddess of Revelation before my eyes, motivating me hopefully to write. Unlimited thanks to her great sense of realization I always adore.

1. **Introduction**:

1.1. Overview.

When we think or hear about polymers, we may immediately come up with an image of some products such as rubber, plastic and clothes. These materials are often insulators, but as a matter of fact, conducting polymers were known before their discovery in the late 1970s.[1] For example, Runge reported the polymerization of aniline via a chemical oxidation reaction in 1834,[2] although at that time, the electrical property of the conducting polymer was not known. Over a century later, however, in 1977, Shirakawa, Heeger, and MacDiarmid, reported the high electrical conductivity of polyacetylene. They were awarded the Nobel Prize in Chemistry in 2000 for the discovery that doping polyacetylene with AsF_5, increased the polymer's conductivity by 220 S/cm at room temperature.[1] Since that discovery, many conducting polymers including poly(para-phenylene ethylene) (PPE), polyaniline (PANI), poly(para-phenylene vinylene) (PPV), polythiophene (PT), polypyrrole (PPY), Poly(para-phenylene) (PPP) many others have been produced, as can be seen in Figure 1.1. These conducting polymers are known as "organic semiconductors" or "synthetic metals."

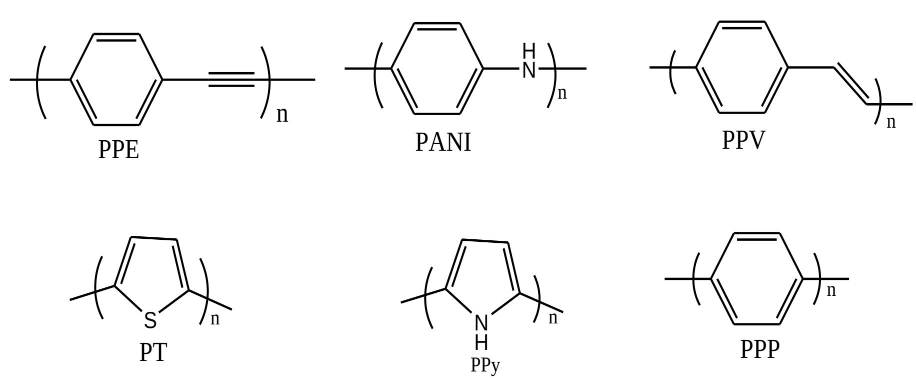

Figure 1.1: structures of several common conjugated polymers.

Conducting polymers (CPs) are considered to be modern materials. Recently, these types of materials have been studied substantially as a result of their unique properties. A great deal of interest is focused on enhancing these materials so that they may replace the currently used semiconductors. Organic conducting polymers provide different beneficial features over inorganic semiconductors such as lightness in weight, resistance to corrosion, nearly infinite numbers of chemical structures of polymers, electronic and optical properties and ease of processability. [3] The key point of focus in CPs use for the development of devices in comparison to other polymers is attributed to their relatively low cost and the ease that they can be cast or molded into a preferable shape from solution or melt.

The electrical properties of conducting polymers are attributed to the mobile charge carriers, which move through the π conjugation system that is constructed by the overlap of the delocalized p-orbitals of the polymer backbone. In contrast, in the undoped state, the conducting polymers display a low electrical conductivity at room temperature.

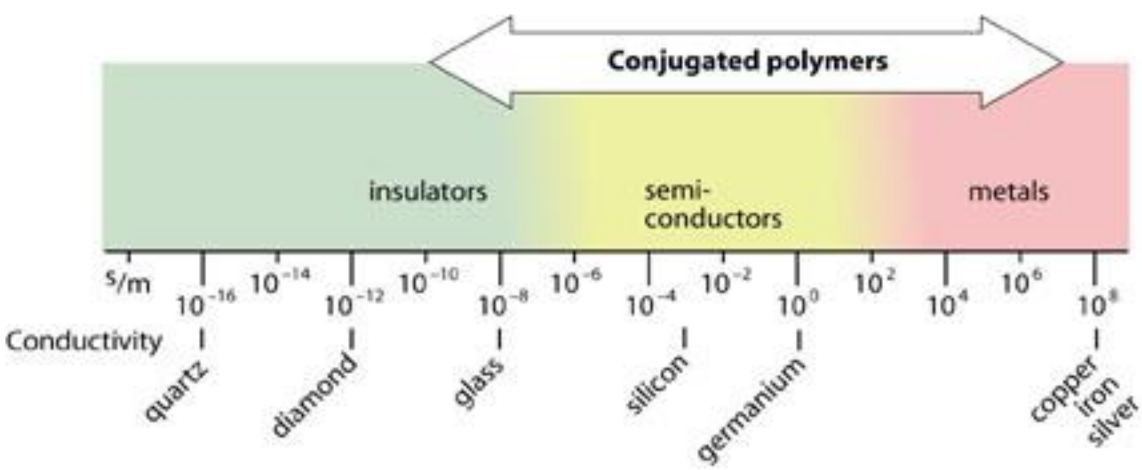

Figure 1.2: Electrical property of conducting polymers in comparison with conventional materials. [4]

Based on the Band Theory [4-7] all materials are classified into three groups: insulators, semiconductors, and conductors. As a result, this is important for understanding why conducting polymers act as either insulators, semiconductors or metals as shown in Figure 1.2. A band model can illustrate why some materials are conductive while others are not. In a band model, electronic bands can be generated due to the overlapping of molecular orbitals.

The band gap (E_g) refers to the energy difference between the top of the valence band and bottom of the conduction band. The exceptional conductivity of metals is attributed to absence of a band gap, which can be due to band overlap or a partially filled band. In the case of insulators, the lack of conductivity of these materials is ascribed to the large band gap. The band gap is smaller in semiconductors than insulators, and the thermal or photon excitation can promote some electrons from the valence band to vacant spaces in the conduction band as illustrated in Figure 1.3.

The π band (valence band) and π* band (conduction band) overlap in conducting polymers after doping by either n-doping or p-doping. The doped polymer undergoes a decrease in the distance between the valence band and conduction band, allowing the polymer to behave as a metal in term of conductivity. [8] Overall, the presence of a small band gap is the fundamental aim in the preparation conducting polymers.

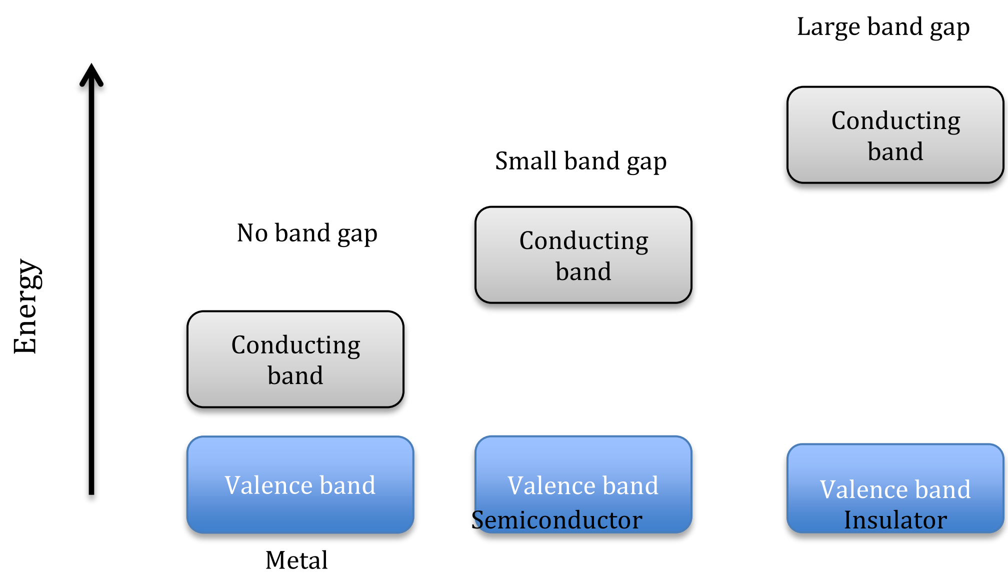

Figure 1.3: The difference in band gaps for Metals, Semiconductors, and Insulators.

1.2. Synthesis of conducting polymer:

Conducting polymers can be produced by either electrochemical or chemical oxidation reaction of the corresponding monomers. [9,10] The processes of synthesizing conducting polymers initiates with the oxidation of the monomer to produce a molecule with low molecular weight (an oligomer). Since the oligomer has a low oxidation potential compared to the monomer, it then undergoes further oxidation to produce the polymer. Ultimately, a polymer is obtained by either precipitation in an appropriate solvent or electrodeposition of the polymer onto an electrode.

Ammonium persulfate $(NH_4)_2S_2O_8$ and Ferric chloride ($FeCl_3$) are common chemical oxidizing agents. A polymer produced using these two agents is regarded as a (p-type) doped polymer. An anion A^- must also be added to balance the change on the polymer backbone, resulting in the production of a stable doped polymer.

Chemical polymerization produces a large amount of the polymer. The synthesis of polypyrrole, for instance, can be easily obtained from aqueous solution, whereas, the successful preparation of polyaniline needs to be in acidic conditions since the level of protonation of the polyaniline is extremely sensitive in terms of the electrical conductivity of the polymer. Unlike polypyrrole and polyaniline, which require aqueous solutions for their polymer synthesis, polymerization of thiophene is often carried out in organic solvents such as acetonitrile because of its poor solubility in aqueous electrolytes.

It is worth mentioning that the oxidation polymerization reaction is not the only approach for synthesizing conducting polymers, but there are also other techniques such as the condensation polymerization reaction and organometallic aryl-aryl coupling. [11,12] However, the doped or oxidized polymer can only be directly prepared by the approach of oxidative polymerization. In other techniques, the neutral polymer is synthesized first and then doped or oxidized in the following step.

1.2.1. Polythiophene (PT) vs Poly(3-alkylthiophene) (P3AT)

1-2-1-1. Overview

Among the many conducting polymers, polythiophenes have attracted considerable interest during the last two decades due to their environmental and thermal stability in both doped and undoped states, (42% weight loss at 900^{o}C) and their very high electrical conductivity ranging from 3.4×10^{-4} to 1.0×10^{-1} S/cm after doping with iodine.[13]

The first synthesis of polythiophene was reported in 1980, and gave an insoluble and unprocessable compound.[14,15]The reason for the poor solubility of polythiophene is attributed to the strong π stacking between thiophenes rings. Various possible approaches of modifying the properties of (P3AT) can be achievable by substitution of an alkyl group in the β position of the thiophene ring. This substitution on the β position results in an improvement in solubility of P3AT in the organic solvents. Therefore, it enhances the ease of processing for many applications and facilitates the characterization of P3ATs,[16] which have several practical applications such as in electrical conductor, smart windows, rechargeable batteries, LED polymers, solar cells, and sensors optical devices, etc.[10]

Generally, the ability to manipulate the properties of P3AT by varying substituted alkyl groups at the β position has become a critical topic in term of design and creation of a novel series of P3AT, hence, promoting new advanced materials and their properties.

1-2-1-2 Chemical Synthesis of Polyalkylthiophene (P3ATs).

The chemical synthesis of P3AT has undergone several improvements. Polymethylthiophene (PMT) was the first synthesized substituted P3AT and was insoluble.[17-19] In 1985, Elsenbamer and his co-workers synthesized the first soluble and stable P3AT.[20-22] Shortly after, chemical and electrochemical syntheses of P3AT were reported.[23-25] It was deduced that the solution and melt processed into film was possible with alkyl group longer than butyl with the electrical conductivity of 1×10^{-5} S/cm. [20-25] The following are several techniques that have been used to prepare P3AT.

Kumada followed the same procedures of synthesis polythiophene [20-22] to prepare P3AT and this reaction is known as cross – coupling polymerization, [26,27] as shown in Scheme (1.1). In addition, it was found that common organic solvents such as chloroform, THF, acetonitrile, methylene chloride, benzonitrile, nitrobenzene, toluene, and xylene can dissolve any P3AT with alkyl group equal to or longer than butyl group.

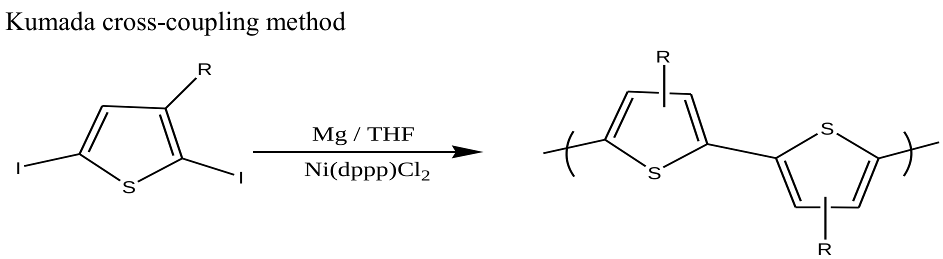

Scheme 1.1: the synthesic approach for Poly (3-alkylthiophene).

The synthesis of P3AT was further developed in 1995 by Curtis el at, [28] 2.5-bis (chloromercurio-3-alkylthiophene was polymerized in the presence of copper powder and $PdCl_2$ in pyridine as shown in Scheme 1.2. In this method, the homopolymer and copolymer were produced, with 3-alkyl and 3- esteric substituents formed with respect to the copolymer. The molecular weight was observed to be 26 K, with a PDI of 2.5 for poly (3-butylthiophene).

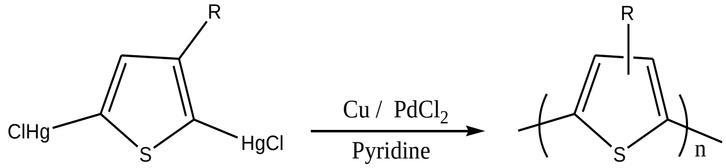

R= alkyl or esters

Scheme 1.2: Curtis' method for the synthesis of P3AT.

In 1986, Sugimoto and his co-workers successfully prepared P3AT using oxidizing agents such as ferric (III) chloride ($FeCl_3$),[23] ruthenium(III) chloride ($RuCl_3$) or molybdenum(III) chloride ($MoCl_3$)[29] in dry chloroform. In general, $FeCl_3$ as an oxidizing agent has frequently been used to synthesize P3AT.[30-35] The molecular weight of polymers prepared by this method ranges from 30 to 300 K with PDI ranging from 1.3 to 5.[34,35] Moreover, there is no α-β (2,4) coupling as a result of the $FeCl_3$ method. The main drawback of this method is that remaining iron can settle in the polymer and alter the properties of the P3AT, which can influence devices performance for some applications such as transistors[36] and light-emitting diodes (LED).[37]

The preparation of PT[29-36,38-45] and P3AT[46] using $FeCl_3$ is a highly effective and simple approach. This reaction is classified as an electrophilic substitution. The general mechanism of the polymerization reaction of 3-alkythiophene is illustrated in Scheme 1.3. The major function of $FeCl_3$ is to initiate the reaction by producing radical cations on the thiophene ring. Thereby, the polymerization chain reaction will continue until addition of methanol to terminate the reaction.

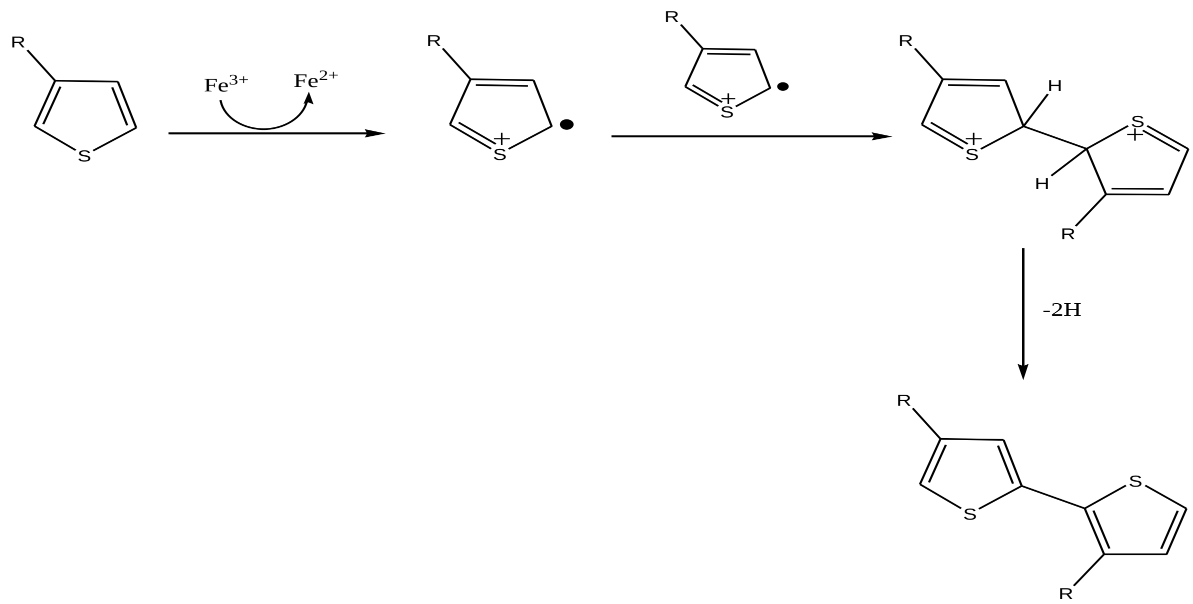

Scheme 1.3: The general mechanism of P3AT synthesis using $FeCl_3$.

1.2.1.3. Regioregular and Regioirregular.

Due to the 3- substituent of the thiophene monomer, P3AT is converted to an asymmetrical molecule. This means that the linkages of the dimer provide three possibilities of coupling: 2,5 or head to tail (HT) coupling, 2,2 or head to head (HH) coupling, and 5,5 or tail to tail (TT) coupling. [47,48] These couplings are arbitrary structures, which are produced in the polymers of P3AT. However, three assorted couplings can generate four regioisomers in the case of P3AT. Scheme 1.4 displayed the three coupling orientations and the four regioisomers of P3AT.

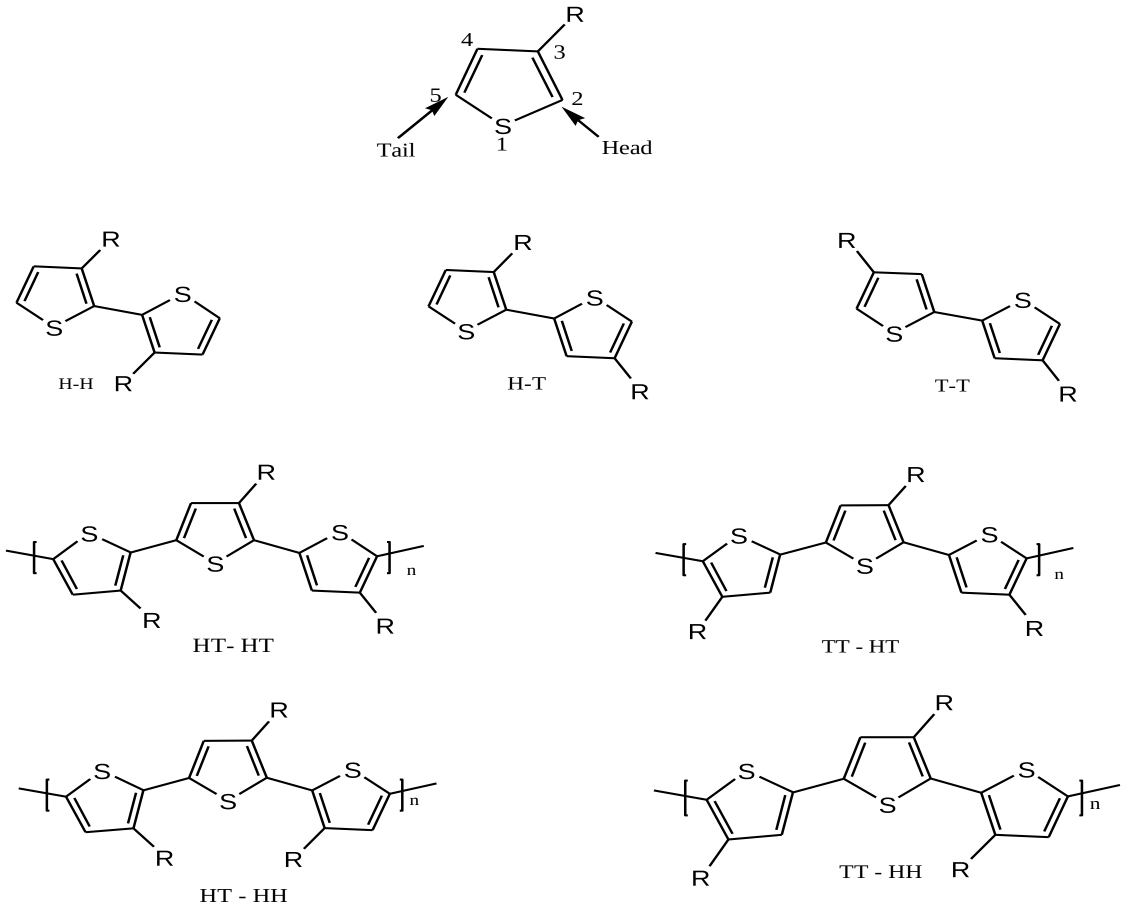

Scheme 1.4:The possible regiochemical couplings in P3AT.

The word “regioirregular” is a term given to a polymer, which has a mixture of these couplings such as HH or TT, which can affect the properties of the polymers. In HH and TT orientation couplings thiophenes are twisted due to the torsion point between thiophenes rings. The regioirregular coupling can affect the properties of P3AT such as loss of the conjugation system, a large band gap, destruction of the conjugated system and other attractive properties of P3AT. In addition, the formation π - π stacking of regioirregular P3AT has less probability to form in HH and TT couplings, which can affect the electronic properties of P3AT.

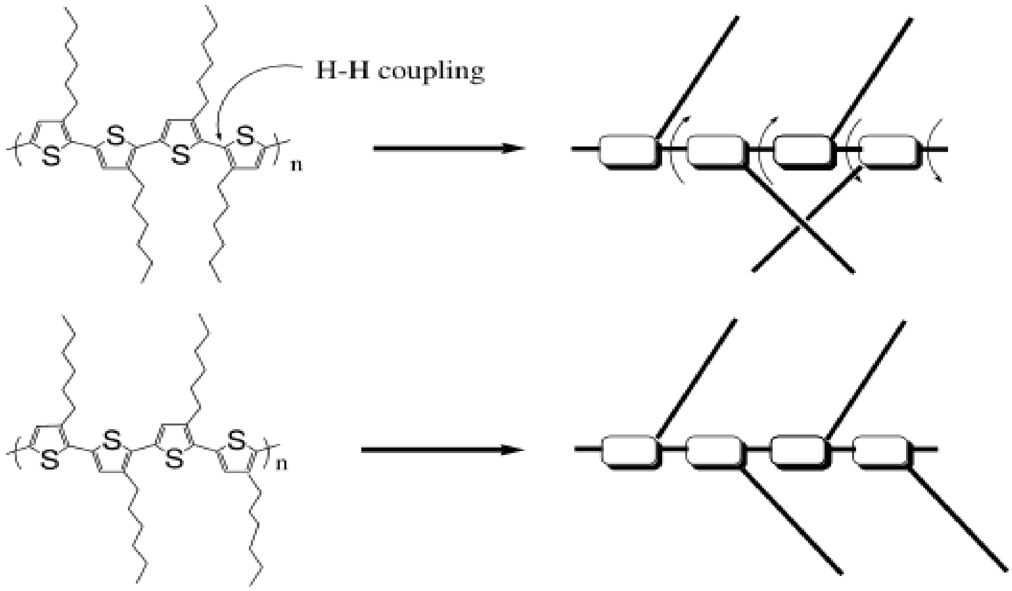

Figure 1.4: Regioirregular (H-H) coupling top and regioregular (H-T) coupling bottom.

Regioregular P3AT, on the other hand, is a polymer which is formed by all head to tail linkages. This type of coupling has been explored enormously because it leads to remarkable properties such as high conductivity, high stability, and high electronic mobility. In addition, 3-dimensional structures can be formed in HT coupling, which leads to a planar configuration. The steric hindrance of the regioregular formation is diminished. In comparison, HH or TT couplings are not desirable coupling due to the increase of band gap and negative effect on the conjugated system of the P3AT. [24]

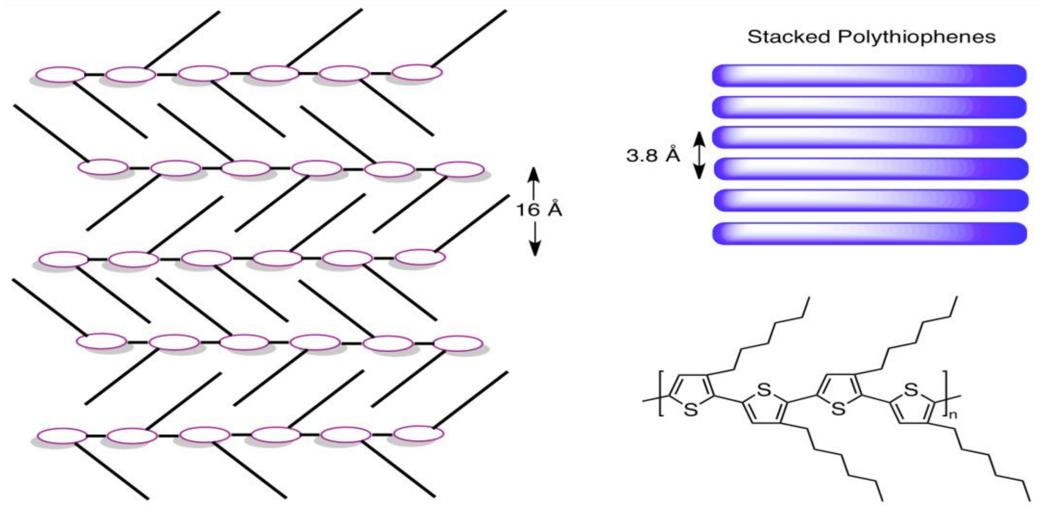

Figure 1.5: Three-dimensional self - assembly of rr-P3AT. [49]

1.2.1.4. Controlling The synthesis of Regioregular Poly(3-alkythiophene).

Various methods to control the synthesis of rr-P3ATs have been reported. McCullough and his co-worker mentioned the first synthesis of the regioregular head to tail P3AT with a yield of nearly 100%. [50] The key element of this method is to react 2-bromo-3-alkyl thiophene with LDA at -76 ^{o}C followed by the addition of MgB_2OEt_2 to form 2-bromo-5-bromomagnesium-3-alkylthiophene, which is then polymerized with a catalytic amount of $Ni(dppp)Cl_2$ via the Kumada cross–coupling method. This method affords a yield of approximately 44 – 69 % of rr-P3AT as shown in Scheme 1.5. In addition, 98-100 % HT-HT coupling was synthesized by the Mcullough method with a typical average molecular weight between 20 K- 40 K and PDI of 1 to 4.

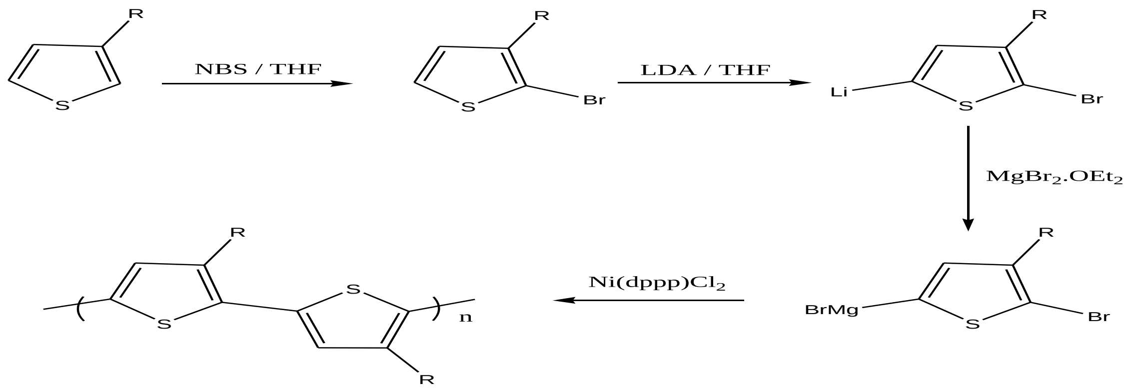

Scheme 1.5: The synthesis of rr-P3AT via the McCullough approach.

Rieke et al described another synthetic approach for preparing regioregular P3AT as illustrated in Scheme 1.6. In this method, the reaction between 2,5-dibromo-3-alkylthiophene with highly reactive zinc results in the formation of an organozinc compound. Subsequently, nickel was utilized as a catalyst for polymerization. [47,51-53]The regioregularity of the resulting polymer relies on the choice of the appropriate catalyst. For example, a regiorandom polymer is formed when using $Pd(PPh_3)$, while $Ni(dppp)Cl_2$ produces a regioregular polymer. The molecular weight and PDI of these polymers are from of 24 K-34 K and 1.4, respectively.

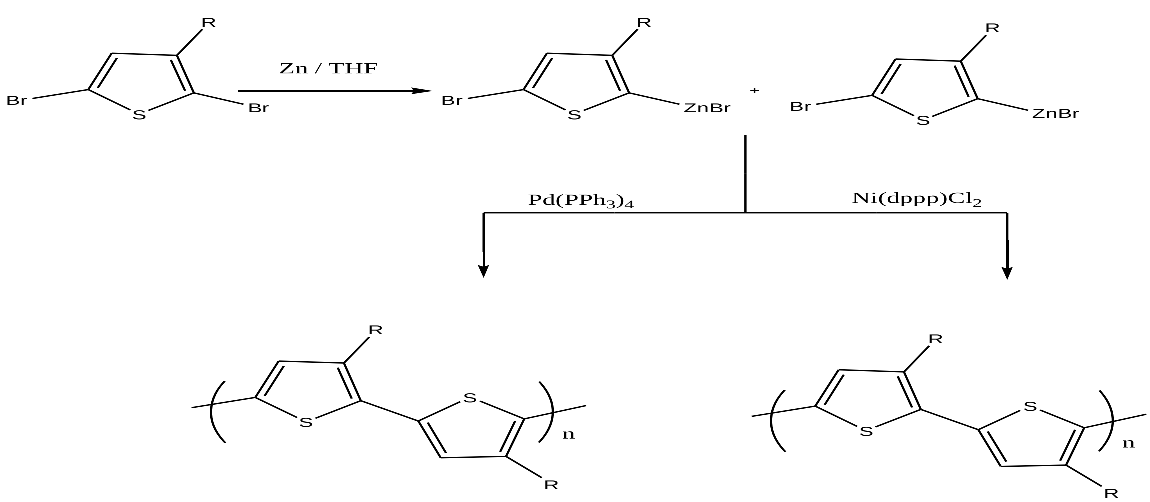

Scheme 1.6: The synthesis of rr-P3AT via the Rieke approach.

The use of highly reactive zinc and multistep procedure are a major drawback of the two aforementioned methods. As a result, in 1999, McCullough developed a novel route for the synthesis of rr-P3AT. This method is widely known as Grignard metathesis (GRIM) method.[54,55]

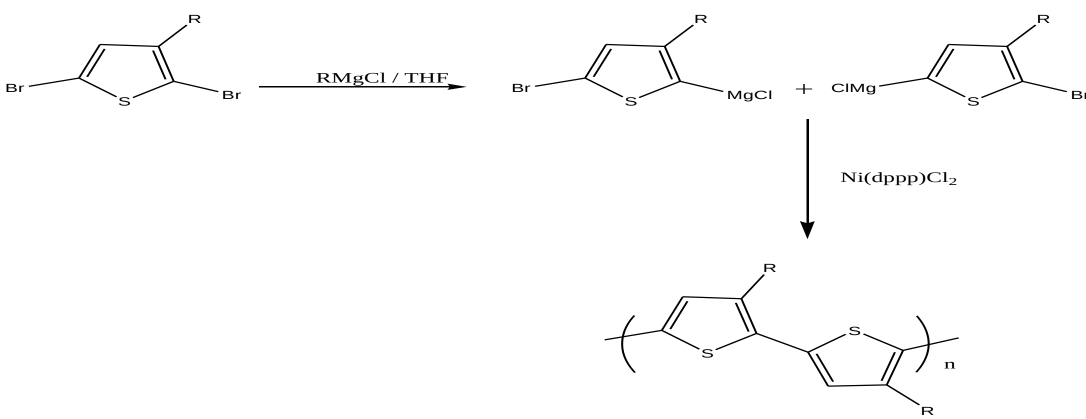

Scheme 1.7: The synthesis of rr-P3AT via GRIM

According to the GRIM method, one equivalent of RMgCl is reacted with 2,5-dibromo-3-alkylthiophene to produce an intermediate mixture as illustrated in Scheme 1.7. The molecular weight of rr-P3AT produced by this method ranges from 20 k to 40 K with a PDI of 1.2 to 1.4.

1-2-2 – Polyaniline

1.2.2.1 Overview.

Polyaniline (PANI) is one of the most attractive conducting polymeric materials. PANI was first discovered in 1934 by Runge.[2] This newly discovered polyaniline was known as “aniline black”, which is a result of an oxidation reaction. Runge observed that heating aniline nitrate and copper (II) resulted in a color change from dark green to black.

The incredibly unique properties of PANI, including high electrical conductivity, high stability, optical, electrochemical, low cost, and lightness [56,57] make it a promising polymer for future use in technological, and scientific applications such as rechargeable batteries, radar absorption, solar cells, catalysts, sensors, and non-linear optical and light-emitting devices. [58-65] Polyaniline commonly refers to a large class of conducting polymers. Polyaniline's structure composes of alternating reduced (benzenoid) and oxidized (quinoid) repeating units as illustrated in Figure 1.6.

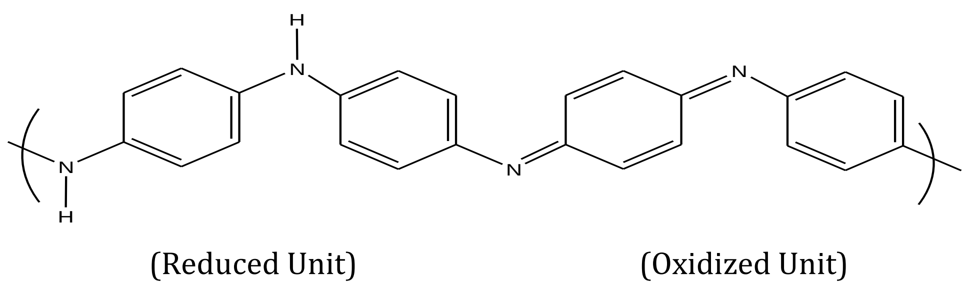

Figure 1.6: General structure of polyaniline.

The major feature of PANI is its ability to interconvert between conducting and insulating properties under specific conditions. [66] This process is known as protonic [67] doping which is the main distinguishing property of PANI amongst other conducting polymers, and as a result, many properties that are relevant to PANI, including vibrational, electrochemical, chemical, and optical, and others properties can be highly altered depending on the incorporation of various dopant anions. Moreover, the oxidation state of PANI plays a crucial function in forming four different types of PANI as shown in Figure 1.7. [68]

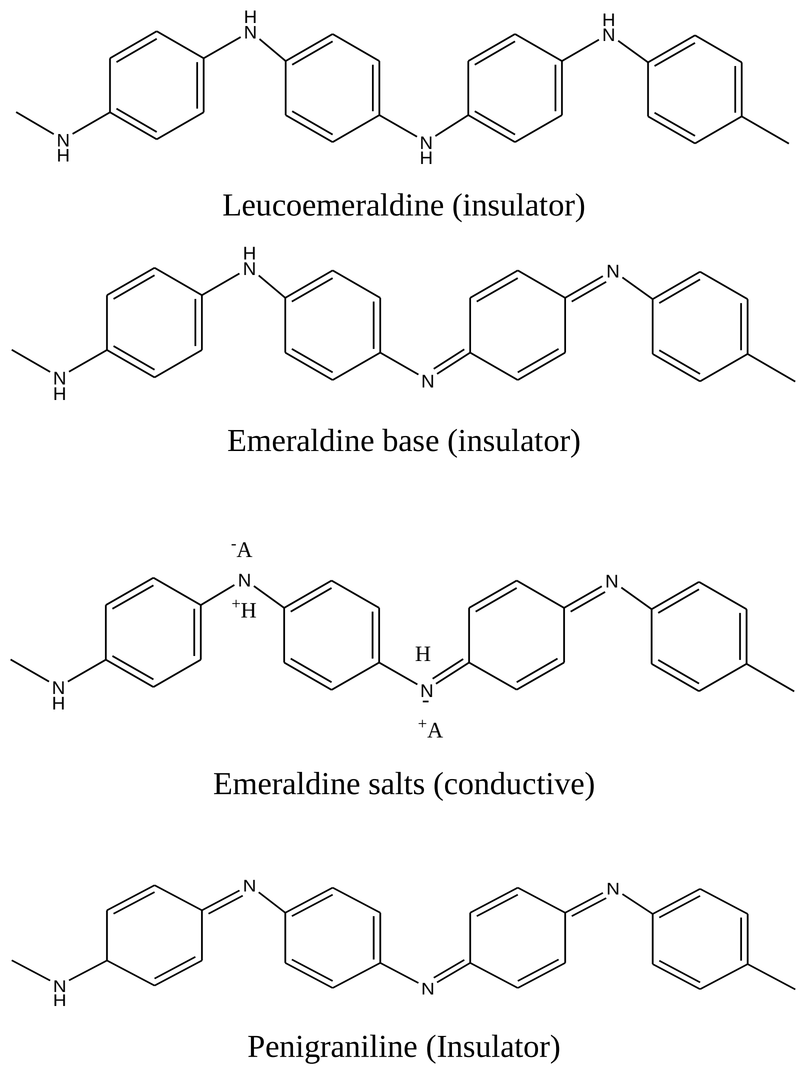

Figure 1.7: Four different oxidation forms of polyaniline.

Leucoemeraldine is a form of PANI, comprised solely of reduced units, and completely oxidized PANI is referred to as pernigraniline, which consists of solely oxidized units. Emeraldine base form of PANI is made up of an equal amounts of reduced and oxidized units. It is essential to mention that all the aforementioned forms of PANI are insulators. In contrast, the emeraldine salt of PANI is highly electrically conducting and stable. This form of PANI can be prepared by a chemical reaction of emeraldine base with protonic acids. The doped PANI (emeraldine salt) displays a spectacular improvement in electrical conductivity of approximately 9 to 10 orders of magnitude compared to non-doped PANI, a conductivity of with 1 to 5 S/cm. [69,70]

1.2.2.2. Synthesis of Polyaniline

PANI can be synthesized by either electrochemical or chemical polymerization methods by using an oxidizing agent in the presence of aqueous acid solution, yielding the emeraldine salt. Other polymerization methods have also been utilized such as enzyme-catalyzed polymerization and photochemically initiated polymerization. [71,72] Regarding chemical polymerization, various oxidizing agents have been used to polymerize the aniline monomer, including ammonium peroxydisulfate (APS), [73,74] hydrogen peroxide, ceric nitrate [75], and ferric chloride. [76] Among these oxidizing agents, the synthesis of PANI via APS produces a polymer with the highest electrical conductivity compared to other oxidizing agents.

The electrochemical polymerization approach is another technique to synthesize PANI in aqueous medium or appropriate electrolytes using constant potential or current. [77-80] Features such as controlling the degree of doping, and ease of preparation are some advantages of the electrochemical synthesis of PANI. However, some properties such as low conductivity and, lower crystallinity are drawbacks of the electrochemical polymerization of PANI. The mechanism of the polymerization reaction is the same regardless of which of the two synthetic methods is used, as can be seen in Scheme 1.8.

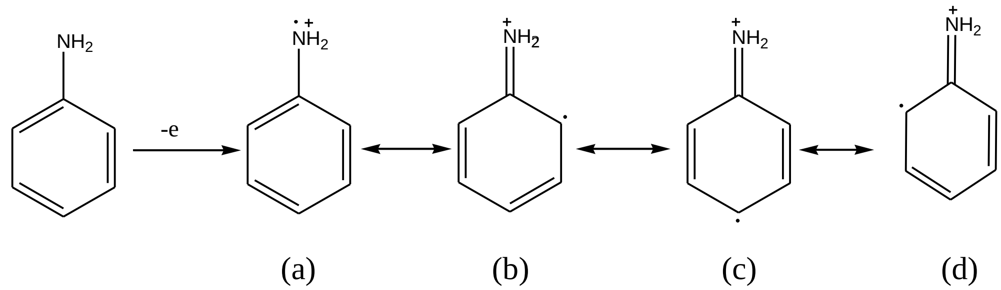

Scheme 1.8: The resonance structures of aniline radical cation.

The first step in synthesizing polyaniline is to generate a radical cation by an electron transfer from the 2s energy level of the aniline nitrogen. The radical cation is resonance stabilized and resonance structure (c) is the most reactive due to its significant substituent inductive influence and is lower sterically less hindered. The next step is to produce a dimer from the aniline monomer by a head to tail coupling between the radical cation (c) in an acidic medium. Subsequently, a new radical cation dimer is generated after oxidizing the dimer. Next, the radical cation dimer reacts with a radical cation monomer to synthesize the trimer. This process continues in a chain reaction.

1.3. Doping of Polymers.

The term “doping” is borrowed from physics. However, in chemistry, it describes the insertion of either anions (p-doing) or cations (n-doping) into a material via electrochemical or chemical reactions. The notion of doping is mainly relevant to conducting polymers, which differentiates the intrinsically conducting polymers from other varieties of polymers. In the intrinsically conjugated polymer, the valence band is completely full by electrons and the conduction band is completely empty. There are two classes of conducting polymers; non-conductive form (non-doped) polymers and conductive form (doped) polymers. In neutral polymers (non-doped state), all conducting organic polymers are either insulators or semiconductors.[81]

The procedure of converting the neutral form of the polymer chain into a charged conjugated polymer is called 'doping', and takes place when the neutral form of the polymer is treated by a small amount ($\leq \sim 10$ %) of dopant species. This causes the electrical, electronic structural, magnetic, and optical properties of the polymer to alter noticeably. In addition, the electrical conductivity of the doped polymer compared to the non-doped polymer is typically higher by 5 – 10 orders of magnitude. Polyacetelyene, for example, is the most common conducting polymer which when doped by an oxidizing agent such as iodine, experiences increase in the electrical conductivity up to 10^{4} S/cm.[4]

Electrochemical and chemical processes are the general approaches to making doped and non-doped polymers. The degree of conductivity can be adjusted by controlling the level of doping. The incorporation of a doped polymer with a conventional polymer can produce conducting blends with the best properties of both types of polymers. Thus, it is possible to employ conducting blends for various applications.

Redox doping such as chemical or electrochemical partial oxidation (p-doping), or partial reduction (n-doping) are classical approaches for doping conjugated polymer.[82] Generally speaking, the doping process is required for the insulating polymer to be transformed into its conducting form. The doping process involves exposing the polymer to either a solution or vapor of the doping agent such as $FeCl_3$ or I_2 [83], arsenic pentachlride, $NOPF_6$, or sodium naphthalide. The most important factor of the dopant agent is its capability of oxidizing or reducing the polymer. During the doping process, there is a rearrangement of the polymer chain into more planar conformation between the monomeric units. [84]

In comparison to other conducting polymers, polyaniline is an exceptional polymer since it has four different oxidation states, leucomemeraldine (fully reduced), emeraldine (half-oxidized), pernigraniline (fully oxidized) [85,86] and emeraldine salt, which is the only electrically conductive form of the polymer. The emeraldine salt is produced by protonation of emeraldine base with an acid. As a result, polyaniline is very vulnerable to PH changes. Polyaniline has redox activity at a pH of 4 or lower. However, polyaniline will deprotonate and loss its redox activity at higher pH.

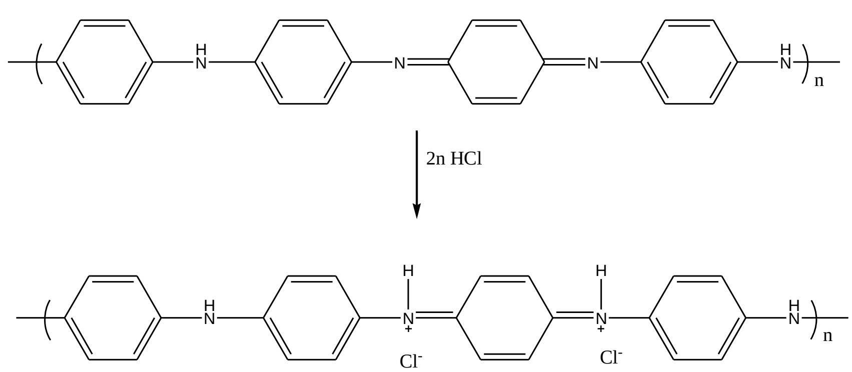

Scheme 1.9: The protonic doping of Emeraldine base by HCl.

The level of oxidation and protonation is the key element of the electrical conductivity of polyaniline. [85,86] The process of preparing emeraldine salts from emeraldine base is known as “protonic acid doping” [67] as shown in Figure 1.9. The electrical conductivity of the emeraldine salts results in a spectacular increase of electrical conductivity to 4×10^{2} S/cm. [70]

Similarly, strong acids can be used to dope other polymers such as poly (3-alkylthiophene), but result in a lack of solubility and processability. Moreover, the doping of polythiophenes by strong acid can convert the sp^2 hybridization of the aromatic ring into sp^3 hybridization as shown in Scheme 1.10. This can affect the π system along the polymer chain, which causes a reduction in conductivity and affects the optical properties of the conducting film. [87]

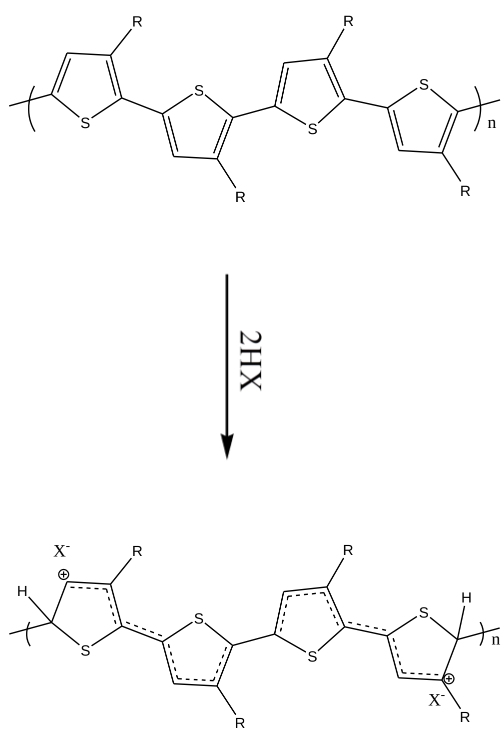

Scheme 1.10: Protonic doping of P3AT.

Polythiophenes can be reduced by a chemical agent such as sodium metal or by an electrochemical approach to produce a polymer with electrical conductivity. The effectiveness of this technique is extremely influenced by two major elements: the cation nature and its efficiency of the solvated size. [88] For example, the reductive doping of polythiophenes bearing crown-ethers becomes more stable under dry-air condition. Scheme 1.11 demonstrates the reduction reaction (doping) of the polythiophene with crown ether. However, this polymer still lacks stability under a humid atmosphere. [89]

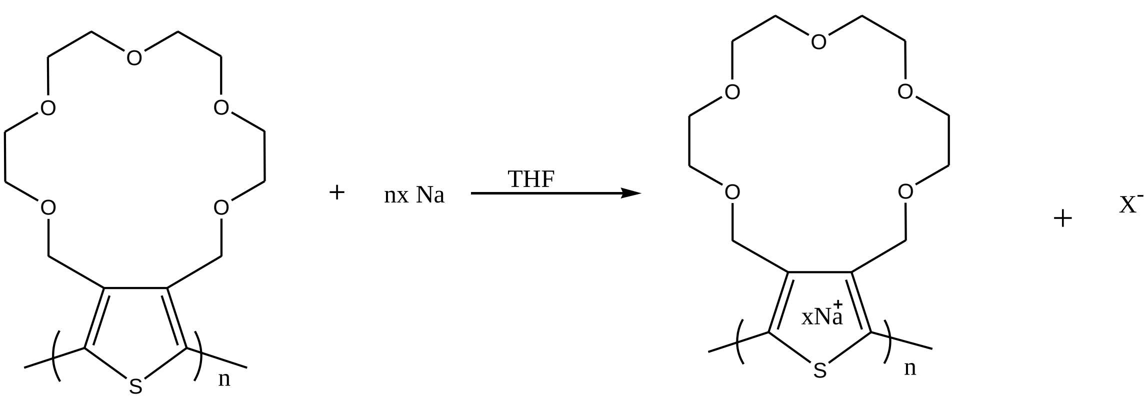

Scheme 1.11: The reduction doping of PT with a crown – ether.

In contrast, the oxidative doping of the conjugated polymer can be accomplished upon various common polymers structure using different oxidizing reagents. However, because of the widespread use of this method, the doping reaction usually represents oxidation of the polymer backbone with the incorporation of anions. The crucial point of for effective oxidative doping is the reduction potential of the oxidant, which should be higher than that the oxidation potential of the polymer. In case of poly(3-alkylthiophene), some oxidizing agents include ferric chloride, gold(III) chloride, iodine, and a salt such as nitrosonium tosylate.

The difference between the oxidation and the reduction potentials of doping agents is governed either by the reversibility of the charge- transfer complex formations, [90,91] such as the doping of polythiophenes by oxygen, or achieved electron transfer when poly(3-alkylthiophene) can be doped by ferric chloride, which is reduced as described in the equation 1:

$$e^- + 2\,FeCl_3 \longrightarrow FeCl_4^- + FeCl_2 \qquad (1)$$

Concerning the doping of P3AT with $FeCl_3$, the chemistry of the doped polymer may be influenced by any remaining reduced dopant [$FeCl_4^-$] and the by-product $FeCl_2$. Poly (3-alkylthiophene) doped with $FeCl_3$ exhibits a low environmental stability, attributed to the photoreduction and photolysis of $FeCl_4^-$, resulted in electrons moving to a charge carrier in the conductive polymer. [90,91] This leads to a decrease in the amount of charge carrier in the doped polymer. Therefore, over time, the electrical conductivity is decreased. In general, the chemistry of any by-product during the doping reaction can have an effect on the stability of the conducting polymer.

It is possible to overcome the problem of residual byproduct during the doping process by using a reaction known as the “full electron-transfer reaction.” This reaction decreases the amount of any by-product by employing oxidizing agents, which form volatile reaction products. For instance, poly(3-alkylthiophene) can be doped by nitrosonium triflate (ONOTf) with NO gas as a byproduct, as seen in equation (2).

$$e^- + ONOTf \longrightarrow NO_{(g)} + OTf^- \quad (2)$$

In the case of doping P3AT with ONOTf, the characterization of the doped polymer indicates absence of the nitrogen as determined by elemental analysis. Also, the IR spectrum displays the lack of the C-N stretches. There is concrete evidence of the low presence of nitration along the polymer chain. Clearly, the [NO^+] cation is driven out of the doped polymer as nitrous oxide.

1.4. Mechanism of Electrical Conductivity.

To describe the conductivity of electrically conjugated polymers, some concepts are borrowed from physics such as polaron, bipolaron, and soliton as shown in Figure 1.8. The oxidation of conducting polymer (p-doping) results in removal of an electron from the top of the valence band, forming a radical cation which is known as (polaron). The radical cation, which has higher energy than energy in the conduction band, delocalizes only on several monomeric segments with a paramagnetic spin. When a further oxidation is applied to the polaronic state, the unpaired electron will be removed, formation of a special dication (bipolaron) which is not independent, formed with a spinless property. Furthermore, a high level of dopant produces many bipolaron levels and ultimately causes a formation of bipolaron band. The soliton is special formation and only exists when a polymer has two equivalent resonance forms (degenerate ground state).

The definite mechanism of electrical transport along the polymer backbone is not entirely understood, although the well-known soliton and bipolaron are the major source of charge carriers. Most of the polymers are disordered, comprising a blend of crystalline and amorphous areas. It is very necessary to take into account the fact that the charge carriers move along, and between the polymeric units and tangled boundaries, and can affect the mechanism of charge transport. Thus, parameters such as temperature, magnetism, doping have been investigated to understand the effect of these factors on charge transport. Several mechanisms have been proposed, and the most commonly excepted explanation is the transformation of the charge carriers between the localized sites, or between polaron, bipolaron, and solitons. Another explanation is that a metallic island is dispersed in an insulating matrix which is created by inhomogenous doping species. The conduction is then dependent on the movement of the charge carriers between different conduction domains, which can also be affected by thermal activation. This means that conduction is temperature dependent.[4-7]

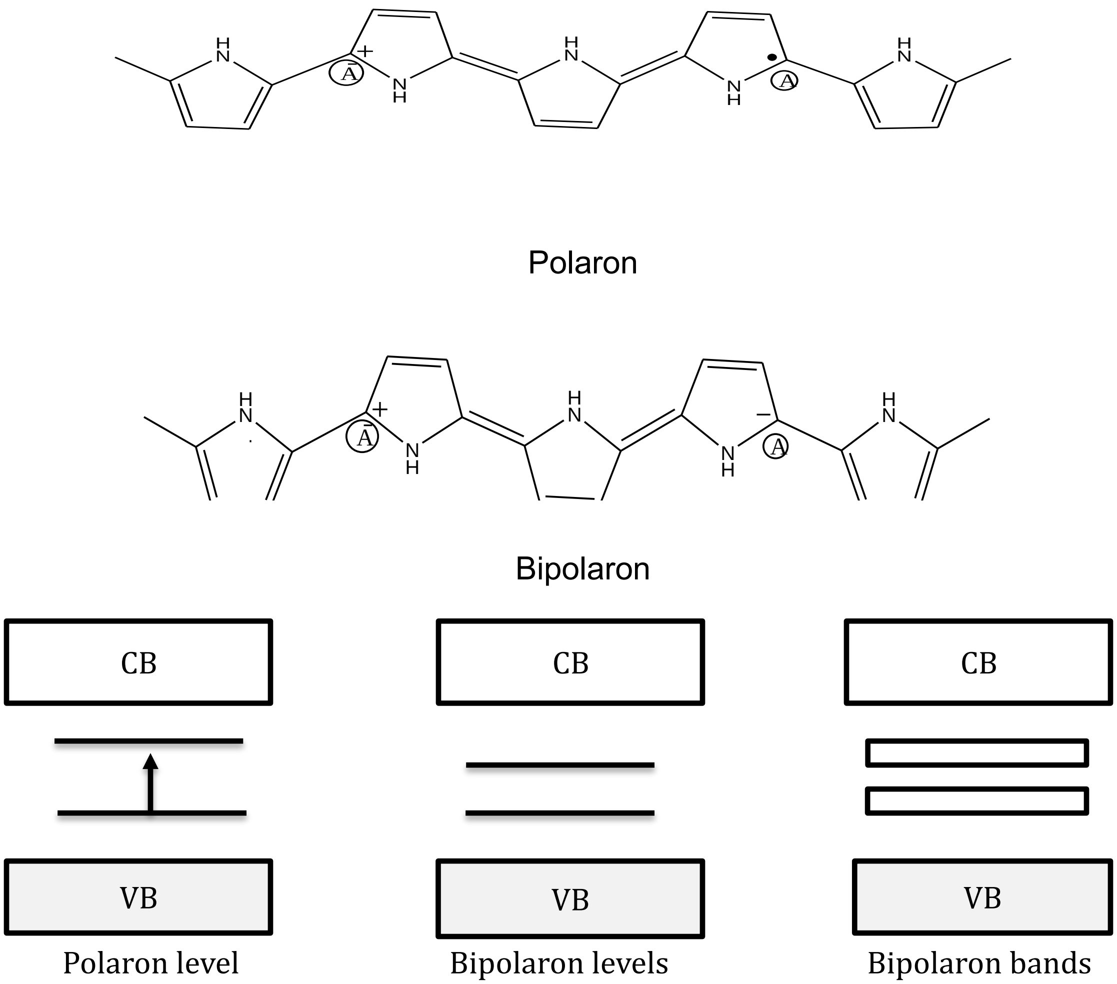

Figure 1.8: The polaron, bipolaron, and their band gaps. [5]

In conducting polymers, not only good charge transport, but also environmental stability is a fundamental factor. There are two classifications of the stability of conducting polymers: extrinsic and intrinsic stabilities. Extrinsic stability refers to the interaction of the surface of the conducting polymers with external environmental factors such as water, oxygen, and peroxide. The charged sites of the polymer are susceptible to attack by free radicals, nucleophilic, or electrophilic substances. As a result, the polymer has to be protected by a stable coating if it is extrinsically unstable.

The degradation mechanism even in the dry air and the lifetime of the conducting polymer play a crucial role in the stability of the polymer. This type refers to intrinsic stability, which is thermodynamic in origin. The intrinsic instability of the polymer can occur between the charged sites of the polymer and the dopant ion or between single and double bond system of the neutral chain by an irreversible chemical reaction. Thus, the conjugation system breaks and renders sp^3-hybridized carbon. The thermodynamically can also lead to the intrinsic instability by making the polymer lose its dopant, and this arises once having unstable charge sites because of the structural changes in the polymer chain. [7,92-94]

Table 1.1 shows the comparison between some conducting polymers in terms of their conductivities, stabilities, and processing possibilities. Temperature, concentration, presence of electrode impurities, pressure, and current [95] all affect the properties of conducting polymers. Additionally, the monomer structure is a determining component in terms of conductivity. Also, the solubility and flexibility of conducting polymer can be improved by attaching alkyl groups. [96-98]

Table 1.1: Stabilities and processing possibilities of conducting polymers. [99]

Polymer	Conductivity S/cm	Stability Doped state	Processing possibilities
Polyacetetylene	10^3 - 10^5	poor	limited
Polyphenylene	1000	poor	limited
Polyphenylenesulfide	100	poor	excellent
Polyphenylenevinylene	1000	poor	limited
Polypyrroles	100	good	good
Polythiophenes	100	good	excellent
Polyanilines	10	good	good

1.5. Application of Conducting Polymers

Since the negative environmental effects of metals have been reported, conducting polymers have been widely investigated for potential applications. Due to the electronic and conductive properties of conducting polymers, the applications are classified into two groups as shown in Table 1.2. The electrical conductivity of polymers is significant for various applications. Due to the lightweight, low cost, biological activity and ease of manufacturing, conductive polymers have an interesting field in many potential applications. Due to the presence of π electron along the conducting polymer, the reversible (oxidation and reduction) reaction can happen chemically or electrochemically. This feature renders a valuable opportunity to utilize conducting polymers for various modern applications. [100]

Table 1.2: Two groups of applications for conducting polymers. [4-7,101-110]

Group 1- Conductivity	Group 2 - Electroactivity
Electrostatic materials	Active electronics (diodes, transistors)
Electromagnetic shielding	Molecular electronics
Conducting adhesives	Rechargeable batteries and solid electrolyte
Ink jet printed material	Chemical, biochemical and thermal sensors
Antistatic clothing	Ion exchange membrane
Piezoceramic	Electromechanical actuators
	"Smart windows"

In corrosion protection, conducting polymers can be utilized for coating metals because of their lightweight and environmental safety. Since metals decompose in the presence of water or moisture and cannot endure long periods of time and have a negative impact on the environment, it has been proposed that coating metals with conducting polymers can effectively protect the metals from corrosion. Therefore, the direct contact between the reactive species such as water and moisture and the metals is avoided.

Moreover, oxidation state plays a major role in transformation the electrical energy to mechanical work. [100] Baughman and his co-worker have reported that conducting polymers can be used as actuators. [111]

Batteries are one of the most significant applications of conducing polymers. The charge capacity of metal is slightly lower than conducting polymers per unit of mass due to the polymer charge being located in three or four adjacent monomeric units. Conducing polymers and metals such as lithium can be used to generate high power densities because of the high potential difference between materials. Cellular phone, computers, cordless drills, and laptops are potential applications of rechargeable batteries. [100]

Electrochromic devices (smart windows) are another application of conducting polymers. There is only a slight dissimilarity between rechargeable batteries and electrochromic device applications. In electrochromic devices, for example, there must be at least one transparent electrode to observe the color changes. In the performance of electrochromic windows, the doped and undoped states of conducting polymers will result from electric potential (sunlight), and as a result, a positive potential is employed leading to p-doping (oxidative doping), which causing the color alters to be visible. Several conducting polymers have been investigated, including polythiophene, polyaniline, and polypyrrole, etc. for potential use in electrochromic devices. [100]

1.6. Transition Metal Dichalcogenides (TMDs):

During the recent past, two- dimensional nanomaterials such as graphene and TMDs have received a tremendous amount of attention due to their outstanding as electrical, [112,113] optical [114-121] and mechanical [122,123] properties. Graphene is one of the well-known 2D nanosheet materials, which exists in atomic-layer thickness with a hexagonal structure. The incredible properties of graphene and its technological applications such as in electronic devices and batteries are attributed to its 2D structural dimensionality. The properties of graphene do not remain in the case of bulk counterpart graphite. Despite the impressive characteristics of graphene and its applications, its inert reactivity is a major drawback. This means that graphene cannot be utilized in various applications unless it is functionalized with a desirable molecule. This can cause graphene to lose some of its exotic properties due to the functionalization. [124]

As a result of the discovery of graphene, a wide range of two-dimensional nanomaterials have rapidly gained a tremendous amount of interest. The 2D nanosheets of layered transition metal dichalcogenides are considered to be a breakthrough in the next technological generation. These materials have a high potential for use in various applications such as energy storage, [125-131] electronic devices, [129,132-139]optoelectronic devices, [140-142] and gas sensing. [129,143-147]

The composition of TMDs is represented by a general formula of MX_2, where M refers to the transition metal of group 4 to 10 and X refers to a chalcogen such as sulfur, selenium, and tellurium. In general, transition metals in groups 4 to 7 display layered structures. On the other hands, transition metals in groups 8 to 10 predominantly show non-layered structures.

Structurally, the transition metal is typically sandwiched between two chalcogen layers with the association of weak van der Waals force between the TMD layers, while the bond between M-X is covalent in nature. The bonding state is filled by four electrons from the metal. The high environmental stability of TMDs materials stems from the absence of the dangling bond and terminal long – pair electrons of chalcogen on the surface of TMDs. The monolayer of TMDs is comprised of a hexagonal or rhombohedral formation with the arrangement of octahedral or trigonal coordination and a thickness ranging from 6 to 7Å. [148]

Various electronic properties can be exhibited by TMD nanomaterials including metallic, semiconductor, superconductor, and insulator. For example, HfS_2 is an insulator, WS_2 and MoS_2 are semiconductors, WTe_2 and $TiSe_2$ are semimetals while $NbSe_2$ and TaS_2 are true metals. The versatile electronic properties of TMDs stems from the occupation of the non-bonding d band from group 4 to group 10 of the transition metals and poses metallic properties once the orbitals are partially occupied. In contrast, they show semiconductor properties once they are completely occupied. The presence of the chalcogen atoms has only a small effect on the electronic structure compared to that of the metal atoms. In contrast, the band gap of TMDs decreases with the increase of the atomic number of the chalcogen. The electronic properties of the layered TMDs are shown in Table 3.

Table 1.3: The Comparison of various layered TMDs' electronic properties. [148]

Group	Metal M	Chalcogen X	Properties
4	Ti, Hf, Zr	S, Se,Te	Semiconducting (E_g = 0.2 ~ 2 eV)
5	V, Nb, Ta	S, Se, Te	Narrow band metals or semimetals
6	Mo, W	S, Se, Te	Sulfides and selenides are semiconducting. Telluride are semietallic
7	Tc, Re	S, Se, Te	Small gap semiconductors.
10	Pd, Pt	S, Se, Te	Sulfides and selenides are semiconducting. Telluride are metallic. $PdTe_2$ is superconducting

Many approaches have been reported for the synthesis of mono and few layers 2D nanocomposites via two main techniques: top-down and bottom-up methods. The most common examples of the top-down method are chemical Li intercalation and exfoliation with butyllithium (BuLi), [149] liquid phase exfoliation in the solvent, [150] and mechanical exfoliation method. [151-153] In the bottom-up method, chemical vapor deposition CVD synthesis [154-159] and wet chemical synthesis [160-162] are common ways to prepare nanocomposites.

Among these techniques, the exfoliation technique is one of the most convenient and effective approaches for the synthesis of the nanocomposites. The exfoliation of bulk TMDs has two major advantages. First, the exfoliation of bulk TMDs does not usually affect the original properties of TMDs in a single layer. This leads to the second advantage, which is the possibility of design and creation of monolayer TMD materials with desirable properties.

This method was utilized to prepare polymer/MoS_2 composite. The initial step is to soak MoS_2 powder into a solution mixture of n-butyl lithium in hexane at room temperature to form $LixMoS_2$ (x is ≈ 1). The following step is to soak the $LixMoS_2$ into the water to accomplish the exfoliated layers of MoS_2 and the guest. The value of x is ≈ 1.

In term of the chemical structure, MoS_2 is the same as WS_2; the exfoliation-adsorption technique method was utilized to prepare WS_2 layers, but it was difficult due to the low Li concentration x=0.4 gained in $LixWS_2$, resulting in challenging to achieve a high degree of exfoliated WS_2. Matte et al. described a technique for the synthesis of exfoliated WS_2 few layers which required the use of thiourea and tungstic acid. The tungstic acid was mixed physically with an excess of thiourea. The ratio of tungstic acid to thiourea is 1:48 mole. After that, the mixture was then heated to 500˚C under a nitrogen atmosphere.

1.7. Polymer – Inorganic nanocomposite.

Polymer–inorganic nanocomposites (PINCs) have received significant technological and scientific interest. In the late 1980s, polymer nanocomposites were improved in commercial research and academic laboratories. Toyota was the first company to use naylon-6/clay nanocomposite material. This composite showed outstanding mechanical integrity. Nanocomposite materials are considered multiphase materials, where one of these phases is a nanoscale particle with a dimension of 100 nm or lower. [163] The existence of these phases in one system and their synergistic influence are anticipated to afford nanocomposites with unique properties. In addition, it is possible to design and create nanocomposites with highly desirable characteristics.

Nanocomposites can be divided into three categories according to their matrix: ceramic matrix nanocomposites, metal matrix nanocomposites, and polymer matrix nanocomposites. The possibility of nanocomposites design and synthesis stimulates researchers to discover and create advanced nanocomposites with unusual physical and chemical properties, which opens a window into use nanocomposites in a diverse range of technological applications.

Polymer- inorganic nanocomposites can be either in a form of exfoliated or intercalated state as shown in Figure 1.9. In the case of an intercalated nanocomposite, the organic polymer is inserted between the layers of inorganic materials leading to an expansion of inter-layer spacing. In an exfoliated case, the layers of the inorganic material are fully separated and dispersed throughout the organic polymer. Many approaches have been used to synthesize polymer-inorganic nanocomposite. *In situ*-polymerization, [164-166] melt intercalation, [167,168] template synthesis, [169,170] sol-gel processes, [171-173] and the direct mixture of polymer and particulates [174-176] are the most common methods for preparing polymer-nanocomposites.

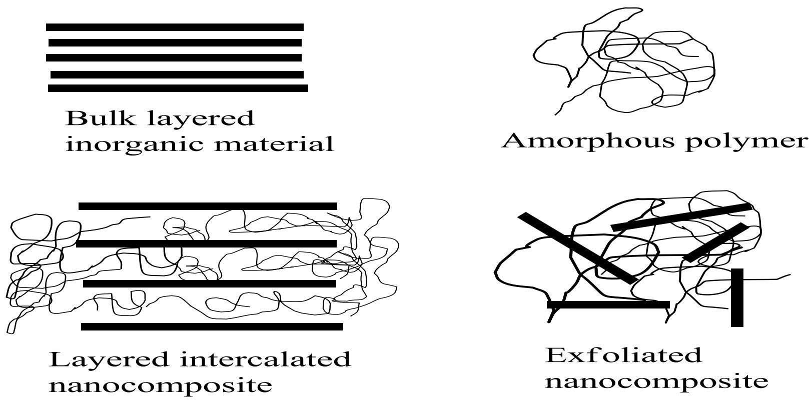

Figure 1.9: Intercalated and exfoliated nanocomposites.

The main reason for using organic polymers are their characteristics such as durability and low-cost, processability, lightweight and ease of fabrication. The main challenge for the polymers is to extend their applications by preserving the aforementioned properties while improving some particular properties such as heat resistance, mechanical properties; strength and modulus. [177,178] In contrast, polymer properties such as mechanical, electrical and thermal are relatively poor when compared to metals and ceramic, although, the several forms of polymers such homo-polymer, co-polymer and blended polymer are not adequate to compensate these properties. [178]

The incorporation of inorganic nanofillers into organic polymer has gained increased interest due to the appearance of spectacular resultant properties. The nanospecies are typically incorporated to improve particular properties of the polymer. [179] The polymer nanocomposites based on nanoclays have attracted a tremendous interest because of their ability to enhance some properties such as thermal, [180,181] fire retardant, [182-186] mechanical, [187-189] and barrier [190,191] properties of the polymer. In addition, the polymer nanocomposites have been displayed that at lower or equal loading showed equal or better properties than the polymer or conventional filler. [192-197]

Generally speaking, the produced nanocomposities exhibit advanced optical, electrical, electronic and mechanical properties. Thus, polymer-nanocompositics can be utilized as materials in different domains in nanotechnology and nanoscience applications such as automotive, aerospace industries, military equipment, safety, and optical and electronic devices. However, these applications often require further properties and functions such as high environmental stability, chemical resistance, electrical conductivity, mechanical properties, flame retardancy and reduced permeability to gasses and water, etc. The properties of the polymer and the nanofillers play a very important role in the effectiveness of polymer nanocomposites' properties. Table 1.4 shows some potential applications of nanocomposite materials. [198,199]

Table 1.4: Potential applications of various nanocomposites.

Nanocomposites	Potential applications
Polycarprolactone/SiO_2	Bone-bioerodible for skeletal tissue repair
PMMA/SiO_2	Dental application, optical devices.
Polyethylacrylate/SiO_2	Catalysis support, stationary phase for chromatography.
Poly(3,4-ethylene-dioxythiphene)/ V_2O_5	Cathode materials for rechargeable lithium batteries.
Shape memory polymers/SiC	Medical devices for gripping or releasing therapeutics within blood vessels
Polyimide/SiO_2	Microelectronics.
Polycarbonate/SiO_2	Abrasion resistant coating.

1.8. Decomposition Kinetics:

The thermal stability of nanocomposite materials is a very important property. DSC and TGA are common characterization techniques for investigation of the thermal properties of materials. In particular, thermogravimetric analysis (TGA) is a powerful technique in which the amount and rate change of a substance's weight as a function of temperature are measured an inert atmosphere.

TGA data is very useful to determine the decomposition point of a substance and anticipate its stability at very high temperatures. TGA can be utilized to acquire further information regarding the decomposition kinetics of any material. The activation energy, for instance, is a very significant element for decomposition materials. Calculating the activation energy can help to determine the appropriate applications for these materials. Ozawa method is one of the most common methods, which have been used to calculate the meaningful activation energy values. The integral method was deduced by Ozawa. [200] The distinct feature of this method is that it does not need to assume any parameter in the kinetic equation. In addition, Ozawa's method is a model-free method because it measures the temperatures proportional to a precise value of the convesion (α) at various heating rates β. Ozawa's method is usually described by the following equation (3):

$$\log \beta = \log\left(\frac{\mathrm{AE}}{\mathrm{R}}\right) - 2.315 - 0.4567\left(\frac{\mathrm{E}}{\mathrm{RT}}\right) - log\ g(\alpha) \qquad (3)$$

Where β is the heating rate, R is the molar gas constant (8.314 J /mol.K), (α) is the decomposed fraction, A is an pre-exponential factor. From the above equation, a new expression can be derived as follows:

$$g(\alpha) = (AE/\ \beta\mathrm{R})\ \mathrm{P(x)} \qquad (4)$$

Then the value of (x) can be determined by:

$$x = \frac{E}{RT} \qquad (5)$$

The conversion of (α) can be computed from the weight loss data as described in the following expression:

$$\alpha = (\ \mathrm{mo} - \mathrm{m}\ )/\ (\ \mathrm{mo} - \mathrm{m}\infty) \qquad (6)$$

Where m_o is the initial weight, m∞ is final weight, m is the actual weight at any temperature during the experiment. A plot of log β against 1/T acquires from the thermogram at various heating rates is supposed to be a straight line. Therefore, the estimation of activation energy can be evaluated from the slope of these straight lines as described in the following expression:

$$E_a = - \text{slope} * (R/0.457) \qquad (7)$$

1.9. Project Goals

The incorporation of nanofiller into conducting polymers can enhance the properties of the produced nanocomposites such as electrical, thermal and optical properties. In this research, various conducting polymers have been used to investigate the effect of the incorporation of different percentages WS_2 within PT, PThN, and PANI. The object of this research is to understand the thermal behavior of various compositions of WS_2 nanocomposites and Ozawa's method was employed to calculate the activation energies of these nanocomposite materials.

Chapter 2:

2.1. Introduction:

Conducting polymers have recently attracted a considerable amount of interest due to their remarkable properties such as high electrical conductivity, high environmental and thermal stability, and ease of preparation. Among these polymers, polythiophene (PT) and its derivatives have been studied extensively, and they have emerged as the most promising conducting polymers for potential applications. The major drawback of PT is its lack of solubility in most organic solvents. However, substitution in the β position of the thiophene ring provides a wide variety of conducting polymers with remarkable properties, which have several potential applications such as in electrical conductor, smart windows, rechargeable batteries, LED polymers, solar cells, and sensors, etc. [10]

Coumarin and its derivatives are extensively distributed in nature, and many of them provide varied and beneficial biological activities [201,202]. Coumarin and its derivatives also have a large number of applications such as stimulation for the central nervous system (CNS), [203] anti-inflammatory, [204-206] antitumor and anti-HIV therapy, [207,208] and antibacterial. [209,210] Moreover, coumarin derivatives are essential parts of fluorescence probes, switches, and sensors. [211,212]The fluorescence of coumarin compounds is extensively utilized as a research tool in polymer science. [213,214]They are also utilized as photo-initiators. [215] Naphthalene-containing monomers have been also synthesized for fluorescence applications because the ultraviolet radiation can be trapped by naphthalene derivatives.[216] Also, β naphthol is a fluorescent compound which can be used in dye applications[217].

Nanocomposites with transition metal chalcogenides have also been investigated for their improved optical, electrical and mechanical properties, etc. The preparation of nanocomposites can be either in exfoliated and intercalated states. Often, exfoliated composites are known as hybrid materials that contain a tiny amount of inorganic fillers. Polymer-based nanocomposites began to receive attention in the late 1980s, with Toyota being the first company using polymer nanocomposite in the 1990s [20]. The interest in utilizing polymer is attributed to their properties such as light weight, ease of synthesis, low cost, processability, and other properties.[218] Therefore, the incorporation of inorganic species into conducting polymers results in the production of nanocomposite materials with outstanding properties. In this work, the exfoliated nanocomposites were prepared. In literature, the exfoliated composites exhibit an improvement in the decomposition temperature and flame retardancy, etc.

In this work, P3AT with different alkyl group namely naphthalene and coumarin were chemically synthesized. In addition, PT-WS_2 nanocomposites were prepared and characterized by Nicole Arsenault,[219] and PThN-WS_2 nanocomposites were synthesized by the *in situ* polymerization method. These nanocomposites were prepared using different percentages by mass of WS_2; 1%, 5%, 10%, 20%, 37%, and 64%. PThN-WS_2 nanocomposites were characterized using techniques such as IR and XRD, and it was found that exfoliated composites resulted from the combination of PThN and WS_2.

Thermogravimetric Analysis (TGA) was used to determine the decomposition kinetics of WS_2-PT and WS_2-PThN nanocomposites. Ozawa's method was used to compute the activation energies for decomposition of these nanocomposites decomposition.

2.2. Experimental:

2.2.1. Material.

All chemicals and solvents were purchased from Sigma Aldrich and used without any further purification.

2.2.2 Synthesis of the monomers.

2.2.2.1. Synthesis of monomer 1.

The monomer synthesis occurred via a Steglich esterification reaction as illustrated in Scheme 2.1. In a solvent mixture of dichloromethane (DCM) and dimethyformaldhyde (DMF) (10 mL and 2 mL, respectively), 2-(3-thienyl) ethanol (1 mmol) was reacted with coumarine-3-carboxylic acid with stirring while under N_2 atmosphere in the presence of N,N-dimethylaminopyridene (DMAP). The mixture was then cooled to 0^oC for 30 minutes. After that, a solution of dicyclohexyl carbodiimide (DCC) (2 mmol) in 1-2 mL of DCM was added to the mixture to in order increase the reactivity. The reaction was stirred for 24 hours at room temperature, after which the solvent was removed in *vacuo*. After that, the crude product was dissolved in the freezer for 30 minutes in order to precipitate dicyclohexylurea (DCU). The DCU was removed from the product using vaccum filtration and was then further purified using chromatography (EtOAc/hexane 1.5:1). Thienyl-coumarine (ThC) was obtained as an off-white product with a yield of 70%.

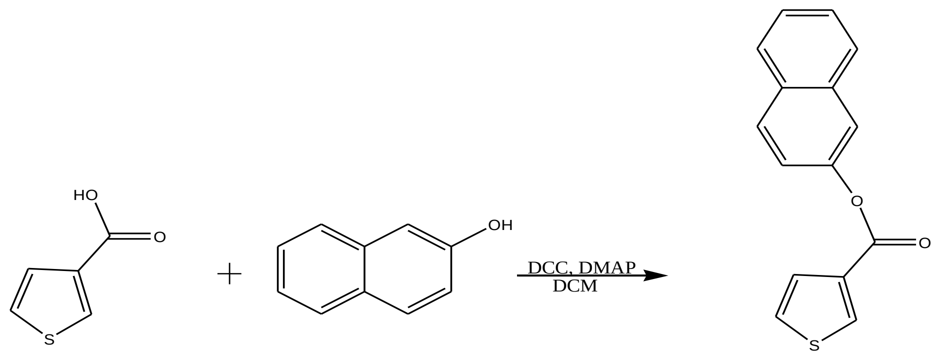

Scheme 2.1: The esterification reaction of 3-thiophenecarboxylic acid with 2-naphthol.

2.2.2.2. Synthesis of monomer 2.

The synthesis of monomer 2 is shown in Scheme 2.2, and was prepared by reacting 3-thiophene carboxylic acid (1mmol) with 2–naphthol (1 mmol) in the presence of DMAP (2 mmol) using a solvent mixture of DCM/DMF (10 mL/2 mL) under N_2 with stirring. A solution of DCC (2 m mol) in 1-2 mL of DCM was added to the mixture after 30 minutes at 0^oC. Solvents were removed in *vacuo,* and the product was redissolved again in DCM and put in the freezer for 30 minutes to precipitate the DCU, which was removed via vacuum filtration. A further purification was performed using column chromatography (EtOAc/hexane) to obtain thiophene-naphthalene (ThN), an off-white solid product, with a yield 70%.

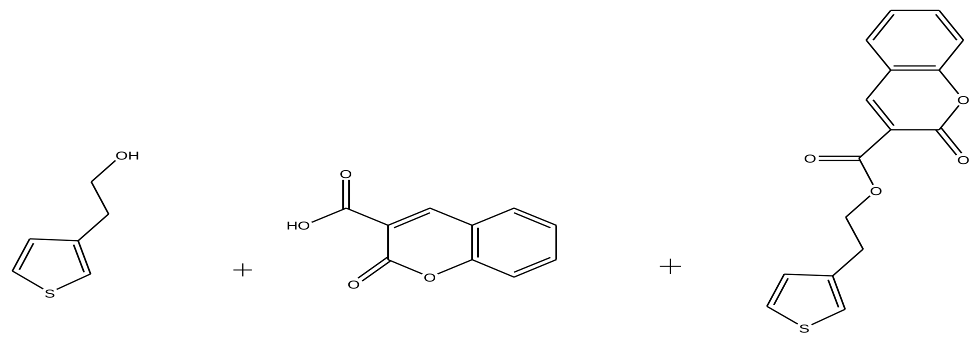

Scheme 2.2: The esterification reaction of 2-(3-thienyl) ethanol with coumarin-3-carboxylic acid.

2.2.3. Synthesis of poly(3-alkylthiophene) with naphthalene and coumarin.

The synthesis of poly(3-alkylthiophene) substituted with naphthalene was performed by an oxidation polymerization reaction using ferric chloride ($FeCl_3$) as an oxidizing agent in a ratio of 1:2 for the monomer and $FeCl_3$ [220]. The naphthalene containing-monomer (0.5g, 1.96 mmol) was first dissolved in 5 mL of chloroform, which was then added dropwise to a solution of $FeCl_3$ (0.638 g, 3.93 mmol) of in 15 mL of chloroform. The reaction solution was stirred under a gentle nitrogen purge for 3 hours at 50 ^oC, and 21 hours at room temperature. The reaction was then terminated by pouring an excess of methanol. The black precipitated product was then filtered and washed several times with distilled water, acetone, methanol and 10% HCl to remove any impurities. The resultant polymer was then dried under vacuum for 4 hours, and the black product was found to be insoluble in most common organic solvents. The same procedures were followed to prepare P3AT with coumarin and the brown product was found to be soluble in $CHCl_3$.

2.2.4. Synthesis of Exfoliated WS_2:

The synthesis of WS_2 was achieved following the method described by Matte et al [221]. A mixture of thiourea and tungstic acid (3.656g, 48 mmol) was placed in a ceramic reaction vessel, which was then put into a ceramic tube placed in a split furnace under a constant flow of nitrogen purge. The split furnace was heated to 500°C for 3.5 hours. The reaction temperature was then reduced to room temperature and allowed to sit overnight under a constant flow of nitrogen. The vessel was then taken from the ceramic tube, and a black solid product was recovered.

2.2.5. Synthesis nanocomposite of Poly(3-alkylthiophene):

The nanocomposites of WS_2-polythiophene and WS_2-poly(3-alkylthiophene) were produced using 1%, 5%, 10%, 20%, 37% and 64% by mass of WS_2. All nanocomposites were synthesized using an identical procedures. The synthesis of 5% WS_2-PThN is used as an example.

Exfoliated of WS_2 (0.0225g) was added to a 50 mL beaker in the presence of 15 mL of chloroform. A probe sonicator was used to disperse the exfoliated WS_2 for 20 minutes. In a 250 mL Schlenk flask, 0.52 g of ferric chloride ($FeCl_3$) was treated with 15 mL of $CHCl_3$ while stirring under a nitrogen purge. The suspension of WS_2 in $CHCl_3$ was then added dropwise to the Schlenk flask. The solution mixture was left stirring under nitrogen for 30 mins. 0.46 g of ThN monomer was dissolved in 1 mL of $CHCl_3$, and the solution was then added dropwise to the mixture of WS_2-$FeCl_3$. The reaction was stirred for 3 hours at 42°C under nitrogen and was then left to sit for 1-2 days until the $CHCl_3$ had evaporated. The dark product was washed with a sufficient amount of methanol, and then dried under vacuum filtration.

2.3. Result and Discussion.

2.3.1. NMR Analysis:

An esterification reaction was conducted between 2-(3-thienyl) ethanol and coumarin-3-carboxlic acid. NMR analysis was performed to identify the ThC monomer and its polymer. Figure 2.1 represents the ^{1}H and ^{13}C NMR spectra of the ThC monomer. Aromatic protons of the heterocyclic thiophene and the coumarin appeared at a low field in the ^{1}H NMR spectrum. However, the aliphatic protons of the 3AT were shown at high field. The disappearance of hydroxyl proton resonances of the 2-(3-thienyl) ethanol at 4.67 ppm and the carboxylic acid proton resonance of coumarin-3- carboxylic acid at 13.18 ppm were observed in the ^{1}H NMR spectrum. It was deduced a successful synthesis of the ThC.

New peaks were observed at 7.48ppm, 7.36ppm, and 7.12 ppm indicating the presence of the thiophene ring. Also, aliphatic protons showed noticeable shifted in the resonance at 3.05 ppm and 5.45ppm. In addition, ^{13}C NMR analysis Table 2.2 was performed to confirm the successful synthesis of ThC monomer. There is a distinct peak detected at 162.52 ppm which refers to the ester carbonyl group while the quaternary carbon of coumarin-3-carboxylic acid next to the ester carbonyl shifted to 117.77 ppm.

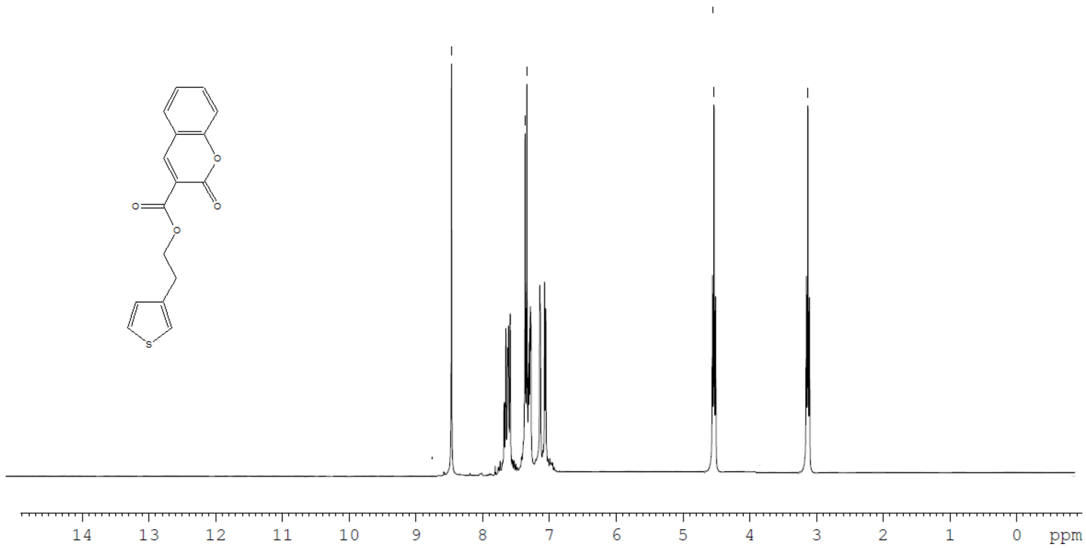

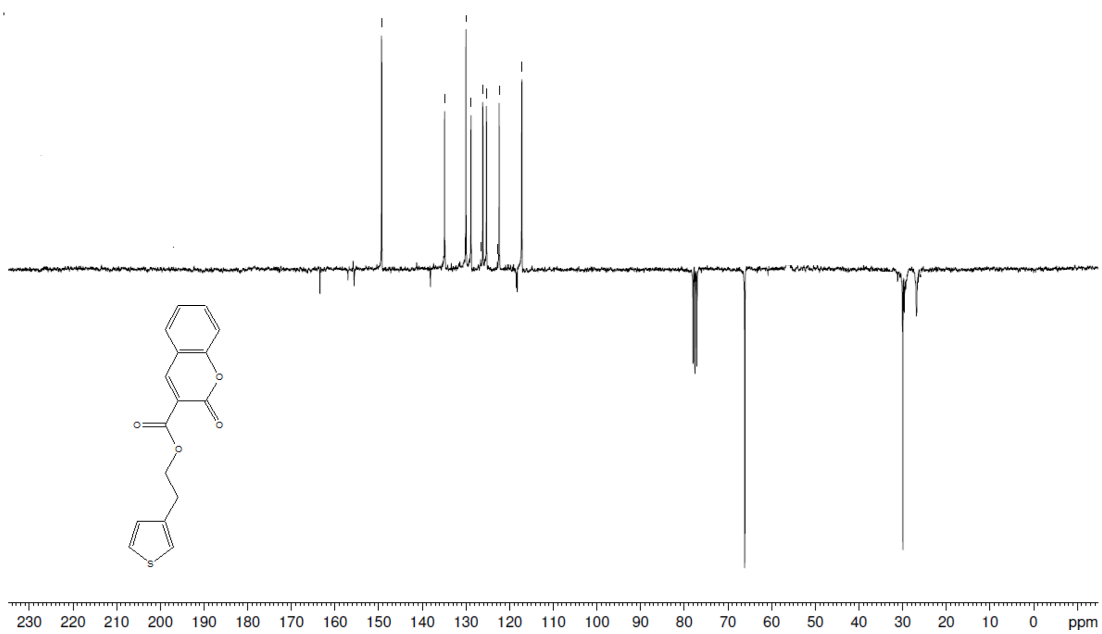

Figure 2.1: ^{1}H NMR (top) and ^{13}C NMR (bottom) of the monomer ThC in $CDCl_3$.

The structural identity of the new PThC polymer was determined by using NMR spectroscopy. Figure 2.2 shows the ^{1}H-NMR spectra of PThC and its ^{13}C NMR. It can be seen that the two spectra of the ThC in Figure 2.1 revealed some similarities and differences. For example, the aliphatic protons of both ThC and PThC at 3.27 ppm, while coumarin aromatic protons resonate at 7.31 ppm. However, differentiation between the two spectra provided evidence that the polymerization reaction had proceeded successfully. The disappearance of two aromatic protons of PThC in the α position at 7.0 ppm and 7.14 ppm indicates that polymerization through α-α coupling has proceeded successfully.

It was also found in ^{13}C spectrum that the two aromatic carbons of thiophene in the α position appear at 122.37 ppm and 128.8 ppm as it is pointing up in the monomer. In the polymer, on the other hand, the same peaks shifted to 117.1 ppm and 149.6 ppm and pointing down which result in a higher intensity of these peaks in comparison to its monomer. Overall, the ^{1}H-NMR and ^{13}C NMR of PThC are not completely clear due to the partial solubility in $CDCl_3$.

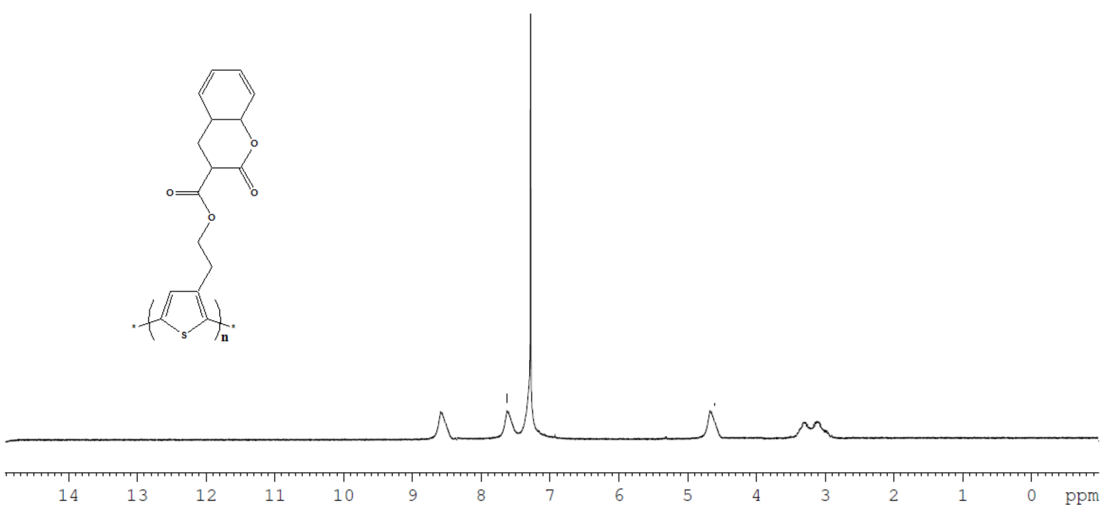

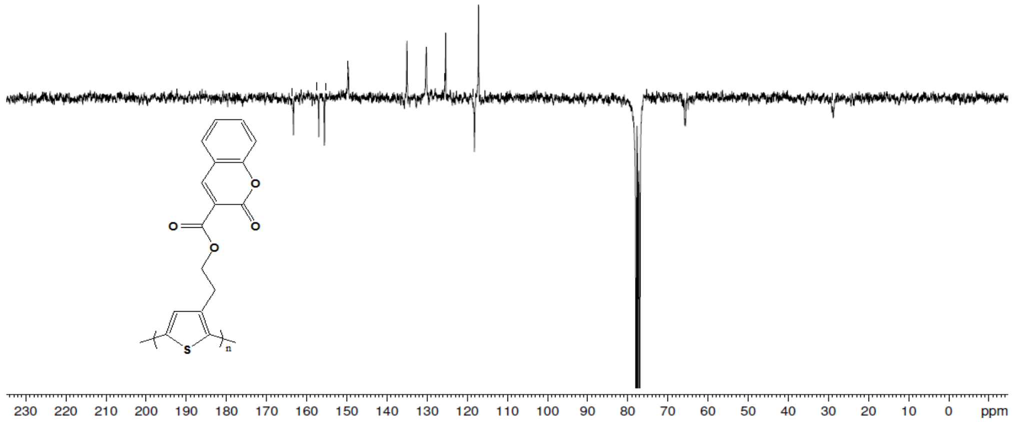

Figure 2.2: [1]H NMR (top) and [13]C NMR (bottom) of the PThC polymer in $CDCl_3$.

Table 2.1: [1]H-NMR of the ThC monomer and PThC polymer.

Compound	Aromatic thiophene	Aromotic cumarin	Others
ThC Monomers	7.01(m, 1H) 7.149 (m, 1H)	7.3(m, 2H), 7.59(m, 2H) 8.4 (S, 1H)	3.13(s, 2H) 4.55(s, 2H
PThC polymer	7.62(s, 1H)	7.29 (s, 4H) 8.5(s, 1H)	3.17(s, 2H) 4.61(s, 2H

Table 2.2: [13]C-NMR of the ThC monomer and PThC polymer.

Compound	Aromatic thiophene	Aromotic cuomarin	Others
ThC Monomer	122.37,126.6 129.99 137.4	117.17 118.1 125.2 128. 134.87 149.29 155.84 156.2	66.61 29.32 162.97
PThC Polymers	117.1 155.7 130.08	118.49 118.7 125.5 134.87 149.72 155.19 157.4	66 28.9 163.57

Another esterification reaction was also conducted between thiophene-3-carboxylic acid and 2-naphthol. NMR analysis was done to prove the synthesized ThN monomer is successful. Figure 2.3 depicts the ^{1}H NMR and ^{13}C NMR spectra of the ThN monomer. Aromatic protons of the heterocyclic thiophene and the naphthol were registered in the ^{1}H NMR peaks in the low field. The disappearance of hydroxyl proton resonances of the thiophene-3- carboxylic acid at 12.64 ppm and the HO proton resonance of 2-naphthol at 9.74 ppm proved the synthesis of the monomer. ^{13}C NMR analysis was also collected to confirm the synthesized monomer. The distinguish peak is the ester carbonyl that resonated at 160.79 ppm.

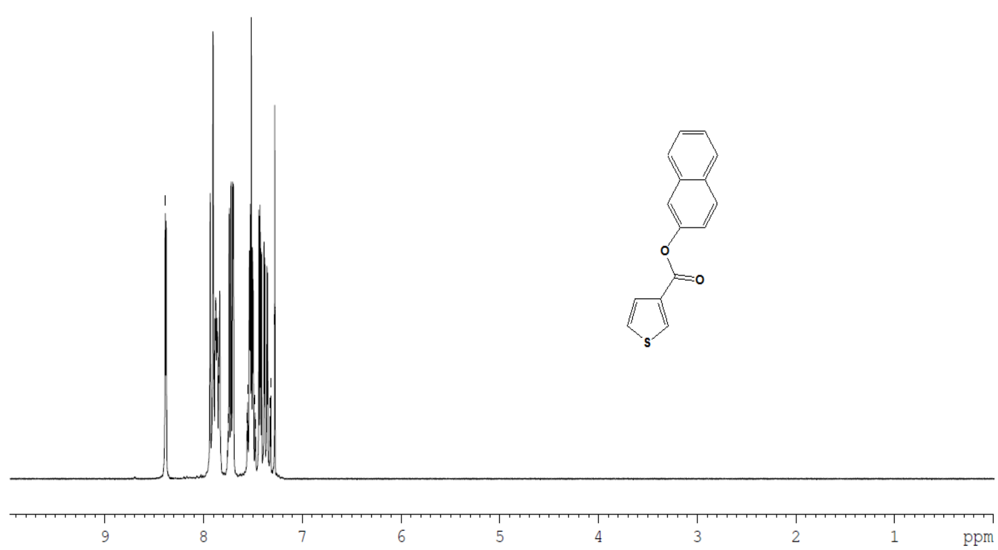

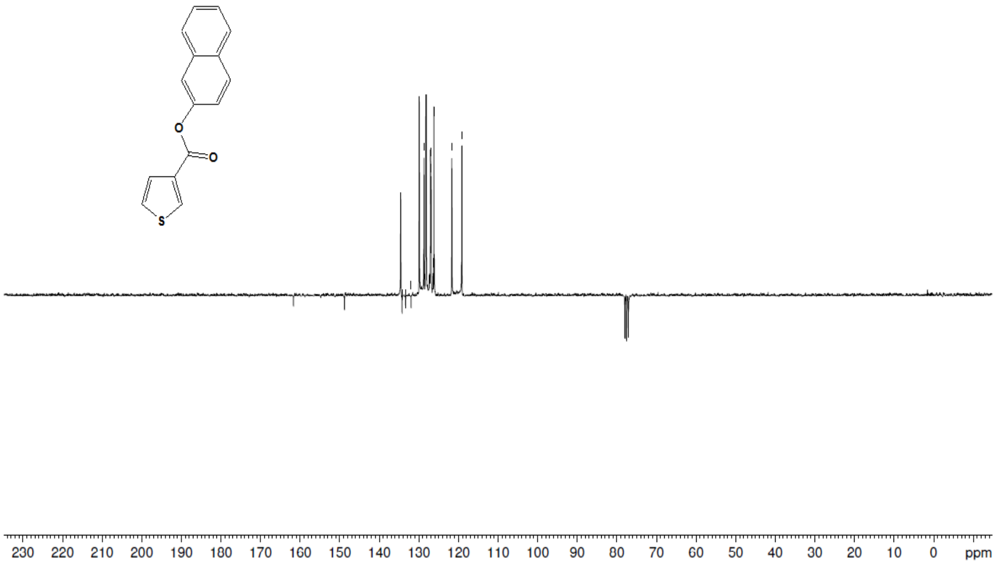

Figure 2.3: [1]H NMR (top) and [13]C NMR (bottom) of the ThN monomer in $CDCl_3$.

Table 2.3: [1]H-NMR of the ThN monomer.

Compound	Aromatic thiophene	Aromatic of 2-naphthol	Others
Monomers	7.01(m, 1H) 7.149 (m, 1H)	7.3(m, 2H), 7.59(m, 2H) 8.4 (S, 1H)	3.13(s, 2H) 4.55(s, 2H

Table 2.4[13]C-NMR of the ThN monomer.

Compond	Aromatic thiophene	Aromatic of 2-naphthol	Other
Monomer	127.07 128.69 134.588 134.21	119.12 121.67 126.19 126.40 126.89 128.21 129.89 132.03 133.31 148.86	161.75

2.3.2. FT-IR Characterization.

Fourier Transform Infra-Red spectroscopy was conducted on the ThN, ThC monomers, PThN, and PThC. FT-IR also was done on each nanocomposite of PThN/WS_2.

FT-IR analysis the monomer and the polymer were carried out. Table 2.1 summarizes the FT-IR stretching band for both the ThN and the PThN, respectively. It is illustrated band in the range of 3123 to 3051 cm^{-1} referred to the C-H (α) and C-H (β) stretching of the thiophene ring. However, C-H (α) almost disappeared in the polymer. The exhibitions of intense peaks of the polymer at 734, 1067 and 1177 cm^{-1} are attributed to the C-H stretching of the aromatic ring. The low intensity of aromatic C-H bands is attributed to the occurrence of the polymerization on para position of the naphthalene [222]. Also, the observation of a characteristic band at 1716 cm^{-1} is assigned to the carbonyl group stretching of the monomer, which appeared at a higher wavenumber for the polymer at 1732 cm^{-1}. The FT-IR exhibited two bands 1398 cm^{-1} and 1511 cm^{-1}, indicating to the C=C of the aromatic rings of the polymer, where they appeared at 1507 cm^{-1}, 1418 cm^{-1} and 1400 cm^{-1} in the monomer. Moreover, the C-H (α) bending is shown at 770 cm^{-1} in the monomer, while a deformation characteristic of thiophene occurred in the polymer, with a disappearance of this band in the polymer which is evidence that the polymerization reaction took place at the (α) - (α) coupling. Also due to the presence of C-H aromatic band, the assignment confounded with other peaks [223]. For instance, two peaks in the FT-IR spectrum of the monomer were shown around 827 and 741cm^{-1}. This may attribute to either C-H “oop” and C-S stretches.

Table 2.5: The FT-IR stretching band for both the ThN and the PThN.

Assigments	Monomer	polymer
C-H α- thiohene stretch	3123 cm^{-1}	-------
C-H β- thiophene stretch	3051 cm^{-1}	3051 cm^{-1}
C-H α- bending	790 cm^{-1}	-------
C=O	1716 cm^{-1}	1732 cm^{-1}
C=C aromatic	1507 cm^{-1}	1511 cm^{-1}
C-H aromatic	2850 cm^{-1}	2850 cm^{-1}
C-S	827 cm^{-1}	815 cm^{-1}

FT-IR analysis of the monomer 2-(3-thienyl) ethanol with coumarin-3-carboxylic acid and its polymer were carried out. All assignments for the ThC monomer and the PThC polymer are listed in Table 2.2. The ThC monomer demonstrated bands at 3108 and 3063 cm^{-1} represented the C-H (α) and C-H (β) stretching of thiophene ring. However, the C-H (α) stretch is disappeared in the polymer spectra, indicating that the polymerization reaction took place on (α) positions. The exhibitions of strong peaks of the polymer at 1564 cm^{-1} are attributed to C=C stretches of the aromatic ring, where they appeared at 1566 of the ThC monomer. Also, the observation of a characteristic band at 1750 cm^{-1} in the polymer indicated to the carbonyl group, which it appeared at 1751 cm-1 in the monomer spectrum. FT-IR spectrum of the PThC displayed the C-H stretch in plane bending at 1121 and 1005 cm^{-1}, whereas they appeared at 1018 and 1125 cm^{-1} for the ThC. Moreover, due to the presence of CH_2, C-S and the aromatic C-H (oop) bands, these bands can confound the assignments somewhat [223]

Table 2.6: The FT-IR stretching band for both the ThC and the PThC.

Assigments	Monomer	polymer
C-H α- thiohene stretch	3108 cm^{-1}	-------
C-H β- thiophene stretch	3063 cm^{-1}	3051 cm^{-1}
C-H α- bending	790 cm^{-1}	-------
C=O	1751 cm^{-1}	1750 cm^{-1}
C=C aromatic	1566 cm^{-1}	1564 cm^{-1}
C-H aromatic	2828 cm^{-1}	2832 cm^{-1}
C-H	1125 cm^{-1}	1121 cm^{-1}
C-S	794 cm^{-1}	786 cm^{-1}

FT-IR spectroscopy for all nanocomposite materials showed changes in the vibrational stretches compared to that of the pristine PThN. Table 2.3 summarizes these changes which are attributed to the interaction between the exfoliated WS_2 and the polymer.

Table 2.3: The vibrational spectrum changes of the functional group for 1%WS_2-PThN nanocomposites in comparison to the pure PThN.

Functional group	Pure polymer	1%WS_2-PThN nanocomposites
C=O ester	1732 cm^{-1} (strong)	1722 cm^{-1} (medium)
C-O ester	1196 cm^{-1} (strong)	1177 cm^{-1} (strong)
C-H aromatic	2850 cm^{-1} (weak)	2852 cm^{-1} (medium)
C=C aromatic	1511 cm^{-1} (medium)	1515 cm^{-1} (medium)
C-H β- thiophene stretch	3051 cm^{-1} (weak)	3051 cm^{-1} (weak)
C-H “oop”	734 cm^{-1} (strong) 812 cm^{-1} (strong)	725 cm^{-1} (strong) 811 cm^{-1} (strong)

2.3.3. XRD Characterization.

XRD was carried out to obtain some structural information of the monomer ThN and ThC monomers, WS_2 and PThN-WS_2 nanocomposites. The synthesized monomers ThN and ThC were demonstrated to be highly crystalline with several sharp peaks as shown in Figure 2.4.

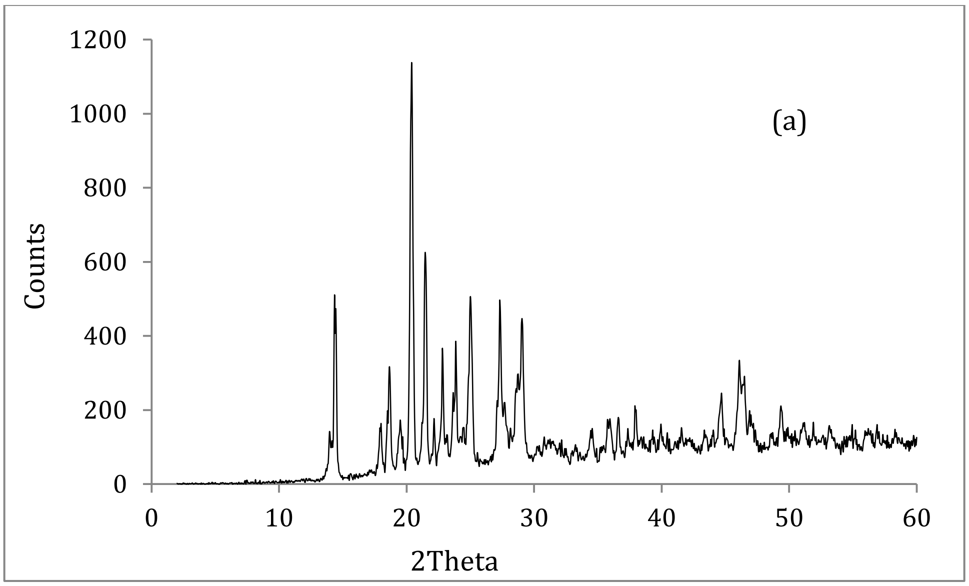

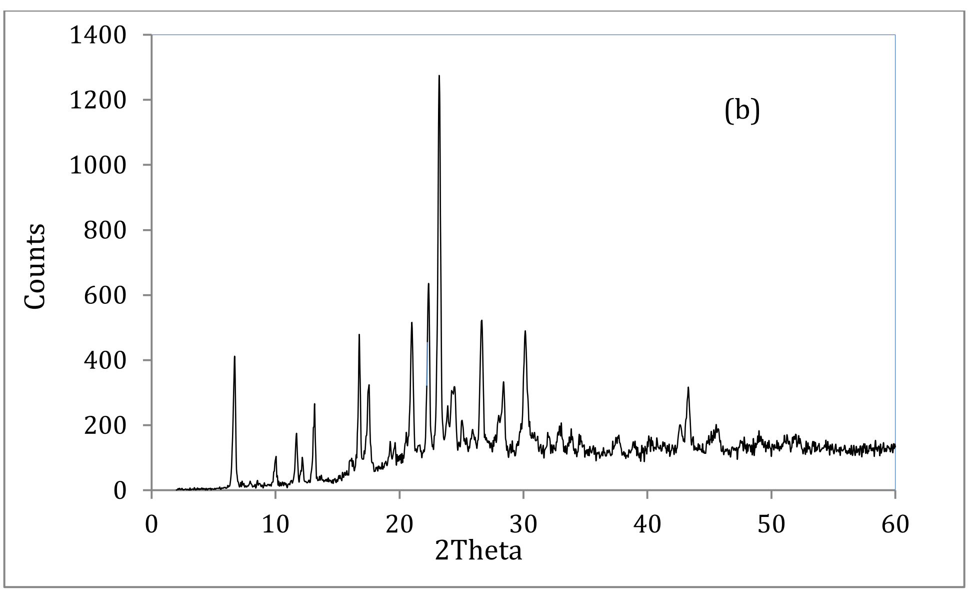

Figure 2.4: XRD of the (a) ThN and (b)ThC monomers.

However, powder XRD diffraction data were collected on the PThN and PThC, which were synthesized via an oxidation reaction using a ratio 1:2 of monomer 3-alkyl thiophene to $FeCl_3$ as shown in Figure 2.5.

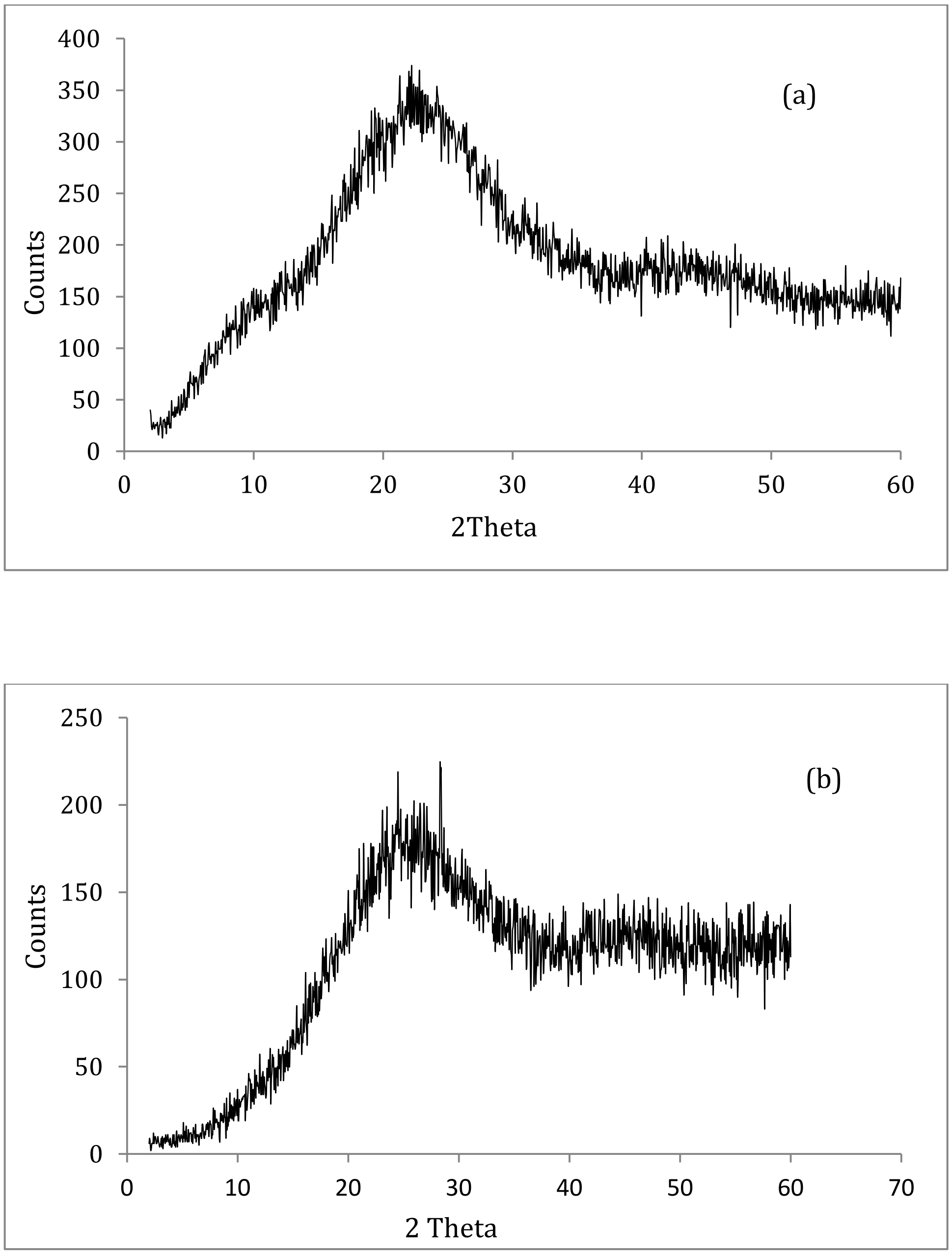

Figure 2.5: XRD of the (a) PThN and (b) PThC polymers

The XRD diffractograms of the PThN and PThC demonstrated that they were highly amorphous with a disappearance of sharps peaks compared to their monomers. They also showed maximum peaks around 22^o and 25^o, respectively. Therefore, it was suggested that the polymerization reaction was done successfully for both monomers.

XRD data of the exfoliated WS_2 which was synthesized from tungstic acid and thiourea with a ratio of (1:48) was also carried out to determine that if the exfoliated WS_2 was done successfully.

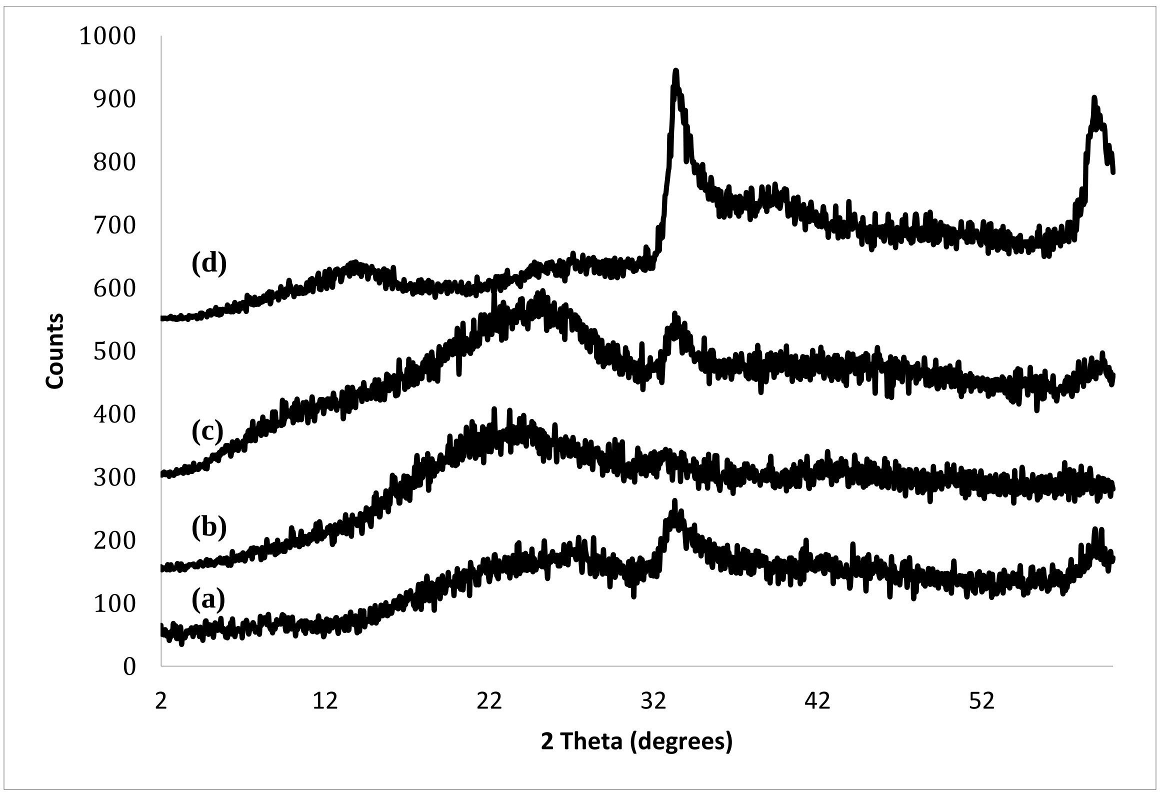

Figure 2.6: XRD of the exfoliated WS_2 (a), 1%WS_2-PThN (b) and 10%WS_2-PThN (c) and 64%WS_2-PThN (d) nanocomposites.

The diffractogram of the exfoliated WS_2 is shown in Figure 2.6 (a). Powder X-ray diffraction data of WS_2 was a highly amorphous material with a lack of crystallinity with only 17.2%. XRD data of WS_2 corresponded to the previous synthesis of the exfoliated WS_2. [224] The XRD data for the WS_2-PThN nanocomposites in Figure 2.6 (b) has revealed that the XRD data of PThN-WS_2 nanocomposites with the percent of WS_2 1%, and 5% did not show a significant change compared to the XRD of pure PThN. This was anticipated because of the small amount of the nanofiller. However, the diffractogram of PThN-WS_2 nanocomposites with the percents such as 20%, 37%, and 64% starts to behave similarly to the diffractogram of WS_2 as shown Figure 2.6 (c). The 10% WS_2-PThN nanocomposites exhibited a clear diffractogram of the two peaks around 22^o and 32^o which are attributed to the PThN and exfoliated WS_2, respectively. The collected XRD data confirmed the successful synthesis of PThN-WS_2 nanocomposites.

2.3.4. Thermogravimetric Analysis.

The thermal stability is an essential factor to consider for a conjugated polymer in its possible applications. [225,226] The thermal properties of the polymer were investigated using TGA under air. Figure 2.7 shows the thermograms for the ThN monomer and PThN polymer. It was noticed that the polymer displays favorable thermal stability at high temperature with an onset decomposition temperature of 487^oC. In comparison, the monomer exhibits weights loss at a lower temperature around 250 ^oC.

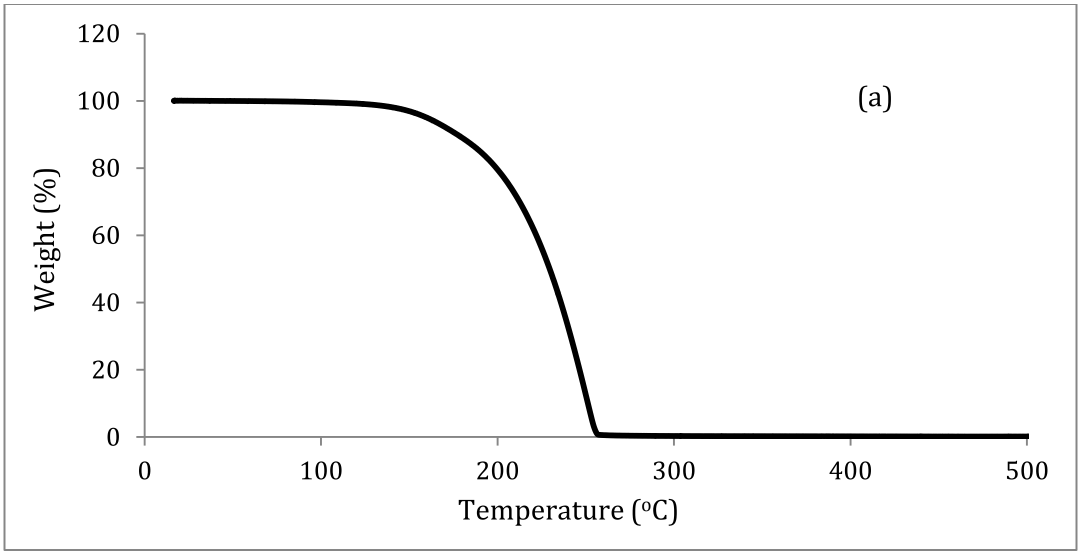

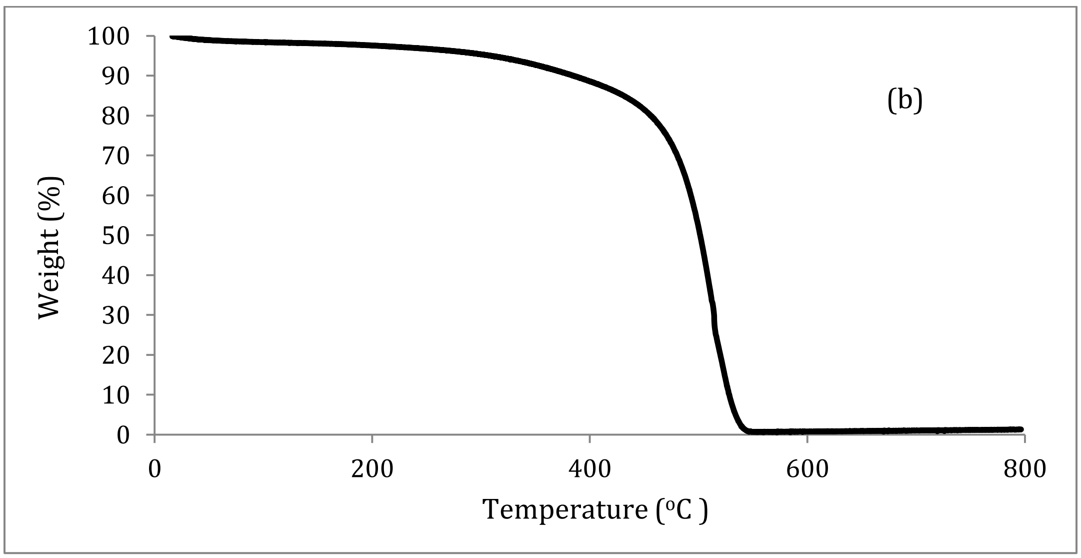

Figure 2.7:The TGA curve ThN monomer (a) and PThN polymer (b).

The thermal stability was also investigated for the ThC monomer and its polymer. It was found that that Figure 2.8 shows the TGA curve for the ThC monomer and PThC polymer. It was found that PThC polymer demonstrated higher thermal stability at evaluated temperature with complete decomposition around 550 ^{o}C. In comparison, the ThC monomer, which showed weights lose at a lower temperature approximately 380^{o}C.

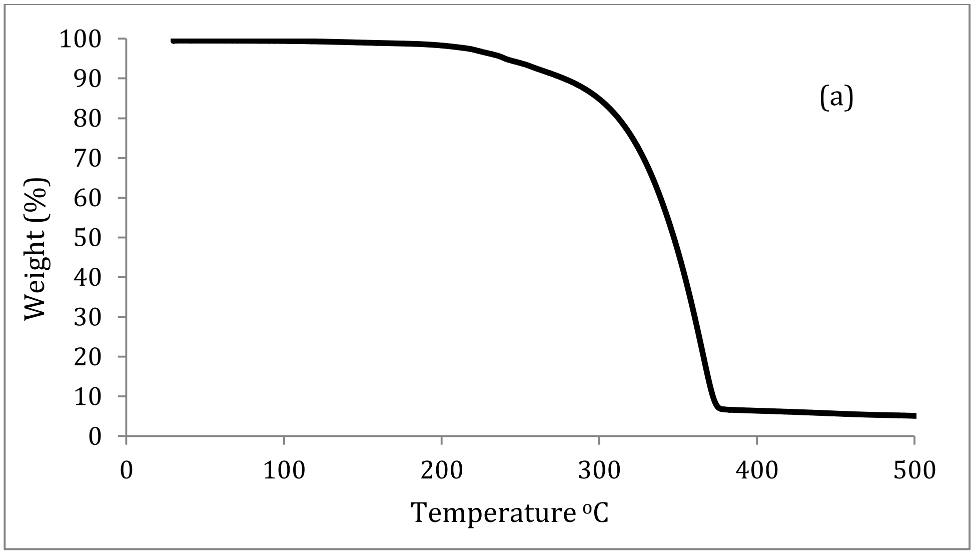

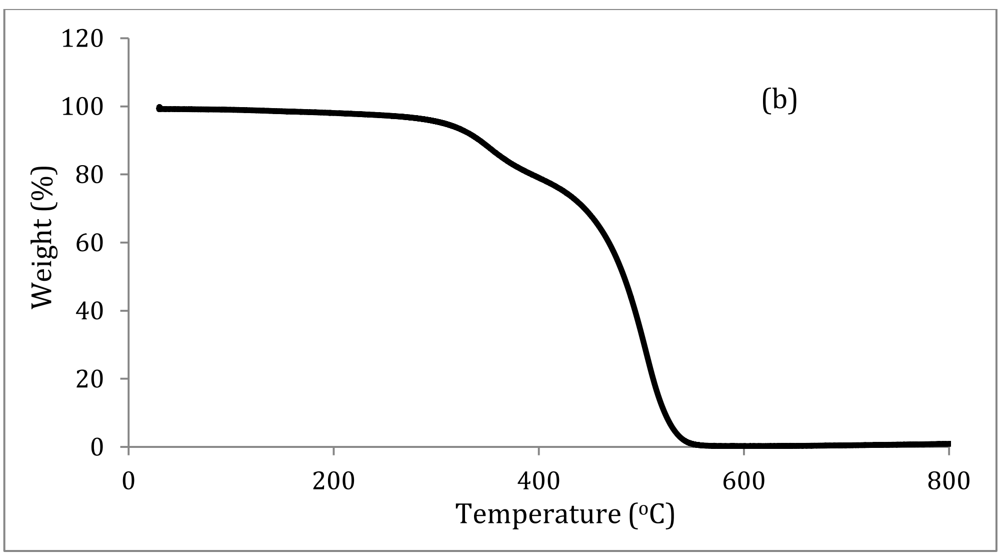

Figure 2.8:The TGA curve ThC monomer (a) and PThC polymer (b).

Transmission electron microscopy (TEM) was utilized to study the PThN and its nanocomposites to obtain more information about the structure of the material. Figure 2.9 displays an example of the TEM micrograph of PThN, which is fully featureless and disordered.

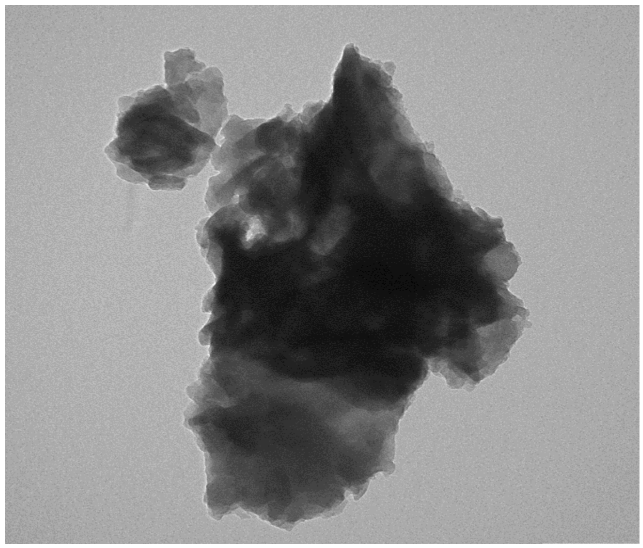

Figure 2.9: TEM micrograph of bulk PThN.

2.3.5. Decomposition Kinetic Measurements of PT-WS_2 and Poly(3-alkylthiophene) with naphthol- WS_2 Nanocomposites.

Thermal degradation of P3AT/WS_2 nanocomposites:

Figure 2.9 represents the thermogram decomposition process of the pure PThN at a heating rate of 5^{o}C/min. As shown in figure 2.10, the onset decomposition temperature of pure PThN occurs around 350^{o}C with a full decomposition at around 500^{o}C.

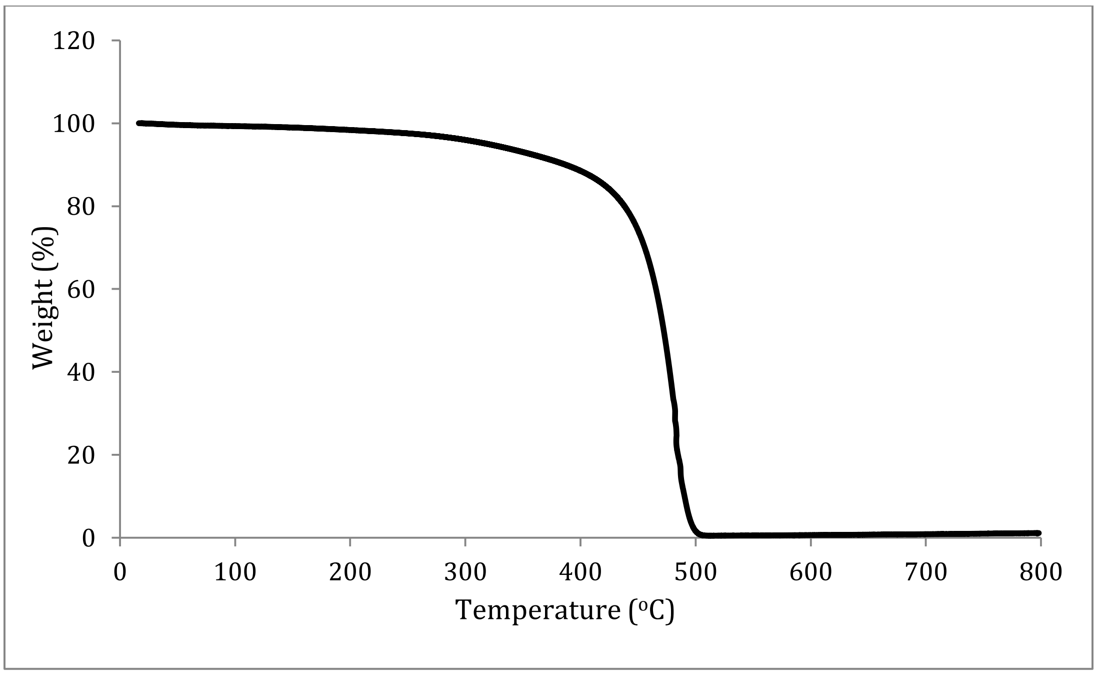

Figure 2.10: The TGA curve of pure PThN at heating rate of 5^{o}C/min.

By applying Ozawa's method, the activation energy of decompositions can be obtained from a set of TGA curves for every individual sample at four heating rates, (5, 10, 20, 40 ^{o}C/min). These heating rates were employed to run all samples to get the activation energy from the TGA data. Figure 2.11 reveals the TGA curves of the PThN/ WS_2 nanocomposites.

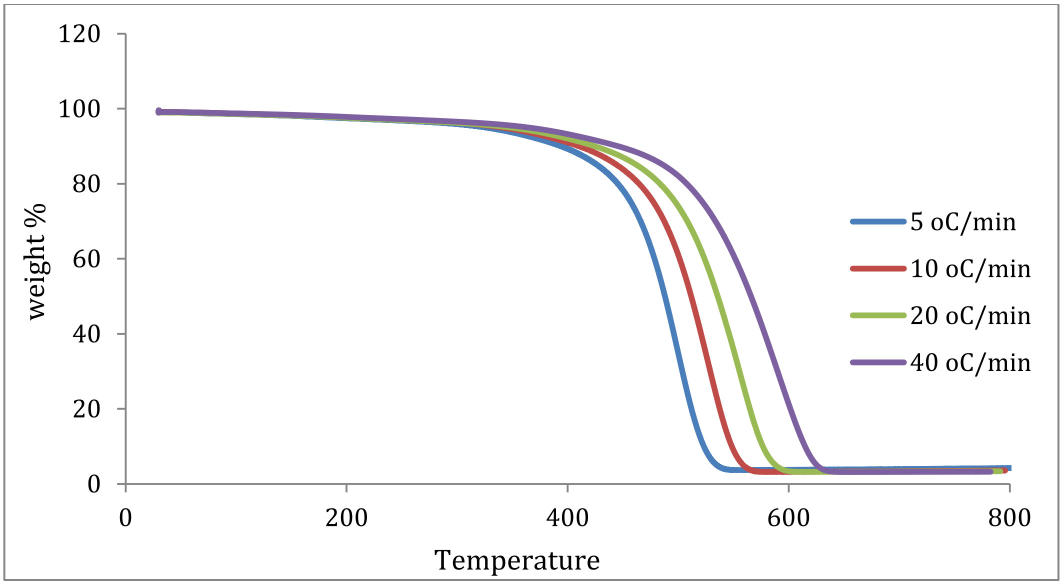

Figure 2.11: TGA of 10% of WS_2 – PThN nanocomposites.

It is obvious from the TGA plots of the 10 % by weight of WS_2 – PThN nanocomposites profiles that same weight losses happened upon increasing the heating rates from 5 to 40^{o}C/min. It is evident that the decomposition process of the polymer starts to occur at a lower temperature with a slower heating rate, and upon raising the heating rate, the decomposition onset temperature of the polymer increases. This is associated with the fact that the polymer does not have adequate time to decompose with an increased heating rate. Therefore, the polymer will not begin to decompose until a higher temperature.

Thermal Degradation Kinetics:

In this research, each sample was examined using TGA at four heating rate. According to Ozawa's method, the conversion (α) is a requirement parameter and can be determined using equation (6):

$$\alpha = \left(\frac{\text{mo} - \text{m}}{mo - m\infty} \right)$$

Where α is the ratio of the actual weight loss to the total weight loss, m_o is the initial sample weight, m is the sample weight at any temperature during the run, and m_∞ is the weight of the sample at the end of the TGA. The conversion (α) was determined for each heating rate and then plotted as a function of temperature for each polymer nanocomposite. Figure 2.12 displays an illustration of the conversion profile for the PThN with 10 % WS_2.

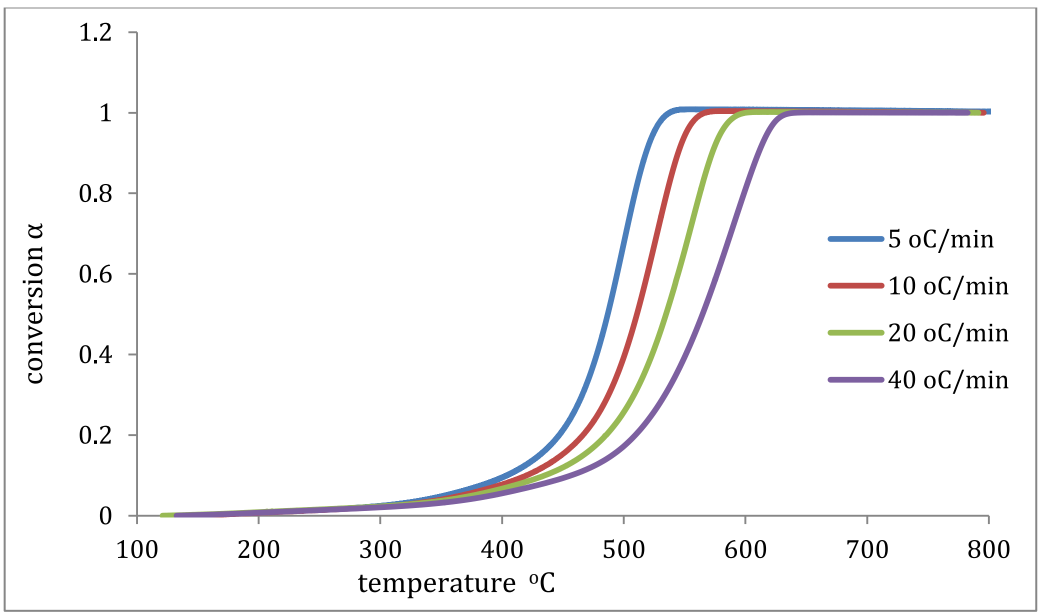

Figure 2.12: The conversion α of 10 %WS_2-PThN nanocomposite.

Figure 2.13 shows the Ozawa plot of Log β versus the inverse of the temperature and it clearly that the relationship is not fully completely linear. As a result, the linear regressions were taken to get the slopes of these lines.

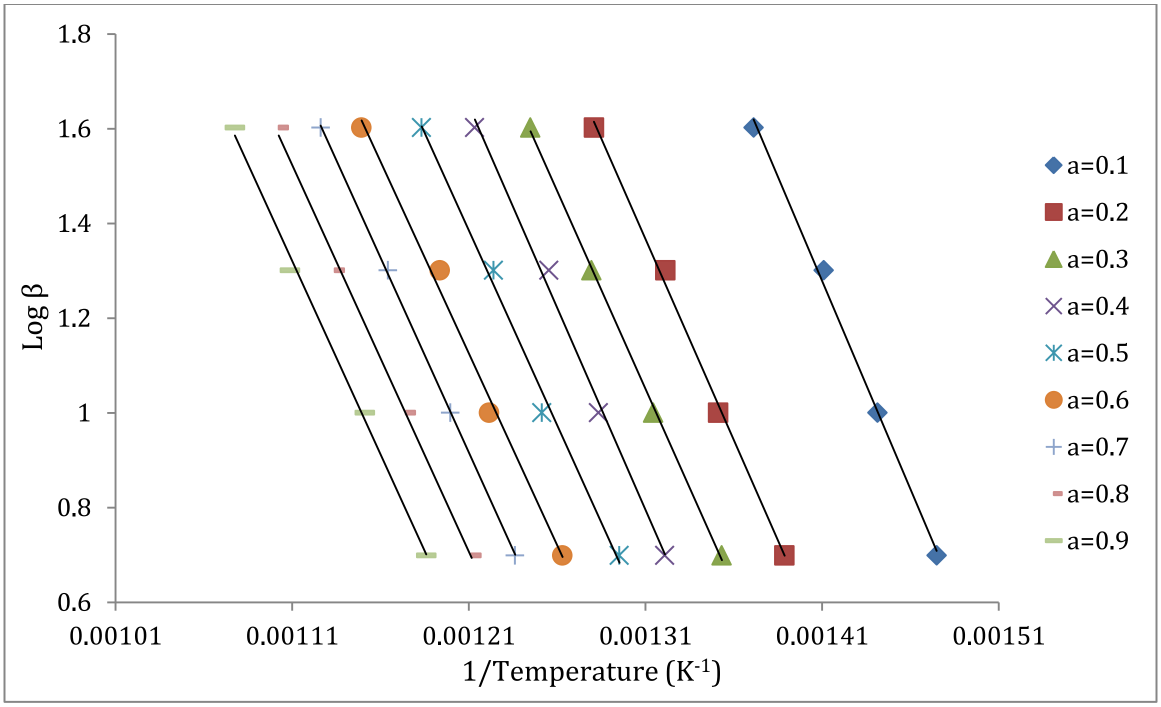

Figure 2.13: The regression lines for conversion of 0.1 -0.9 based on the Ozawa's method for PThN-WS_2 10%.

By utilizing the following equation, the activation energy can be estimated from these regression lines.

$$E_a = - \text{slope} * (R/0.457) \quad (7)$$

Where R is the gas constant (8.314 J/mol.K). The value of the correlation coefficients (R) and the activation energies for the 10% PThN-WS_2 nanocomposites are presented in Table 2.8.

Table 2.8: The correlation coefficient (R) and the activation energy (E_a) obtained using Ozawa's method for 10% WS_2-PThN.

Sample	Conversion α	R	Ea (kJ/mol)
10 % WS_2 by weight	0.1	0.9956	158.8
	0.2	0.9990	153.0
	0.3	0.9993	148.4
	0.4	0.9993	143.4
	0.5	0.9990	138.4
	0.6	0.9986	138.0
	0.7	0.9984	141.2
	0.8	0.9974	139.6
	0.9	0.9968	143.4
Average			144.9

The coefficient R is above 0.99 for each conversion. The value of the activation energy (E_a) was calculated for conversions (α) from 0.1 to 0.9 exhibited values varying from 138 kJ/mol to 158 kJ/mol for the nanocomposites of PThN with 10 % by weight WS_2. The average of these activation energies for each conversion was 145.0 kJ/mol. The same methodologies were employed to determine the Ea for polythiophene (PTh), pure PThN, 1%, 5%, 10%, 20%, 37%, 64% by weight PTh/WS_2, and PThN/WS_2 nanocomposites. The Ea values and their standard deviations for all nanocomposites are registered in Table 2.9.

Table 2.9: The activation energy values of pure PTh, PThN and all the nanocomposites.

% by weight of WS_2	Ea (KJ/mol) of PT	Standard Deviations (KJ/mol)	Ea (KJ/mol) of PThN	Standard Deviations (KJ/mol)
0	79.9	±10.4	145.6	±26.0
1	83.5	±7.2	144.9	±7.1
5	87.1	±4.1	145.0	±6.7
10	78.5	±9.1	149.1	±7.2
20	124.9	±8.1	198.7	±19.6
37	97.0	±2.1	209.5	±19.0
64	113.8	±10.6	204.9	±28.2

Overall, the values of the activation energies for nanocomposite were increased with incorporating higher percents of WS_2 in comparison to that of pure PT or PThN. The pure PThN showed an enhancement in the Ea with 145.6 kJ/mol in comparison to pure PTh with 79.9 kJ/mol. In addition, at a lower percentage of WS_2 such as 1%, 5, 10%, the Ea values did not exhibit a major change in the activation energies for these nanocomposites. The activation energies against the weight percentages of WS_2 is plotted in Figure 2.14 for PTh-WS_2 and Figure 2.15 for PThN-WS_2.

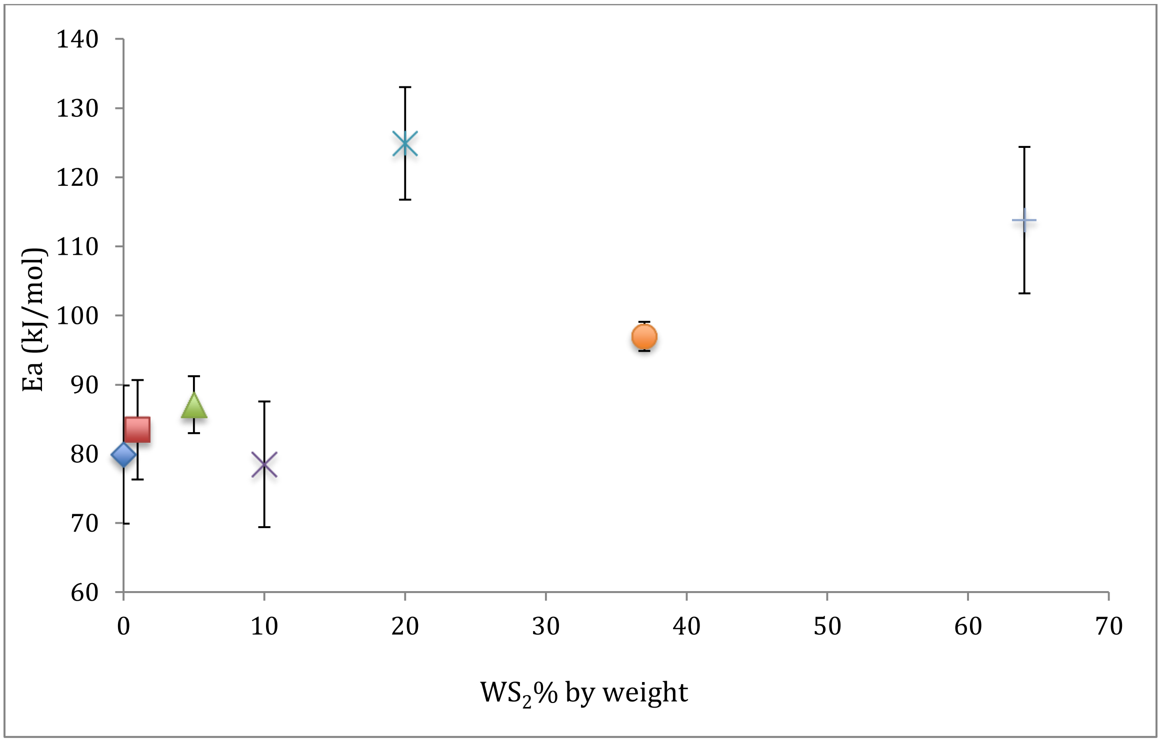

Figure 2.14: The plot of activation energy of pure PTh and WS_2 – PTh nanocomposites against the weight percentages of WS_2.

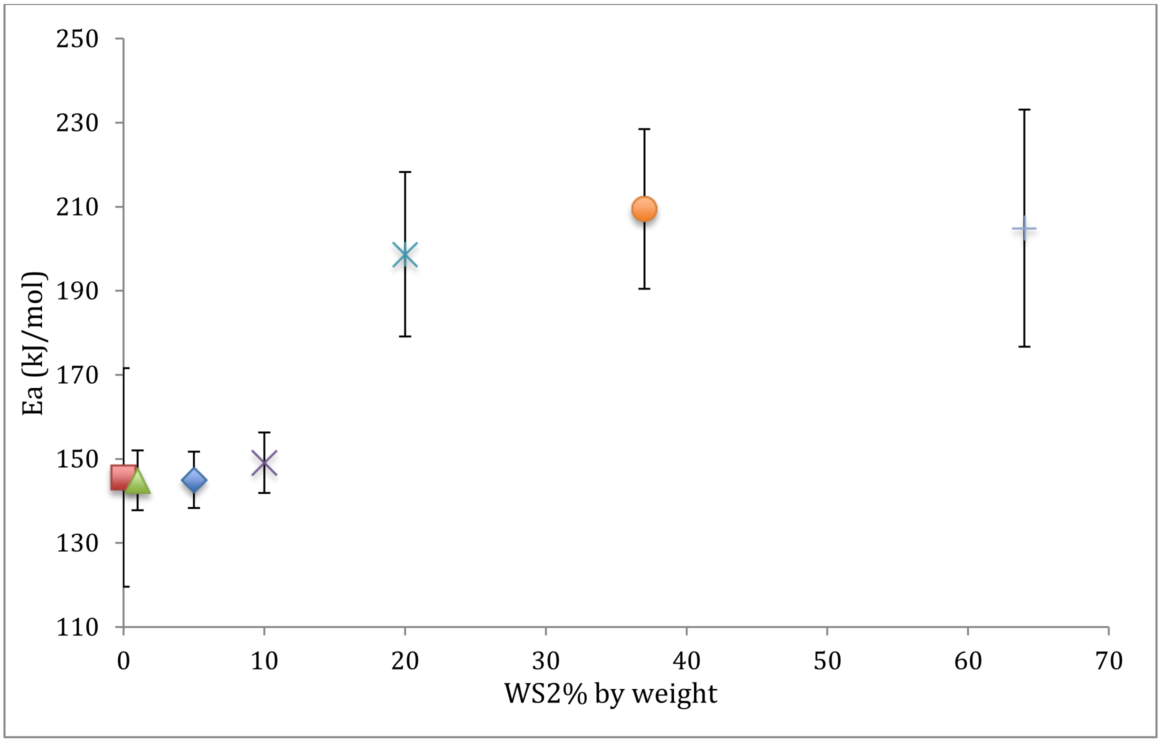

Figure 2.15: The plot of activation energy of pure PThN and WS_2 – PThN nanocomposites against the weight percentages of WS_2.

The Ea values for PTh - WS_2 nanocomposites modified upon increasing the mass of WS_2. As we can see in figure 2.15, 20 % by weight of WS_2 demonstrated the greatest value of Ea 124.9 kJ/mol. However, 1%, 5% and 10% PThN - WS_2 nanocomposites presented a nearly equivalent value of Ea with 83.1 kJ/mol, 85.3 kJ/mol and 78.5 kJ/mol, respectively. Moreover, 64% of WS_2-PTh has illustrated an increase in the Ea by around 34 kJ/mol in comparison to the Ea of pure PTh.

On the other hand, the activation energy values for PThN - WS_2 nanocomposites changed upon raising the amount of WS_2. As we can see in Figure 2.14, 37 % by weight of WS_2 revealed the largest value of Ea 209.5 kJ/mol. Also, 1%, 5% and 10% PThN - WS_2 nanocomposites showed a relatively same value of Ea with 145.0 kJ/mol, 149.9

kJ/mol and 151.6 kJ/mol, respectively. Furthermore, around 52 kJ/mol, and 58 kJ/mol observed an enhancement of the Ea in comparison to the Ea of pure PThN for 20% and 64% of WS_2-PThN nanocomposites, respectively.

2.3.6 Conclusion:

This work demonstrated the kinetics decomposition measurement of several PTh-WS_2 and PThN-WS_2 nanocomposites. Ozawa's method was employed to measure the Ea of nanocomposite with several percents of WS_2 hosting PTh and PThN using the TGA.

It was found that the Ea of pristine PTh was 79.9 kJ/mol. Also, 20% and 64% wt of WS_2-PTh composition showed a major improvement in the Ea value with 124.9 kJ/mol and 113.8 kJ/mol respectively. The Ea of exfoliated PTh nanocomposite at lower percentages such as1%, 5%, and 10% of WS_2 did not display a noticeable change in the Ea.

In contrast, the Ea of pure PThN was 145.6 kJ/mol, and the 37 % wt of WS_2-PThN composition demonstrating a significant development in the Ea with the greatest value, 209 kJ/mol. The remainder of the PThN-WS_2 nanocomposite series exhibited enhanced activation energies ranging from 198 to 204 kJ/mol. On the other hand, the Ea of 1%, 5%, and 10% nanocomposites are almost the same as pure PThN.

Generally speaking, the addition of the exfoliated WS_2 exhibited a significant the activation energies values of the polythiophene and poly(3-alkylthiophene nanocomposites. The molecular connection between the polymer and nanofiller demonstrate a noticeable increase in the activation energy of the decomposition. Furthermore, the incoporation of nanofiller produce good heat distribution inside the polymer –nanocomposit.

Decomposition Kinetic Measurements of WS_2 - polyaniline nanocomposites.

3.1. Introduction

In recent decades, conducting or electroactive polymers have been the subject of substantial interest due to their outstanding properties, including environmental stability in the doped and undoped state, high electrical conductivity [227,228] and ease of preparation. [229] They also have potential applications such as rechargeable batteries [230,231], smart windows, [232] light emitting diode, [233,234] energy storage, [235] optical and electronic devices, [233,236-238] and sensors. [239] The thermal stability of conducting polymers is one of the most important reasons for their use in many potential applications such as Light emitting diode (LED), optical materials, and electrochromic devices. [237,238] However, conducting polymers are vulnerable to undergoing different degradation reactions at elevated temperatures under any environmental conditions during the processing and service life. This may inhibit the use these materials in their potential applications due to the destruction of the required properties by degradations such as distortion of the conjugated system and a decrease of the efficiency of the mechanical properties.

Recently, the incorporation of nanoparticles of layered inorganic compounds such as MoS_2, V_2O_5, WS_2, and MoO_3 at the molecular level into organic conducting polymers such as polyaniline, polythiophene, and Polypyrrole has attracted significant attention. The resulting nanocomposite can compensate the relatively poor mechanical properties of the organic polymer and enhance its electrical conductivity and thermal properties compared to the pure polymer. [122,123,240,241] For example, it has been reported that the exfoliated PANI/WS_2 nanocomposites, which were synthesized by an *in situ* polymerization technique, has shown an enhancement in electrical conductivity was 9 S/cm which is a three-fold increase compared to the pure PANI. [242]

In this study, the PANI/WS_2 exfoliated nanocomposites were prepared via an *in situ polymerization* technique. The aim of this work is to understand the thermal behavior of different compositions of WS_2 nanocomposites. This was performed by determining the impact of the different heating rates on the onset decomposition temperature, determining calculating the activation energy of various WS_2 – polyaniline percentages nanocomposites using thermogravimetric (TGA) analysis in a nitrogen atmosphere. Furthermore, Ozawa's method was utilized to compute the apparent activation energy of these filling materials. [200]

3.2. Experimental.

3.2.1. Preparation of Polyaniline

In a 500 mL Erlenmeyer flask, 2.51 g of distilled aniline was added to 40 mL of 1M HCl at 0^{o}C in an ice bath. In a125 mL Erlenmeyer flask, 0.1623 g of APS was dissolved in 40 ml of 1M HCl. This solution was cooled to 0^{o}C and then added dropwise to the aniline/HCl solution. The solution was then stirred for 1.5 hours with the temperature maintained between 0 to 5^{o}C. The ratio of aniline to ASP was 1:1. The resultant product was filtered and washed with 500 mL of 1M HCl.

3.2.2. *In Situ* polymerization of exfoliated 20% WS_2- PANI nanocomposites.

The PANI/WS_2 nanocomposites were synthesized chemically via an *in situ polymerization* following a previously described procedure.[224] Distilled aniline (0.251g) was placed in a 500 mL Erlenmeyer flask in the presence of 40 mL 1M HCl. The solution was stirred and maintained at 0°C in an ice bath. In a 125 mL Erlenmeyer flask, 6.1134 g of APS was dissolved in 40 ml of 1M HCl, and the solution was cooled to 0°C.

In a 50 mL beaker, 0.5067g of exfoliated WS_2 was added to 30 mL of deionized water. This suspension was ultrasonicated at 30% amplitude for 20 min, and was then added dropwise to the aniline/HCl solution. The APS/HCl solution was then added dropwise to the aniline/WS_2 solution. The reaction was then stirred at 0°C for 1.5 hours. A black product was obtained after vacuum filtration, which was then washed with 500 ml of 1M HCl. The same procedures were followed to synthesize others compositions of WS2; 1%, 5%, 7.5%, 10%, 12.5%, 15%, 20%, 37%, and 64%.

3.2.3. Instrumentation.

Thermogravimetric experiments were carried out in a TGA Q500 instrument under nitrogen environment. The nitrogen flow rate to the sample chamber was maintained at 60 mL/min by the instrument. Each sample was run at four different heating rates: 5, 10, 20 and 40°C/min. Thermogravimetric curves were obtained for each sample, and the kinetic measurements were collected for each trial. The activation energy can be computed using the decomposition temperature of each sample and the information of weight loss at every heating rate.

3.3. Result and Discussion.

Thermal degradation of PANI/WS_2 nanocomposites:

The same previous procedures in chapter 2 were followed to calculate the decomposition kinetic of PANI-WS_2 nancomposites. Figure 3.1 depicts the thermogram of the pristine polyaniline at a heating rate of 10^{o}C/min. As shown in figure 1, the onset decomposition temperature of pure polyaniline begins around 340^{o}C with a complete decomposition at approximately 600^{o}C.

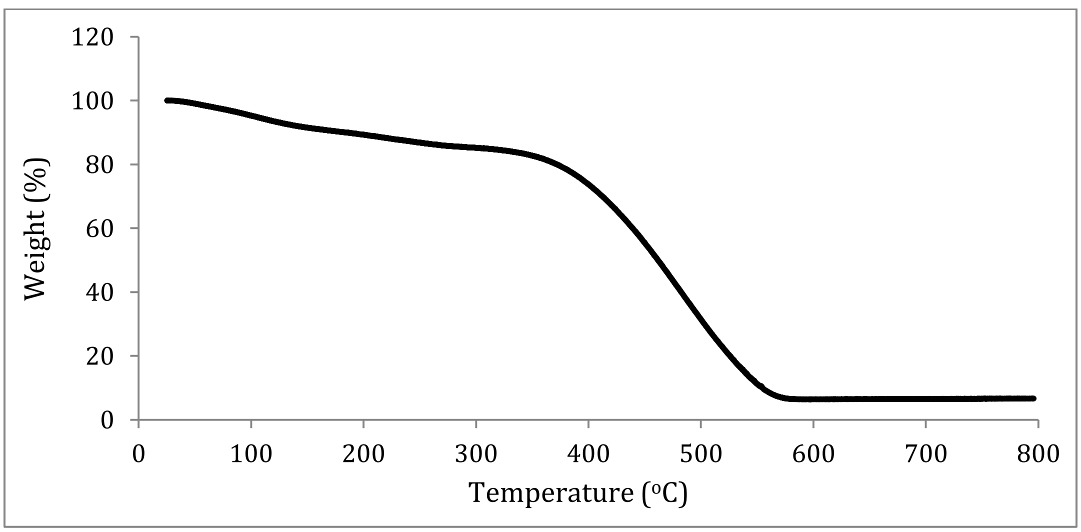

Figure 3.1: The TGA curve of pure polyaniline at heating rate of 10 ^{o}C/min.

(5, 10, 20, 40 ^{o}C/min) heating rates were used to run each sample in order to obtain the activation energy from the TGA data. Figure 2.3 shows the TGA curves of the polyaniline/ WS_2 nanocomposites at selected heating rate.

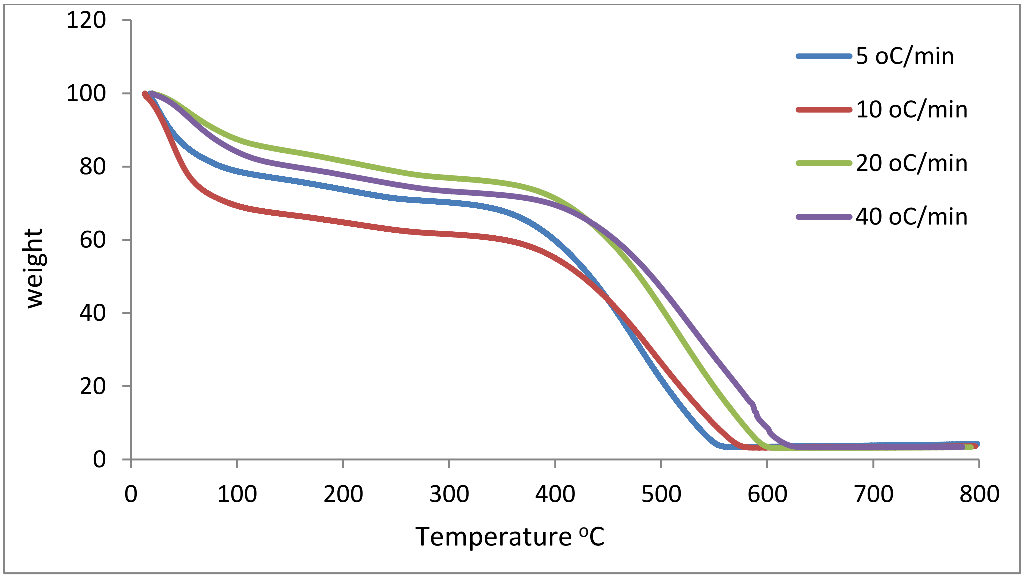

Figure 3.2: TGA of 12.5 of WS_2 – polyaniline nanocomposite.

It was apparent from the TGA curves of the 12.5 % by weight WS_2 – polyaniline nanocomposites profiles that various trends of the weight losses occurred upon changing the heating rates from 5 to 40 ^{o}C/min. It is clear that the onset decomposition of the polymer occurred at a lower temperature with a slower heating rate, and upon increasing the heating rate, the onset decomposition temperature of the polymer increases. This phenomenon is attributed to the fact that the polymer does not have adequate time to decompose with an increased heating rate. Therefore, the polymer will not begin to decompose until a higher temperature.

Thermal Degradation Kinetics:

The conversion (α) is a prerequisite parameter and can be calculated using equation (6). Figure 3.3 shows an example of the conversion profile for the polyaniline nanocomposite with 12.5 % WS_2.

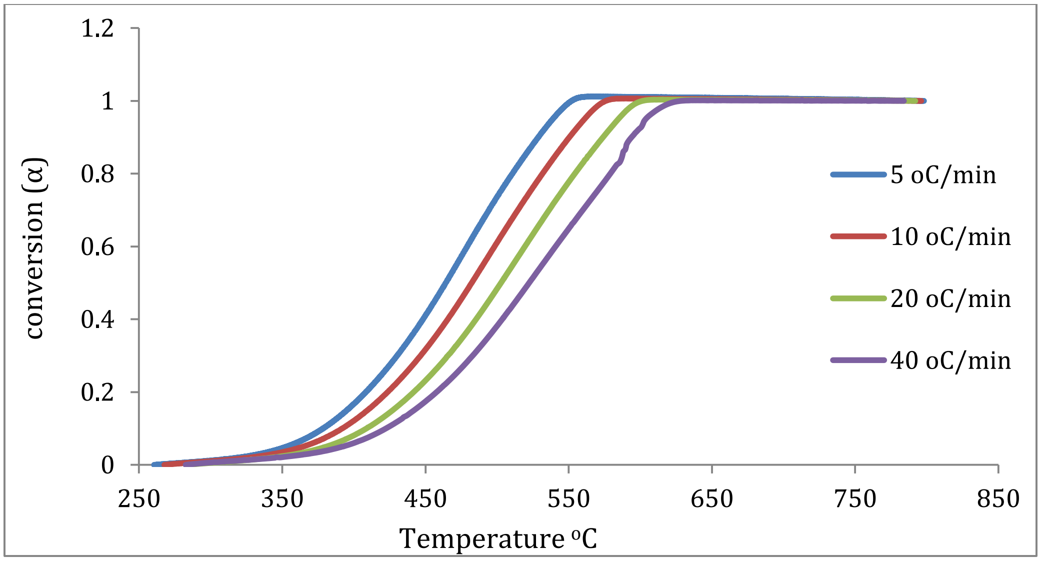

Figure 3.3: The conversion of 12.5 % WS_2 - PANI nanocomposite.

The regression lines, according to Ozawa's method, are plotted in Figure 3.4 as Log β against the inverse of the temperature and the slops were taken to compute the Ea.

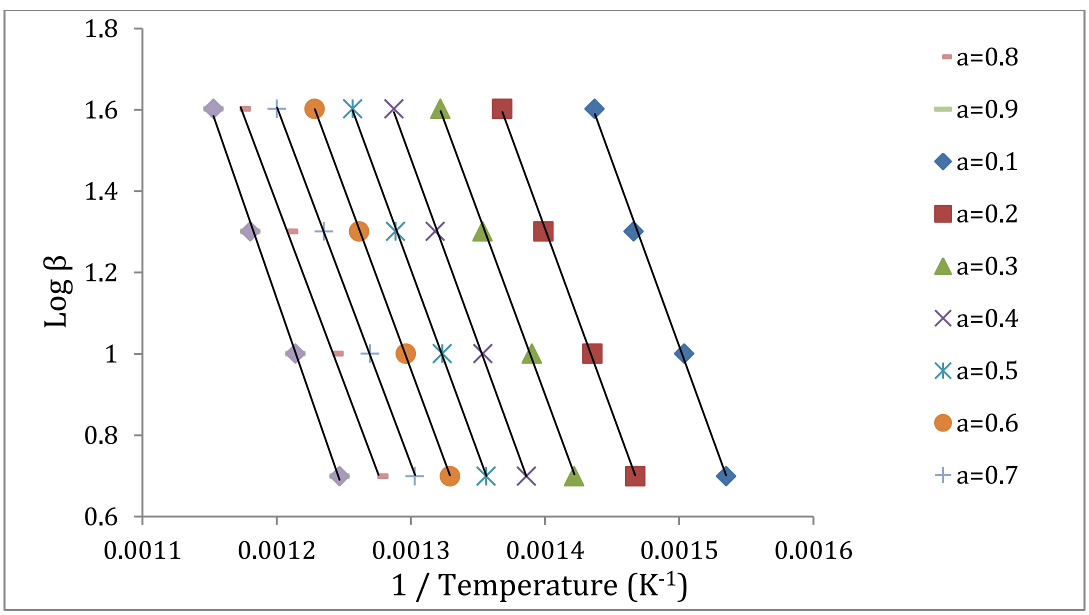

Figure 3.4: The regression lines for conversion of 0.1 -0.9 based on the Ozawa's method for PANI-WS_2 12.5 %.

The activation energy can be then calculated from the slope of these regression lines using equation (7). The value of the correlation coefficients (R) and the activation energies for the 12.5% polyaniline-WS_2 nanocomposites are given in Table 3.1.

Table 3.1: The correlation coefficient (R) and the activation energy (Ea) obtained using Ozawa's method for 12.5 % WS2-PANI.

Sample	Conversion α	R	Ea (kJ/mol)
12.5 % WS_2 by weight	0.1	0.9979	164.9
	0.2	0.9989	163.9
	0.3	0.9991	163.1
	0.4	0.9993	165.1
	0.5	0.9998	164.2
	0.6	0.9999	162.5
	0.7	0.9999	159.9
	0.8	0.9999	160.2
	0.9	0.9980	173.2
Average			164.1

It is apparent that the coefficient R is above 0.99 for each case. The value of the activation energy (E_a) computed by the isothermal method for conversions (α) from 0.1 to 0.9 exhibited values ranging from 159 kJ/mol to 173 kJ/mol for the nanocomposites of polyaniline with 12.5 % by weight WS_2. The average of these activation energies for each conversion was 164 kJ/mol, which is higher than the activation energy of pristine polyaniline at 133 kJ/mol. The same procedures were used to calculate the activation energy for pure PANI, 1, 5, 7.5, 10, 15, 20, 37, and 64% by weight polyaniline/WS_2 nanocomposites. The activation energy value for each nanocomposite is listed in Table 3.2

Table 3.2: The activation energy values of pure PANI and all of the PANI/WS_2 nanocomposites.

% by mass of WS_2	Ea (kJ/mol)	Standard Deviations (KJ/mol)
0	129.2	± 6.9
1	147.7	± 4.7
1 (b)	138.5	±8.5
5	131.1	± 5.1
5 (b)	138.5	±22.4
7.5	147.7	± 19.0
10	153.3	± 3.8
12.5	164.1	± 3.8
12.5 (b)	162.1	± 4.5
15	151.2	± 4.5
20	152.3	±14.2
20 (b)	151.5	±21.1
37	148.5	± 5.8
64	152.0	±12.1

In general, it is obvious that the values of the activation energy for each nanocomposite were increased in comparison to that of pure polyaniline. The activation energy against the weight percentages of WS_2 is plotted in Figure 3.5.

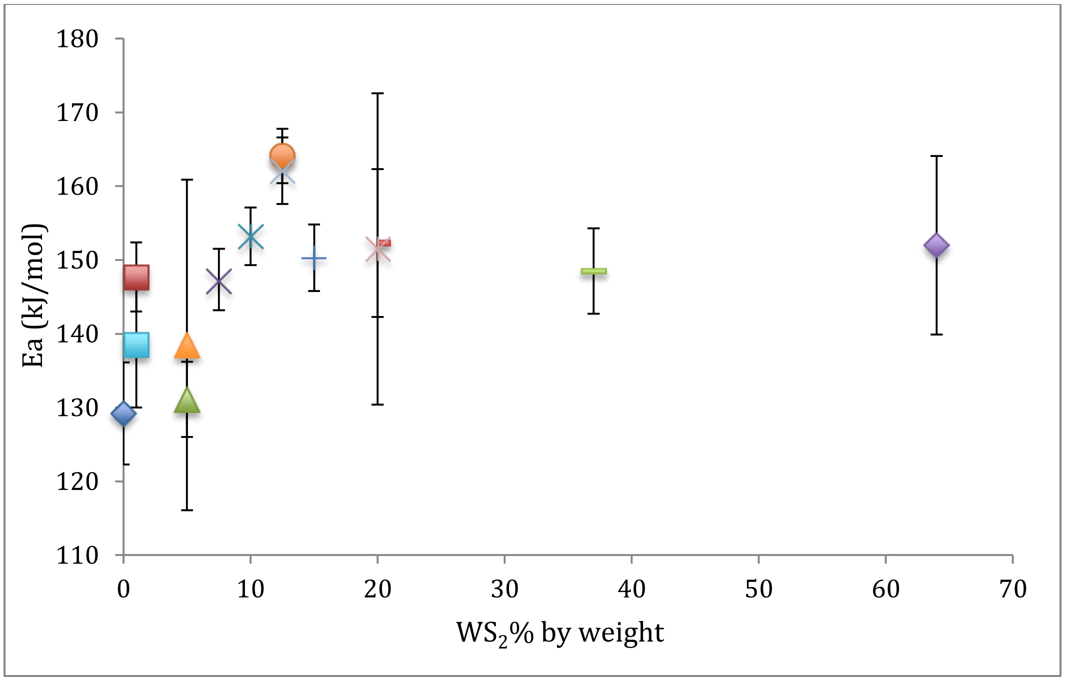

Figure 3.5: The plot of activation energy of pure PANI and WS_2–PANI nanocomposites against the weight percentages of WS_2.

The activation energy values for polyaniline-WS_2 nanocomposites vary upon increasing the amount of WS_2. As we can see, 12.5 % by weight of WS_2 displayed the highest activation energy value of 164 kJ/mol. In addition, the 1, 10, 15, 20, 37 and 64% polyaniline - WS_2 nanocomposites exhibited good improvement in the value of the activation energy with 146 kJ/mol, 152.3 151 kJ/mol, 145 kJ/mol, 152.3 kJ/mol and 152 kJ/mol respectively. However, 5% WS_2-PANI nanocomposite showed no significant change in activation energy at the first run while in the second run displayed an enhancement by 10 kJ/mol in comparison to the pure polyaniline with 129.2 kJ/mol.

3.4. Conclusion:

This work illustrated the decomposition kinetics of various PANI-WS_2 nanocomposites. Ozawa's method was applied to compute the activation energy of decomposition of the PANI-WS_2 nanocomposite. The activation of decomposition of pristine polyaniline was 129 kJ/mol, with PANI-12.5 %WS_2 composition displaying a significant increase in the activation energy of decomposition 165 kJ/mol. The remainder of the PANI-WS_2 nanocomposite series displayed increased activation energies ranging from 147.7 to 152.7 kJ/mol, with the exception of the 5% nanocomposites which did not show a significant increase in activation energy. Overall, the incorporation of the exfoliated WS_2 nanofiller enhanced the activation energies values of the polymer matrix. The molecular interaction between the polymer matrix and nanofiller enhance activation energy of the decomposition. Moreover, the incorporation of nanofiller affords better heat distribution within the polymer -nanocomposite.

Chapter 4: Future Work.

The current research has afforded us with interesting and exciting results of the exfoliated PTh, PThN, and PANI with various WS_2 compositions, and more extensive research can be carried out in the future.

One of the primary aims is to achieve a more extensive range in the variation of the composition of the WS_2-PThN nanocomposites. Nanocomposites samples prepared in this project consisted of WS_2 at 1, 5, 10, 20, 37, and 64 mass percentages. These percentages of the nanofiller were randomly selected, and in the future, it would be advantageous to fabricate exfoliated nanomaterials with other percents of WS_2 in order to obtain a comprehensive understanding of the effect of WS_2 on the PTh and PThN.

Finally, one of the possible future aims would be to attempt to incorporate exfoliated WS_2 into the synthesis of various compositions comprising either substituted polyanilines, polythiophene and other electronically conductive polymers such as polyphenylene sulfide, polypyrroles, and poly(para-phenylene). These conducting polymers are preferred because they have gained a considerable amount of interest.

5. **References.**

1. Shirakawa, H.; Louis, E. J.; MacDiarmid, A. G.; Chiang, C. K.; Heeger, A. J. Synthesis of electrically conducting organic polymers: halogen derivatives of polyacetylene,(CH) x. *Journal of the Chemical Society, Chemical Communications* **1977**, 578-580.

2. Runge, F. Ueber einige Produkte der Steinkohlendestillation. *Annalen der Physik* **1834**, *107*, 65-78.

3. Skotheim, T. A. *Handbook of conducting polymers;* CRC press: 1997; .

4. MacDiarmid, A. G. "Synthetic metals": A novel role for organic polymers (Nobel lecture). *Angewandte Chemie International Edition* **2001**, *40*, 2581-2590.

5. Chandrasekhar, P. Conducting polymers. *Fundamentals and Applications: A Practical Approach* **1999**, 83.

6. Taliani, C.; Gebauer, W.; Fichou, D. Handbook of Oligo and Polythiophenes. **1999**.

7. Heeger, A. J. Semiconducting and metallic polymers: the fourth generation of polymeric materials (Nobel lecture). *Angewandte Chemie International Edition* **2001**, *40*, 2591-2611.

8. Krane, K. S. Modern physics. *Modern Physics, 2nd Edition, by Kenneth S.Krane, pp.608.ISBN 0-471-82872-6.Wiley-VCH, August 1995.* **1995**, *1*.

9. Wallace, G.; Moulton, S.; Misoska, V.; Kane-Maguire, L.; Innis, P. In *In Nanostructure based on inherently conducting polymers;* Materials Forum; 2002; Vol. 26, pp 29-38.

10. Reynolds, J. R.; Skotheim, T. A.; Elsenbaumer, R. L. *Handbook of conducting polymers;* Marcel Dekker: 1998.

11. Weder, C. Organometallic conjugated polymer networks. *Journal of Inorganic and Organometallic Polymers and Materials* **2006**, *16*, 101-113.

12. Cheng, Y.; Luh, T. Synthesizing optoelectronic heteroaromatic conjugated polymers by cross-coupling reactions. *Journal of organometallic chemistry* **2004**, *689*, 4137-4148.

13. Skotheim, T. A.; Reynolds, J. *Handbook of Conducting Polymers, 2 Volume Set;* CRC press: 2007; .

14. Yamamoto, T.; Sanechika, K.; Yamamoto, A. Preparation of thermostable and electric- conducting poly (2, 5-thienylene). *Journal of Polymer Science: Polymer Letters Edition* **1980**, *18*, 9-12.

15. Lin, J. W.; Dudek, L. P. Synthesis and properties of poly (2, 5-thienylene). *Journal of Polymer Science: Polymer Chemistry Edition* **1980**, *18*, 2869-2873.

16. Springborg, M. The electronic properties of polythiophene. *Journal of Physics: Condensed Matter* **1992**, *4*, 101.

17. Amer, A.; Zimmer, H.; Mulligan, K. J.; Mark, H. B.; Pons, S.; McAleer, J. F. Polymerization of 3- methyl-2, 5-dibromothiophene utilizing n-butyl lithium and copper (II) chloride. *Journal of Polymer Science: Polymer Letters Edition* **1984**, *22*, 77-82.

18. Yamamoto, T.; Sanechika, K.; Yamamoto, A. Preparation and characterization of poly (thienylene) s. *Bull. Chem. Soc. Jpn.* **1983**, *56*, 1497-1502.

19. Kaneto, K.; Yoshino, K.; Inuishi, Y. Electrical and optical properties of polythiophene prepared by electrochemical polymerization. *Solid State Commun.* **1983**, *46*, 389-391.

20. Jen, K.; Miller, G. RL Elsenbaumer J. *Chem.Soc., Chem.Commun* **1986**, 1346.

21. Jen, K.; Oboodi, M.; Elsenbaumer, R. In *In Processible and environmentally stable conducting polymers;* ABSTRACTS OF PAPERS OF THE AMERICAN CHEMICAL SOCIETY; AMER CHEMICAL SOC 1155 16TH ST, NW, WASHINGTON, DC 20036: 1985; Vol. 190, pp 17-PME.

22. Elsenbaumer, R.; Jen, K. Y.; Oboodi, R. Processible and environmentally stable conducting polymers. *Synth. Met.* **1986**, *15*, 169-174.

23. Sugimoto, R.; Takeda, S.; Gu, H.; Yoshino, K. Preparation of soluble polythiophene derivatives utilizing transition metal halides as catalysts and their property. *Chem.Express* **1986**, *1*, 635-638.

24. Sato, M.; Tanaka, S.; Kaeriyama, K. Soluble conducting polythiophenes. *Journal of the Chemical Society, Chemical Communications* **1986**, 873-874.

25. Hotta, S.; Rughooputh, S.; Heeger, A.; Wudl, F. Spectroscopic studies of soluble poly (3-alkylthienylenes). *Macromolecules* **1987**, *20*, 212-215.

26. Yamamoto, T.; Sanechika, K.; Yamamoto, A. Preparation of thermostable and electric- conducting poly (2, 5-thienylene). *Journal of Polymer Science: Polymer Letters Edition* **1980**, *18*, 9-12.

27. Kobayashi, M.; Chen, J.; Chung, T.; Moraes, F.; Heeger, A.; Wudl, F. Synthesis and properties of chemically coupled poly (thiophene). *Synth. Met.* **1984**, *9*, 77-86.

28. McClain, M. D.; Whittington, D. A.; Mitchell, D. J.; Curtis, M. D. Novel Poly (3-alkylthiophene) and Poly (3-alkylthienyl ketone) Syntheses via Organomercurials. *J. Am. Chem. Soc.* **1995**, *117*, 3887-3888.

29. Yoshino, K.; Hayashi, S.; Sugimoto, R. Preparation and properties of conducting heterocyclic polymer films by chemical method. *Japanese Journal of Applied Physics* **1984**, *23*, L899.

30. Österholm, J.; Laakso, J.; Nyholm, P.; Isotalo, H.; Stubb, H.; Inganäs, O.; Salaneck, W. Melt and solution processable poly (3-alkylthiophenes) and their blends. *Synth. Met.* **1989**, *28*, 435-444.

31. Hotta, S.; Soga, M.; Sonoda, N. Novel organosynthetic routes to polythiophene and its derivatives. *Synth. Met.* **1988**, *26*, 267-279.

32. Yoshino, K.; Nakajima, S.; Sugimoto, R. Fusibility of polythiophene derivatives with substituted long alkyl chain and their properties. *Japanese journal of applied physics* **1987**, *26*, L1038.

33. Kulszewicz-Bajer, I.; Pawlicka, A.; Plenkiewicz, J.; Proń, A.; Lefrant, S. Poly (3-n-Butylthiophene) tetrachloroferrate: Preparation, spectroscopic and morphological studies. *Synth. Met.* **1989**, *30*, 335-339.

34. Leclerc, M.; Diaz, F. M.; Wegner, G. Structural analysis of poly (3-alkylthiophene) s. *Die Makromolekulare Chemie* **1989**, *190*, 3105-3116.

35. Pomerantz, M.; Tseng, J. J.; Zhu, H.; Sproull, S. J.; Reynolds, J. R.; Uitz, R.; Arnott, H. J.; Haider, M. I. Processable polymers and copolymers of 3-alkylthiophenes and their blends. *Synth. Met.* **1991**, *41*, 825-830.

36. Abdou, M. S.; Lu, X.; Xie, Z. W.; Orfino, F.; Deen, M. J.; Holdcroft, S. Nature of Impurities in. pi.-Conjugated Polymers Prepared by Ferric Chloride and Their Effect on the Electrical Properties of Metal-Insulator-Semiconductor Structures. *Chemistry of materials* **1995**, *7*, 631-641.

37. Chen, F.; Mehta, P. G.; Takiff, L.; McCullough, R. D. Improved electroluminescence performance of poly (3-alkylthiophenes) having a high head-to-tail (HT) ratio. *J.Mater.Chem.* **1996**, *6*, 1763-1766.

38. Chen, F.; Mehta, P. G.; Takiff, L.; McCullough, R. D. Improved electroluminescence performance of poly (3-alkylthiophenes) having a high head-to-tail (HT) ratio. *J.Mater.Chem.* **1996**, *6*, 1763-1766.

39. Niemi, V.; Knuuttila, P.; Österholm, J.; Korvola, J. Polymerization of 3-alkylthiophenes with FeCl3. *Polymer* **1992**, *33*, 1559-1562.

40. Järvinen, H.; Lahtinen, L.; Näsman, J.; Hormi, O.; Tammi, A. A new method to prepare 3-octylthiophene and poly-(3-octylthiophene). *Synth. Met.* **1995**, *69*, 299-300.

41. Loponen, M.; Taka, T.; Laakso, J.; Väkiparta, K.; Suuronen, K.; Valkeinen, P.; Österholm, J. Doping and dedoping processes in poly (3-alkylthiophenes). *Synth. Met.* **1991**, *41*, 479-484.

42. Yoshino, K.; Nakajima, S.; Fujii, M.; Sugimoto, R. Conducting polymer fibre prepared by melt-spinning method from fusible polythiophene derivative. *Polymer communications* **1987**, *28*, 309-310.

43. Inganäs, O.; Salaneck, W.; Österholm, J.; Laakso, J. Thermochromic and solvatochromic effects in poly (3-hexylthiophene). *Synth. Met.* **1988**, *22*, 395-406.

44. Reynolds, J. R.; Ruiz, J. P.; Child, A. D.; Nayak, K.; Marynick, D. S. Electrically conducting polymers containing alternating substituted phenylenes and bithiophene repeat units. *Macromolecules* **1991**, *24*, 678-687.

45. Yoshino, K.; Nakajima, S.; Onoda, M.; Sugimoto, R. Electrical and optical properties of poly (3-alkylthiophene). *Synth. Met.* **1989**, *28*, 349-357.

46. Gautun, O. R.; Carlsen, P. H.; Samuelsen, E. J.; Mårdalen, J. Synthesis and studies of polythiophenes substituted with polydeuterated side chains. Isotope effects in the polymerization of 3-alkylthiophenes. *Synth. Met.* **1993**, *58*, 115-121.

47. Chen, T.; Wu, X.; Rieke, R. D. Regiocontrolled synthesis of poly (3-alkylthiophenes) mediated by Rieke zinc: their characterization and solid-state properties. *J. Am. Chem. Soc.* **1995**, *117*, 233-244.

48. McCullough, R. D. The chemistry of conducting polythiophenes. *Adv Mater* **1998**, *10*, 93-116.

49. Taliani, C.; Gebauer, W.; Fichou, D. Handbook of Oligo and Polythiophenes. **1999**.

50. McCullough, R. ACS Polymer Preprints 1992, 33 (1), 195.(c) McCullough, RD; Lowe, RD; Jayaraman, M. *Anderson, DLJ Org.Chem* **1993**, *58*, 904.

51. Wu, X.; Chen, T.; Rieke, R. D. Synthesis of regioregular head-to-tail poly [3-(alkylthio) thiophenes]. A highly electroconductive polymer. *Macromolecules* **1995**, *28*, 2101-2102.

52. Chen, T. A.; O'Brien, R. A.; Rieke, R. D. Use of highly reactive zinc leads to a new, facile synthesis for polyarylenes. *Macromolecules* **1993**, *26*, 3462-3463.

53. Chen, T.; Rieke, R. D. Polyalkylthiophenes with the smallest bandgap and the highest intrinsic conductivity. *Synth. Met.* **1993**, *60*, 175-177.

54. Iovu, M. C.; Sheina, E. E.; Gil, R. R.; McCullough, R. D. Experimental evidence for the quasi-“living” nature of the grignard metathesis method for the synthesis of regioregular poly (3-alkylthiophenes). *Macromolecules* **2005**, *38*, 8649-8656.

55. Loewe, R. S.; Ewbank, P. C.; Liu, J.; Zhai, L.; McCullough, R. D. Regioregular, head-to-tail coupled poly (3-alkylthiophenes) made easy by the GRIM method: investigation of the reaction and the origin of regioselectivity. *Macromolecules* **2001**, *34*, 4324-4333.

56. Stejskal, J.; Gilbert, R. Polyaniline. Preparation of a conducting polymer (IUPAC technical report). *Pure and Applied Chemistry* **2002**, *74*, 857-867.

57. Bhadra, S.; Singha, N. K.; Khastgir, D. Electrochemical synthesis of polyaniline and its comparison with chemically synthesized polyaniline. *J Appl Polym Sci* **2007**, *104*, 1900-1904.

58. MacDiarmid, A.; Yang, L.; Huang, W.; Humphrey, B. Polyaniline: Electrochemistry and application to rechargeable batteries. *Synth. Met.* **1987**, *18*, 393-398.

59. De Chanterac, H.; Roduit, P.; Belhadj-Tahar, N.; Fourrier-Lamer, A.; Djigo, Y.; Aeiyach, S.; Lacaze, P. Electromagnetic absorption of polyanilines at microwave frequencies. *Synth. Met.* **1992**, *52*, 183-192.

60. Mäkelä, T.; Sten, J.; Hujanen, A.; Isotalo, H. High frequency polyaniline shields. *Synth. Met.* **1999**, *101*, 707.

61. MacDiarmid, A. G.; Epstein, A. J. In *In Conducting polymers: past, present and future…;* MRS Proceedings; Cambridge Univ Press: 1993; Vol. 328, pp 133.

62. Wang, H.; MacDiarmid, A.; Wang, Y.; Gebier, D.; Epstein, A. J. Application of polyaniline (emeraldine base, EB) in polymer light-emitting devices. *Synth. Met.* **1996**, *78*, 33-37.

63. Dutta, D.; Sarma, T. K.; Chowdhury, D.; Chattopadhyay, A. A polyaniline-containing filter paper that acts as a sensor, acid, base, and endpoint indicator and also filters acids and bases. *J. Colloid Interface Sci.* **2005**, *283*, 153-159.

64. Drelinkiewicz, A.; Waksmundzka-Góra, A.; Sobczak, J.; Stejskal, J. Hydrogenation of 2-ethyl-9, 10-anthraquinone on Pd-polyaniline (SiO 2) composite catalyst: The effect of humidity. *Applied Catalysis A: General* **2007**, *333*, 219-228.

65. Chang, M.; Wu, C.; Chen, Y.; Hsieh, B.; Huang, W.; Ho, K.; Hsieh, T.; Han, Y. Polymer solar cells incorporating one-dimensional polyaniline nanotubes. *Organic Electronics* **2008**, *9*, 1136-1139.

66. Feast, W.; Tsibouklis, J.; Pouwer, K.; Groenendaal, L.; Meijer, E. Synthesis, processing and material properties of conjugated polymers. *Polymer* **1996**, *37*, 5017-5047.

67. Chiang, J.; MacDiarmid, A. G. 'Polyaniline': protonic acid doping of the emeraldine form to the metallic regime. *Synth. Met.* **1986**, *13*, 193-205.

68. Masters, J.; Sun, Y.; MacDiarmid, A.; Epstein, A. Polyaniline: allowed oxidation states. *Synth. Met.* **1991**, *41*, 715-718.

69. Stafström, S.; Bredas, J.; Epstein, A.; Woo, H.; Tanner, D.; Huang, W.; MacDiarmid, A. Polaron lattice in highly conducting polyaniline: theoretical and optical studies. *Phys. Rev. Lett.* **1987**, *59*, 1464.

70. Campos, M.; Bello Jr, B. Mechanism of conduction in doped polyaniline. *J. Phys. D* **1997**, *30*, 1531.

71. Teasdale, P. R.; Kane-Maguire, A.; Wallace, G. G.; Spinks, G. M.; Press, C. Conductive electroactive polymers intelligent materials systems. **2002**.

72. Liu, W.; Cholli, A. L.; Nagarajan, R.; Kumar, J.; Tripathy, S.; Bruno, F. F.; Samuelson, L. The role of template in the enzymatic synthesis of conducting polyaniline. *J. Am. Chem. Soc.* **1999**, *121*, 11345-11355.

73. MacDiarmid, A.; Chiang, J.; Richter, A.; Somasiri, N. AJ Epstein in:“Conducting Polymers”, ed. L. Alcacér. **1987**.

74. Willstätter, R.; Dorogi, S. Über Anilinschwarz. III. *Berichte der deutschen chemischen Gesellschaft* **1909**, *42*, 4118-4135.

75. Hand, R. L.; Nelson, R. F. The Anodic Decomposition Pathways of Ortho- and Meta- substituted Anilines. *J. Electrochem. Soc.* **1978**, *125*, 1059-1069.

76. Yasuda, A.; Shimidzu, T. Chemical and electrochemical analyses of polyaniline prepared with FeCl3. *Synth. Met.* **1993**, *61*, 239-245.

77. Mohilner, D. M.; Adams, R. N.; Argersinger, W. J. Investigation of the kinetics and mechanism of the anodic oxidation of aniline in aqueous sulfuric acid solution at a platinum electrode. *J. Am. Chem. Soc.* **1962**, *84*, 3618-3622.

78. Genies, E.; Tsintavis, C. Redox mechanism and electrochemical behaviour or polyaniline deposits. *Journal of electroanalytical chemistry and interfacial electrochemistry* **1985**, *195*, 109-128.

79. Huang, W.; Humphrey, B. D.; MacDiarmid, A. G. Polyaniline, a novel conducting polymer. Morphology and chemistry of its oxidation and reduction in aqueous electrolytes. *Journal of the Chemical Society, Faraday Transactions 1: Physical Chemistry in Condensed Phases* **1986**, *82*, 2385-2400.

80. Genies, E.; Lapkowski, M. Spectroelectrochemical study of polyaniline versus potential in the equilibrium state. *Journal of electroanalytical chemistry and interfacial electrochemistry* **1987**, *220*, 67-82.

81. Bittihn, R.; Ely, G.; Woeffler, F.; Münstedt, H.; Naarmann, H.; Naegele, D. In *In Polypyrrole as an electrode material for secondary lithium cells;* Makromolekulare Chemie. Macromolecular Symposia; Wiley Online Library: 1987; Vol. 8, pp 51-59.

82. Casanovas, J.; Cho, L. Y.; Ocampo, C.; Alemán, C. A theoretical study of the effects produced by N-hydroxyalkyl substitution in pyrrole oligomers. *Synth. Met.* **2005**, *151*, 239-245.

83. Saxman, A.; Liepins, R.; Aldissi, M. Polyacetylene: its synthesis, doping and structure. *Progress in polymer science* **1985**, *11*, 57-89.

84. Lauritzen, M. V. *Solvato-Controlled Doping of Poly (3-alkyithiophene)~ and Other Conjugated Polymers Using Silver (1) Triflate;* 1998; .

85. De Albuquerque, J.; Mattoso, L.; Faria, R.; Masters, J.; MacDiarmid, A. Study of the interconversion of polyaniline oxidation states by optical absorption spectroscopy. *Synth. Met.* **2004**, *146*, 1-10.

86. Albuquerque, J.; Mattoso, L. C.; Balogh, D.; Faria, R.; Masters, J.; MacDiarmid, A. A simple method to estimate the oxidation state of polyanilines. *Synth. Met.* **2000**, *113*, 19-22.

87. Chen, S. A.; Hua, M. Y. Structure and doping level of the self-acid-doped conjugated conducting polymers: poly [n-(3'-thienyl) alkanesulfonic acids]. *Macromolecules* **1993**, *26*, 7108-7110.

88. Mastragostino, M.; Soddu, L. Electrochemical characterization of “n” doped polyheterocyclic conducting polymers—I. Polybithiophene. *Electrochim. Acta* **1990**, *35*, 463-466.

89. Yamamoto, T.; Omote, M.; Miyazaki, Y.; Kashiwazaki, A.; Lee, B.; Kanbara, T.; Osakada, K.; Inoue, T.; Kubota, K. Poly (thiophene-2, 5-diyl) s with a crown ethereal subunit. Preparation, optical properties, and n-doped state stabilized against air. *Macromolecules* **1997**, *30*, 7158-7165.

90. Abdou, M. S.; Orfino, F. P.; Xie, Z. W.; Deen, M. J.; Holdcroft, S. Reversible charge transfer complexes between molecular oxygen and poly (3-alkylthiophene) s. *Adv Mater* **1994**, *6*, 838-841.

91. Abdou, M. S.; Orfino, F. P.; Son, Y.; Holdcroft, S. Interaction of oxygen with conjugated polymers: charge transfer complex formation with poly (3-alkylthiophenes). *J. Am. Chem. Soc.* **1997**, *119*, 4518-4524.

92. Sönmez, G.; Saraç, A. S. In situ spectroelectrochemistry and colorimetry of poly (pyrrole-acrylamide) s. *J. Mater. Sci.* **2002**, *37*, 4609-4614.

93. Väterlein, C.; Ziegler, B.; Gebauer, W.; Neureiter, H.; Stoldt, M.; Weaver, M.; Bäuerle, P.; Sokolowski, M.; Bradley, D.; Umbach, E. Electrical conductivity and oxygen doping of vapour-deposited oligothiophene films. *Synth. Met.* **1996**, *76*, 133-136.

94. Sarac, A. S.; Evans, U.; Serantoni, M.; Clohessy, J.; Cunnane, V. J. Electrochemical and morphological study of the effect of polymerization conditions on poly (terthiophene). *Surface and Coatings Technology* **2004**, *182*, 7-13.

95. Friend, R.; Gymer, R.; Holmes, A.; Burroughes, J.; Marks, R.; Taliani, C.; Bradley, D.; Dos Santos, D.; Bredas, J.; Lögdlund, M. Electroluminescence in conjugated polymers. *Nature* **1999**, *397*, 121-128.

96. Schnöller, M.; Wersing, W.; Naarman, H. In *Intrinsically conductive organic polymers as electrode material for functional ceramics in electronics;* Makromolekulare Chemie. Macromolecular Symposia; Wiley Online Library: 1987; Vol. 8, pp 83-95.

97. Bittihn, R.; Ely, G.; Woeffler, F.; Münstedt, H.; Naarmann, H.; Naegele, D. In *Polypyrrole as an electrode material for secondary lithium cells;* Makromolekulare Chemie. Macromolecular Symposia; Wiley Online Library: 1987; Vol. 8, pp 51-59.

98. Casanovas, J.; Cho, L. Y.; Ocampo, C.; Alemán, C. A theoretical study of the effects produced by N-hydroxyalkyl substitution in pyrrole oligomers. *Synth. Met.* **2005**, *151*, 239-245.

99. Dalgakiran, S. *DESIGN AND ELECTROCHEMICAL CHARACTERIZATION OF NOVEL FUNCTIONALIZED POLYTHIOPHENE AND POLYSILOXANE DERIVATIVES* **2012**.

100. Harun, M. H.; Saion, E.; Kassim, A.; Yahya, N.; Mahmud, E. Conjugated conducting polymers: A brief overview. *UCSI Academic Journal: Journal for the Advancement of Science & Arts* **2007**, *2*, 63-68.

101. Rammelt, U.; Nguyen, P.; Plieth, W. Protection of mild steel by modification with thin films of polymethylthiophene. *Electrochim. Acta* **2001**, *46*, 4251-4257.

102. Speakman, S. P.; Rozenberg, G. G.; Clay, K. J.; Milne, W. I.; Ille, A.; Gardner, I. A.; Bresler, E.; Steinke, J. H. High performance organic semiconducting thin films: Ink jet printed polythiophene [rr-P3HT]. *Organic Electronics* **2001**, *2*, 65-73.

103. Alcácer, L. *Conducting Polymers;* Springer: 1987; .

104. Saxena, V.; Malhotra, B. Prospects of conducting polymers in molecular electronics. *Current Applied Physics* **2003**, *3*, 293-305.

105. Kurian, M.; Galvin, M. E.; Trapa, P. E.; Sadoway, D. R.; Mayes, A. M. Single-ion conducting polymer–silicate nanocomposite electrolytes for lithium battery applications. *Electrochim. Acta* **2005**, *50*, 2125-2134.

106. Adhikari, B.; Majumdar, S. Polymers in sensor applications. *Progress in polymer science* **2004**, *29*, 699-766.

107. Weidlich, C.; Mangold, K.; Jüttner, K. EQCM study of the ion exchange behaviour of polypyrrole with different counterions in different electrolytes. *Electrochim. Acta* **2005**, *50*, 1547-1552.

108. Han, G.; Shi, G. High-response tri-layer electrochemical actuators based on conducting polymer films. *J Electroanal Chem* **2004**, *569*, 169-174.

109. Mirmohseni, A.; Price, W.; Wallace, G. G. Electrochemically controlled transport across conducting polymer composites—basis of smart membrane materials. *Polym. Gels Networks* **1993**, *1*, 61-77.

110. Margolis, J. Conductive Polymers and Plastics 1989.

111. Stenger-Smith, J. D. Intrinsically electrically conducting polymers. Synthesis, characterization, and their applications. *Progress in Polymer Science* **1998**, *23*, 57-79.

112. Radisavljevic, B.; Radenovic, A.; Brivio, J.; Giacometti, V.; Kis, A. Single-layer MoS2 transistors. *Nature nanotechnology* **2011**, *6*, 147-150.

113. Lopez-Sanchez, O.; Lembke, D.; Kayci, M.; Radenovic, A.; Kis, A. Ultrasensitive photodetectors based on monolayer MoS_2. *Nature nanotechnology* **2013**, *8*, 497-501.

114. Zeng, H.; Dai, J.; Yao, W.; Xiao, D.; Cui, X. Valley polarization in MoS_2 monolayers by optical pumping. *Nature nanotechnology* **2012**, *7*, 490-493.

115. Zhang, W.; Chuu, C.; Huang, J.; Chen, C.; Tsai, M.; Chang, Y.; Liang, C.; Chen, Y.; Chueh, Y.; He, J. Ultrahigh-gain photodetectors based on atomically thin graphene-MoS_2 heterostructures. *Scientific reports* **2014**, *4*.

116. Cong, C.; Shang, J.; Wu, X.; Cao, B.; Peimyoo, N.; Qiu, C.; Sun, L.; Yu, T. Synthesis and Optical Properties of Large-Area Single-Crystalline 2D Semiconductor WS2 Monolayer from Chemical Vapor Deposition. *Advanced Optical Materials* **2014**, *2*, 131-136.

117. Splendiani, A.; Sun, L.; Zhang, Y.; Li, T.; Kim, J.; Chim, C.; Galli, G.; Wang, F. Emerging photoluminescence in monolayer MoS_2. *Nano letters* **2010**, *10*, 1271-1275.

118. Li, T.; Galli, G. Electronic properties of MoS_2 nanoparticles. *The Journal of Physical Chemistry C* **2007**, *111*, 16192-16196.

119. Mak, K. F.; Lee, C.; Hone, J.; Shan, J.; Heinz, T. F. Atomically thin MoS_2: a new direct-gap semiconductor. *Phys. Rev. Lett.* **2010**, *105*, 136805.

120. Lee, C.; Yan, H.; Brus, L. E.; Heinz, T. F.; Hone, J.; Ryu, S. Anomalous lattice vibrations of single-and few-layer MoS_2. *ACS nano* **2010**, *4*, 2695-2700.

121. Li, H.; Lu, G.; Yin, Z.; He, Q.; Li, H.; Zhang, Q.; Zhang, H. Optical Identification of Single-and Few-Layer MoS_2 Sheets. *Small* **2012**, *8*, 682-686.

122. Castellanos-Gomez, A.; Poot, M.; Steele, G. A.; van der Zant, Herre SJ; Agraït, N.; Rubio-Bollinger, G. Elastic properties of freely suspended MoS2 nanosheets. *Adv Mater* **2012**, *24*, 772-775.

123. Bertolazzi, S.; Brivio, J.; Kis, A. Stretching and breaking of ultrathin MoS_2. *ACS nano* **2011**, *5*, 9703-9709.

124. Loh, K. P.; Bao, Q.; Eda, G.; Chhowalla, M. Graphene oxide as a chemically tunable platform for optical applications. *Nature chemistry* **2010**, *2*, 1015-1024.

125. Palacin, M. R. Recent advances in rechargeable battery materials: a chemist's perspective. *Chem. Soc. Rev.* **2009**, *38*, 2565-2575.

126. Whittingham, M. S. Lithium batteries and cathode materials. *Chem. Rev.* **2004**, *104*, 4271-4302.

127. Du, G.; Guo, Z.; Wang, S.; Zeng, R.; Chen, Z.; Liu, H. Superior stability and high capacity of restacked molybdenum disulfide as anode material for lithium ion batteries. *Chemical Communications* **2010**, *46*, 1106-1108.

128. Xiao, J.; Choi, D.; Cosimbescu, L.; Koech, P.; Liu, J.; Lemmon, J. P. Exfoliated MoS2 nanocomposite as an anode material for lithium ion batteries. *Chemistry of Materials* **2010**, *22*, 4522-4524.

129. Huang, X.; Yin, Z.; Wu, S.; Qi, X.; He, Q.; Zhang, Q.; Yan, Q.; Boey, F.; Zhang, H. Graphene-based materials: synthesis, characterization, properties, and applications. *small* **2011**, *7*, 1876-1902.

130. Conway, B. Electrochemical supercapacitor. *Scientific Fundamentals and Technological Applications* **1999**.

131. Soon, J. M.; Loh, K. P. Electrochemical double-layer capacitance of MoS2 nanowall films. *Electrochemical and Solid-State Letters* **2007**, *10*, A250-A254.

132. Radisavljevic, B.; Radenovic, A.; Brivio, J.; Giacometti, V.; Kis, A. Single-layer MoS2 transistors. *Nature nanotechnology* **2011**, *6*, 147-150.

133. Zhang, Y.; Tang, T.; Girit, C.; Hao, Z.; Martin, M. C.; Zettl, A.; Crommie, M. F.; Shen, Y. R.; Wang, F. Direct observation of a widely tunable bandgap in bilayer graphene. *Nature* **2009**, *459*, 820-823.

134. Yoon, Y.; Ganapathi, K.; Salahuddin, S. How good can monolayer MoS2 transistors be? *Nano letters* **2011**, *11*, 3768-3773.

135. Zhang, Y.; Ye, J.; Matsuhashi, Y.; Iwasa, Y. Ambipolar MoS2 thin flake transistors. *Nano letters* **2012**, *12*, 1136-1140.

136. Pu, J.; Yomogida, Y.; Liu, K.; Li, L.; Iwasa, Y.; Takenobu, T. Highly flexible MoS2 thin-film transistors with ion gel dielectrics. *Nano letters* **2012**, *12*, 4013-4017.

137. Kim, S.; Konar, A.; Hwang, W.; Lee, J. H.; Lee, J.; Yang, J.; Jung, C.; Kim, H.; Yoo, J.; Choi, J. High-mobility and low-power thin-film transistors based on multilayer MoS_2 crystals. *Nature communications* **2012**, *3*, 1011.

138. Radisavljevic, B.; Whitwick, M. B.; Kis, A. Integrated circuits and logic operations based on single-layer MoS2. *ACS nano* **2011**, *5*, 9934-9938.

139. Wang, H.; Yu, L.; Lee, Y.; Shi, Y.; Hsu, A.; Chin, M. L.; Li, L.; Dubey, M.; Kong, J.; Palacios, T. Integrated circuits based on bilayer MoS_2 transistors. *Nano letters* **2012**, *12*, 4674-4680.

140. Yin, Z.; Li, H.; Li, H.; Jiang, L.; Shi, Y.; Sun, Y.; Lu, G.; Zhang, Q.; Chen, X.; Zhang, H. ACS Nano, 2012, 6, 74;(b) O. Lopez-Sanchz, D. Lembke, M. Kayci, A. Radenovic and A. Kis. *Nat.Nanotechnol* **2013**, *8*, 497.

141. Frey, G. L.; Reynolds, K. J.; Friend, R. H.; Cohen, H.; Feldman, Y. Solution-processed anodes from layer-structure materials for high-efficiency polymer light-emitting diodes. *J. Am. Chem. Soc.* **2003**, *125*, 5998-6007.

142. Zhong, C.; Duan, C.; Huang, F.; Wu, H.; Cao, Y. Materials and Devices toward Fully Solution Processable Organic Light-Emitting Diodes†. *Chemistry of materials* **2010**, *23*, 326-340.

143. Li, H.; Yin, Z.; He, Q.; Li, H.; Huang, X.; Lu, G.; Fam, D. W. H.; Tok, A. I. Y.; Zhang, Q.; Zhang, H. Fabrication of Single-and Multilayer MoS_2 Film-Based Field-Effect Transistors for Sensing NO at Room Temperature. *small* **2012**, *8*, 63-67.

144. Zeng, Z.; Yin, Z.; Huang, X.; Li, H.; He, Q.; Lu, G.; Boey, F.; Zhang, H. Single-Layer Semiconducting Nanosheets: High-Yield Preparation and Device Fabrication. *Angewandte Chemie International Edition* **2011**, *50*, 11093-11097.

145. He, Q.; Wu, S.; Yin, Z.; Zhang, H. Graphene-based electronic sensors. *Chemical Science* **2012**, *3*, 1764-1772.

146. He, Q.; Zeng, Z.; Yin, Z.; Li, H.; Wu, S.; Huang, X.; Zhang, H. Fabrication of Flexible MoS_2 Thin-Film Transistor Arrays for Practical Gas-Sensing Applications. *Small* **2012**, *8*, 2994-2999.

147. Wu, S.; Zeng, Z.; He, Q.; Wang, Z.; Wang, S. J.; Du, Y.; Yin, Z.; Sun, X.; Chen, W.; Zhang, H. Electrochemically Reduced Single-Layer MoS_2 Nanosheets: Characterization, Properties, and Sensing Applications. *Small* **2012**, *8*, 2264-2270.

148. Chhowalla, M.; Shin, H. S.; Eda, G.; Li, L.; Loh, K. P.; Zhang, H. The chemistry of two-dimensional layered transition metal dichalcogenide nanosheets. *Nature chemistry* **2013**, *5*, 263-275.

149. Ramakrishna Matte, H.; Gomathi, A.; Manna, A. K.; Late, D. J.; Datta, R.; Pati, S. K.; Rao, C. MoS_2 and WS_2 analogues of graphene. *Angewandte Chemie* **2010**, *122*, 4153-4156.

150. Feng, J.; Sun, X.; Wu, C.; Peng, L.; Lin, C.; Hu, S.; Yang, J.; Xie, Y. Metallic few-layered VS_2 ultrathin nanosheets: high two-dimensional conductivity for in-plane supercapacitors. *J. Am. Chem. Soc.* **2011**, *133*, 17832-17838.

151. Novoselov, K. S.; Geim, A. K.; Morozov, S. V.; Jiang, D.; Zhang, Y.; Dubonos, S. V.; Grigorieva, I. V.; Firsov, A. A. Electric field effect in atomically thin carbon films. *Science* **2004**, *306*, 666-669.

152. Novoselov, K. S.; Jiang, D.; Schedin, F.; Booth, T. J.; Khotkevich, V. V.; Morozov, S. V.; Geim, A. K. Two-dimensional atomic crystals. *Proc. Natl. Acad. Sci. U. S. A.* **2005**, *102*, 10451-10453.

153. Lee, C.; Li, Q.; Kalb, W.; Liu, X. Z.; Berger, H.; Carpick, R. W.; Hone, J. Frictional characteristics of atomically thin sheets. *Science* **2010**, *328*, 76-80.

154. Wang, Q. H.; Kalantar-Zadeh, K.; Kis, A.; Coleman, J. N.; Strano, M. S. Electronics and optoelectronics of two-dimensional transition metal dichalcogenides. *Nature nanotechnology* **2012**, *7*, 699-712.

155. Liu, K.; Zhang, W.; Lee, Y.; Lin, Y.; Chang, M.; Su, C.; Chang, C.; Li, H.; Shi, Y.; Zhang, H. Growth of large-area and highly crystalline MoS2 thin layers on insulating substrates. *Nano letters* **2012**, *12*, 1538-1544.

156. Lee, H. S.; Min, S.; Chang, Y.; Park, M. K.; Nam, T.; Kim, H.; Kim, J. H.; Ryu, S.; Im, S. MoS_2 nanosheet phototransistors with thickness-modulated optical energy gap. *Nano letters* **2012**, *12*, 3695-3700.

157. Shi, Y.; Zhou, W.; Lu, A.; Fang, W.; Lee, Y.; Hsu, A. L.; Kim, S. M.; Kim, K. K.; Yang, H. Y.; Li, L. Van der Waals epitaxy of MoS_2 layers using graphene as growth templates. *Nano letters* **2012**, *12*, 2784-2791.

158. Zhan, Y.; Liu, Z.; Najmaei, S.; Ajayan, P. M.; Lou, J. Large-area vapor-phase growth and characterization of MoS_2 atomic layers on a SiO_2 substrate. *Small* **2012**, *8*, 966-971.

159. Lee, Y.; Zhang, X.; Zhang, W.; Chang, M.; Lin, C.; Chang, K.; Yu, Y.; Wang, J. T.; Chang, C.; Li, L. Synthesis of Large-Area MoS_2 Atomic Layers with Chemical Vapor Deposition. *Adv Mater* **2012**, *24*, 2320-2325.

160. Jang, J.; Jeong, S.; Seo, J.; Kim, M.; Sim, E.; Oh, Y.; Nam, S.; Park, B.; Cheon, J. Ultrathin zirconium disulfide nanodiscs. *J. Am. Chem. Soc.* **2011**, *133*, 7636-7639.

161. Jeong, S.; Yoo, D.; Jang, J.; Kim, M.; Cheon, J. Well-defined colloidal 2-D layered transition-metal chalcogenide nanocrystals via generalized synthetic protocols. *J. Am. Chem. Soc.* **2012**, *134*, 18233-18236.

162. Vaughn, D. D.; In, S.; Schaak, R. E. A precursor-limited nanoparticle coalescence pathway for tuning the thickness of laterally-uniform colloidal nanosheets: the case of SnSe. *ACS nano* **2011**, *5*, 8852-8860.

163. Schadler, L. In Nanocomposite Science and Technology; Ajayan, PM; Schadler, LS; Braun, PV, Eds. **2003**.

164. Park, S.; Bernet, N.; De La Roche, S.; Hahn, H. Processing of iron oxide-epoxy vinyl ester nanocomposites. *J. Composite Mater.* **2003**, *37*, 465-476.

165. Evora, V. M.; Shukla, A. Fabrication, characterization, and dynamic behavior of polyester/TiO_2 nanocomposites. *Materials Science and Engineering: A* **2003**, *361*, 358-366.

166. Aymonier, C.; Bortzmeyer, D.; Thomann, R.; Mülhaupt, R. Poly (methyl methacrylate)/palladium nanocomposites: synthesis and characterization of the morphological, thermomechanical, and thermal properties. *Chemistry of Materials* **2003**, *15*, 4874-4878.

167. Vaia, R. A.; Giannelis, E. P. Lattice model of polymer melt intercalation in organically-modified layered silicates. *Macromolecules* **1997**, *30*, 7990-7999.

168. Kawasumi, M.; Hasegawa, N.; Kato, M.; Usuki, A.; Okada, A. Preparation and mechanical properties of polypropylene-clay hybrids. *Macromolecules* **1997**, *30*, 6333-6338.

169. Carrado, K. A.; Xu, L. In situ synthesis of polymer-clay nanocomposites from silicate gels. *Chemistry of materials* **1998**, *10*, 1440-1445.

170. Tomasko, D. L.; Han, X.; Liu, D.; Gao, W. Supercritical fluid applications in polymer nanocomposites. *Current Opinion in Solid State and Materials Science* **2003**, *7*, 407-412.

171. Avadhani, C.; Chujo, Y. Polyimide–silica gel hybrids containing metal salts: preparation via the sol–gel reaction. *Applied organometallic chemistry* **1997**, *11*, 153-161.

172. Liu, J.; Gao, Y.; Wang, F.; Li, D.; Xu, J. Preparation and characteristic of a new class of silica/polyimide nanocomposites. *J. Mater. Sci.* **2002**, *37*, 3085-3088.

173. Kickelbick, G. Concepts for the incorporation of inorganic building blocks into organic polymers on a nanoscale. *Progress in Polymer Science* **2003**, *28*, 83-114.

174. Gyoo, P. M.; Venkataramani, S.; Kim, S. C. Morphology, thermal, and mechanical properties of polyamide 66/clay nanocomposites with epoxy-modified organoclay. *J Appl Polym Sci* **2006**, *101*, 1711-1722.

175. Erdem, N.; Cireli, A. A.; Erdogan, U. H. Flame retardancy behaviors and structural properties of polypropylene/nano-SiO_2 composite textile filaments. *J Appl Polym Sci* **2009**, *111*, 2085-2091.

176. Du, H.; Xu, G.; Chin, W.; Huang, L.; Ji, W. Synthesis, characterization, and nonlinear optical properties of hybridized CdS-polystyrene nanocomposites. *Chemistry of materials* **2002**, *14*, 4473-4479.

177. Jordan, J.; Jacob, K. I.; Tannenbaum, R.; Sharaf, M. A.; Jasiuk, I. Experimental trends in polymer nanocomposites—a review. *Materials science and engineering: A* **2005**, *393*, 1-11.

178. Berta, M.; Lindsay, C.; Pans, G.; Camino, G. Effect of chemical structure on combustion and thermal behaviour of polyurethane elastomer layered silicate nanocomposites. *Polym. Degrad. Stab.* **2006**, *91*, 1179-1191.

179. Wypych, G. *Handbook of fillers;* 1999; Vol. 1.

180. Zanetti, M.; Camino, G.; Reichert, P.; Mülhaupt, R. Thermal behaviour of poly (propylene) layered silicate nanocomposites. *Macromolecular Rapid Communications* **2001**, *22*, 176-180.

181. Modesti, M.; Lorenzetti, A.; Bon, D.; Besco, S. Thermal behaviour of compatibilised polypropylene nanocomposite: effect of processing conditions. *Polym. Degrad. Stab.* **2006**, *91*, 672-680.

182. Hull, T. R.; Price, D.; Liu, Y.; Wills, C. L.; Brady, J. An investigation into the decomposition and burning behaviour of Ethylene-vinyl acetate copolymer nanocomposite materials. *Polym. Degrad. Stab.* **2003**, *82*, 365-371.

183. Qin, H.; Zhang, S.; Zhao, C.; Hu, G.; Yang, M. Flame retardant mechanism of polymer/clay nanocomposites based on polypropylene. *Polymer* **2005**, *46*, 8386-8395.

184. Gilman, J. W.; Jackson, C. L.; Morgan, A. B.; Harris, R.; Manias, E.; Giannelis, E. P.; Wuthenow, M.; Hilton, D.; Phillips, S. H. Flammability properties of polymer-layered-silicate nanocomposites. Polypropylene and polystyrene nanocomposites. *Chemistry of Materials* **2000**, *12*, 1866-1873.

185. Zanetti, M.; Kashiwagi, T.; Falqui, L.; Camino, G. Cone calorimeter combustion and gasification studies of polymer layered silicate nanocomposites. *Chemistry of Materials* **2002**, *14*, 881-887.

186. Tang, Y.; Hu, Y.; Li, B.; Liu, L.; Wang, Z.; Chen, Z.; Fan, W. Polypropylene/montmorillonite nanocomposites and intumescent, flame- retardant montmorillonite synergism in polypropylene nanocomposites. *Journal of Polymer Science Part A: Polymer Chemistry* **2004**, *42*, 6163-6173.

187. Hasegawa, N.; Kawasumi, M.; Kato, M.; Usuki, A.; Okada, A. Preparation and mechanical properties of polypropylene-clay hybrids using a maleic anhydride-modified polypropylene oligomer. *J Appl Polym Sci* **1998**, *67*, 87-92.

188. Bureau, M.; Denault, J.; Glowacz, F. In *In Mechanical behavior and crack propagation in injection-molded polyamide 6/clay nanocomposites.* Antec 2001 Conference proceedings; 2001; , pp 5.

189. Svoboda, P.; Zeng, C.; Wang, H.; Lee, L. J.; Tomasko, D. L. Morphology and mechanical properties of polypropylene/organoclay nanocomposites. *J Appl Polym Sci* **2002**, *85*, 1562-1570.

190. Gorrasi, G.; Tortora, M.; Vittoria, V.; Kaempfer, D.; Mülhaupt, R. Transport properties of organic vapors in nanocomposites of organophilic layered silicate and syndiotactic polypropylene. *Polymer* **2003**, *44*, 3679-3685.

191. Osman, M. A.; Atallah, A. High-Density Polyethylene Micro- and Nanocomposites: Effect of Particle Shape, Size and Surface Treatment on Polymer Crystallinity and Gas Permeability. *Macromolecular rapid communications* **2004**, *25*, 1540-1544.

192. Manias, E.; Touny, A.; Wu, L.; Strawhecker, K.; Lu, B.; Chung, T. Polypropylene/montmorillonite nanocomposites. Review of the synthetic routes and materials properties. *Chemistry of Materials* **2001**, *13*, 3516-3523.

193. Hwang, W.; Wei, K.; Wu, C. Mechanical, thermal, and barrier properties of NBR/organosilicate nanocomposites. *Polymer Engineering & Science* **2004**, *44*, 2117-2124.

194. Nabok, A. *Organic And Inorganic Nanostructures (Artech House Mems and Sensors Library);* Artech House Publishers Hardcover: 286 pages: 2005.

195. Markarian, J. Automotive and packaging offer growth opportunities for nanocomposites. *Plastics, Additives and Compounding* **2005**, *7*, 18-21.

196. Presting, H.; König, U. Future nanotechnology developments for automotive applications. *Materials Science and Engineering: C* **2003**, *23*, 737-741.

197. Gao, F.; Beyer, G.; Yuan, Q. A mechanistic study of fire retardancy of carbon nanotube/ethylene vinyl acetate copolymers and their clay composites. *Polym. Degrad. Stab.* **2005**, *89*, 559-564.

198. Sanchez, C.; Julian, B.; Belleville, P.; Popall, M. Applications of hybrid organic–inorganic nanocomposites. *Journal of Materials Chemistry* **2005**, *15*, 3559-3592.

199. Camargo, P. H. C.; Satyanarayana, K. G.; Wypych, F. Nanocomposites: synthesis, structure, properties and new application opportunities. *Materials Research* **2009**, *12*, 1-39.

200. Ozawa, T. Kinetic analysis of derivative curves in thermal analysis. *Journal of Thermal Analysis and Calorimetry* **1970**, *2*, 301-324.

201. Borges, F.; Roleira, F.; Milhazes, N.; Santana, L.; Uriarte, E. Simple coumarins and analogues in medicinal chemistry: occurrence, synthesis and biological activity. *Curr. Med. Chem.* **2005**, *12*, 887-916.

202. Egan, D.; O'kennedy, R.; Moran, E.; Cox, D.; Prosser, E.; Thornes, R. D. The pharmacology, metabolism, analysis, and applications of coumarin and coumarin-related compounds. *Drug Metab. Rev.* **1990**, *22*, 503-529.

203. Moffett, R. B. Central nervous system depressants. VII. 1 pyridyl coumarins. *J. Med. Chem.* **1964**, *7*, 446-449.

204. Fylaktakidou, K. C.; Hadjipavlou-Litina, D. J.; Litinas, K. E.; Nicolaides, D. N. Natural and synthetic coumarin derivatives with anti-inflammatory/antioxidant activities. *Curr. Pharm. Des.* **2004**, *10*, 3813-3833.

205. Bucolo, C.; Cuzzocrea, S.; Mazzon, E.; Caputi, A. P. Effects of cloricromene, a coumarin derivative, on endotoxin-induced uveitis in Lewis rats. *Invest. Ophthalmol. Vis. Sci.* **2003**, *44*, 1178-1184.

206. Bucolo, C.; Ward, K. W.; Mazzon, E.; Cuzzocrea, S.; Drago, F. Protective effects of a coumarin derivative in diabetic rats. *Invest. Ophthalmol. Vis. Sci.* **2009**, *50*, 3846-3852.

207. Harvey, R. G.; Cortez, C.; Ananthanarayan, T.; Schmolka, S. A new coumarin synthesis and its utilization for the synthesis of polycyclic coumarin compounds with anticarcinogenic properties. *J. Org. Chem.* **1988**, *53*, 3936-3943.

208. Kostova, I.; Raleva, S.; Genova, P.; Argirova, R. Structure-Activity Relationships of Synthetic Coumarins as HIV-1 Inhibitors. *Bioinorg Chem. Appl.* **2006**, 68274.

209. Al-Haiza, M.; Mostafa, M.; El-Kady, M. Synthesis and biological evaluation of some new coumarin derivatives. *Molecules* **2003**, *8*, 275-286.

210. Musicki, B.; Periers, A.; Laurin, P.; Ferroud, D.; Benedetti, Y.; Lachaud, S.; Chatreaux, F.; Haesslein, J.; Iltis, A.; Pierre, C. Improved antibacterial activities of coumarin antibiotics bearing 5′, 5′-dialkylnoviose: biological activity of RU79115. *Bioorg. Med. Chem. Lett.* **2000**, *10*, 1695-1699.

211. De Silva, A. P.; Gunaratne, H. N.; Gunnlaugsson, T.; Huxley, A. J.; McCoy, C. P.; Rademacher, J. T.; Rice, T. E. Signaling recognition events with fluorescent sensors and switches. *Chem. Rev.* **1997**, *97*, 1515-1566.

212. de Silva, A. P.; Vance, T. P.; West, M. E.; Wright, G. D. Bright molecules with sense, logic, numeracy and utility. *Organic & biomolecular chemistry* **2008**, *6*, 2468-2480.

213. Soutar, I. The application of luminescence techniques in polymer science. *Polym. Int.* **1991**, *26*, 35-49.

214. Morawetz, H. On the versatility of fluorescence techniques in polymer research. *Journal of Polymer Science Part A: Polymer Chemistry* **1999**, *37*, 1725-1735.

215. Sarker, A. M.; Kaneko, Y.; Neckers, D. C. Photochemistry and photophysics of novel photoinitiators: N, N, N-tributyl-N-(4-methylene-7-methoxycoumarin) ammonium borates. *J. Photochem. Photobiol. A.* **1998**, *117*, 67-74.

216. Abd-El-Aziz, A.; Dalgakiran, S.; Kucukkaya, I.; Wagner, B. Synthesis, electrochemistry and fluorescence behavior of thiophene derivatives decorated with coumarin, pyrene and naphthalene moieties. *Electrochim. Acta* **2013**, *89*, 445-453.

217. Booth, G.; Zollinger, H.; McLaren, K.; Sharples, W. G.; Westwell, A. Dyes, general survey. *Ullmann's Encyclopedia of Industrial Chemistry* **2000**.

218. Skotheim, T. A. *Handbook of conducting polymers;* CRC press: 1997; .

219. Nicole. "Electrical conductivity of polythiophenes exfoliated nanocomposites: a thesis presented in partial fulfilment of the requirements for the Honor in Chemistry at University Prince Edward Island" (2014).

220. Sugimoto, R.; Takeda, S.; Gu, H.; Yoshino, K. Preparation of soluble polythiophene derivatives utilizing transition metal halides as catalysts and their property. *Chem.Express* **1986**, *1*, 635-638.

221. Ramakrishna Matte, H.; Gomathi, A.; Manna, A. K.; Late, D. J.; Datta, R.; Pati, S. K.; Rao, C. MoS2 and WS2 analogues of graphene. *Angewandte Chemie* **2010**, *122*, 4153-4156.

222. Abd-El-Aziz, A. S.; De Denus, C. R.; Todd, E. K.; Bernardin, S. A. Design of polyaromatic ethers using cyclopentadienyliron complexes. *Macromolecules* **2000**, *33*, 5000-5005.

223. Ramos, J. C.; Souto-Maior, R. M.; Navarro, M. Synthesis and characterization of chiral polythiophenes: Poly [(R)-(−) and (S)-( )-2-(3′-thienyl) ethyl N-(3 ″, 5 ″-dinitrobenzoyl)-α-phenylglycinate]. *Polymer* **2006**, *47*, 8095-8100.

224. Lane, B.; Alsaedi, W. H.; Dahn, D. C.; Kucukkaya, I.; Bissessur, R.; Abd-El-Aziz, A. S. In *In Exfoliated polyaniline-WS2 nanocomposites;* ABSTRACTS OF PAPERS OF THE AMERICAN CHEMICAL SOCIETY; AMER CHEMICAL SOC 1155 16TH ST, NW, WASHINGTON, DC 20036 USA: 2014; Vol. 248.

225. Lim, E.; Jung, B.; Shim, H. Synthesis and characterization of a new light-emitting fluorene-thieno [3, 2-b] thiophene-based conjugated copolymer. *Macromolecules* **2003**, *36*, 4288-4293.

226. Ma, W.; Yang, C.; Gong, X.; Lee, K.; Heeger, A. J. Thermally stable, efficient polymer solar cells with nanoscale control of the interpenetrating network morphology. *Advanced Functional Materials* **2005**, *15*, 1617-1622.

227. Tourillon, G.; Garnier, F. New electrochemically generated organic conducting polymers. *Journal of Electroanalytical Chemistry and Interfacial Electrochemistry* **1982**, *135*, 173-178.

228. Chen, S. A.; Fang, W. G. Electrically conductive polyaniline-poly (vinyl alcohol) composite films: Physical properties and morphological structures. *Macromolecules* **1991**, *24*, 1242-1248.

229. Chiang, J.; MacDiarmid, A. G. 'Polyaniline': protonic acid doping of the emeraldine form to the metallic regime. *Synth. Met.* **1986**, *13*, 193-205.

230. Duek, E. A.; De Paoli, M.; Mastragostino, M. An electrochromic device based on polyaniline and prussian blue. *Adv Mater* **1992**, *4*, 287-291.

231. Kaneko, M.; Nakamura, H. Photoresponse of a liquid junction polyaniline film. *Journal of the Chemical Society, Chemical Communications* **1985**, 346-347.

232. Kanatzidis, M. G. Conductive polymers. *Chemical & engineering news* **1990**, *68*.

233. Gustafsson, G.; Cao, Y.; Treacy, G.; Klavetter, F.; Colaneri, N.; Heeger, A. Flexible light-emitting diodes made from soluble conducting polymers. *Nature* **1992**, *357*, 477-479.

234. Parker, I. D. Carrier tunneling and device characteristics in polymer light- emitting diodes. *J. Appl. Phys.* **1994**, *75*, 1656-1666.

235. Trinidad, F.; Montemayor, M.; Fatas, E. Performance Study of Zn/ZnCl2, NH 4Cl/Polyaniline/Carbon Battery. *J. Electrochem. Soc.* **1991**, *138*, 3186-3189.

236. Nishino, H.; Yu, G.; Heeger, A.; Chen, T.; Rieke, R. Electroluminescence from blend films of poly (3-hexylthiophene) and poly (N-vinylcarbazole). *Synth. Met.* **1995**, *68*, 243-247.

237. Genies, E.; Lapkowski, M.; Santier, C.; Vieil, E. Polyaniline, spectroelectrochemistry, display and battery. *Synth. Met.* **1987**, *18*, 631-636.

238. Duek, E. A.; De Paoli, M.; Mastragostino, M. An electrochromic device based on polyaniline and prussian blue. *Adv Mater* **1992**, *4*, 287-291.

239. Deshpande, M.; Amalnerkar, D. Biosensors prepared from electrochemically-synthesized conducting polymers. *Progress in polymer science* **1993**, *18*, 623-649.

240. Radisavljevic, B.; Radenovic, A.; Brivio, J.; Giacometti, V.; Kis, A. Single-layer MoS2 transistors. *Nature nanotechnology* **2011**, *6*, 147-150.

241. Lopez-Sanchez, O.; Lembke, D.; Kayci, M.; Radenovic, A.; Kis, A. Ultrasensitive photodetectors based on monolayer MoS2. *Nature nanotechnology* **2013**, *8*, 497-501.

6-Apendix.

Table 2.10: The vibrational spectrum changes of the functional group for 10%WS_2-PThN nanocomposites in comparison to the pure PThN.

Functional group	Pure polymer	10%WS_2-PThN nanocomposites
C=O ester	1732 cm^{-1} (strong)	1713 cm^{-1} (medium)
C-O ester	1177 cm^{-1} (strong)	1180 cm^{-1} (strong)
C-H β- thiophene stretch	3096 cm^{-1} (weak)	3073 cm^{-1} (medium)
C=C aromatic	1511cm^{-1} (weak)	1584 cm^{-1} (weak)
C-H "oop"	734 cm^{-1} (strong) 812 cm^{-1} (strong)	738 cm^{-1} (strong) 807 cm^{-1} (strong)
C-H aromatic	2850 cm^{-1} (weak)	2848 cm^{-1} (medium)

Table 2.11: The vibrational spectrum changes of the functional group for 20%WS_2-PThN nanocomposites in comparison to the pure PThN.

Functional group	Pure polymer	20%WS_2-PThN nanocomposites
C=O ester	1732 cm^{-1} (strong)	1616 cm^{-1} (medium)
C-O ester	1177 cm^{-1} (strong)	1180 cm^{-1} (strong)
C-H β- thiophene stretch	3096 cm^{-1} (weak)	3048 cm^{-1} (weak)
C=C aromatic	1511 cm^{-1} (weak)	1557 cm^{-1} (medium)
C-H "oop"	734 cm^{-1} (strong) 812 cm^{-1} (strong)	749 cm^{-1} (strong) 803 cm^{-1} (strong)
C-H aromatic	2850 cm^{-1} (weak)	2854cm^{-1} (medium)

Table 2.12: The vibrational spectrum changes of the functional group for 37 %WS_2-PThN nanocomposites in comparison to the pure PThN.

Functional group	Pure polymer	37%WS_2-PThN nanocomposites
C=O ester	1732 cm^{-1} (strong)	1622 cm^{-1}(medium)
C-O ester	1177 cm^{-1} (strong)	1194 cm^{-1} (strong)
C-H β- thiophene stretch	3096 cm^{-1} (weak)	3041 cm^{-1} (weak)
C=C aromatic	1511 cm^{-1} (weak)	1557 cm^{-1} (medium)
C-H "oop"	734 cm^{-1} (strong) 812 cm^{-1} (strong)	747 cm^{-1} (strong) 802 cm^{-1} (strong)
C-H aromatic	2850 cm^{-1} (weak)	2845 cm^{-1} (medium)

Table 2.13: The vibrational spectrum changes of the functional group for 64%WS_2-PThN nanocomposites in comparison to the pure PThN.

Functional group	Pure polymer	64%WS_2-PThN nanocomposites
C=O ester	1732 cm^{-1} (strong)	1664 cm^{-1} (medium)
C-O ester	1177 cm^{-1} (strong)	1197 cm^{-1} (strong)
C-H β- thiophene stretch	3096 cm^{-1} (weak)	3037 cm^{-1} (weak)
C=C aromatic	1511 cm^{-1} (weak)	1595 cm^{-1} (medium)
C-H "oop"	734 cm^{-1} (strong) 812 cm^{-1} (strong)	727 cm^{-1} (strong) 804 cm^{-1} (strong)
C-H aromatic	2850 cm^{-1} (weak)	2849 cm^{-1} (medium)

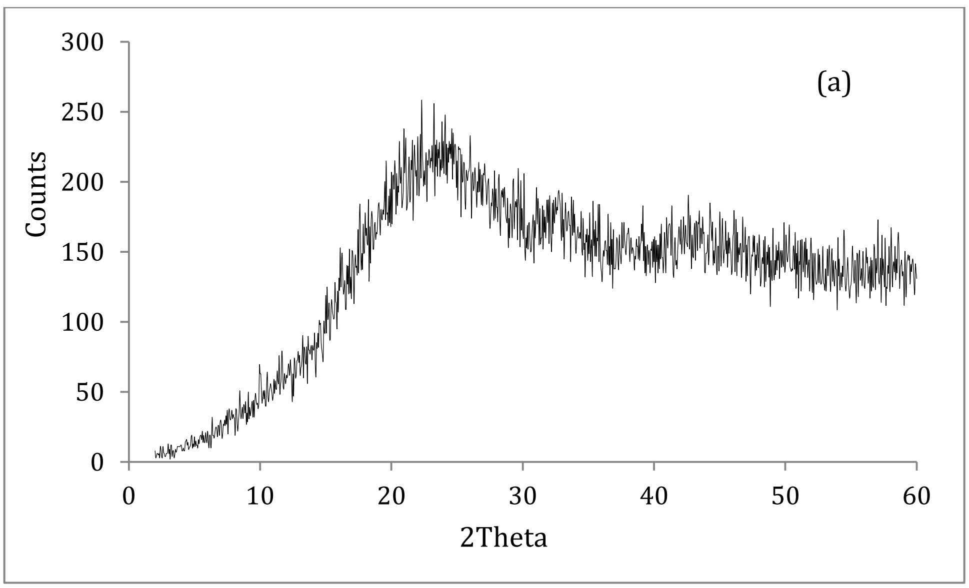

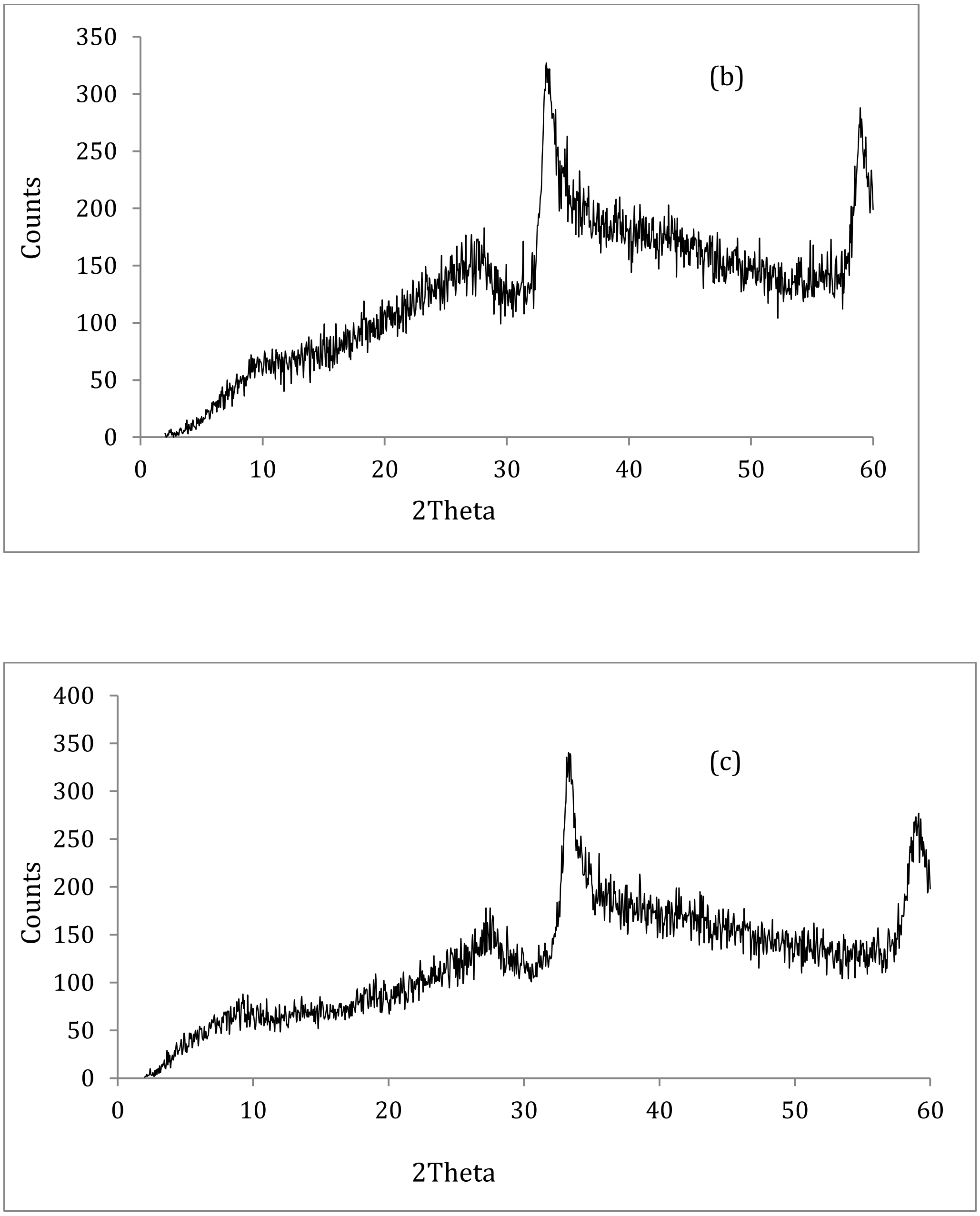

Figure 2.15: The XRD of 5% (a), 20 (b), 37% WS_2-PThN (c) nanocomposite.

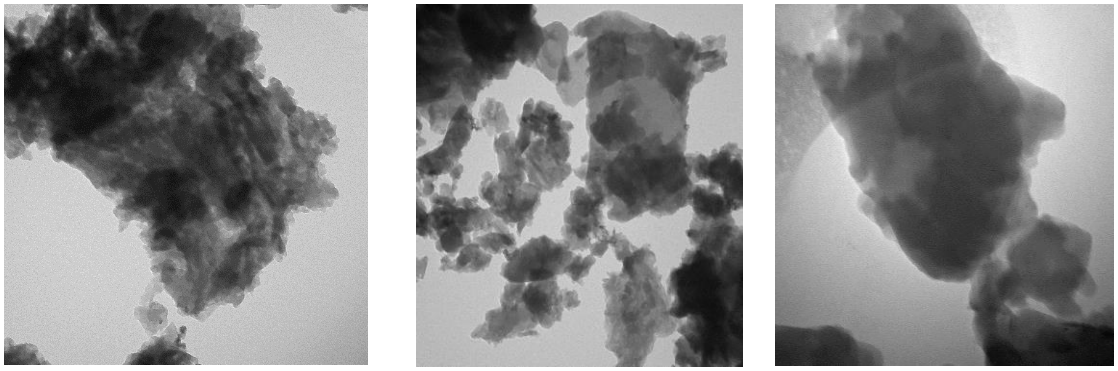

Figure 2.16:TEM micrograph of 1% WS_2-PThN (left), 20% WS_2-PThN and 64% WS_2-PThN nanocomposites.

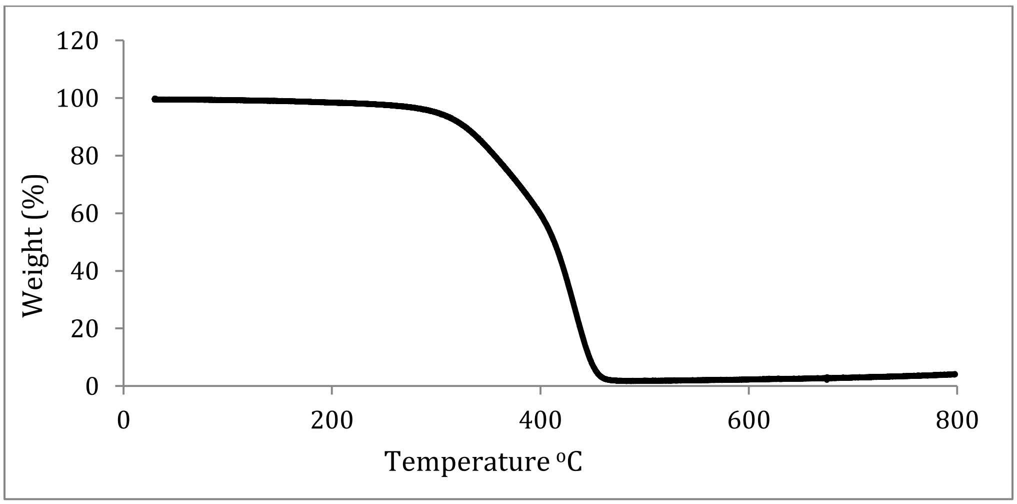

Figure 2.16: Overlay TGA of pure PTh at 5°C/min.

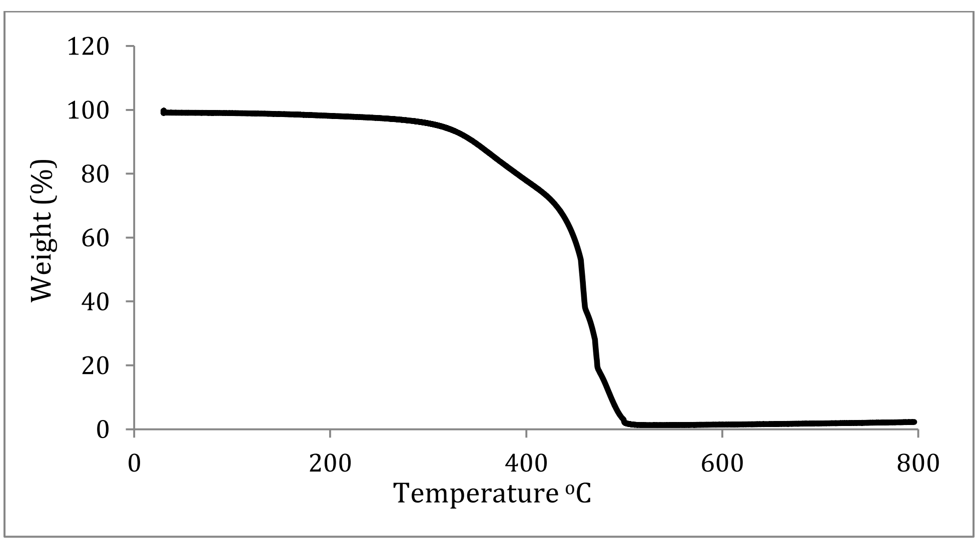

Figure2.17: Overlay TGA of pure PTh at 10°C/min.

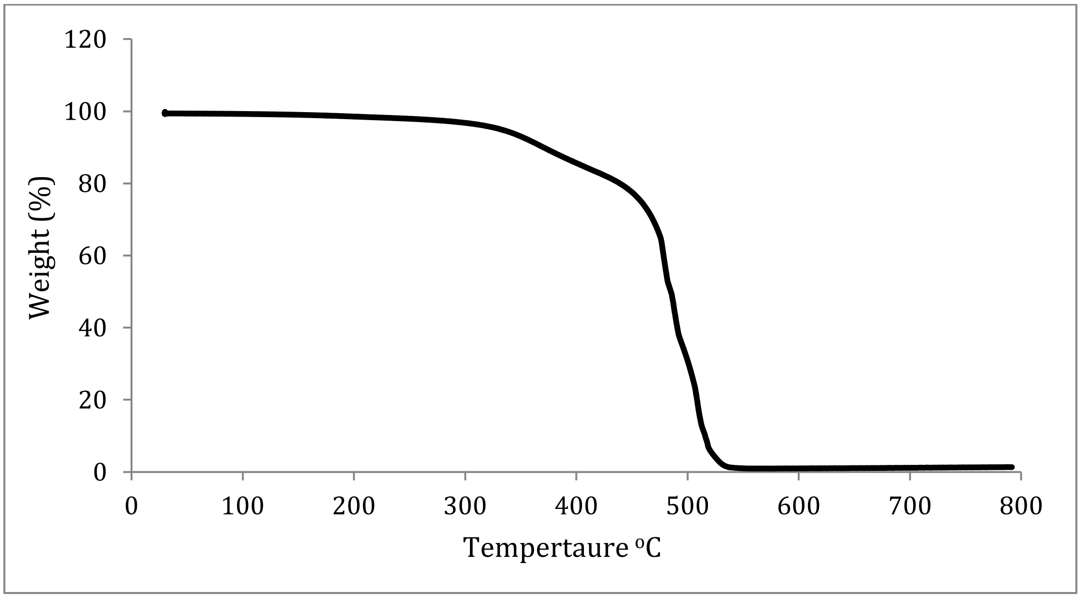

Figure 2.18: Overlay TGA of pure PTh at 20°C/min.

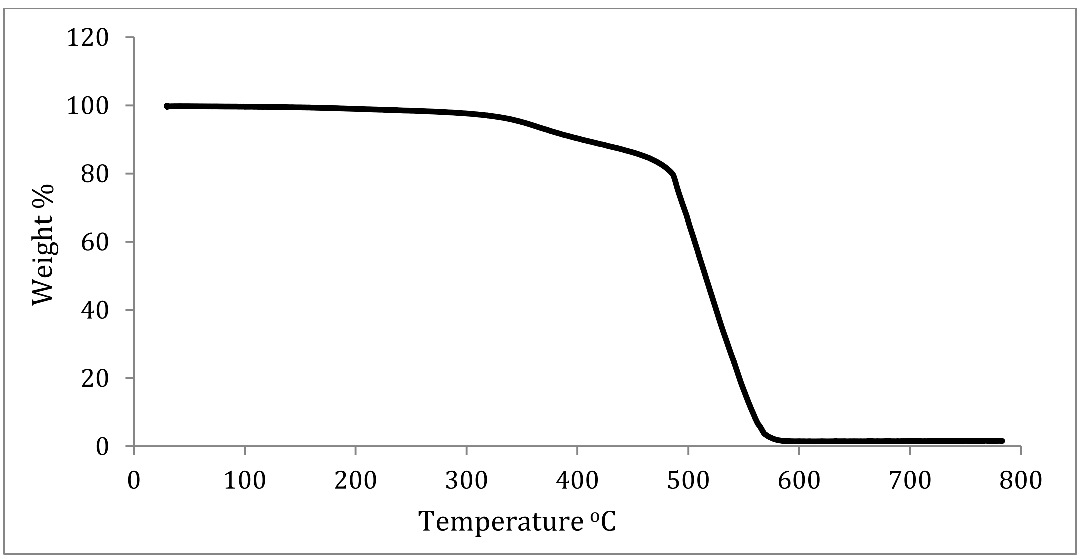

Figure 2.19: Overlay TGA of pure PTh at 40°C/min.

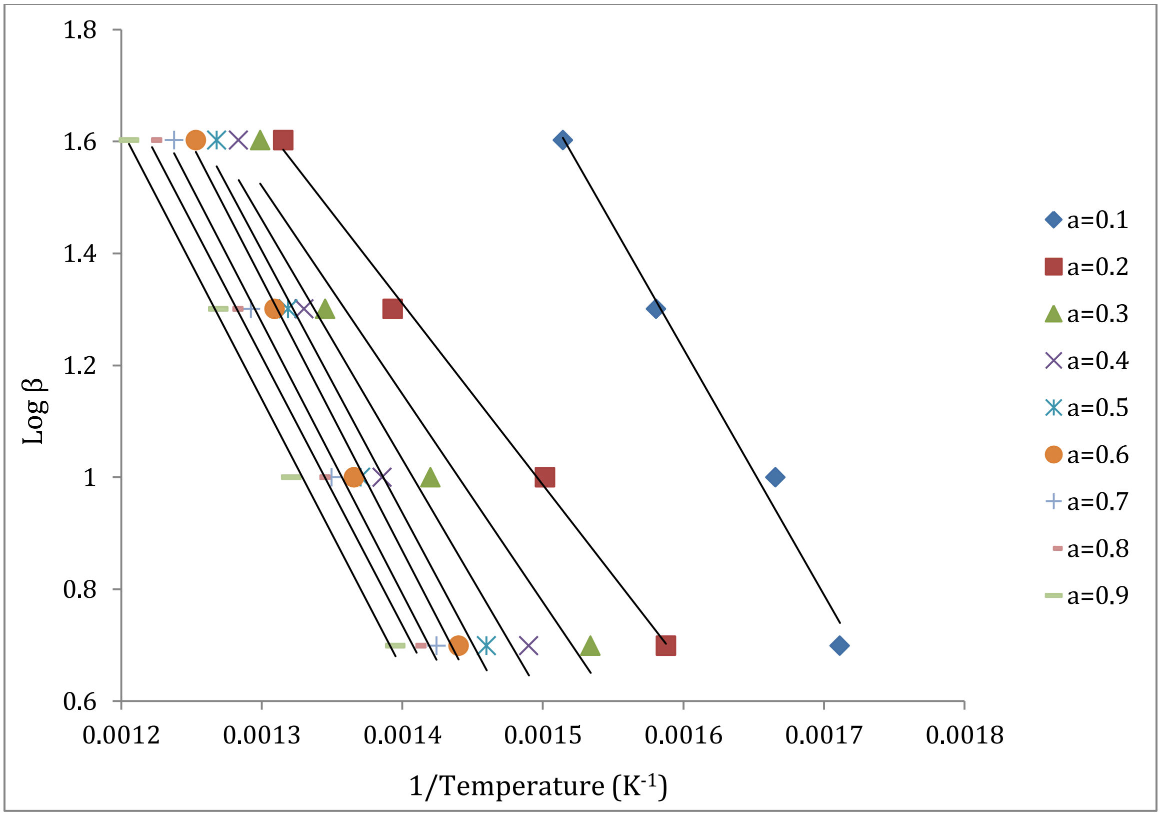

Figure 2.20: The regression lines for conversion of 0.1 -0.9 based on the Ozawa's method for pure PTh.

Table 2.14: The correlation coefficient (R) and the activation energy (Ea) obtained using Ozawa's method for pure PTh.

Sample	Conversion α	R	Ea (kJ/mol)
0% WS_2 by weight	0.1	0.9882	78.2
	0.2	0.9963	58.9
	0.3	0.9635	67.6
	0.4	0.9614	77.9
	0.5	0.9780	85.3
	0.6	0.9947	88.2
	0.7	0.9943	88.1
	0.8	0.9986	87.2
	0.9	0.9955	87.8
Average			79.9

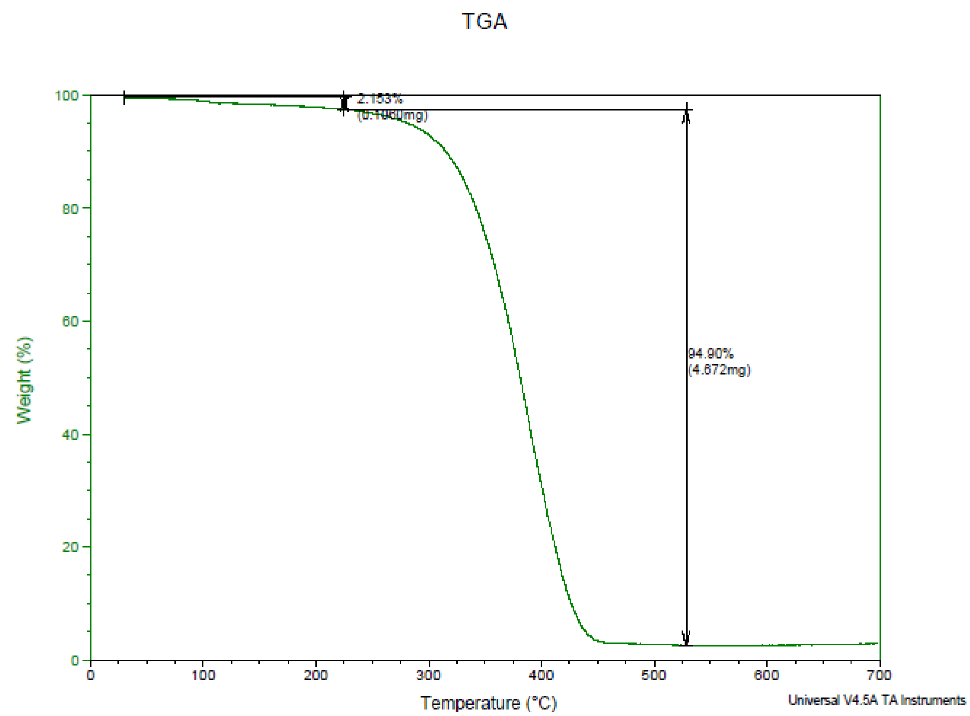

Figure 2.21: Overlay TGA of 1% WS_2- PTh at 5°C/min.

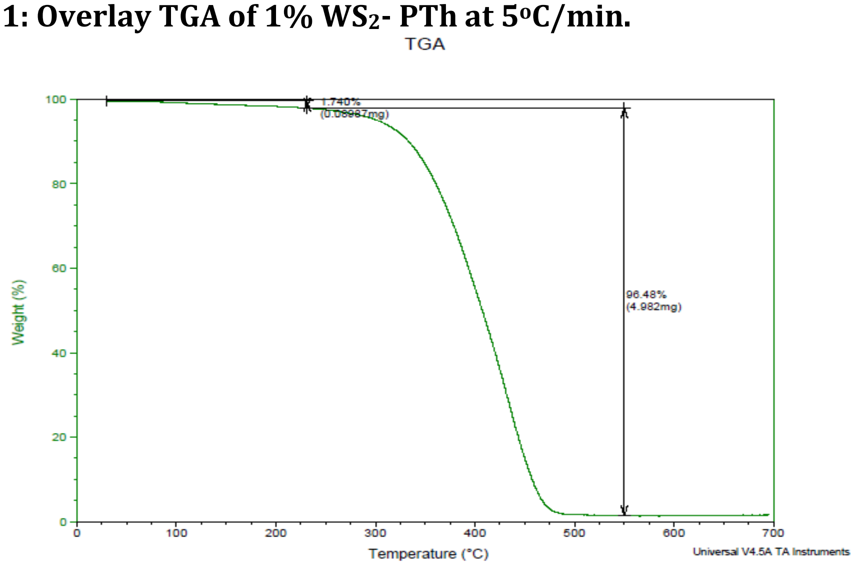

Figure 2.22: Overlay TGA of 1% WS_2- PTh at 10°C/min

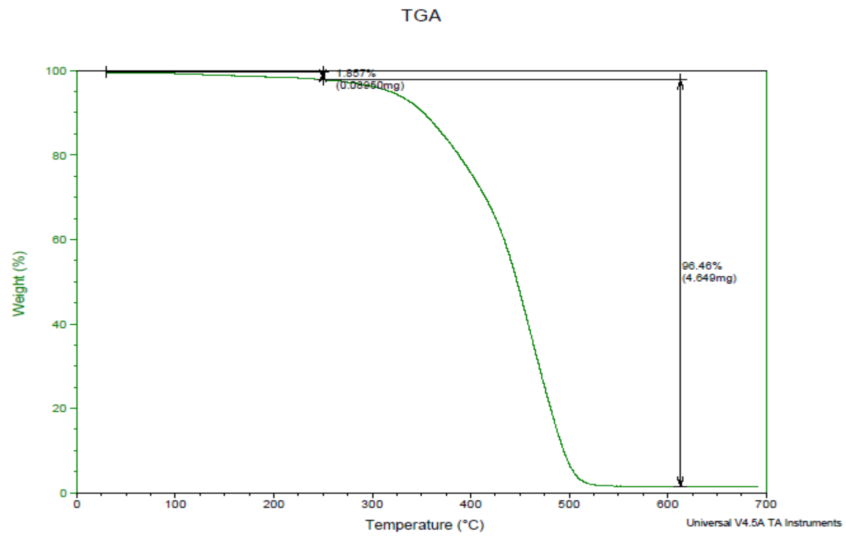

Figure 2.23: Overlay TGA of 1% WS_2- PTh at 20^{o}C/min.

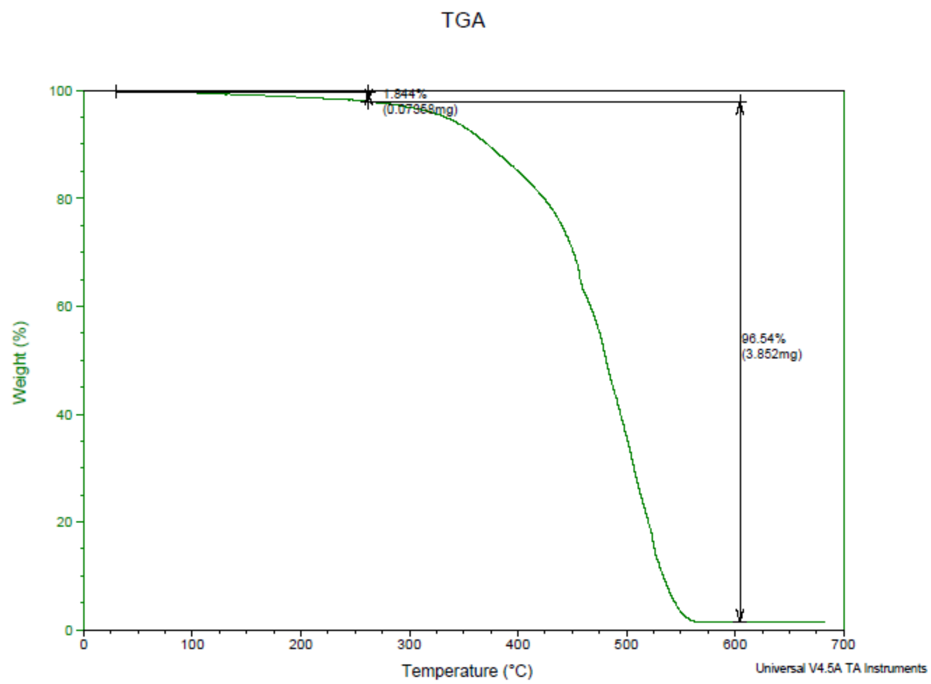

Figure 2.24: Overlay TGA of 1% WS_2- PTh at 40^{o}C/min.

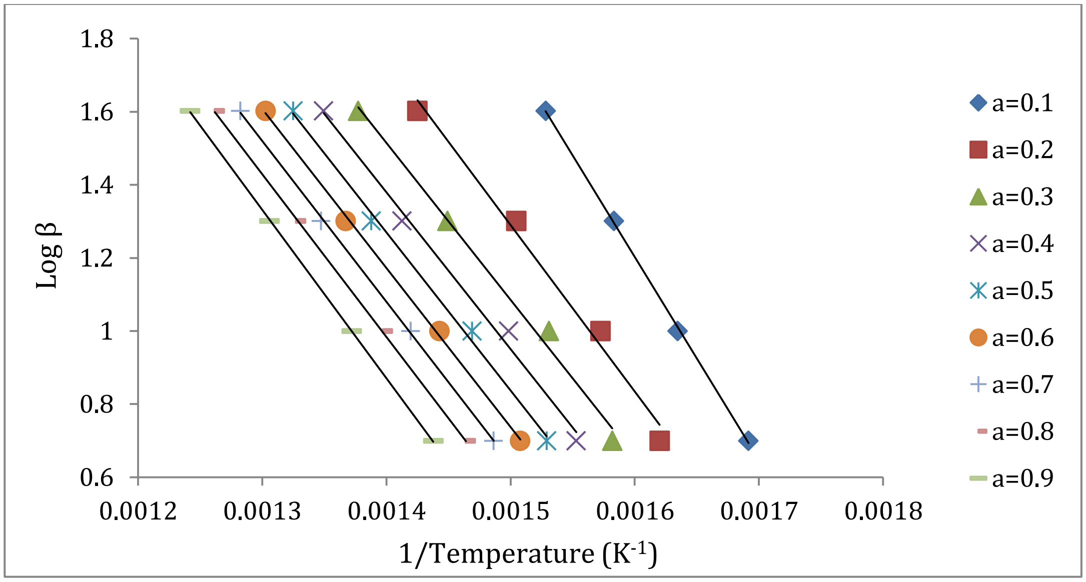

Figure 2.25: The regression lines for conversion of 0.1 -0.9 based on the Ozawa's method for 1%WS_2-PTh.

Table 2.15: The correlation coefficient (R) and the activation energy (Ea) obtained using Ozawa's method for 1%WS_2-PTh nanocomposite.

Sample	Conversion α	R	Ea (kJ/mol)
1% WS_2 by weight	0.1	0.9989	101.1
	0.2	0.9878	82.8
	0.3	0.9920	78.1
	0.4	0.9931	87.2
	0.5	0.9966	78.6
	0.6	0.9990	79.2
	0.7	0.9996	80.0
	0.8	0.9998	81.0
	0.9	0.9999	83.8
Average			83.1

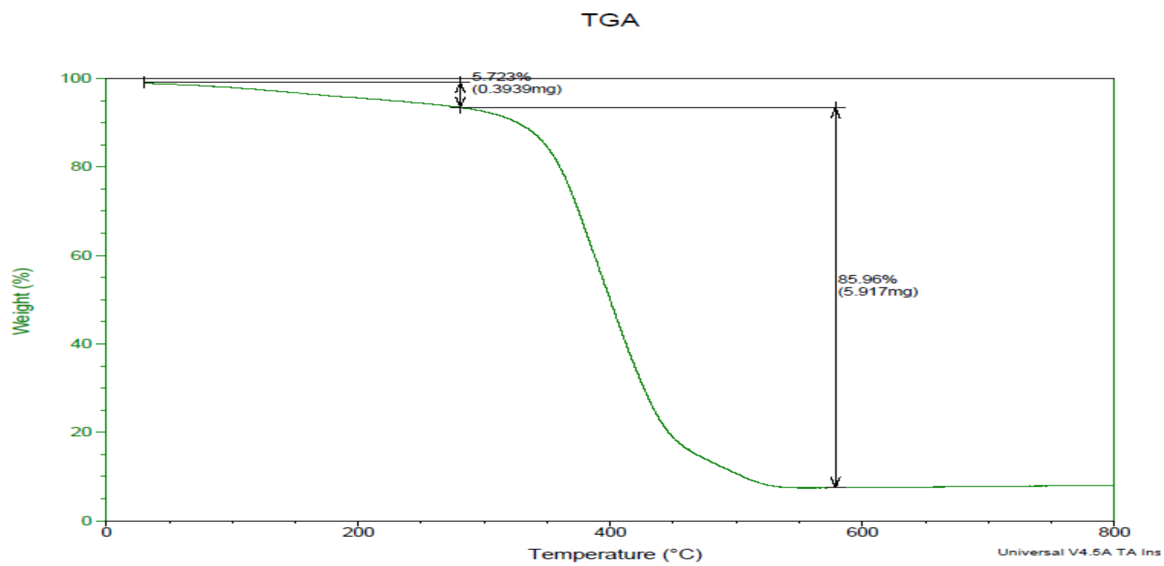

Figure 2.26: Overlay TGA of 5 % WS_2- PTh at 5°C/min.

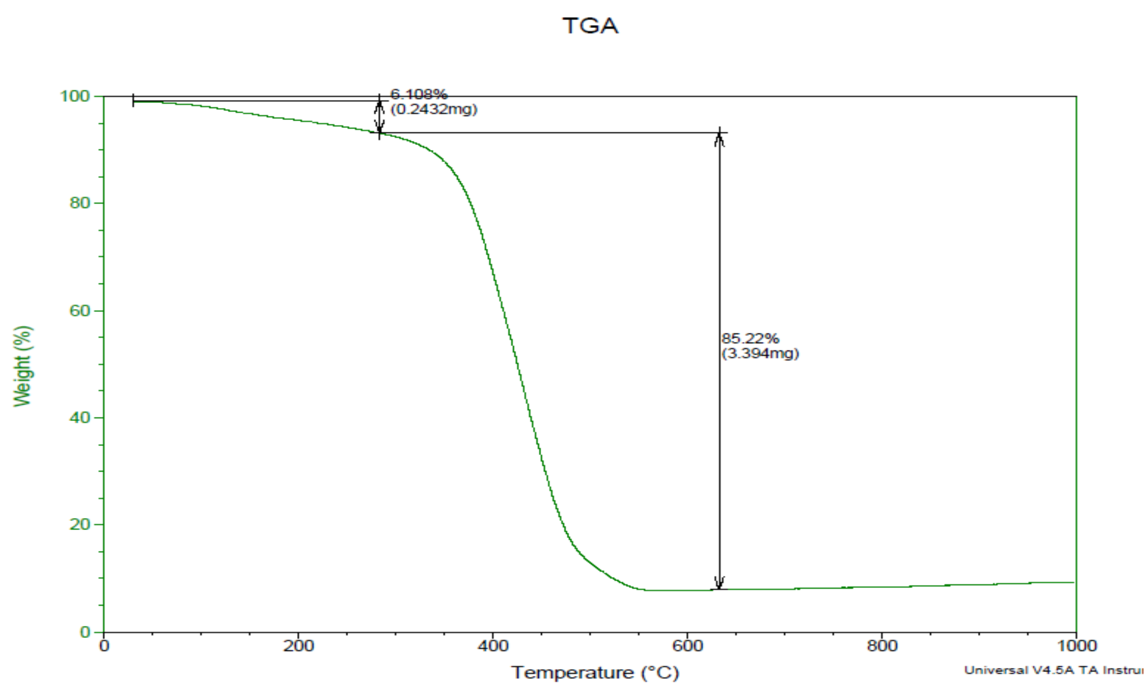

Figure 2.27: Overlay TGA of 5 % WS_2- PTh at 10°C/min.

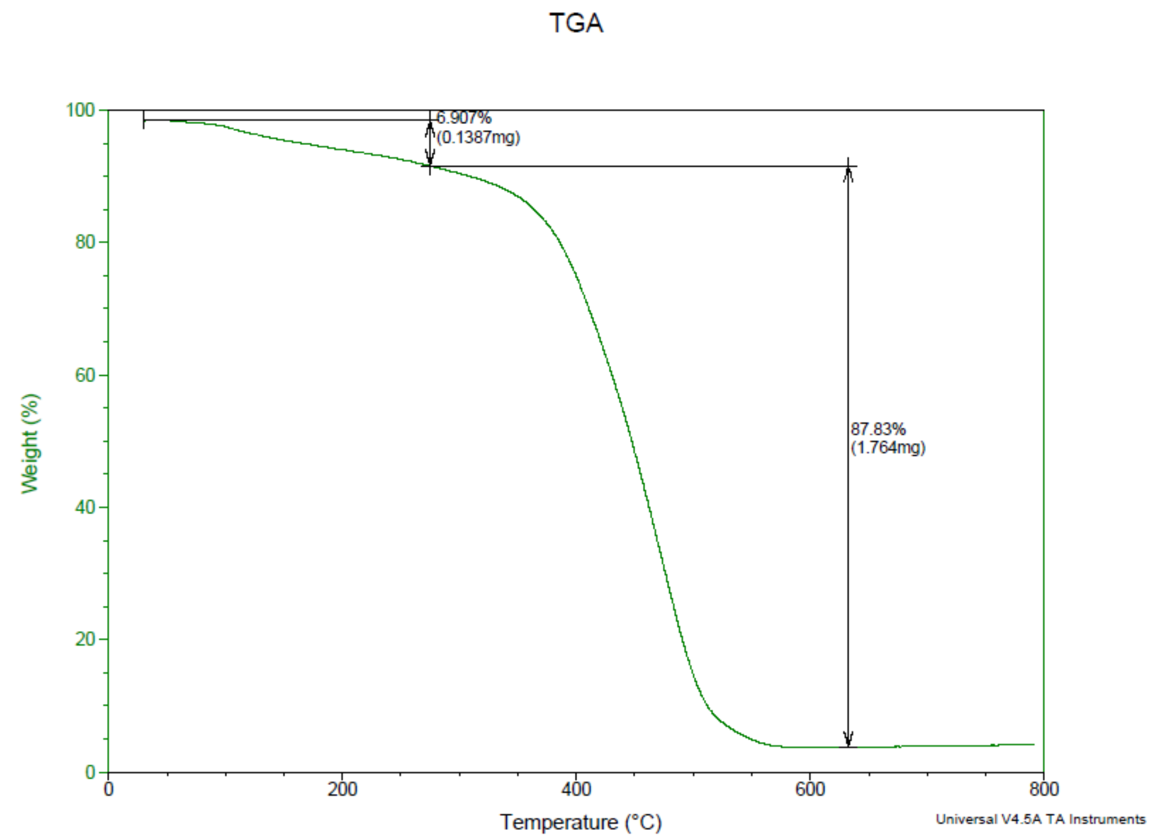

Figure 2.28: Overlay TGA of 5 % WS_2- PTh at 20^{o}C/min.

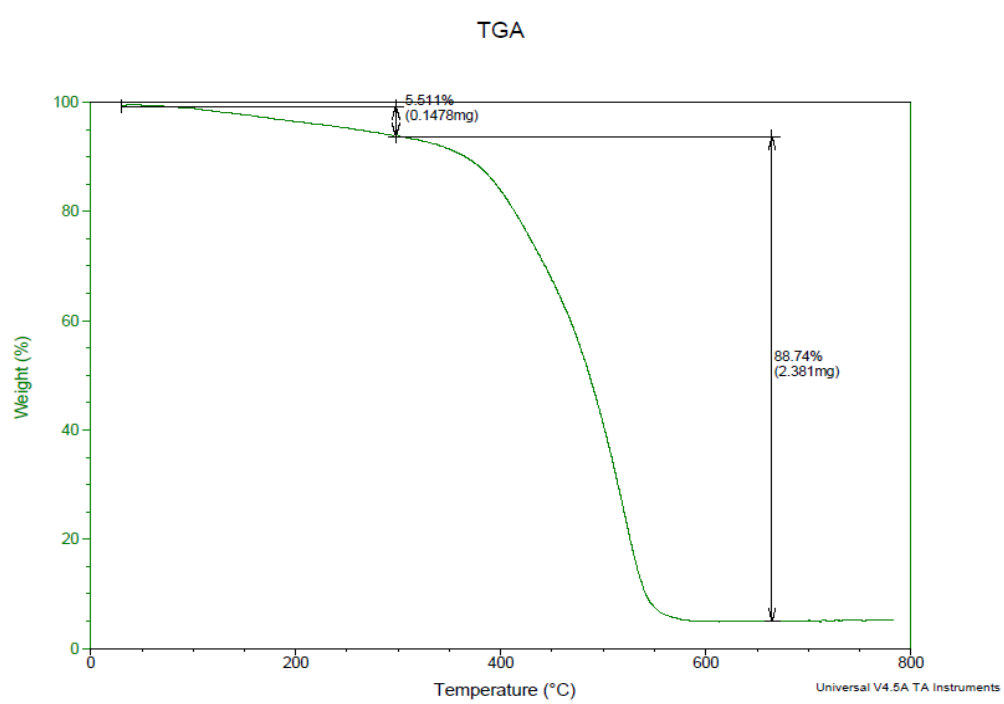

Figure 2.29: Overlay TGA of 5 % WS_2- PTh at 40^{o}C/min.

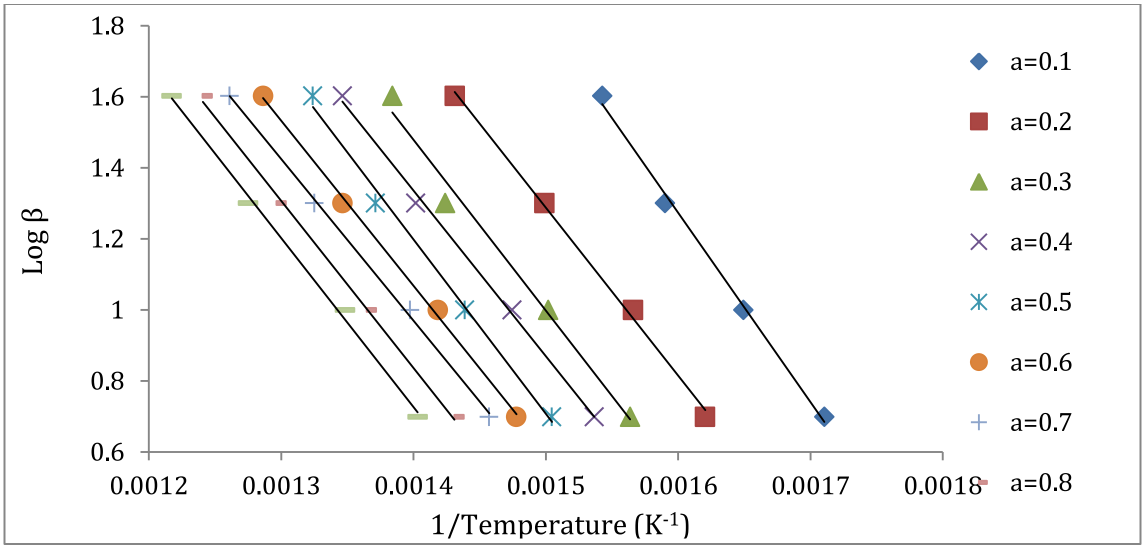

Figure 2.30: The regression lines for conversion of 0.1 -0.9 based on the Ozawa's method for pure 5%WS_2-PTh.

Table 2.16: The correlation coefficient (R) and the activation energy (Ea) obtained using Ozawa's method for 5%WS_2-PTh.

Sample	Conversion α	R	Ea (kJ/mol)
5% WS_2 by weight	0.1	0.9968	96.9
	0.2	0.9975	86.0
	0.3	0.9978	87.5
	0.4	0.9966	84.8
	0.5	0.9935	89.3
	0.6	0.9998	84.6
	0.7	0.9987	82.7
	0.8	0.9949	85.5
	0.9	0.9994	86.5
Average			87.1

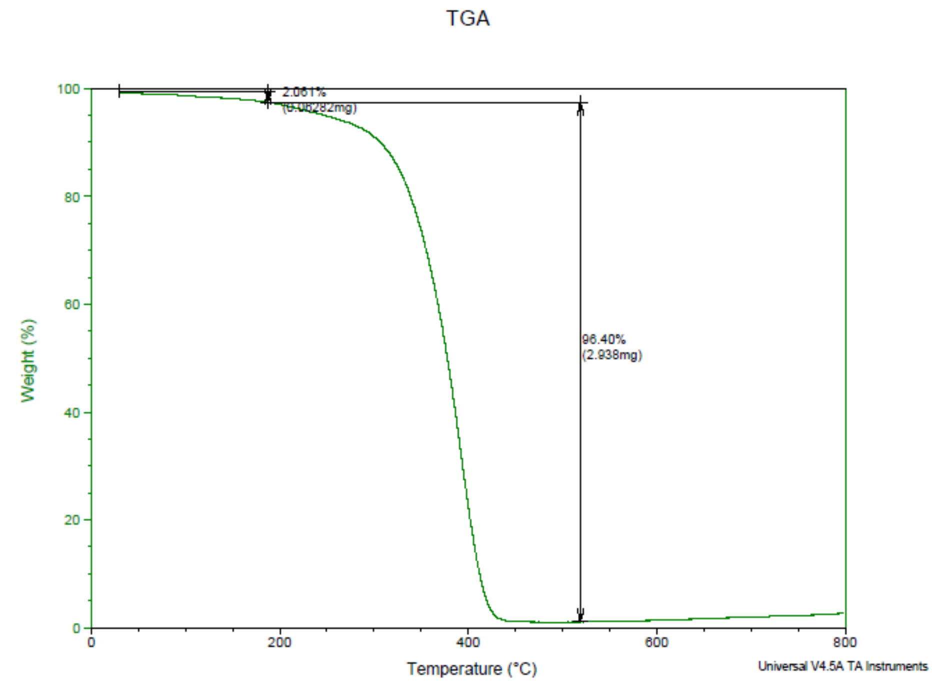

Figure 2.31: Overlay TGA of 10% WS_2- PTh at 5°C/min.

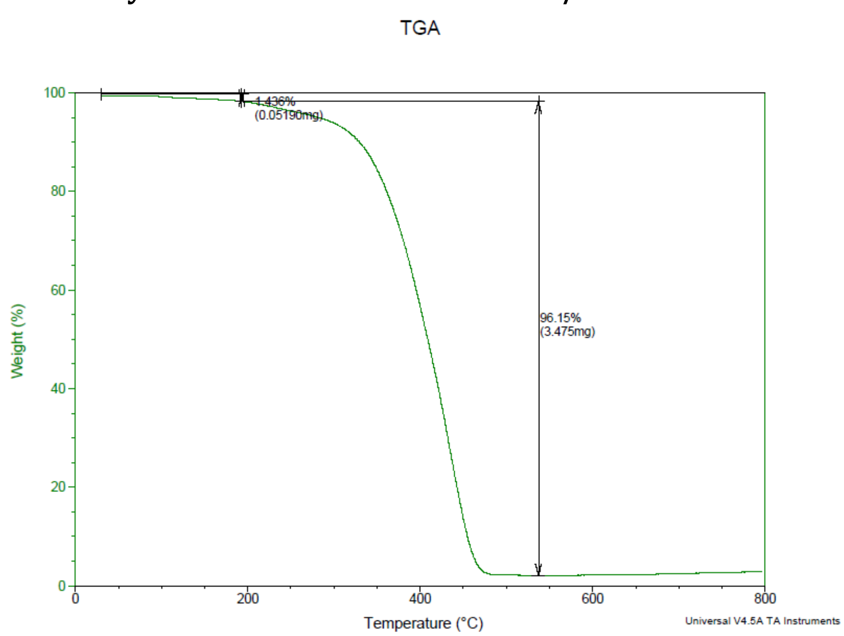

Figure 2.32 : Overlay TGA of 10% WS_2- PTh at 10°C/min

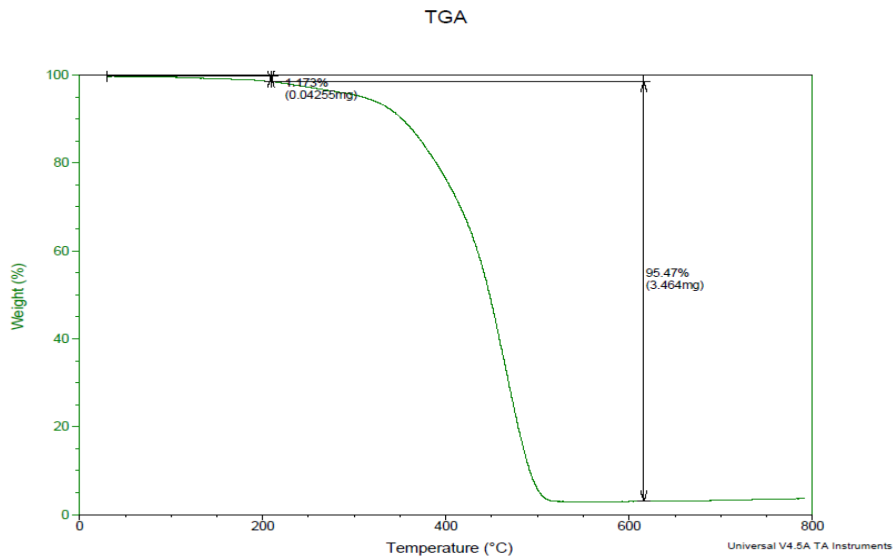

Figure 2.33: Overlay TGA of 10% WS_2- PTh at 20^{o}C/min

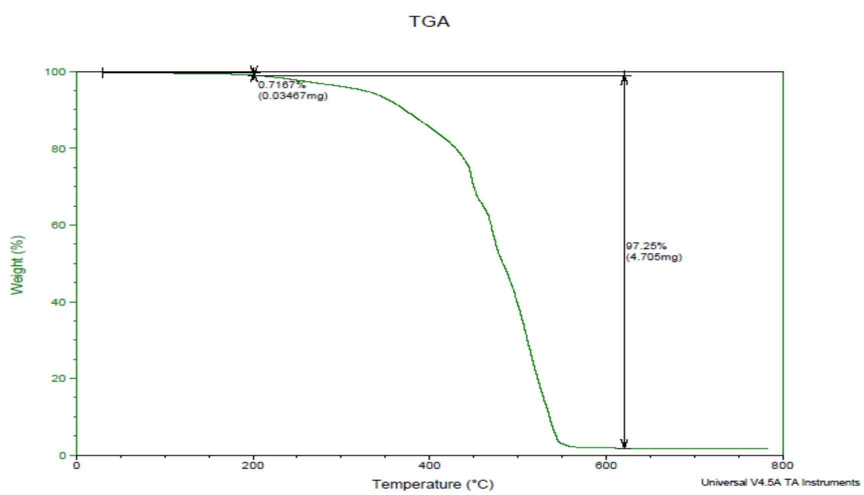

Figure 2.34: Overlay TGA of 10% WS_2- PTh at 40^{o}C/min

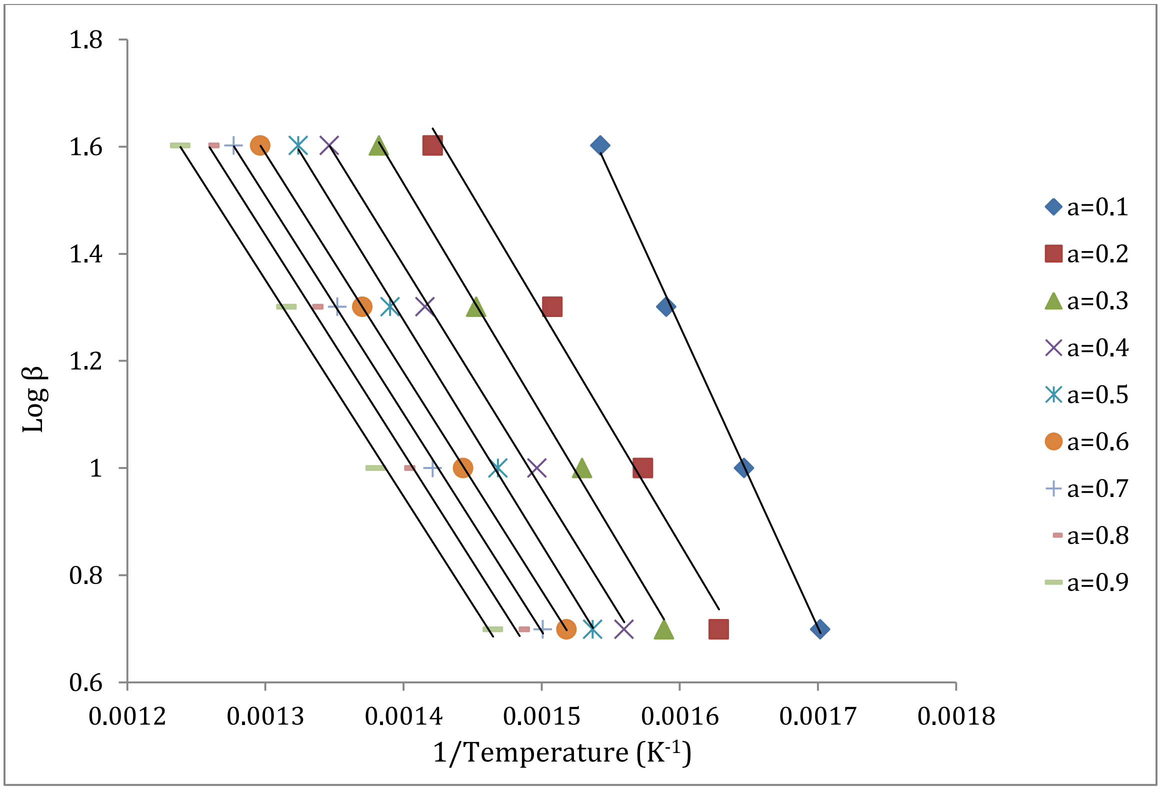

Figure 2.35: The regression lines for conversion of 0.1 -0.9 based on the Ozawa's method for 10%WS_2-PTh.

Table 2.17: The correlation coefficient (R) and the activation energy (Ea) obtained using Ozawa's method for 10%WS_2-PTh.

Sample	Conversion α	R	Ea (kJ/mol)
10 % WS_2 by weight	0.1	0.9986	102.4
	0.2	0.9891	78.8
	0.3	0.9975	78.5
	0.4	0.9979	75.7
	0.5	0.9990	76.2
	0.6	0.9999	74.2
	0.7	0.9993	73.8
	0.8	0.9983	73.8
	0.9	0.9975	73.4
Average			78.5

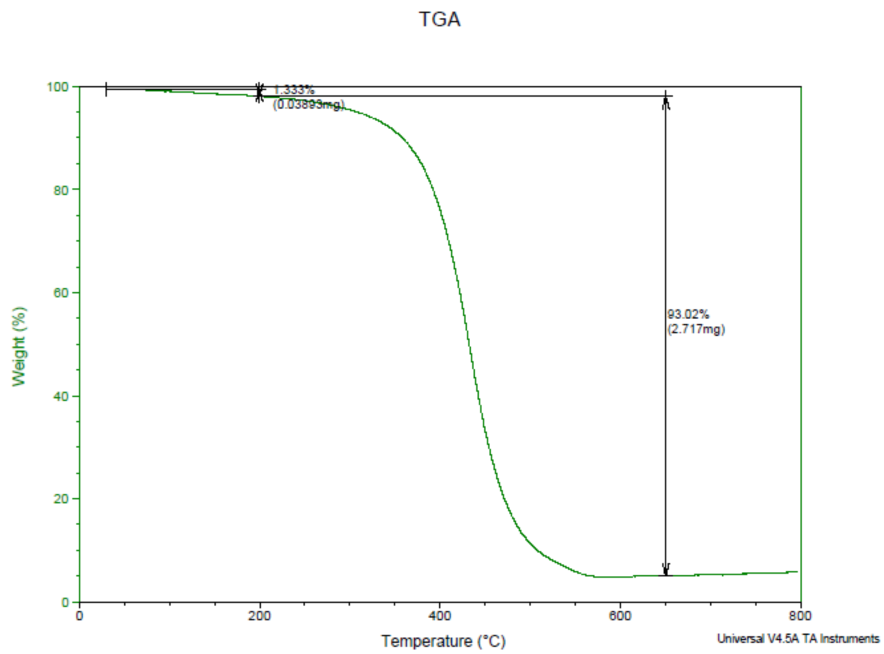

Figure 2.36: Overlay TGA of 20% WS_2- PTh at 5°C/min

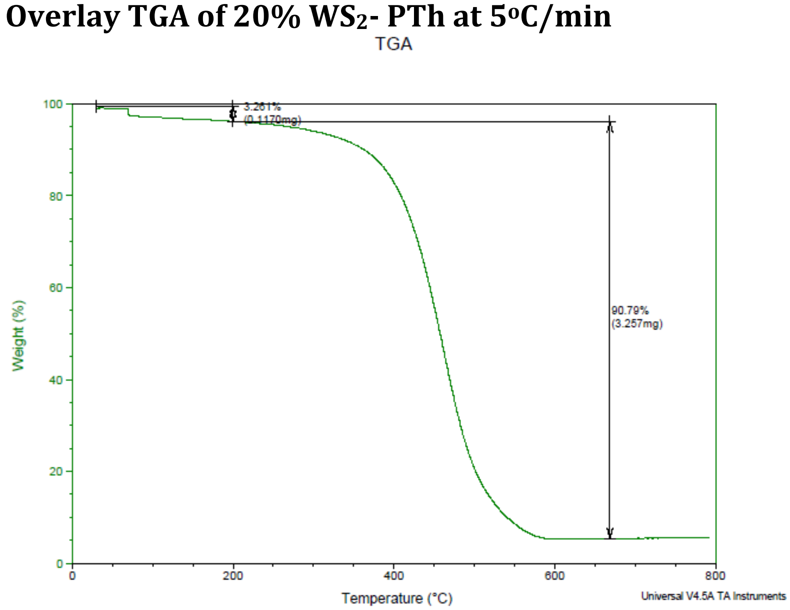

Figure 2.37: Overlay TGA of 20% WS_2- PTh at 10°C/min

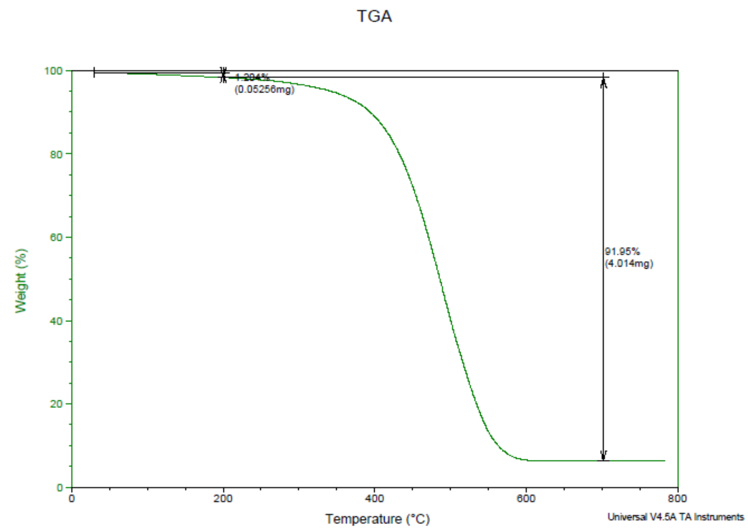

Figure 2.38: Overlay TGA of 20% WS_2- PTh at 20°C/min

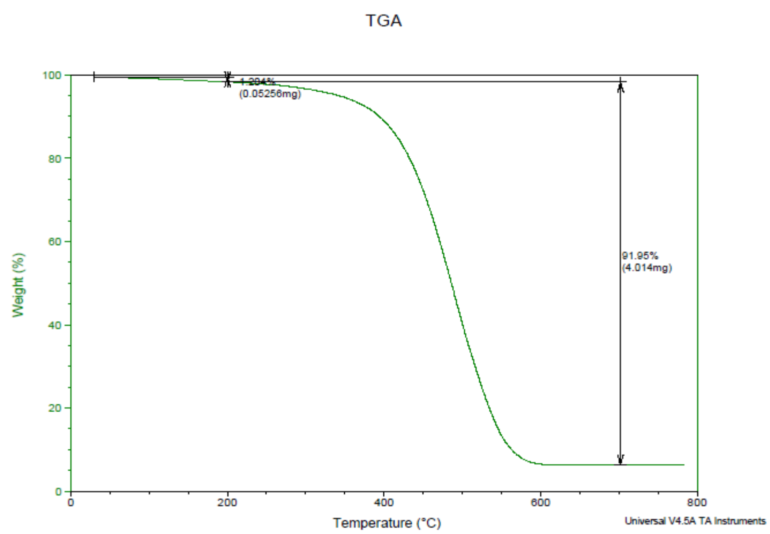

Figure 2.39: Overlay TGA of 20% WS_2- PTh at 40°C/min

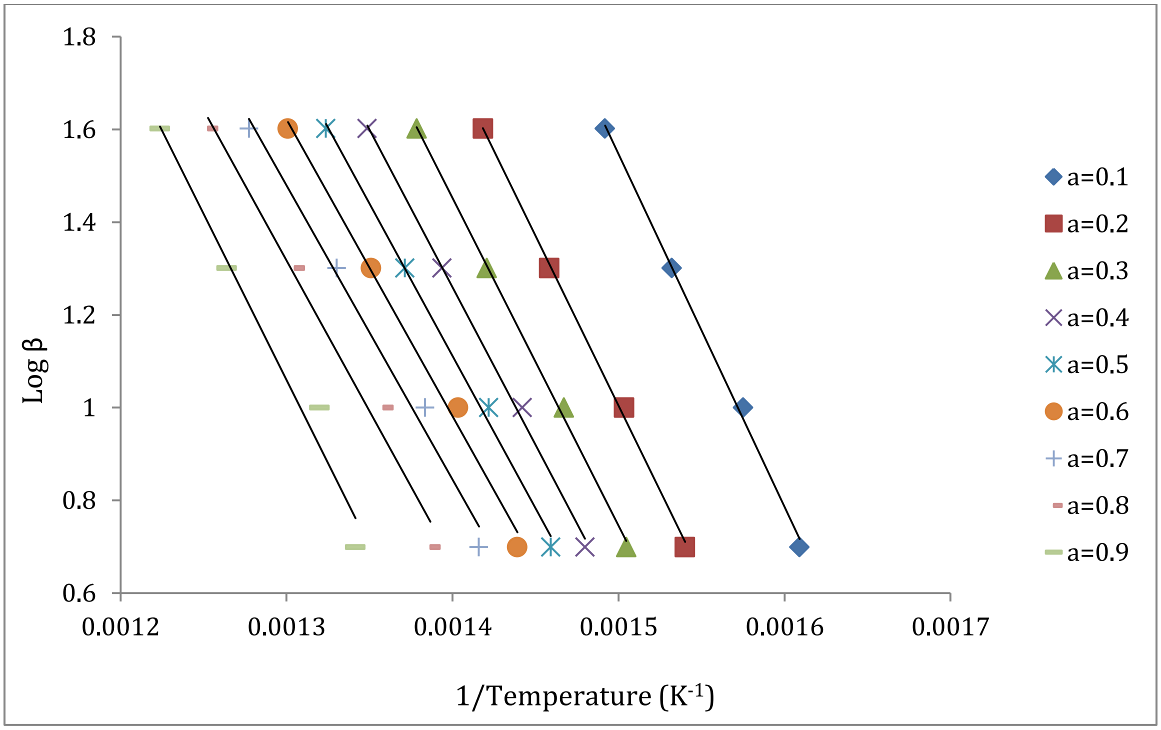

Figure 2.40: The regression lines for conversion of 0.1 -0.9 based on the Ozawa's method for 20 %WS_2-PTh.

Table 2.18: The correlation coefficient (R) and the activation energy (Ea) obtained using Ozawa's method for 20%WS_2-PTh.

Sample	Conversion α	R	Ea (kJ/mol)
20 % WS_2 by weight	0.1	0.9977	138.5
	0.2	0.9986	133.3
	0.3	0.9984	128.5
	0.4	0.9976	123.6
	0.5	0.9961	119.4
	0.6	0.9936	116.5
	0.7	0.9886	115.5
	0.8	0.9831	118.2
	0.9	0.9752	130.4
Average			124.9

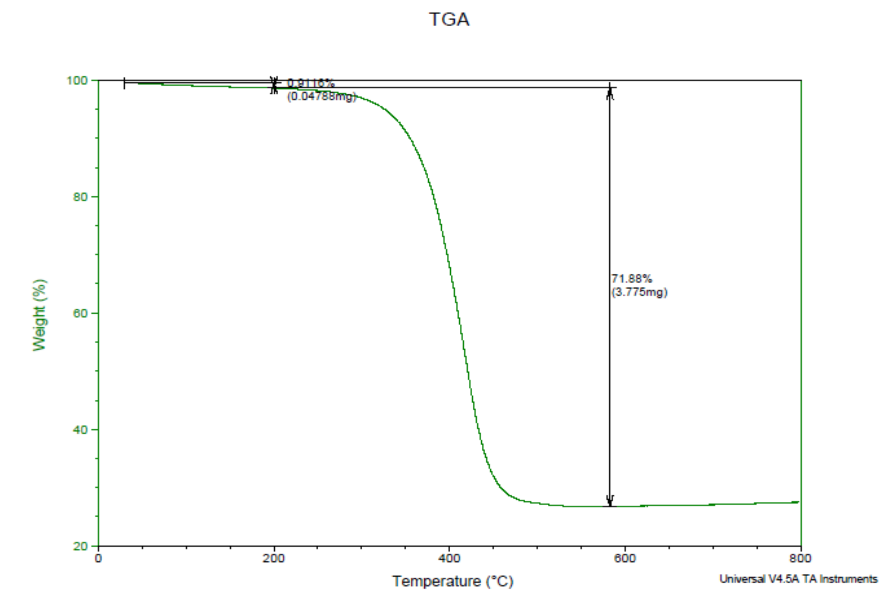

Figure 2.41: Overlay TGA of 37% WS_2- PTh at 5°C/min

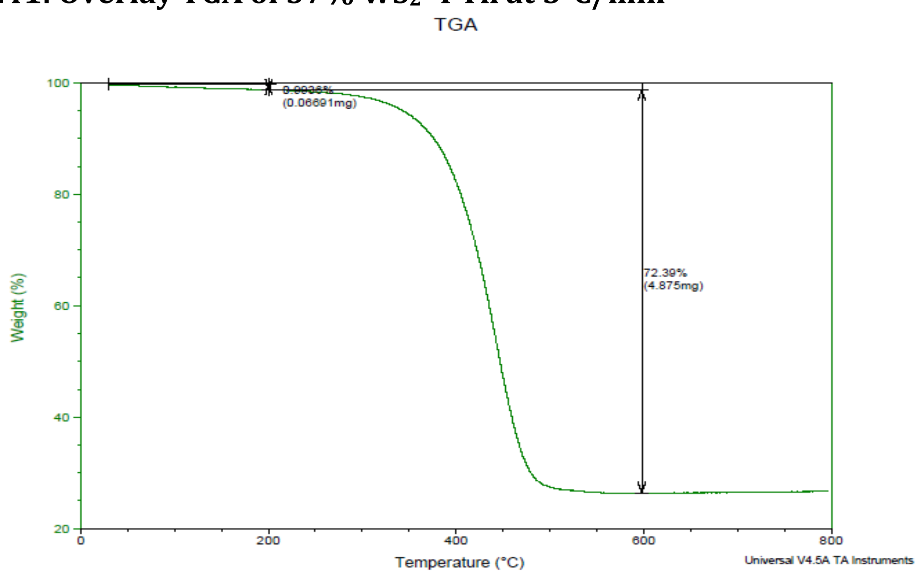

Figure 2.42: Overlay TGA of 37% WS_2- PTh at 10°C/min

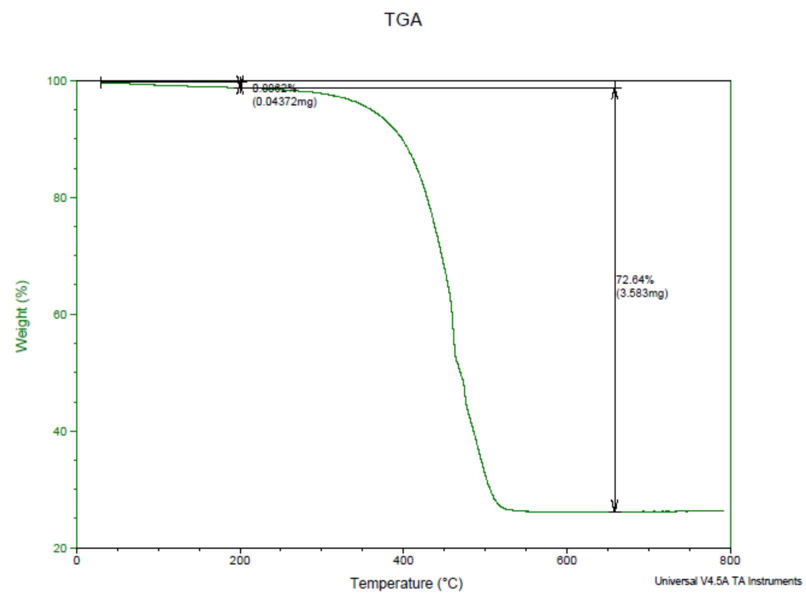

Figure 2.43: Overlay TGA of 37% WS_2- PTh at 20°C/min

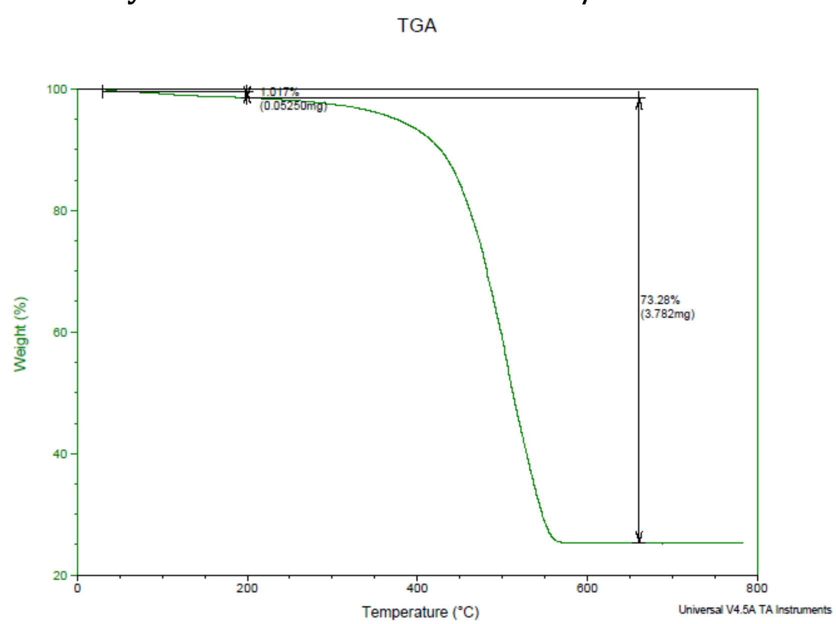

Figure 2.44: Overlay TGA of 37% WS_2- PTh at 40°C/min

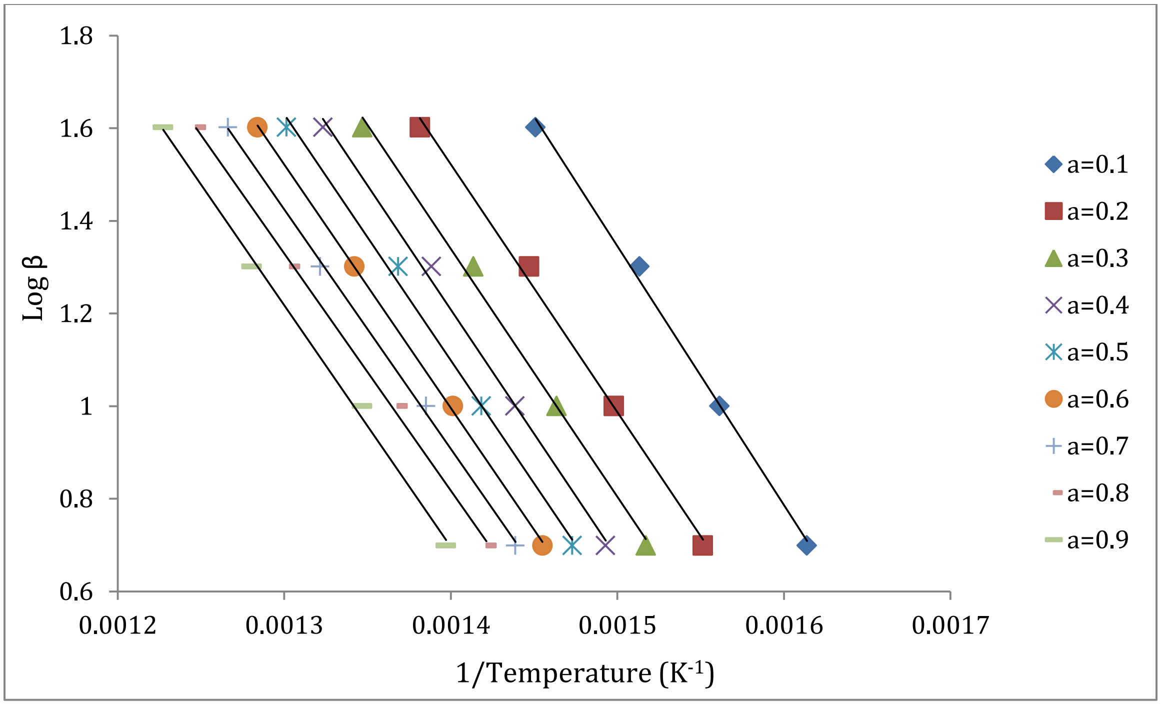

Figure 2.45: The regression lines for conversion of 0.1 -0.9 based on the Ozawa's method for 37 %WS$_2$-PTh.

Table 2.19: The correlation coefficient (R) and the activation energy (Ea) obtained using Ozawa's method for 37%WS$_2$-PTh.

Sample	Conversion α	R	Ea (kJ/mol)
37 % WS$_2$ by weight	0.1	0.9971	101.7
	0.2	0.9967	97.3
	0.3	0.9959	97.3
	0.4	0.9961	97.6
	0.5	0.9995	96.6
	0.6	0.9989	95.6
	0.7	0.9905	94.1
	0.8	0.9961	95.1
	0.9	0.9927	97.2
Average			124.9

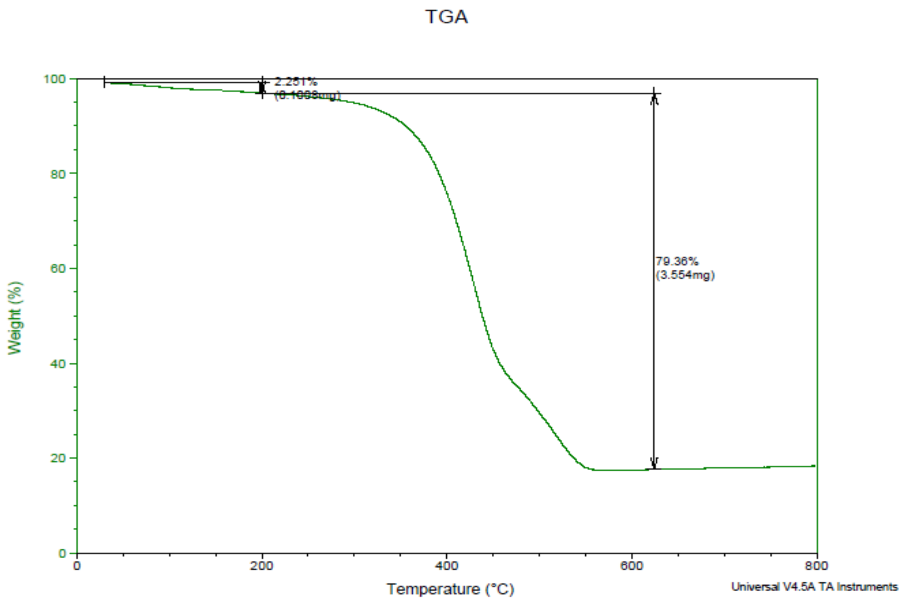

Figure 2.46: Overlay TGA of 64% WS_2- PTh at 5°C/min

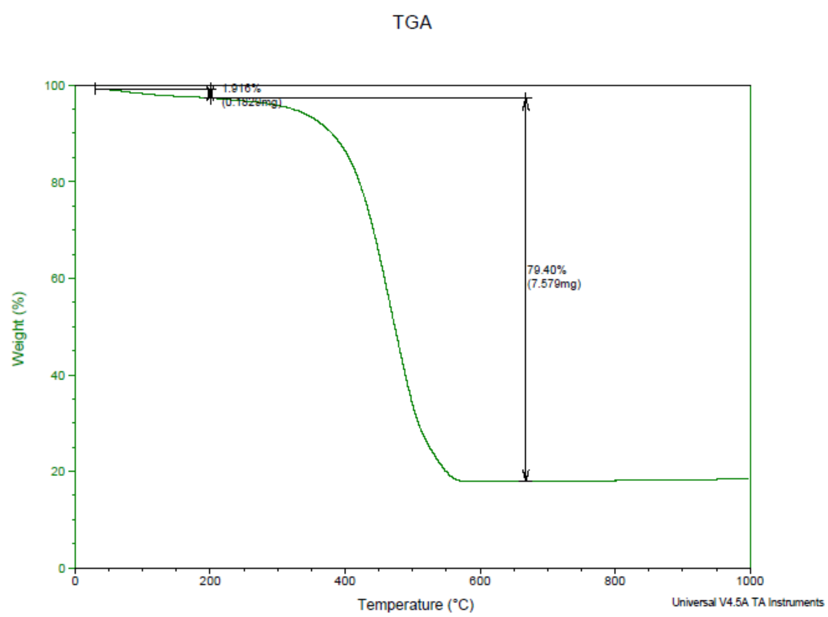

Figure 2.47: Overlay TGA of 64% WS_2- PTh at 10°C/min

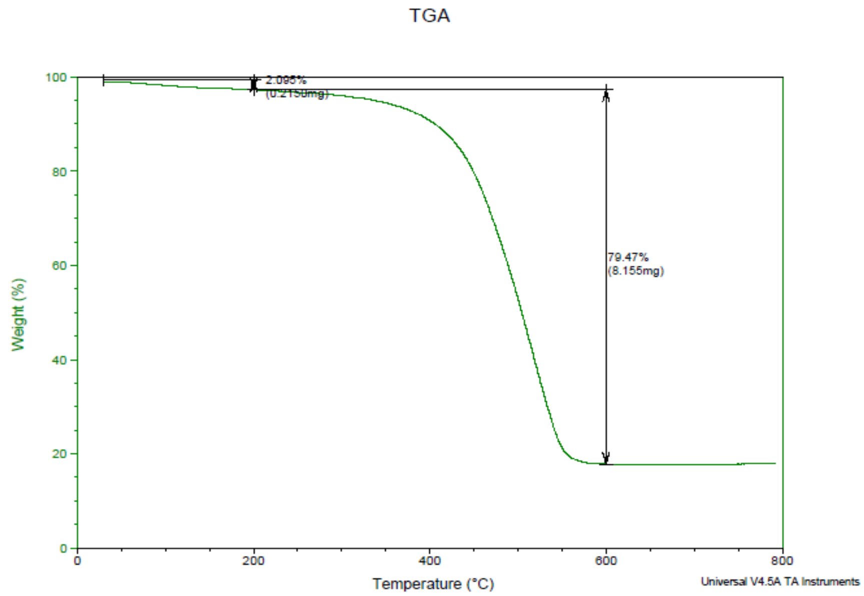

Figure 2.48: Overlay TGA of 64% WS_2- PTh at 20°C/min

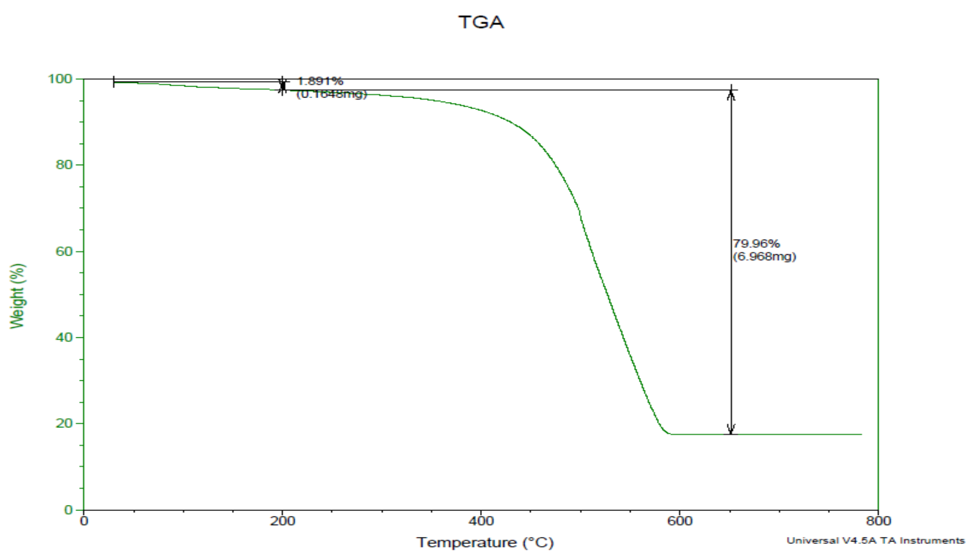

Figure 2.49: Overlay TGA of 64% WS_2- PTh at 40°C/min

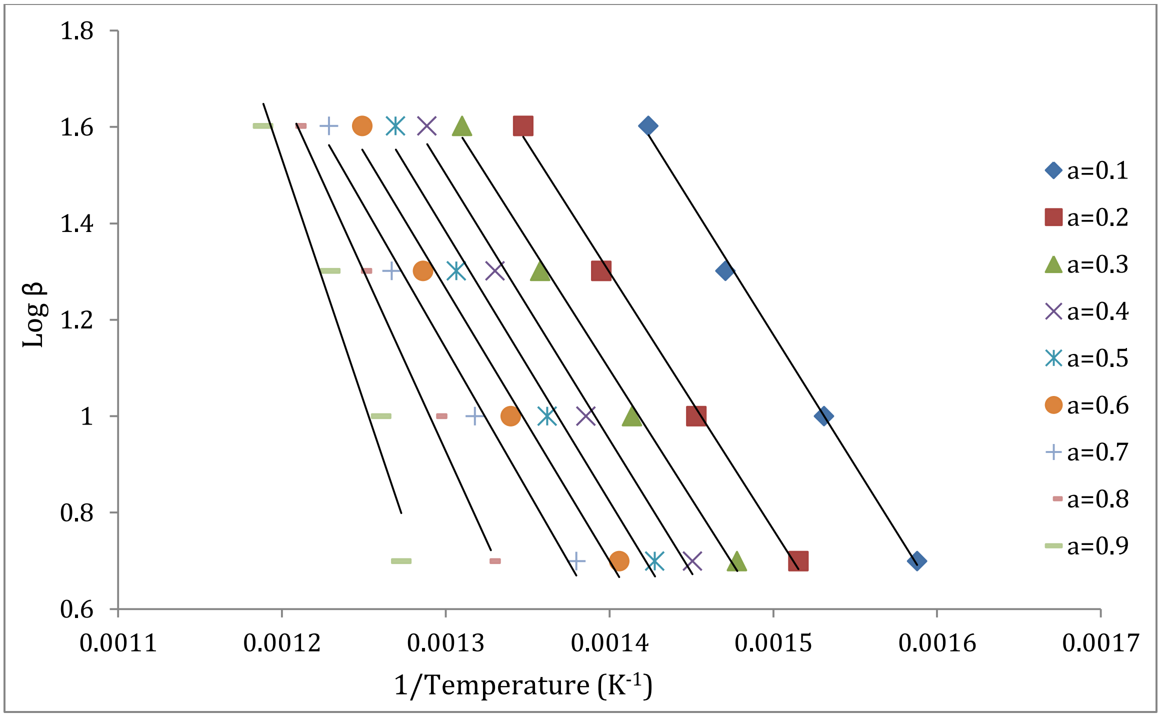

Figure 2.50: The regression lines for conversion of 0.1 -0.9 based on the Ozawa's method for 64 %WS_2-PTh.

Table 2.20: The correlation coefficient (R) and the activation energy (Ea) obtained using Ozawa's method for 64%WS_2-PTh.

Sample	Conversion α	R	Ea (kJ/mol)
64 % WS_2 by weight	0.1	0.9974	108.0
	0.2	0.9965	109.8
	0.3	0.9957	110.1
	0.4	0.9906	107.4
	0.5	0.9985	110.9
	0.6	0.9984	106.5
	0.7	0.9893	107.5
	0.8	0.9959	135.6
	0.9	0.9698	128.7
Average			113.8

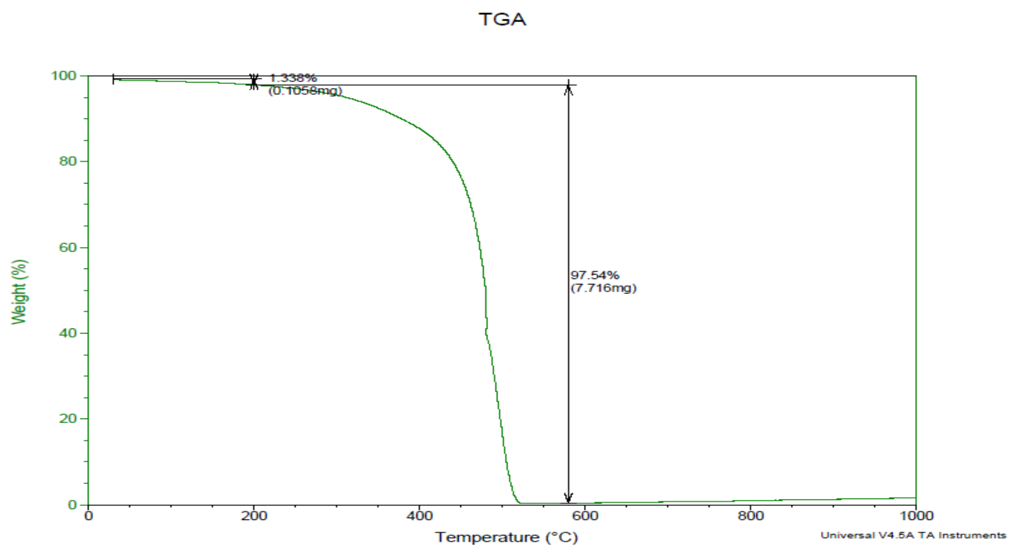

Figure 2.51: The TGA curve of pure PThN at heating rate of 5°C/min

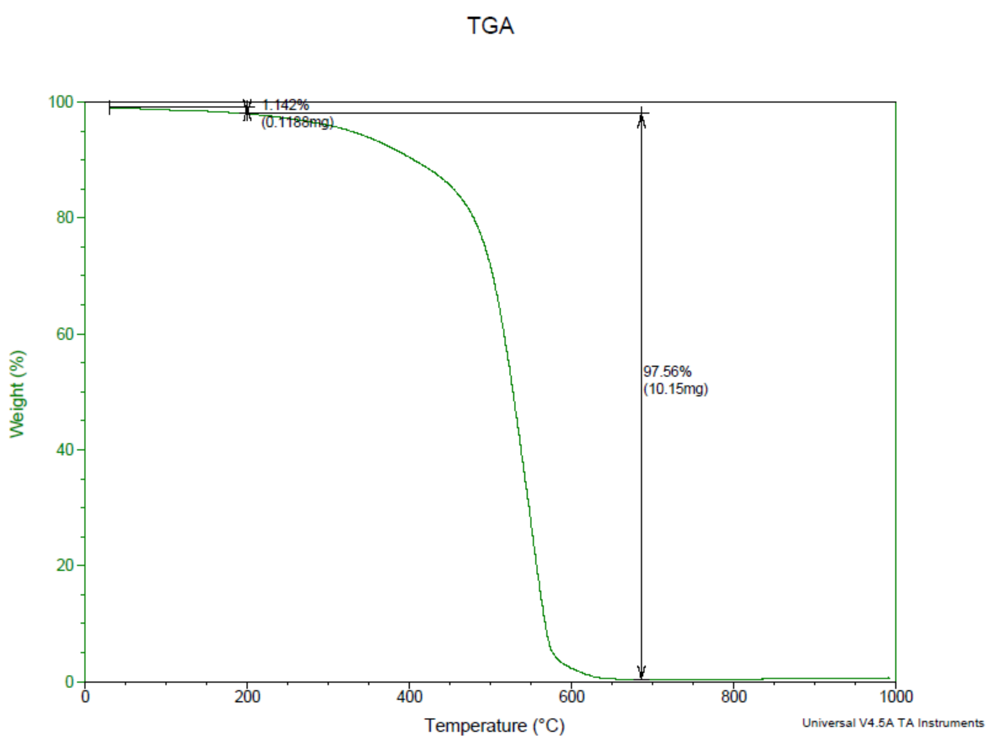

Figure 2.52: The TGA curve of pure PThN at heating rate of 20°C/min.

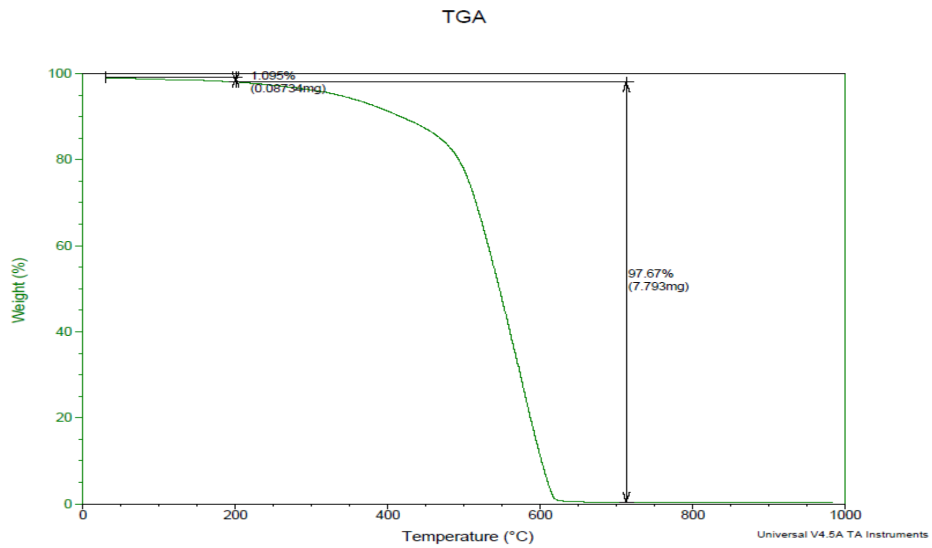

Figure 2.53: The TGA curve of pure PThN at heating rate of 40°C/min.

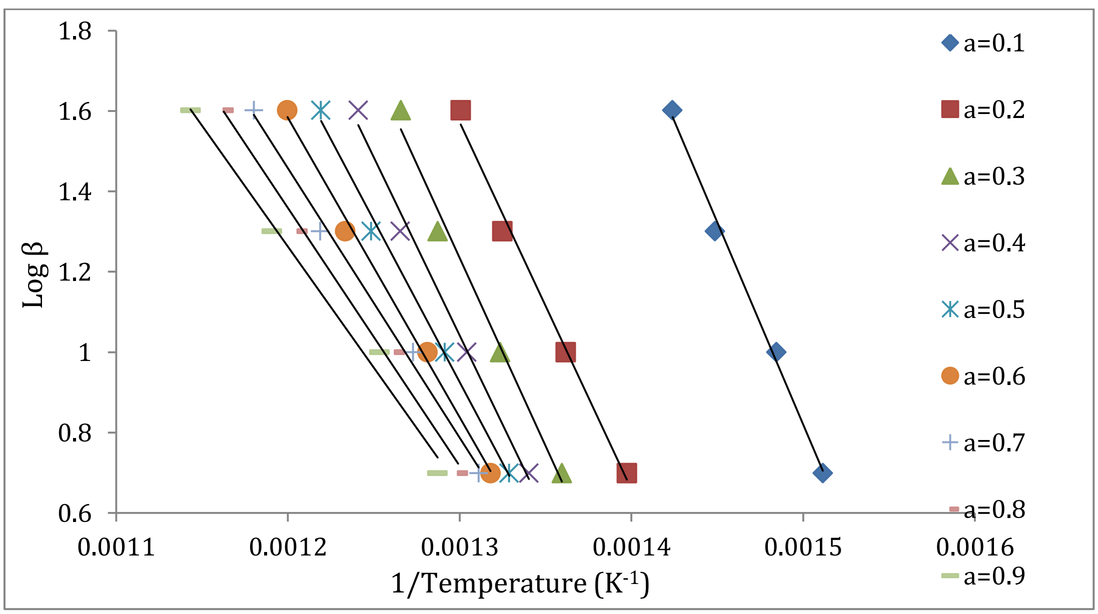

Figure 2.54: The regression lines for conversion of 0.1 -0.9 based on the Ozawa's method for pure PThN.

Table 2.21: The correlation coefficient (R) and the activation energy (Ea) obtained using Ozawa's method for pure PThN.

Sample	Conversion α	R	Ea (kJ/mol)
0 % WS_2 by weight	0.1	0.9955	182.8
	0.2	0.9923	166.0
	0.3	0.9873	170.1
	0.4	0.9916	161.2
	0.5	0.9949	146.5
	0.6	0.9957	135.3
	0.7	0.9952	122.0
	0.8	0.9939	116.7
	0.9	0.9883	109.5
Average			145.6

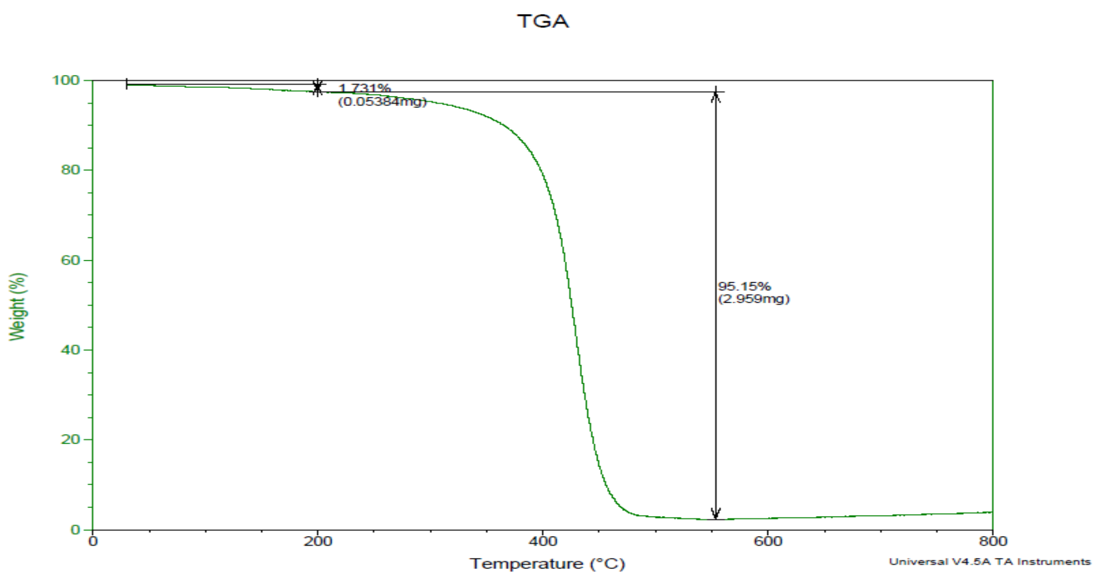

Figure 2.55: Overlay TGA of 1% WS_2- PThN at 5°C/min

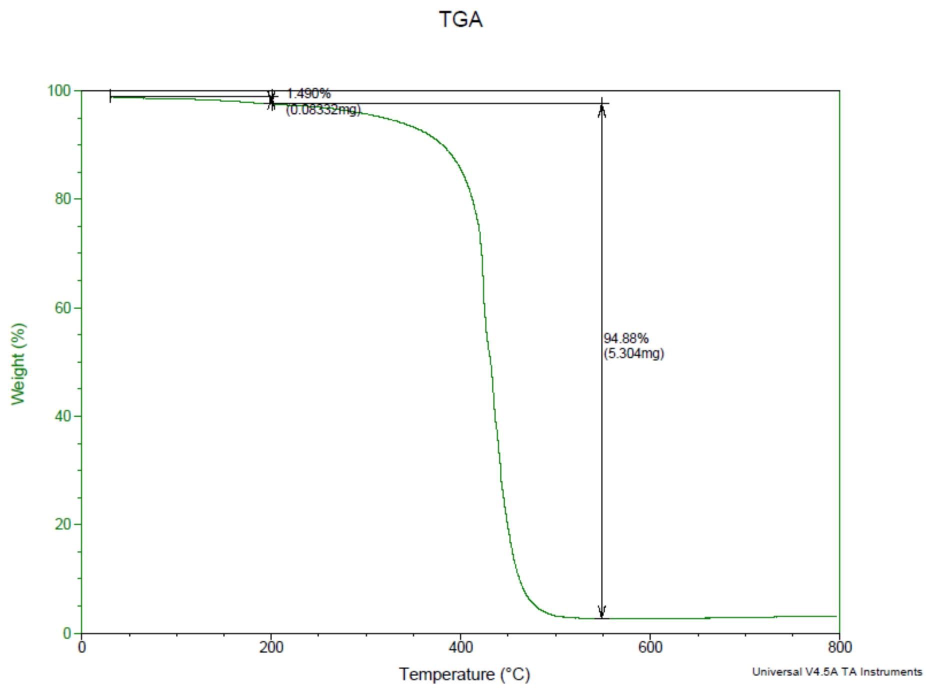

Figure 2.56: Overlay TGA of 1% WS_2- PThN at 10^{o}C/min

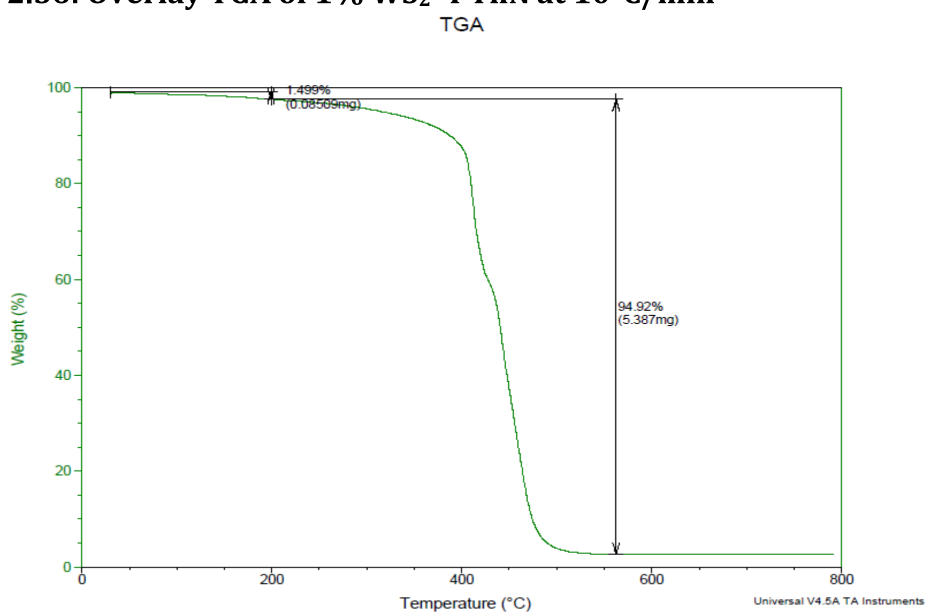

Figure 2.57: Overlay TGA of 1% WS_2- PThN at 20^{o}C/min

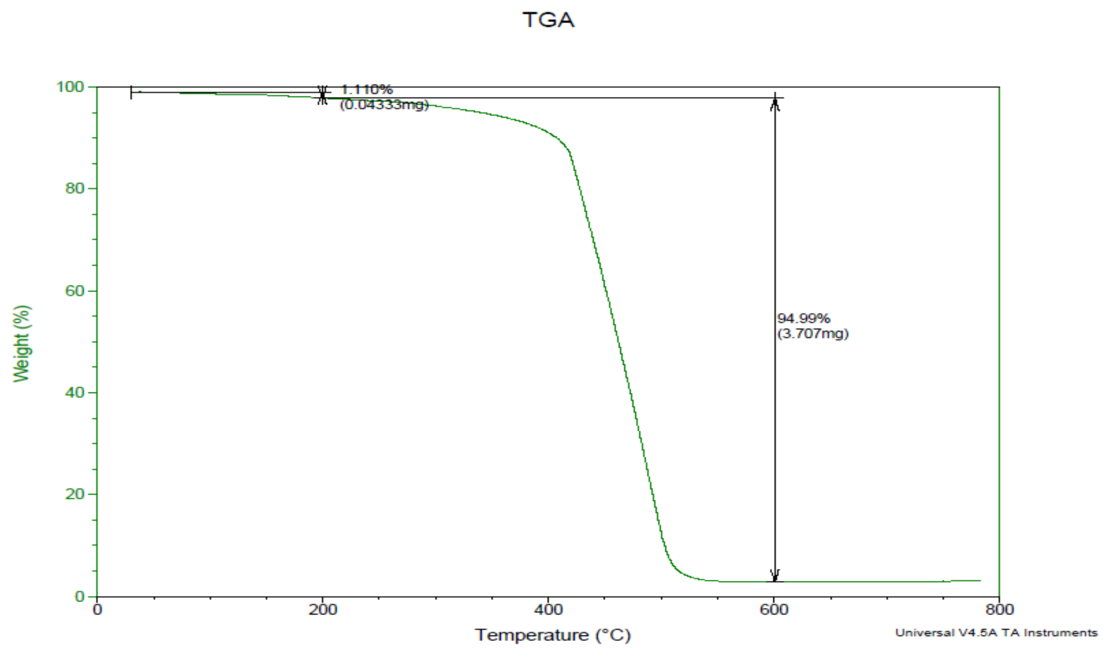

Figure 2.58: Overlay TGA of 1% WS_2- PThN at 40°C/min

Table 2.22: The correlation coefficient (R) and the activation energy (Ea) obtained using Ozawa's method for 1% WS_2- PThN.

Sample	Conversion α	R	Ea (kJ/mol)
1 % WS_2 by weight	0.1	0.9956	158.8
	0.2	0.9990	153.0
	0.3	0.9993	148.4
	0.4	0.9993	143.4
	0.5	0.9990	138.4
	0.6	0.9986	138.0
	0.7	0.9984	141.2
	0.8	0.9974	139.6
	0.9	0.9968	143.4
Average			144.9

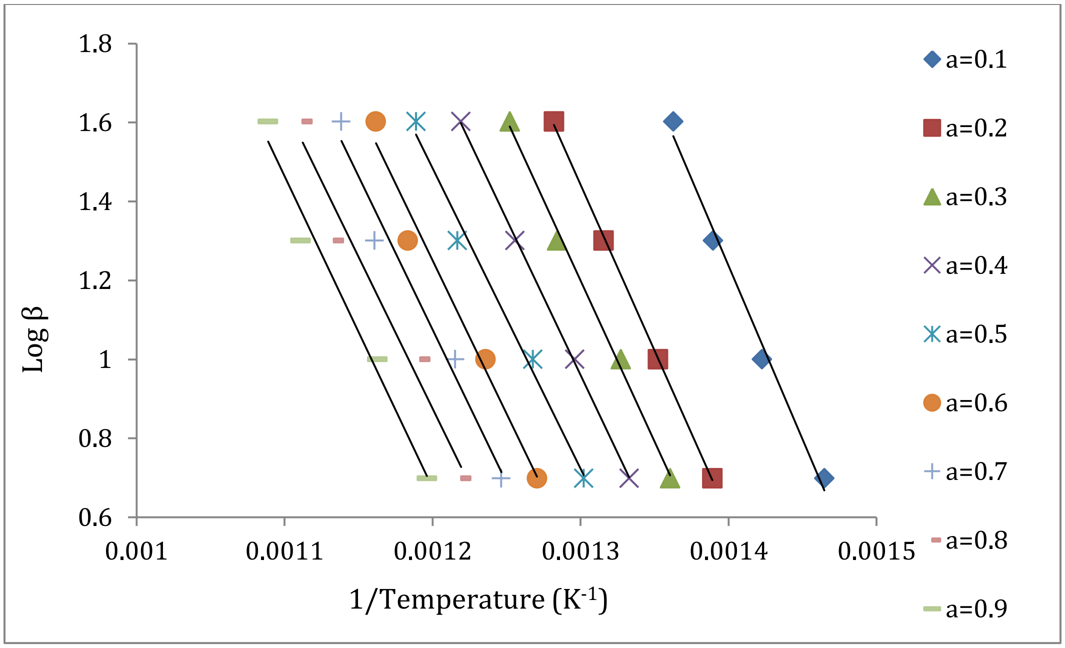

Figure 2.59: The regression lines for conversion of 0.1 -0.9 based on the Ozawa's method for 1% WS_2- PThN.

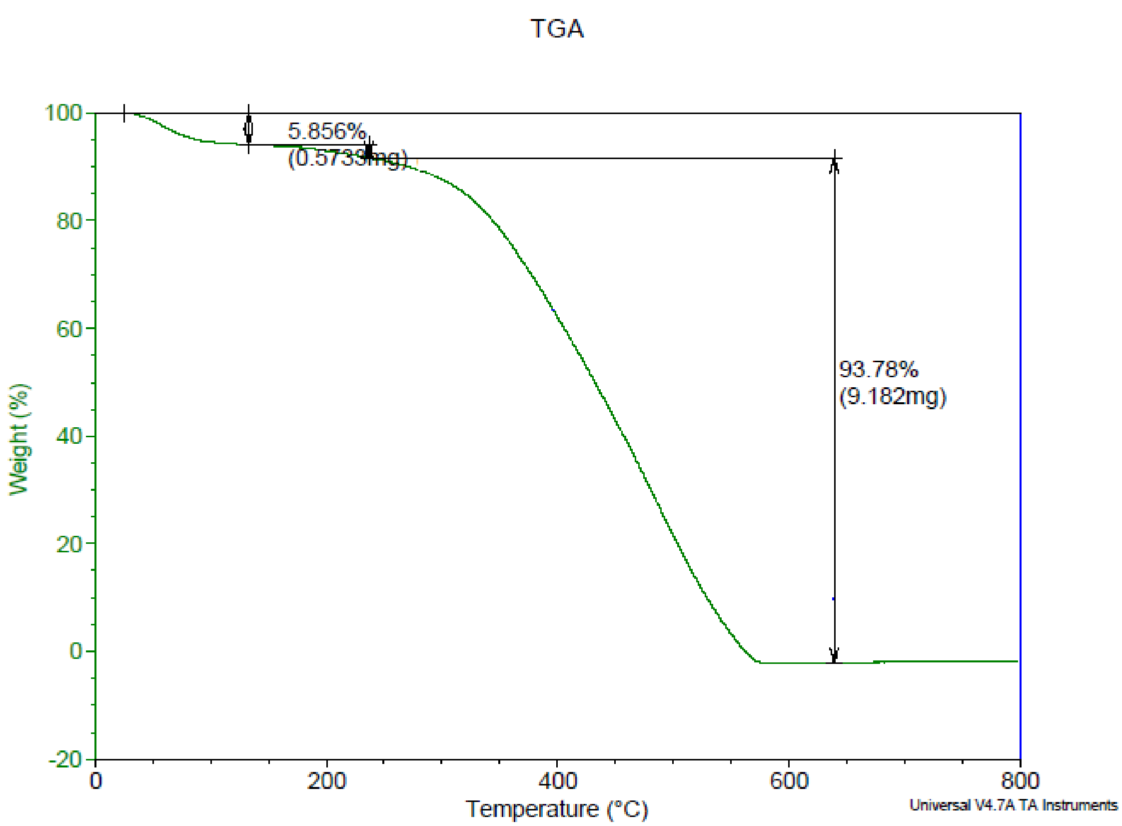

Figure 2.60: Overlay TGA of 5% WS_2- PThN at 5°C/min

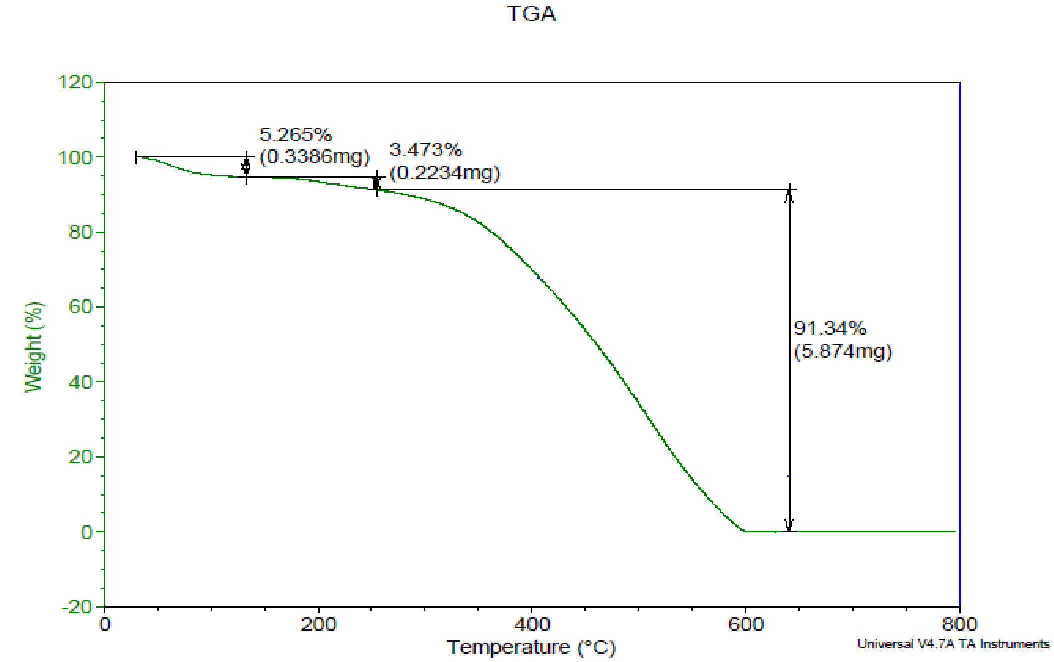

Figure 2.61: Overlay TGA of 5% WS_2- PThN at 10°C/min

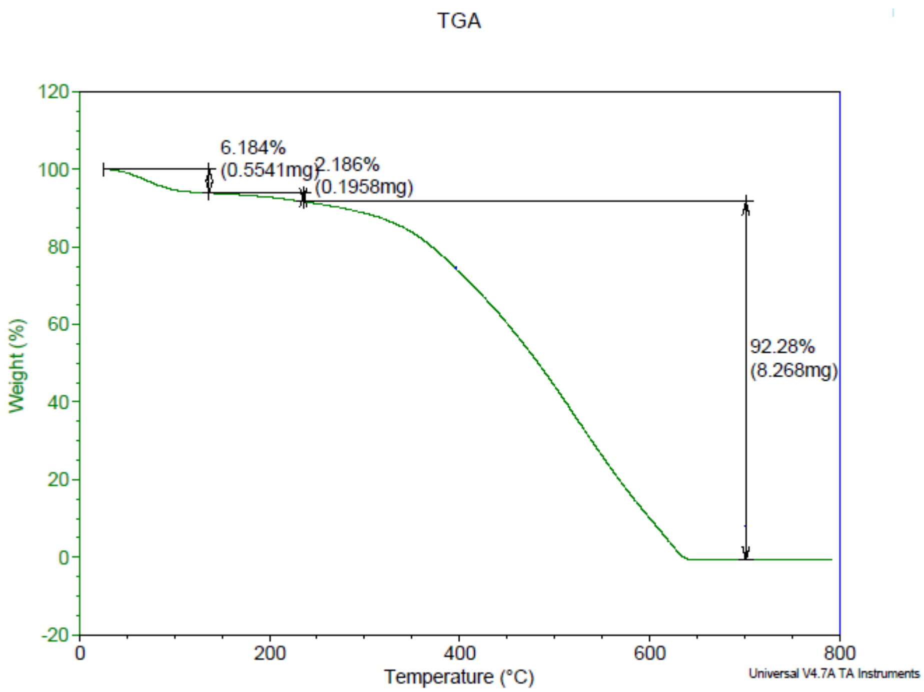

Figure 2.62: Overlay TGA of 5% WS_2- PThN at 20°C/min

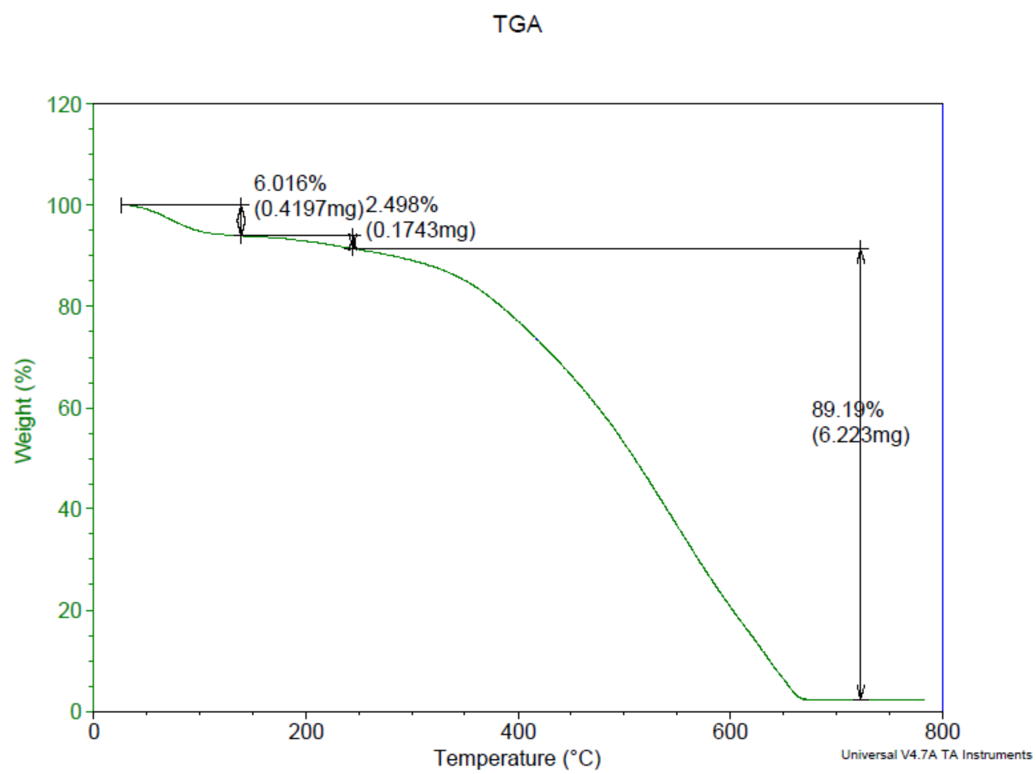

Figure 2.63: Overlay TGA of 5% WS_2- PThN at 40°C/min.

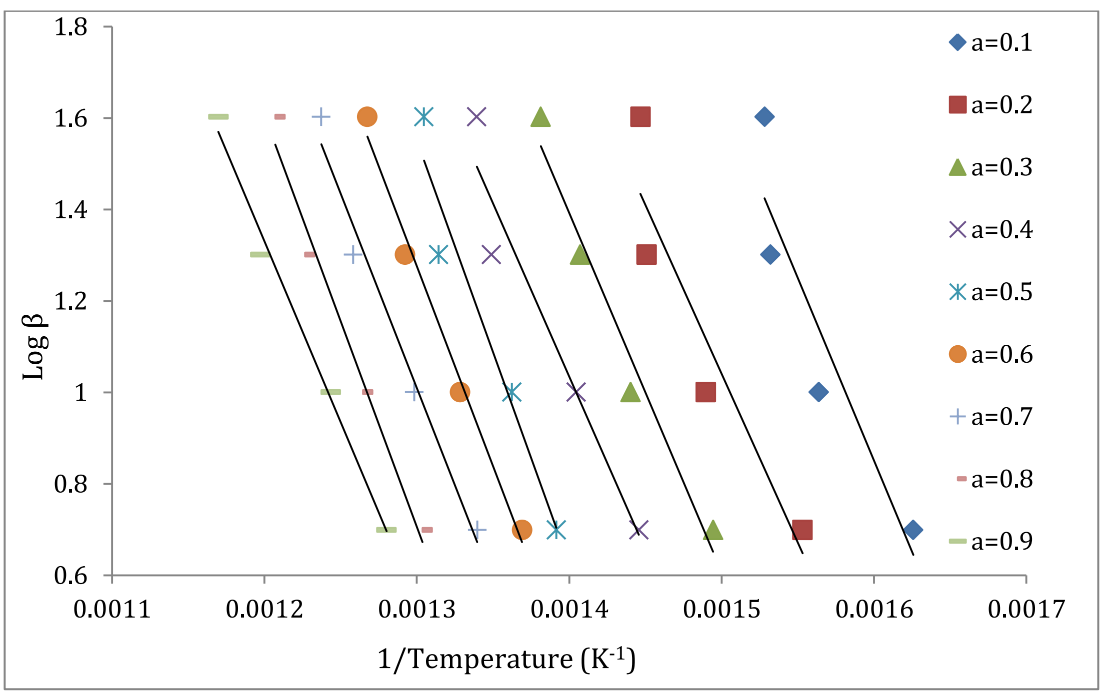

Figure 2.64: The regression lines for conversion of 0.1 -0.9 based on the Ozawa's method for 5% WS_2- PThN.

Table 2.23: The correlation coefficient (R) and the activation energy (Ea) obtained using Ozawa's method for 5% WS_2- PThN.

Sample	Conversion α	R	Ea (kJ/mol)
5 % WS_2 by weight	0.1	0.9936	145.0
	0.2	0.9977	134.3
	0.3	0.9985	142.6
	0.4	0.9996	137.4
	0.5	0.9982	168.1
	0.6	0.9982	159.0
	0.7	0.9566	154.6
	0.8	0.9902	163.9
	0.9	0.9924	143.9
Average			149.9

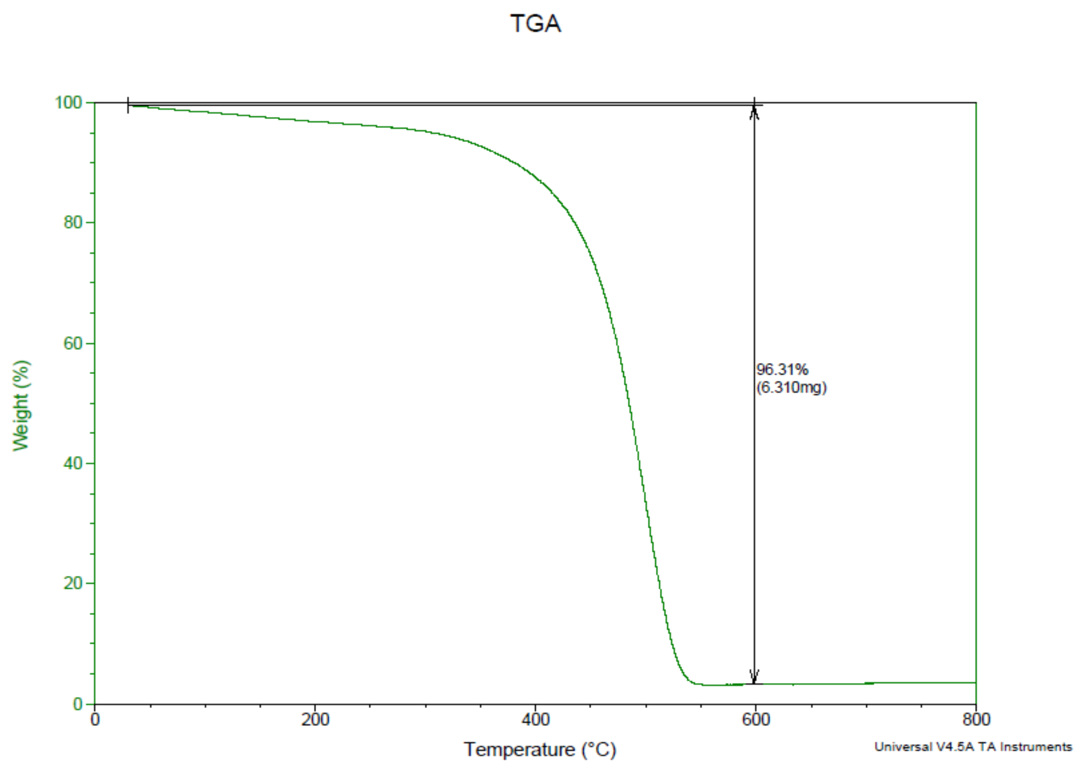

Figure 2.65: Overlay TGA of 10% WS_2- PThN at 5°C/min.

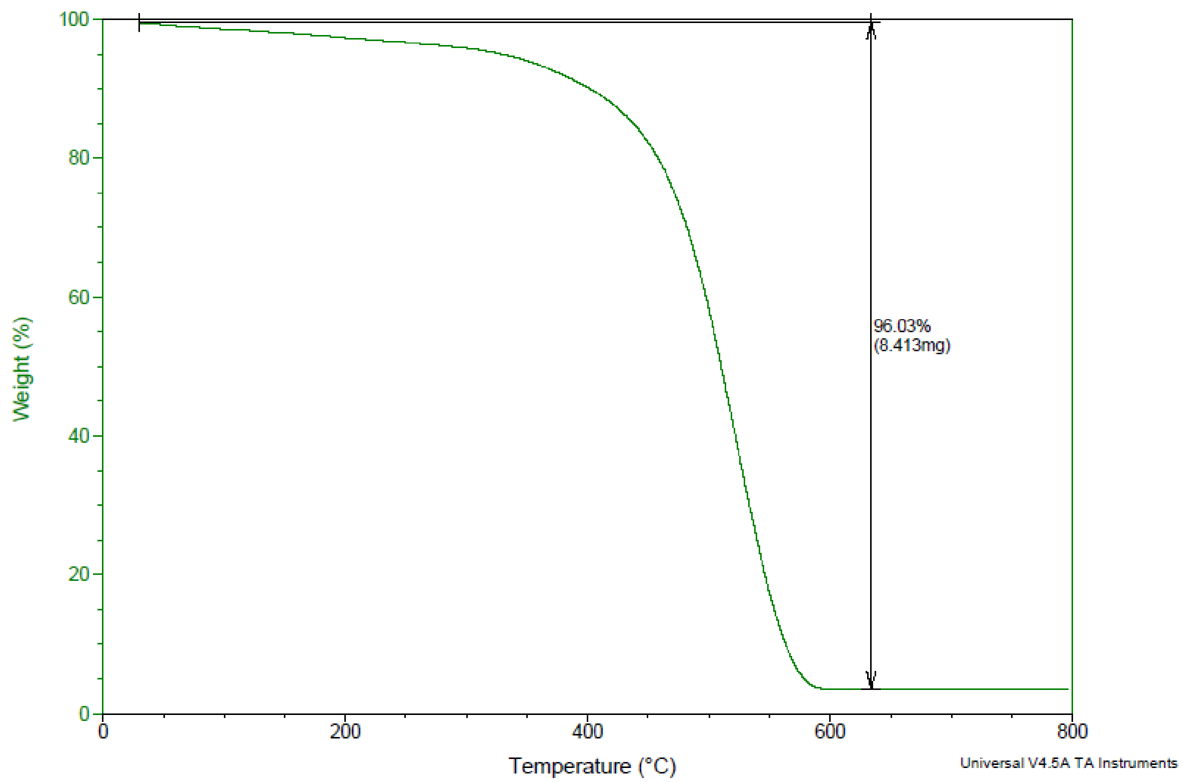

Figure 2.66: Overlay TGA of 10% WS_2- PThN at 10^oC/min.

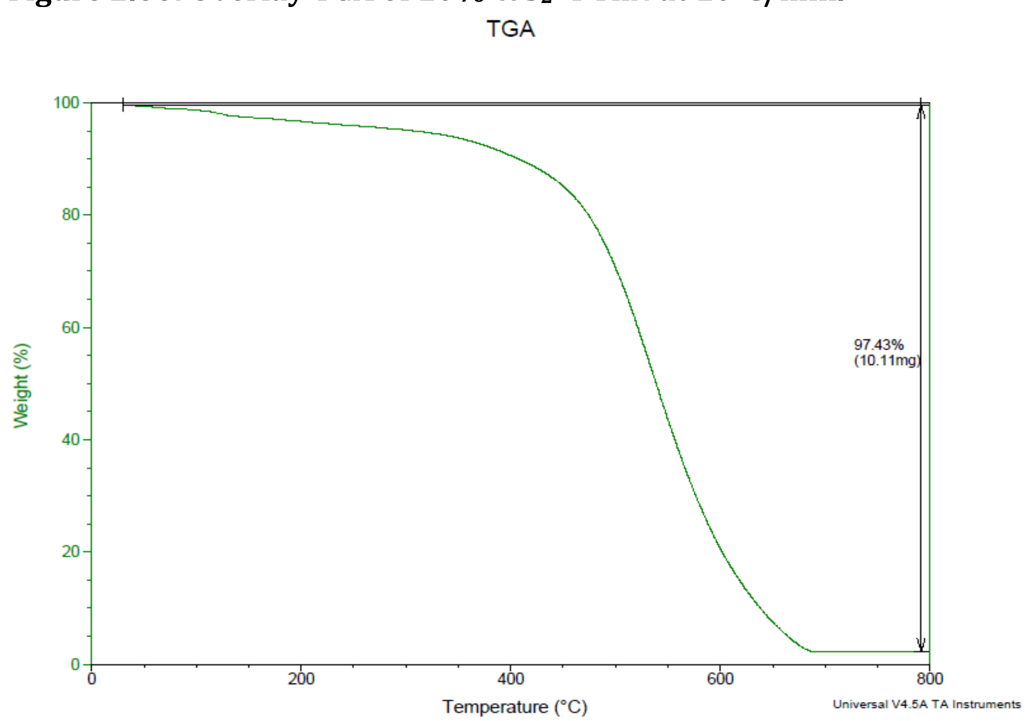

Figure 2.67: Overlay TGA of 10% WS_2- PThN at 20^oC/min.

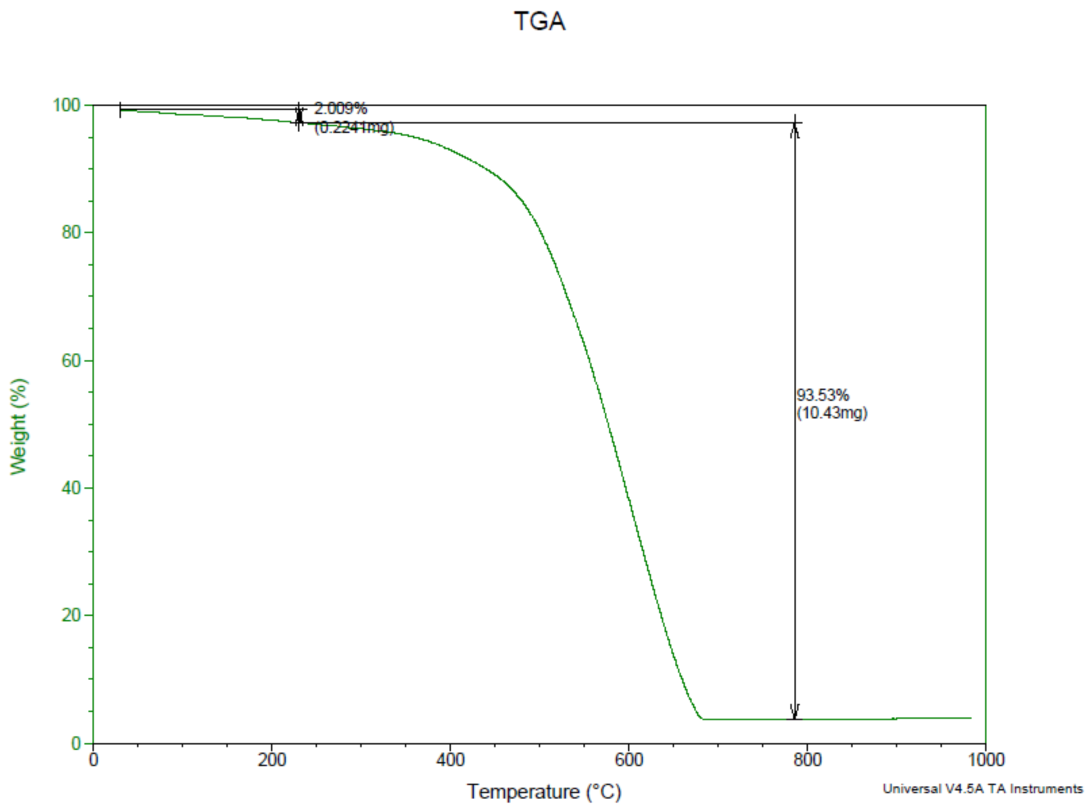

Figure 2.68: Overlay TGA of 10% WS_2- PThN at 40°C/min.

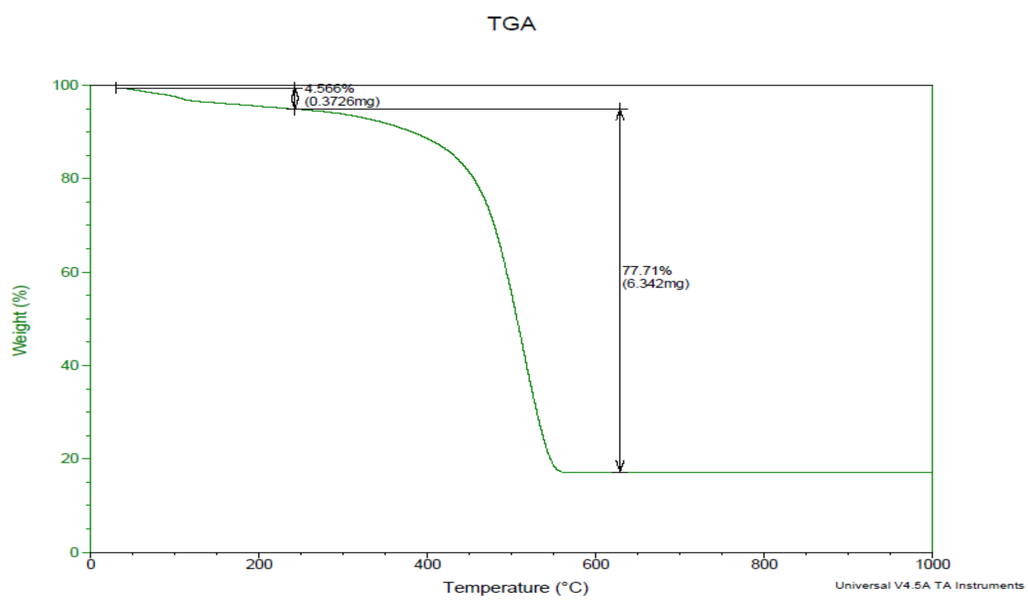

Figure 2.69: Overlay TGA of 20% WS_2- PThN at 5°C/min

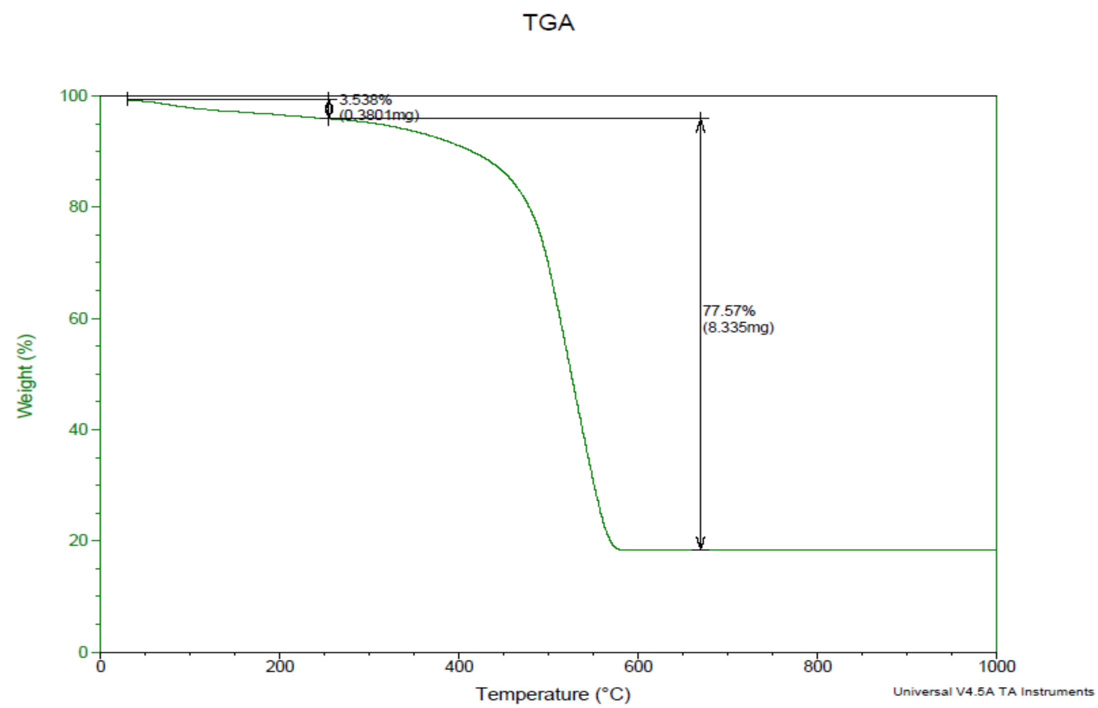

Figure 2.70: Overlay TGA of 20% WS_2- PThN at 10°C/min

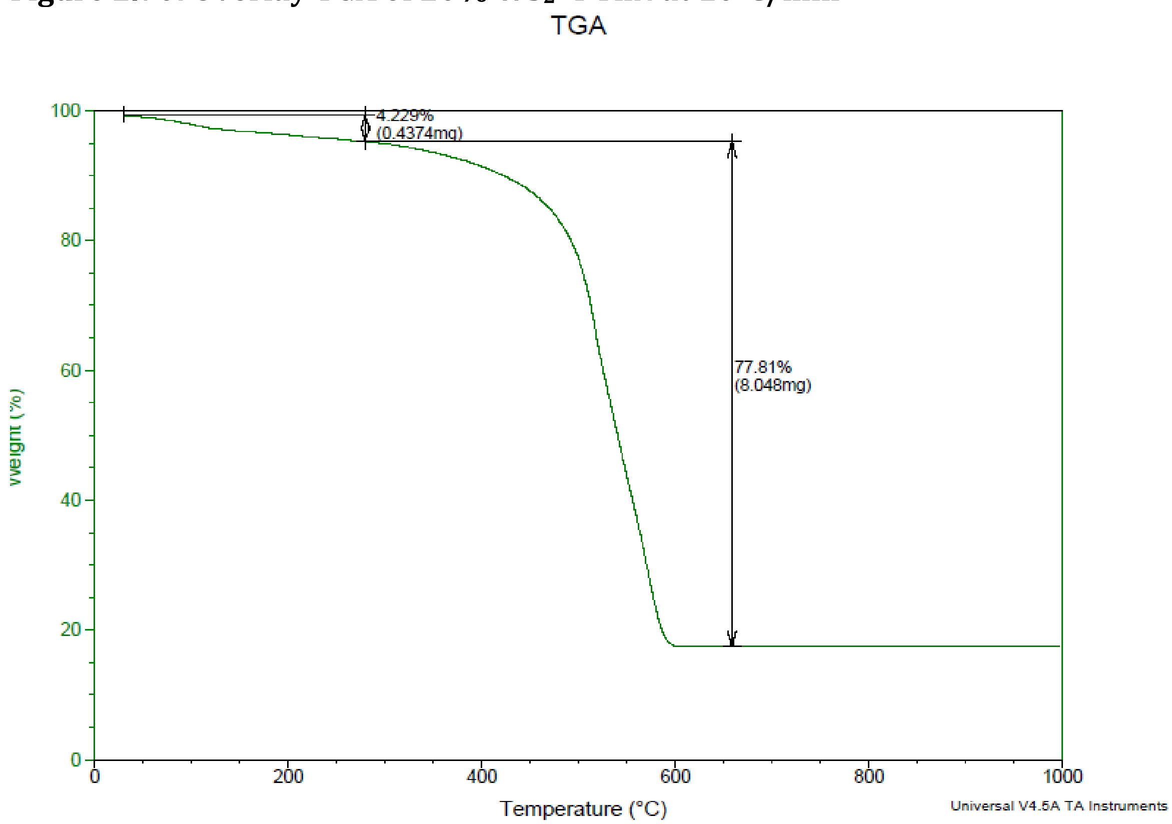

Figure 2.71: Overlay TGA of 20% WS_2- PThN at 20°C/min

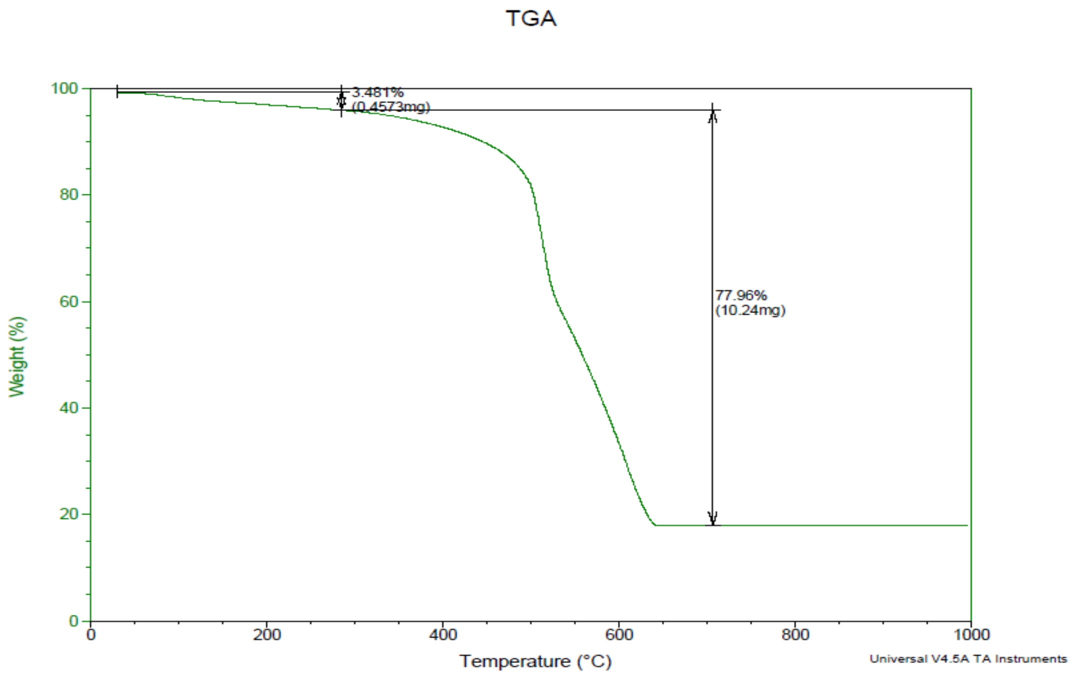

Figure 2.72: Overlay TGA of 20% WS_2- PThN at 40^{o}C/min

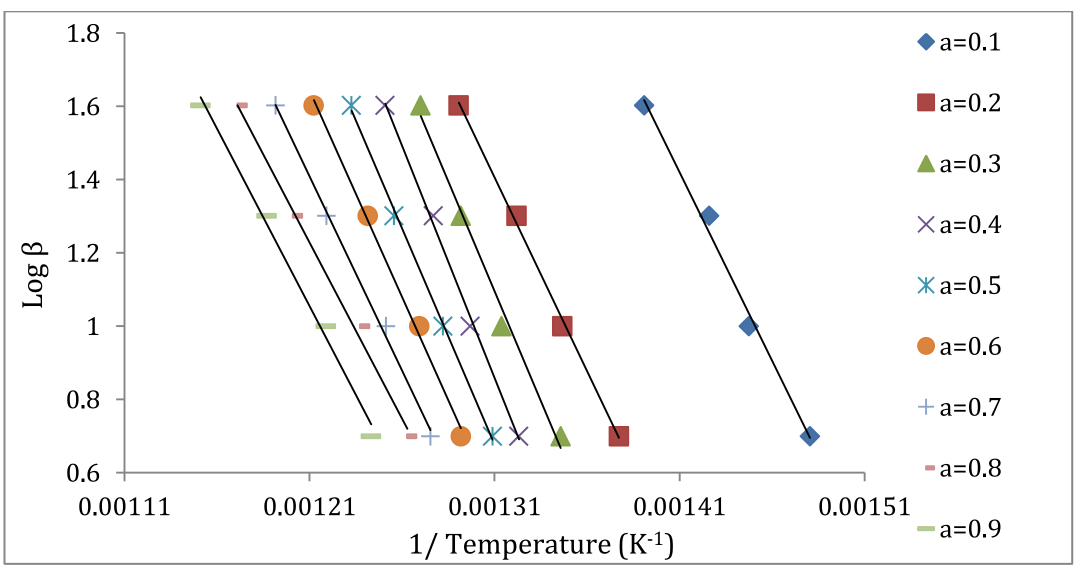

Figure 2.73: The regression lines for conversion of 0.1 -0.9 based on the Ozawa's method for 20% WS_2- PThN.

Table 2.24: The correlation coefficient (R) and the activation energy (Ea) obtained using Ozawa's method for 20% WS_2- PThN.

Sample	Conversion α	R	Ea (kJ/mol)
20 % WS_2 by weight	0.1	0.9898	187.1
	0.2	0.9737	192.3
	0.3	0.9048	217.7
	0.4	0.8874	230.7
	0.5	0.9587	214.1
	0.6	0.9992	205.7
	0.7	0.9962	192.6
	0.8	0.9891	174.2
	0.9	0.9778	174.2
Average			198.7

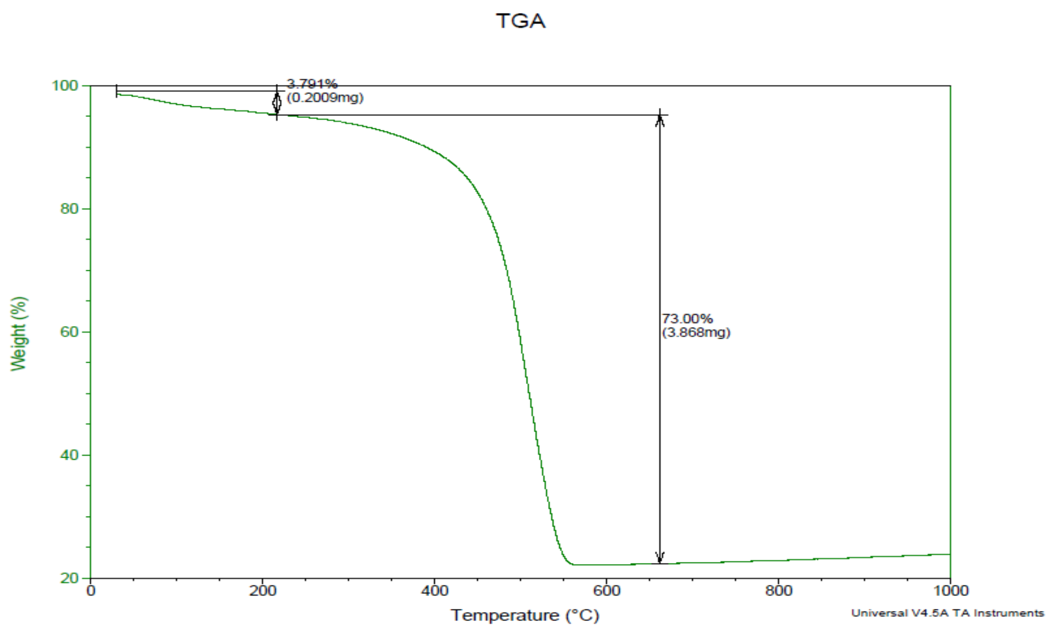

Figure 2.74: Overlay TGA of 37% WS_2- PThN at 5°C/min

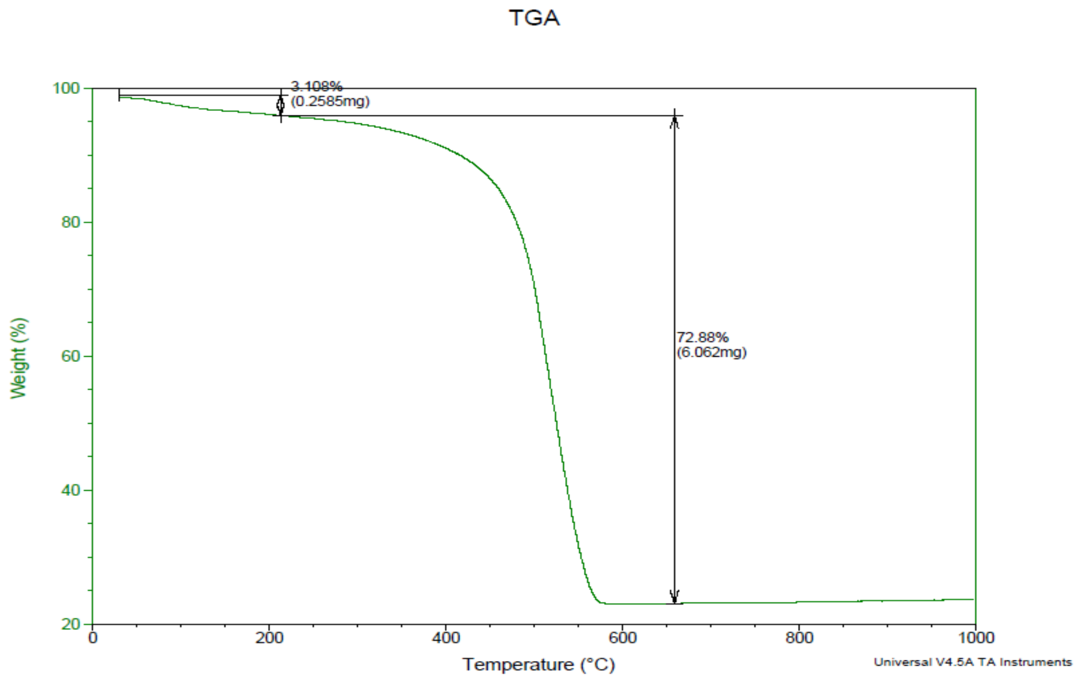

Figure 2.75: Overlay TGA of 37% WS_2- PThN at 10°C/min

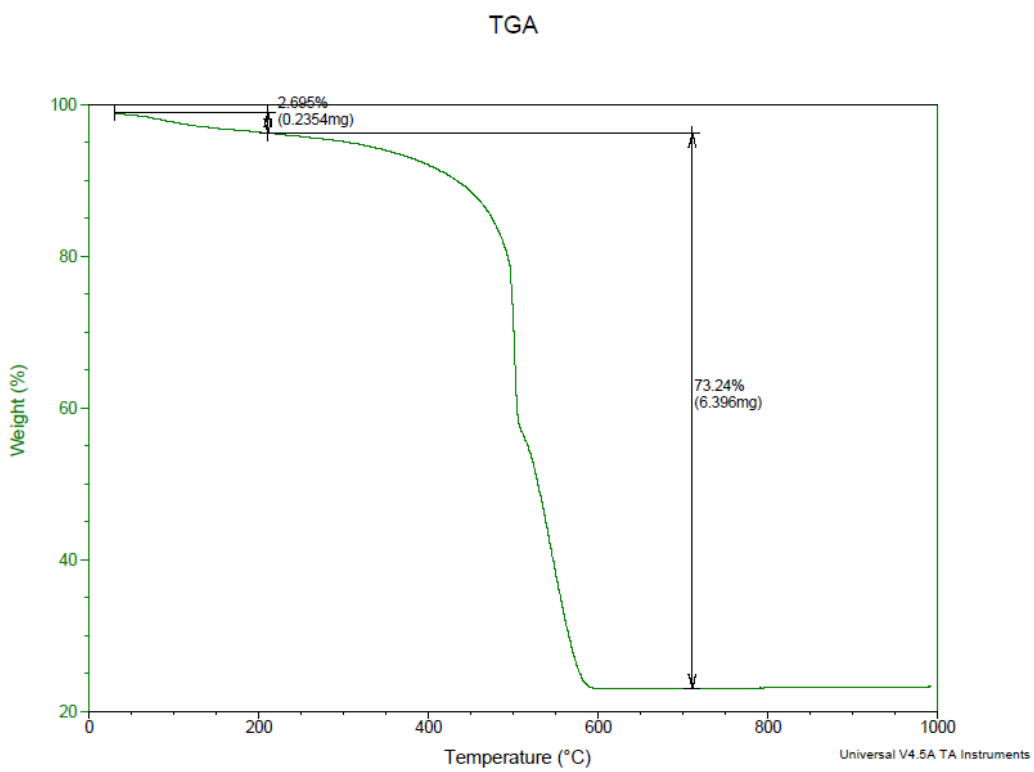

Figure 2.76: Overlay TGA of 37% WS_2- PThN at 20°C/min

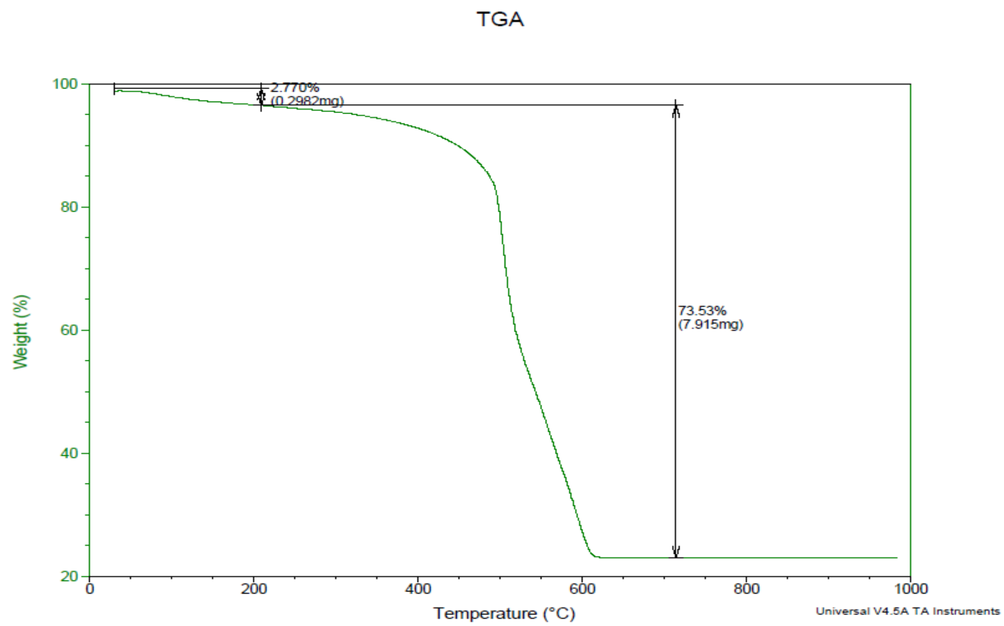

Figure 2.77: Overlay TGA of 37% WS_2- PThN at 40°C/min

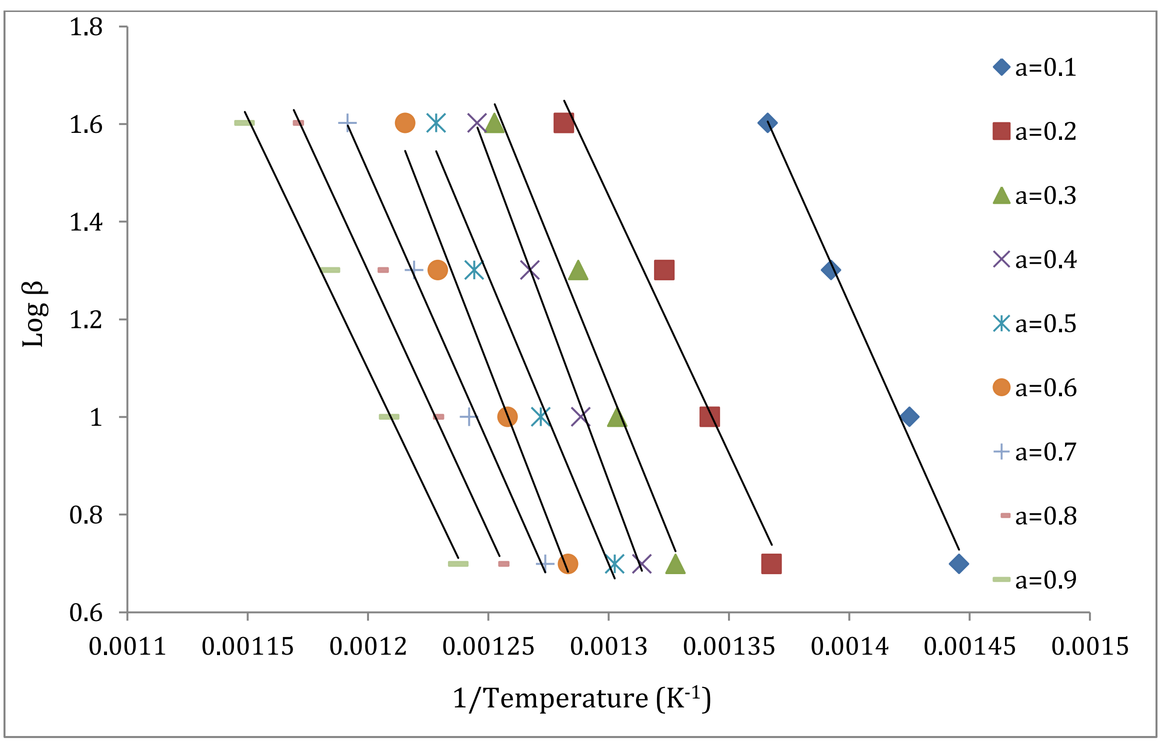

Figure 2.78: The regression lines for conversion of 0.1 -0.9 based on the Ozawa's method for 37% WS_2- PThN.

Table 2.25: The correlation coefficient (R) and the activation energy (Ea) obtained using Ozawa's method for 37% WS_2- PThN.

Sample	Conversion α	R	Ea (kJ/mol)
37 % WS_2 by weight	0.1	0.9932	200.6
	0.2	0.9977	191.8
	0.3	0.9945	221.6
	0.4	0.9949	241.8
	0.5	0.9988	214.5
	0.6	0.9999	231.8
	0.7	0.9988	202.3
	0.8	0.9993	194.0
	0.9	0.9969	187.1
Average			209.5

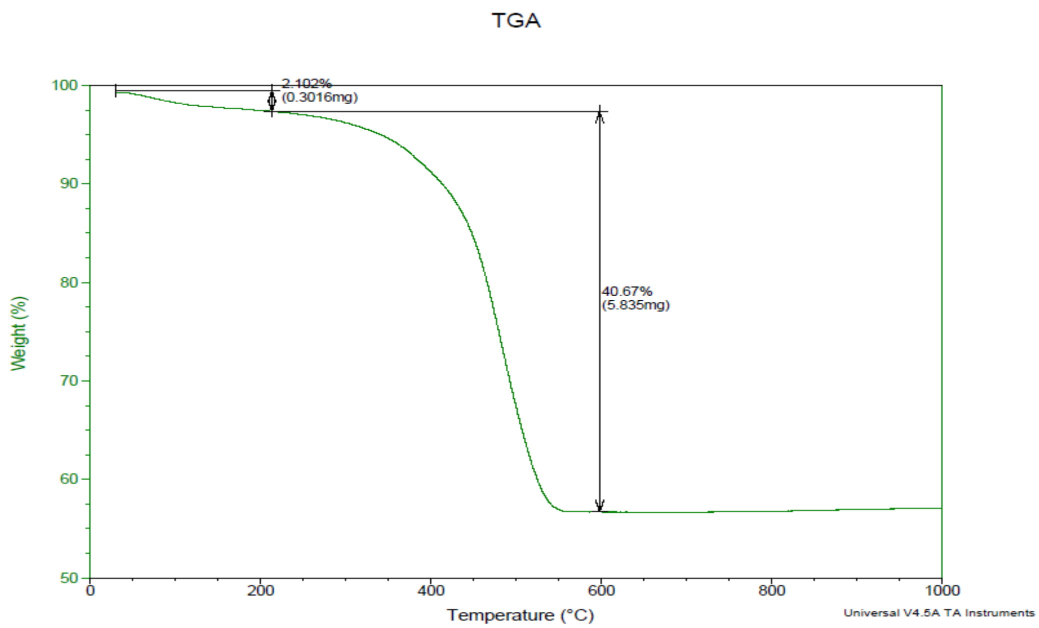

Figure 2.79: Overlay TGA of 64% WS_2- PThN at 5°C/min

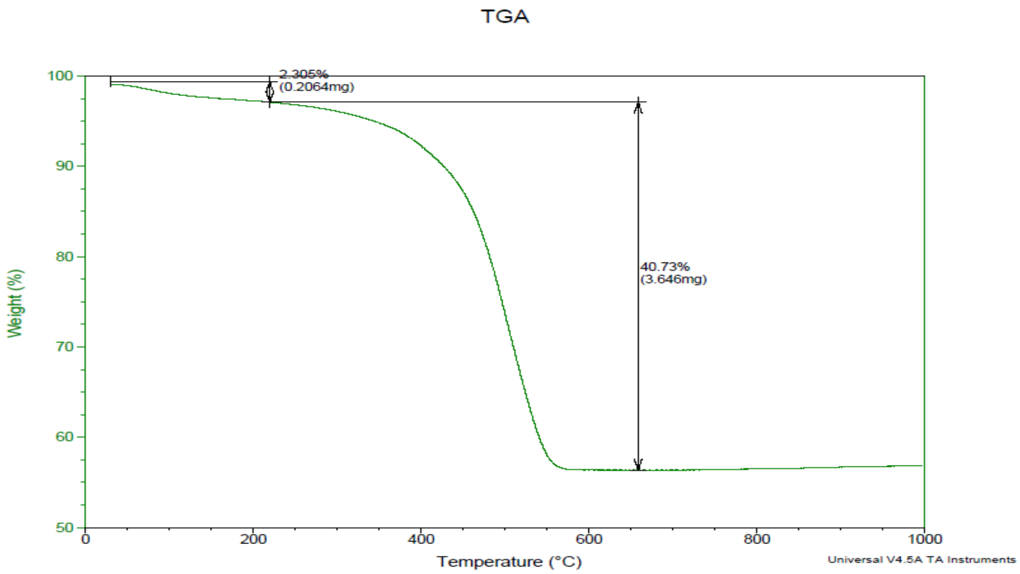

Figure 2.80: Overlay TGA of 64% WS_2- PThN at 10°C/min

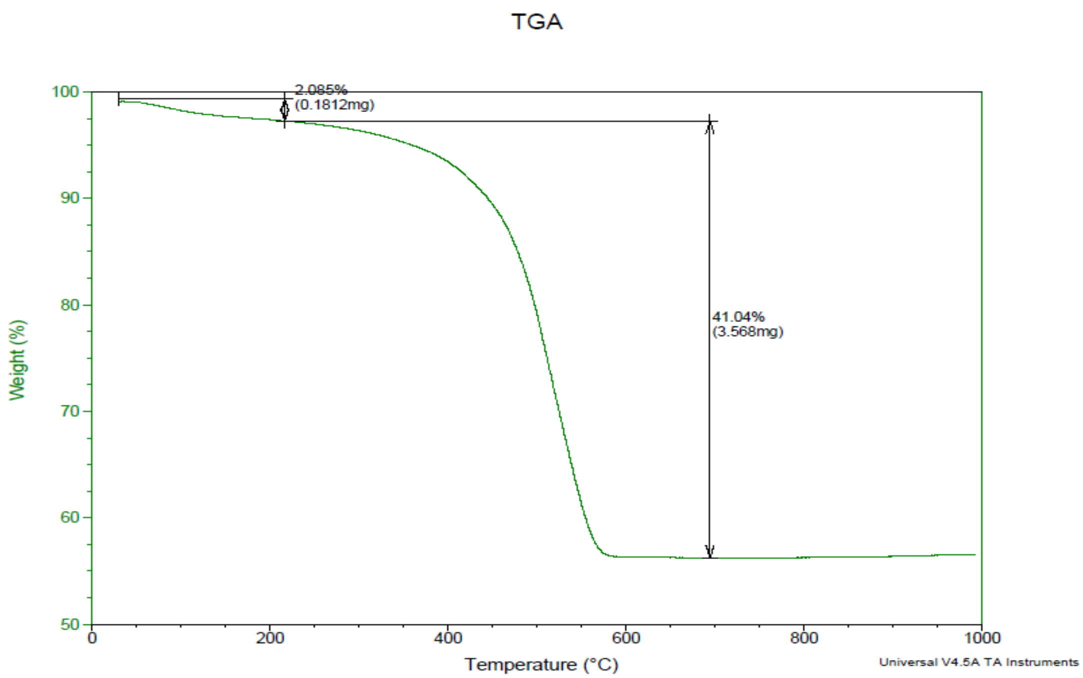

Figure 2.81: Overlay TGA of 64% WS_2- PThN at 20°C/min

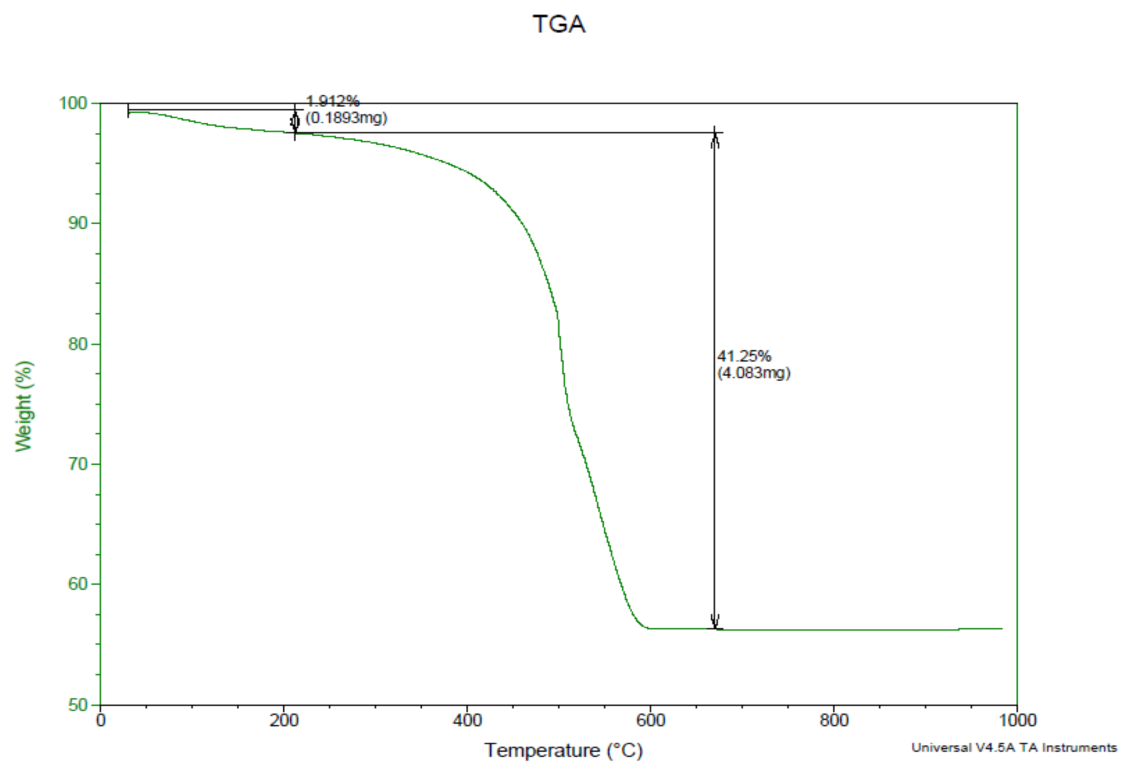

Figure 2.82: Overlay TGA of 64% WS_2- PThN at 40°C/min

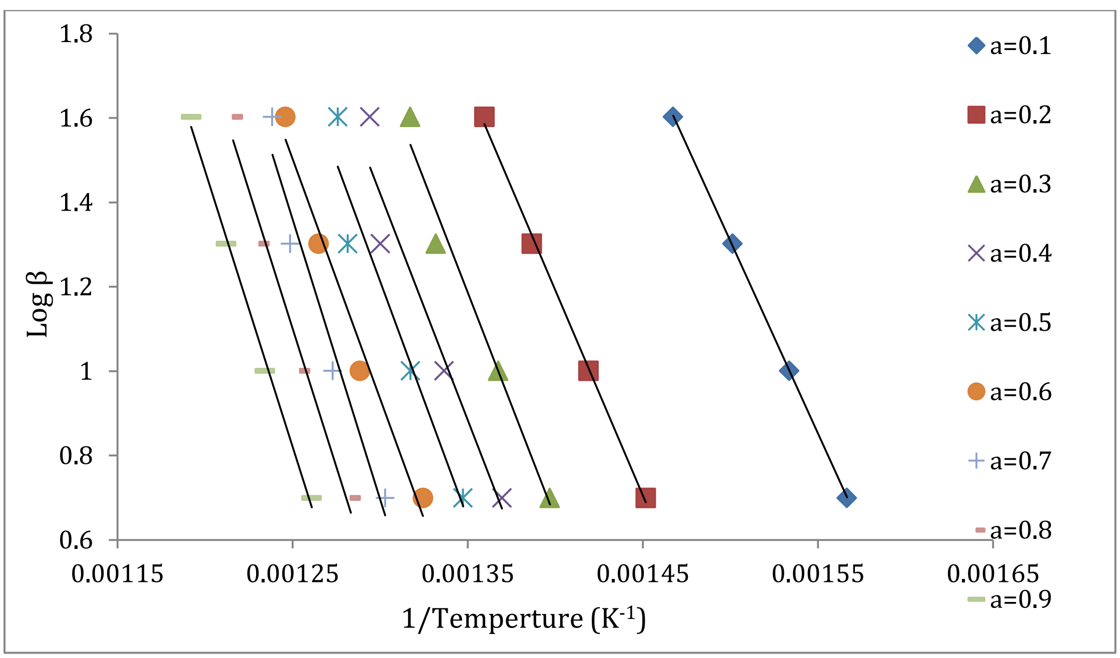

Figure 2.83: The regression lines for conversion of 0.1 -0.9 based on the Ozawa's method for 64% WS_2- PThN.

Table 2.26: The correlation coefficient (R) and the activation energy (Ea) obtained using Ozawa's method for 64% WS_2- PThN.

Sample	Conversion α	R	Ea (kJ/mol)
64 % WS_2 by weight	0.1	0.9999	165.7
	0.2	0.9981	176.9
	0.3	0.9995	194.2
	0.4	0.9954	195.2
	0.5	0.9998	187.9
	0.6	0.9978	206.1
	0.7	0.9594	241.2
	0.8	0.9815	238.5
	0.9	0.9954	238.4
Average			204.9

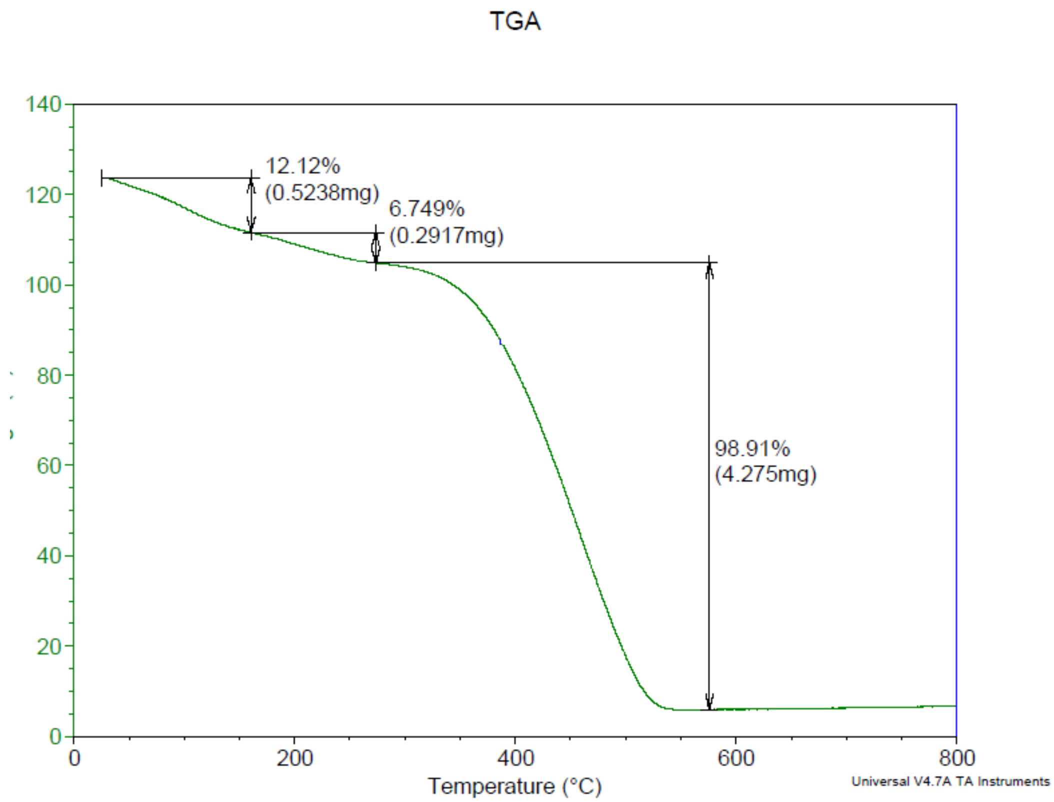

Figure 3.6: Overlay TGA of pure PANI at heating rate 5 °C/min

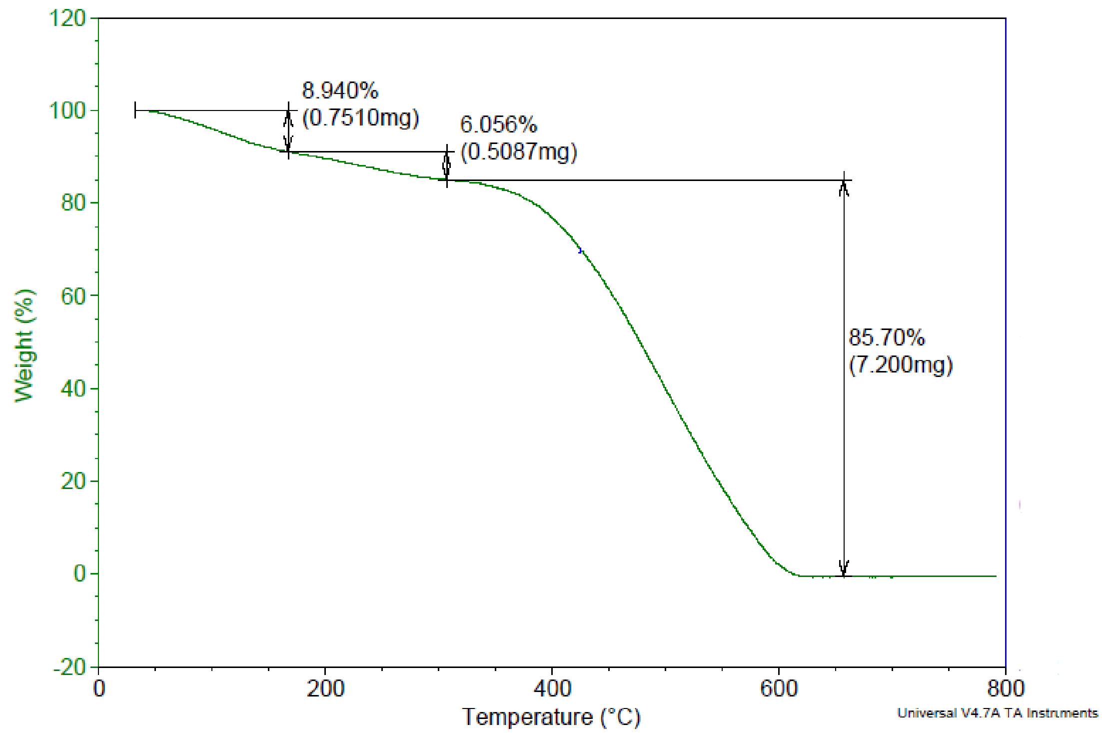

Figure 3.7: Overlay TGA of pure PANI at heating rate 20 $^{o}C/min$

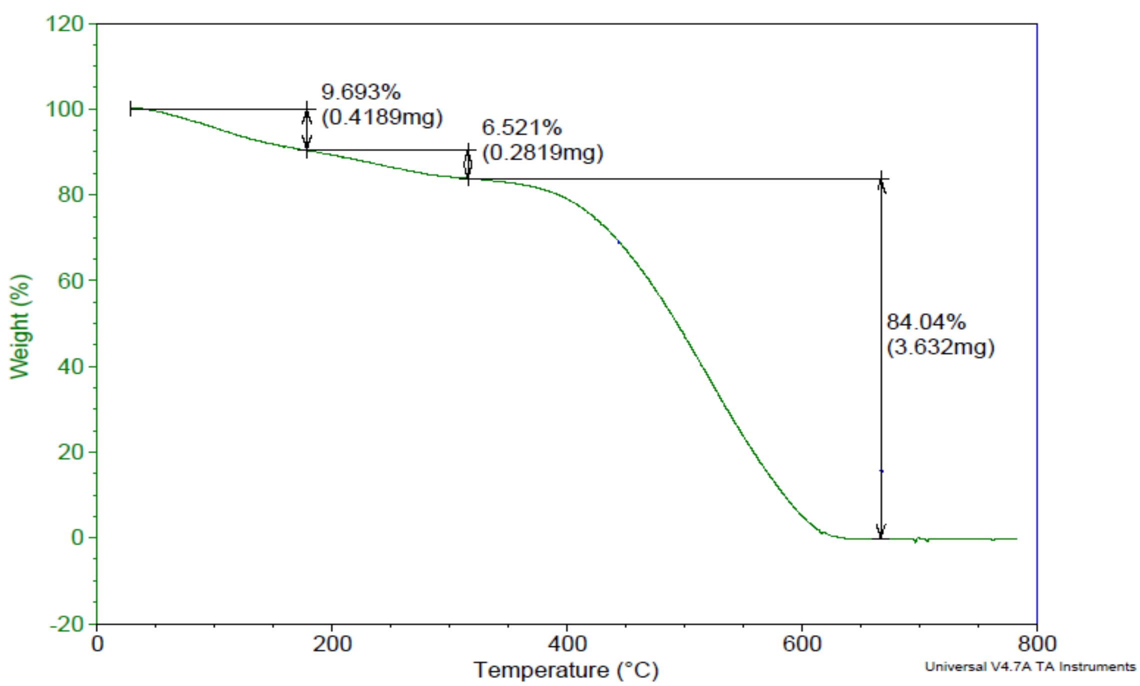

Figure 3.8: Overlay TGA of pure PANI at heating rate 40 $^{o}C/min$

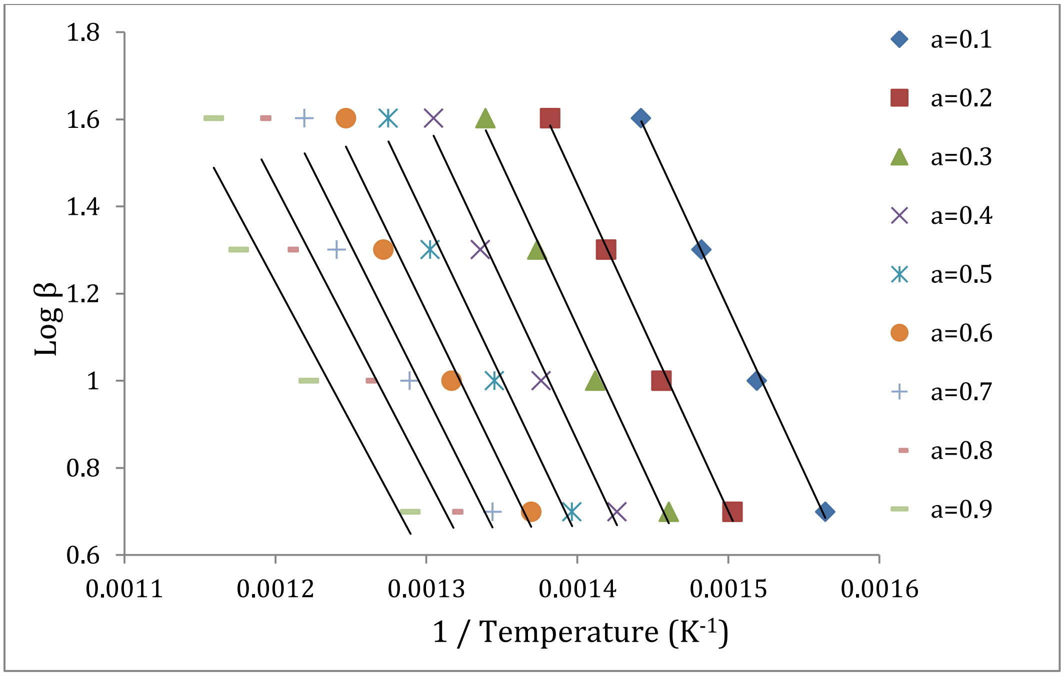

Figure 3.9: The regression lines for conversion of 0.1 -0.9 based on the Ozawa's method for pure PANI.

Table 3.3: The correlation coefficient (R) and the activation energy (Ea) obtained using Ozawa's method for pure PANI.

Sample	Conversion α	R	Ea (kJ/mol)
0 % WS_2 by weight	0.1	0.9982	135.8
	0.2	0.9963	136.6
	0.3	0.9935	135.3
	0.4	0.9889	133.9
	0.5	0.9832	132.1
	0.6	0.9768	129.4
	0.7	0.9671	125.5
	0.8	0.9569	120.9
	0.9	0.9367	117.4
Average			129.6

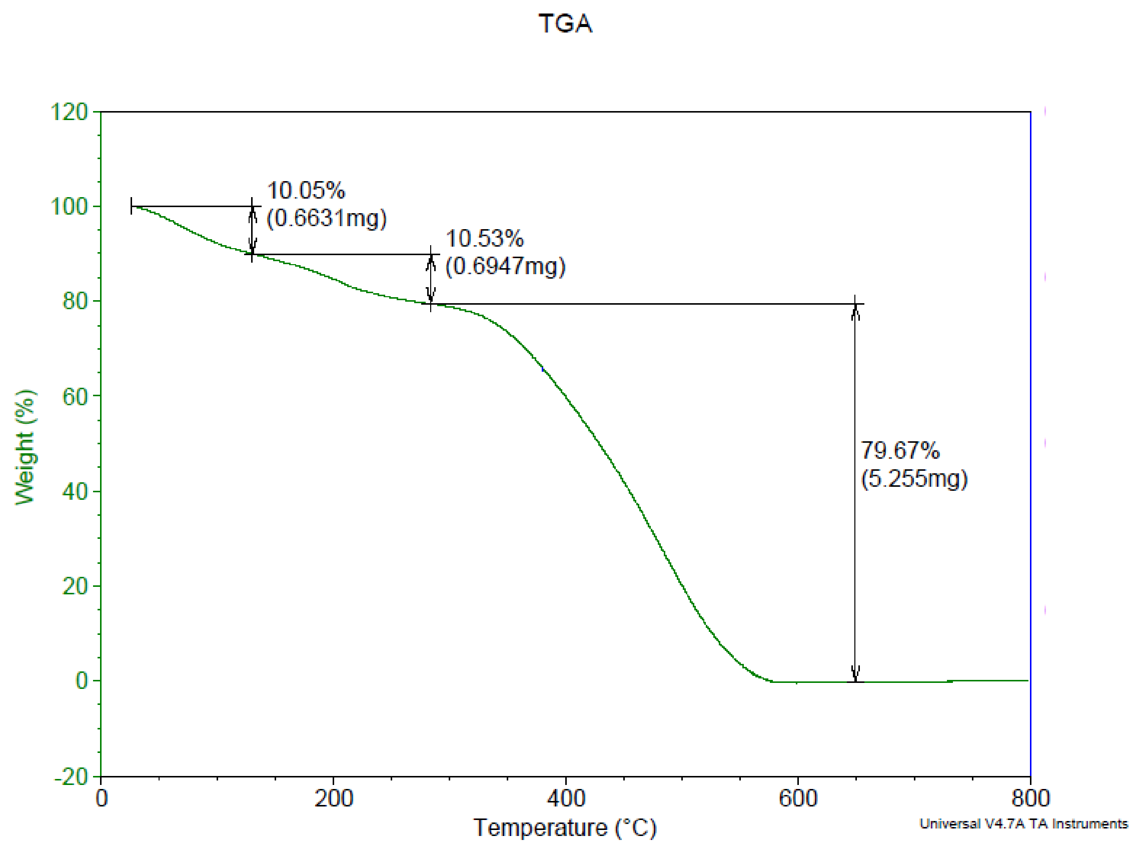

Figure 3.10: Overlay TGA of 1% WS2-PANI at 5 °C/min.

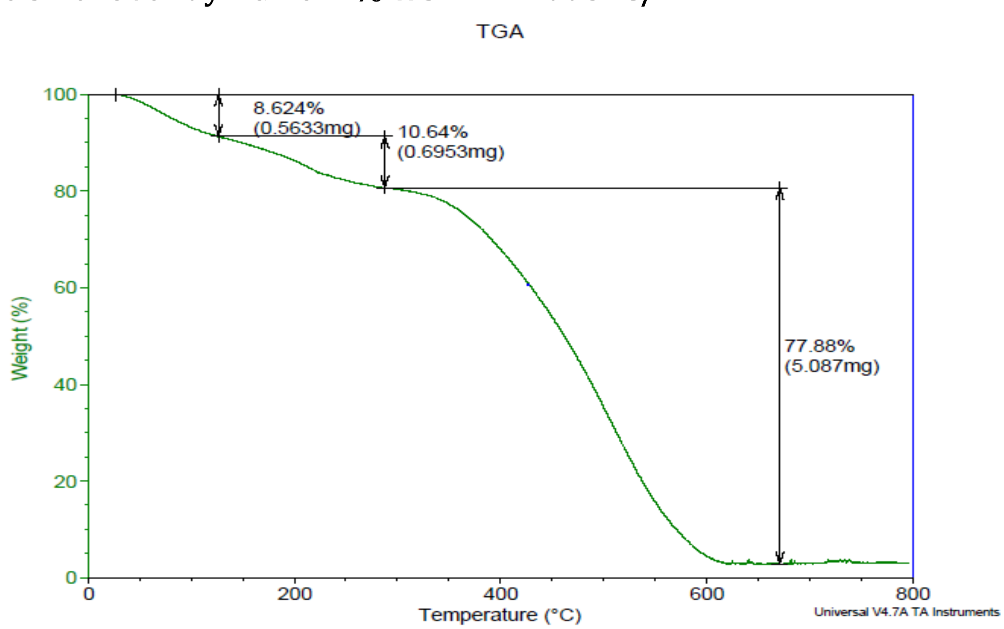

Figure 3.11: Overlay TGA of 1% WS_2-PANI at 10 °C/min.

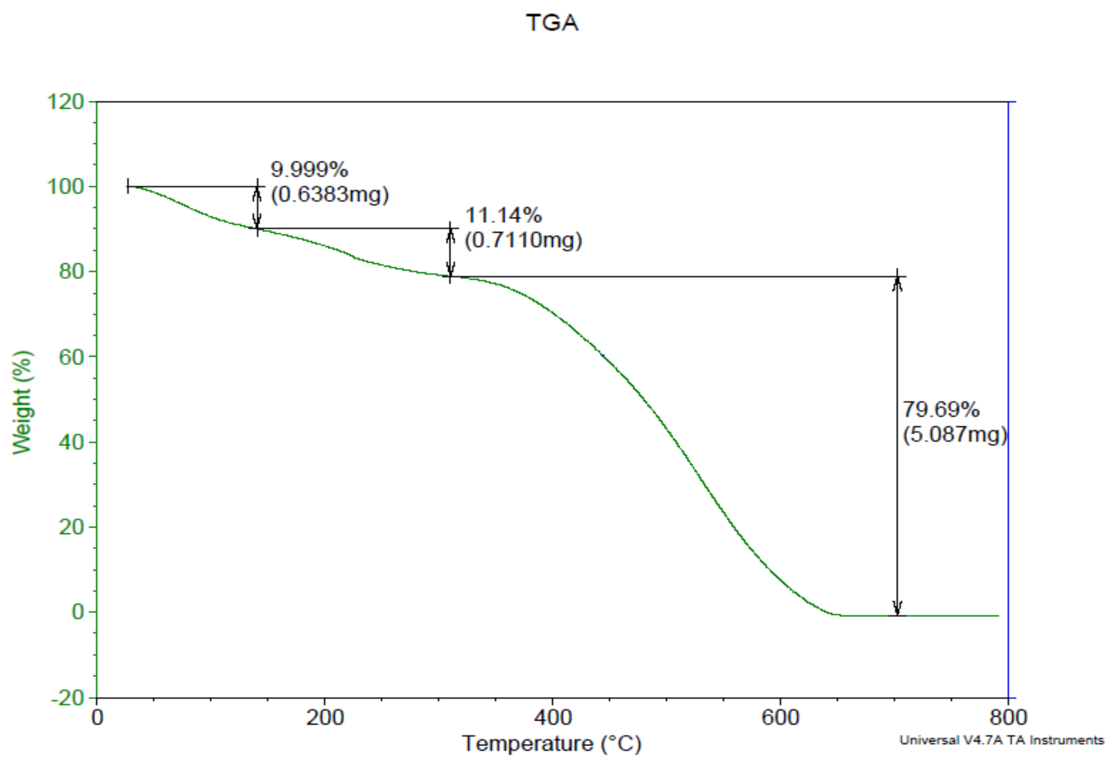

Figure 3.12: Overlay TGA of 1% WS_2-PANI at 20 °C/min.

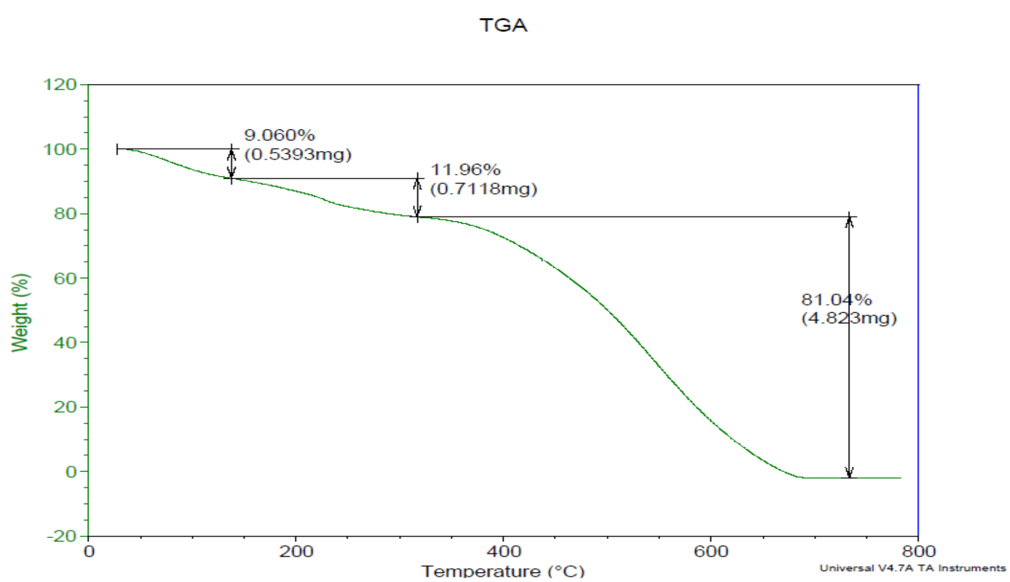

Figure 3.13: Overlay TGA of 1% WS_2-PANI at 40 °C/min.

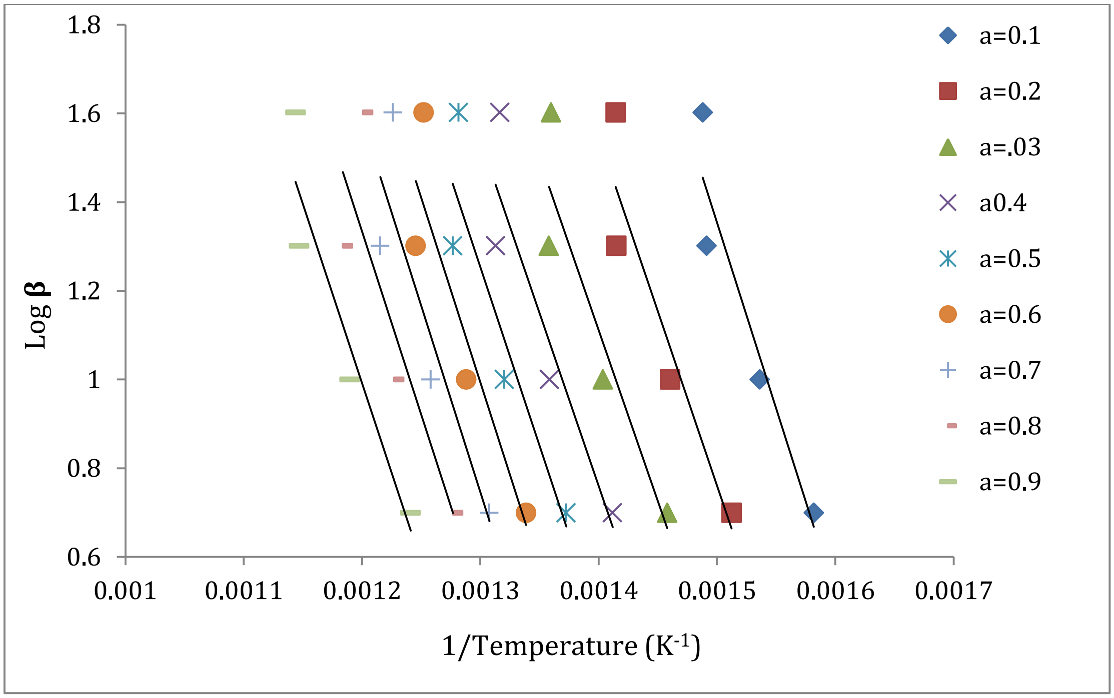

Figure 3.14: The regression lines for conversion of 0.1 -0.9 based on the Ozawa's method for 1 % WS_2-PANI.

Table 3.4: The correlation coefficient (R) and the activation energy (Ea) obtained using Ozawa's method for 1 % WS_2-PANI.

Sample	Conversion α	R	Ea (kJ/mol)
1 % WS_2 by weight	0.1	0.9094	152.6
	0.2	0. 8867	143.1
	0.3	0. 8699	140.1
	0.4	0. 8593	142.1
	0.5	0. 8483	146.6
	0.6	0. 8354	151.2
	0.7	0. 8030	152.9
	0.8	0. 7434	150.4
	0.9	0. 7434	147.2
Average			147.7

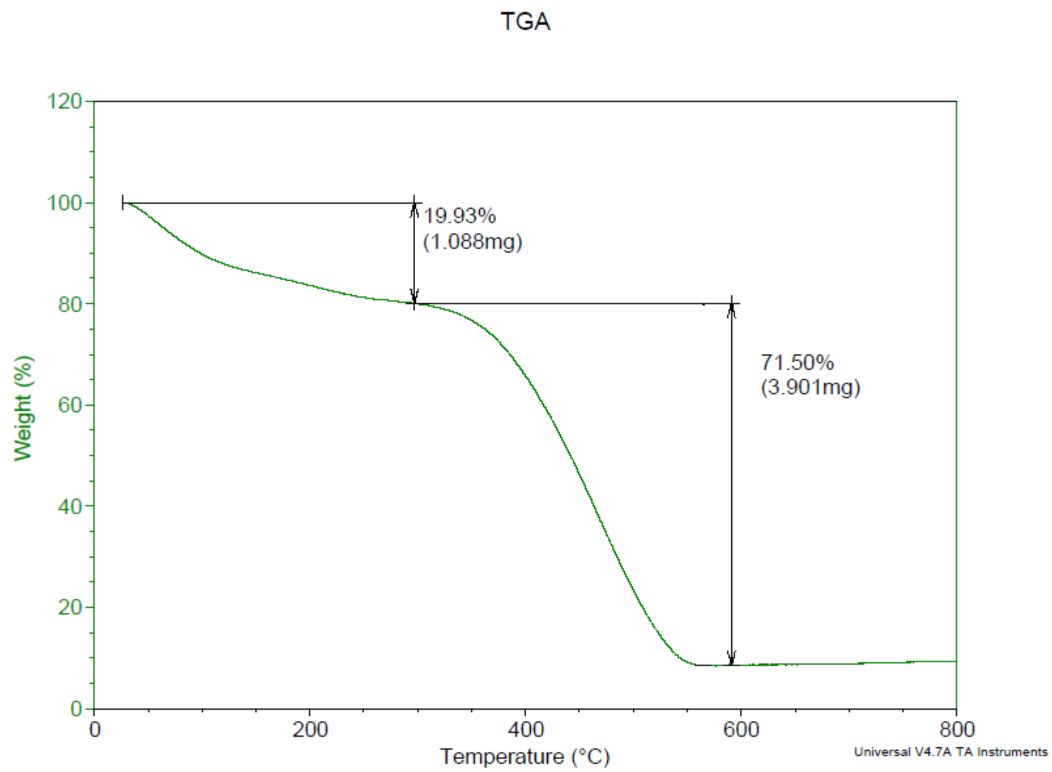

Figure 3.15: Overlay TGA of 5% WS_2-PANI at 5°C/min.

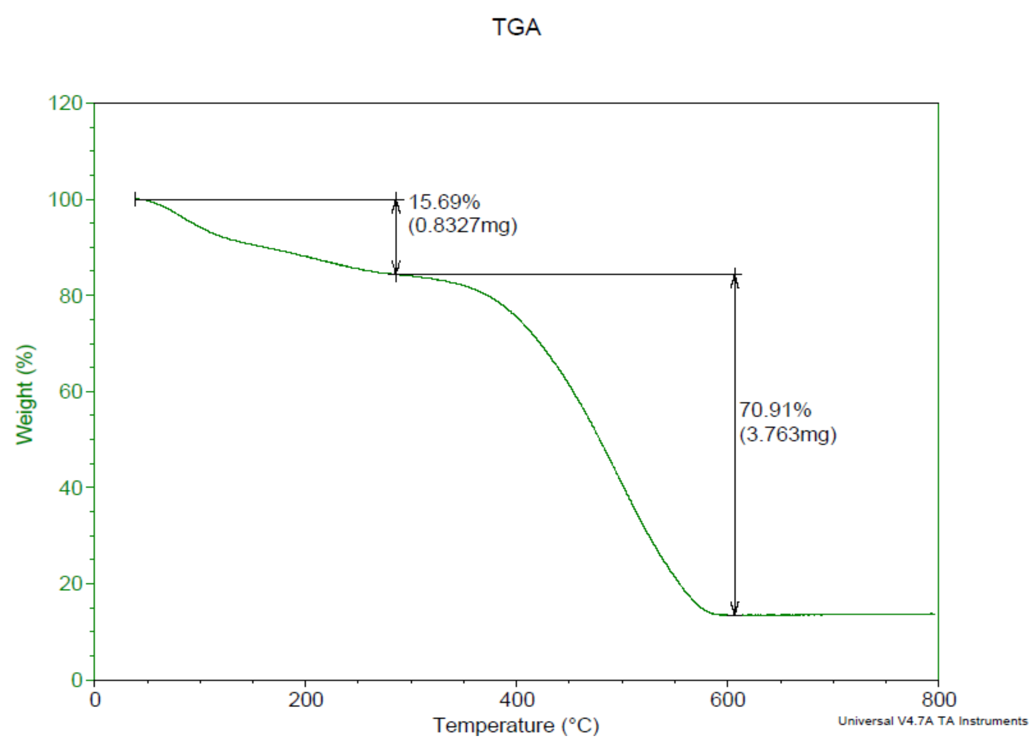

Figure 3.16: Overlay TGA of 5% WS_2-PANI at 10°C/min.

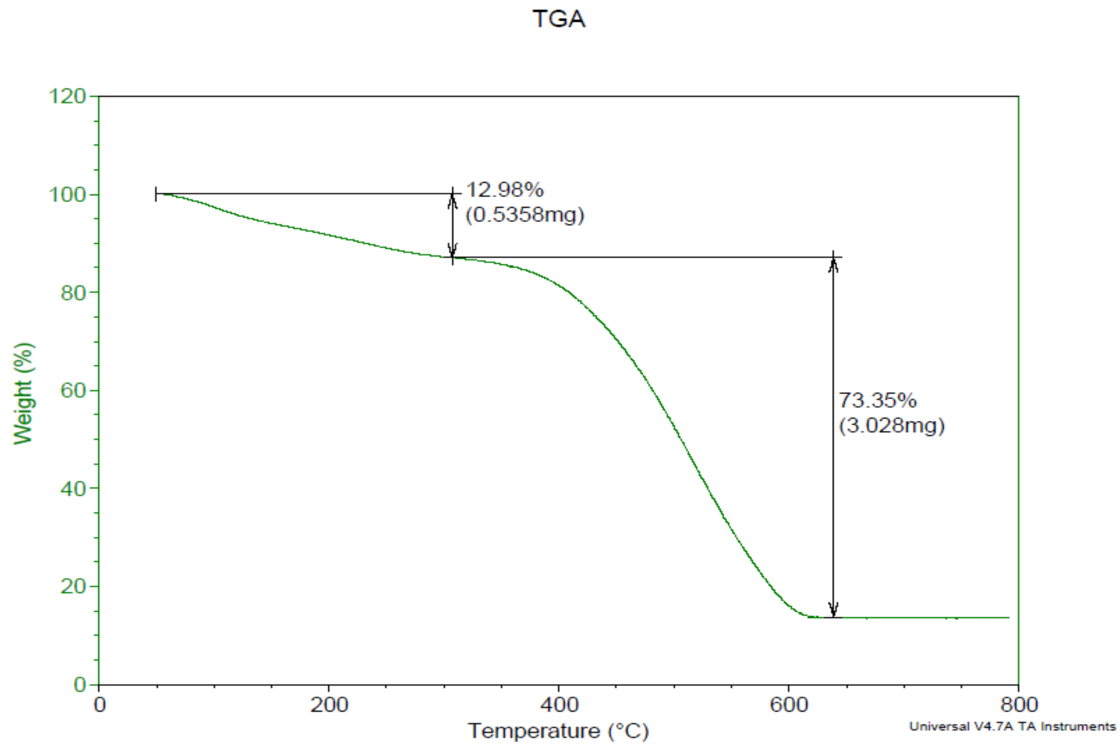

Figure 3.17: Overlay TGA of 5% WS_2-PANI at 20°C/min.

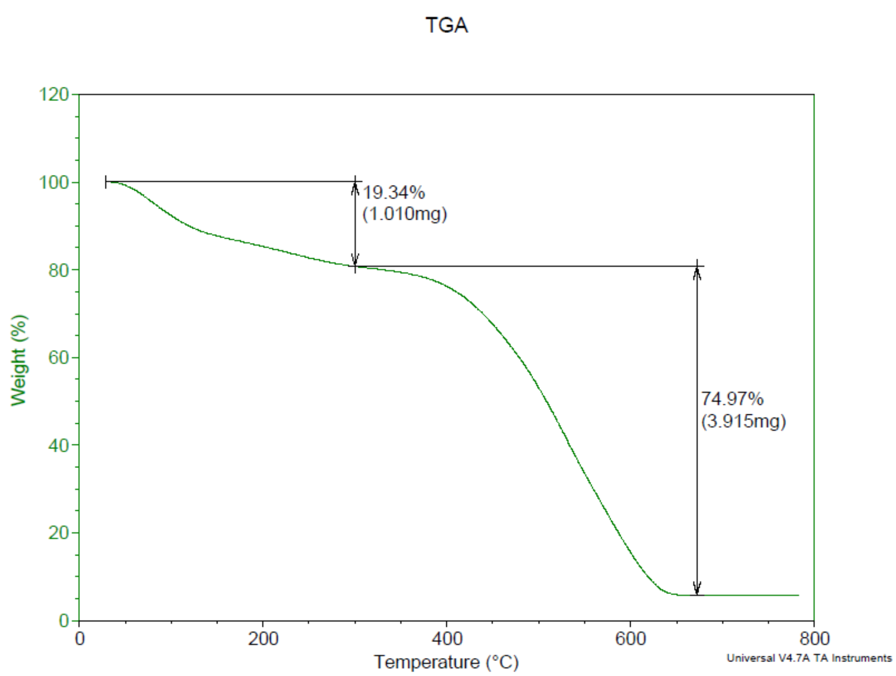

Figure 3.18: Overlay TGA of 5% WS_2-PANI at 40°C/min.

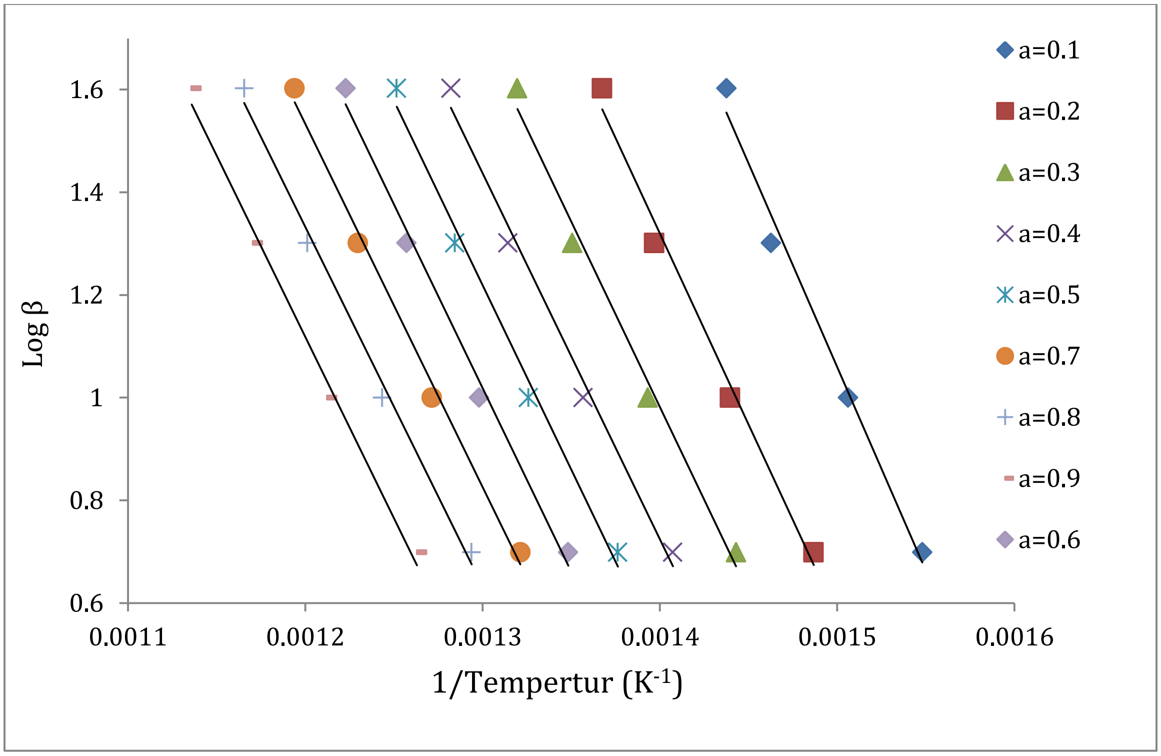

Figure 3.19: The regression lines for conversion α of 0.1 -0.9 based on the Ozawa's method for 5% WS_2-PANI.

Table 3.5: The correlation coefficient (R) and the activation energy (Ea) obtained using Ozawa's method for 5% WS_2-PANI.

Sample	Conversion α	R	Ea (kJ/mol)
5% WS_2 by weight	0.1	0.9873	144.1
	0.2	0.9899	135.2
	0.3	0.9897	131.3
	0.4	0.9905	129.7
	0.5	0.9915	130.5
	0.6	0.9928	130.2
	0.7	0.9944	128.5
	0.8	0.9941	127.4
	0.9	0.9928	128.4
Average			131.7

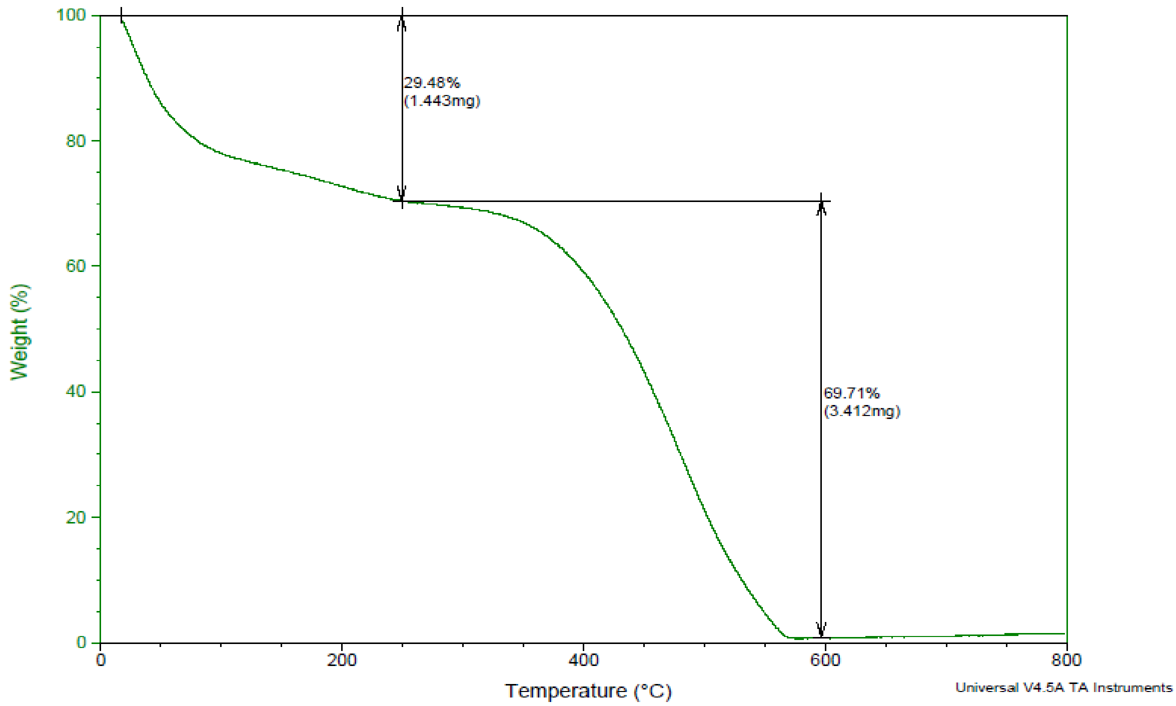

Figure 3.20: Overlay TGA of 7.5% WS_2-PANI at 5 ^{o}C/min.

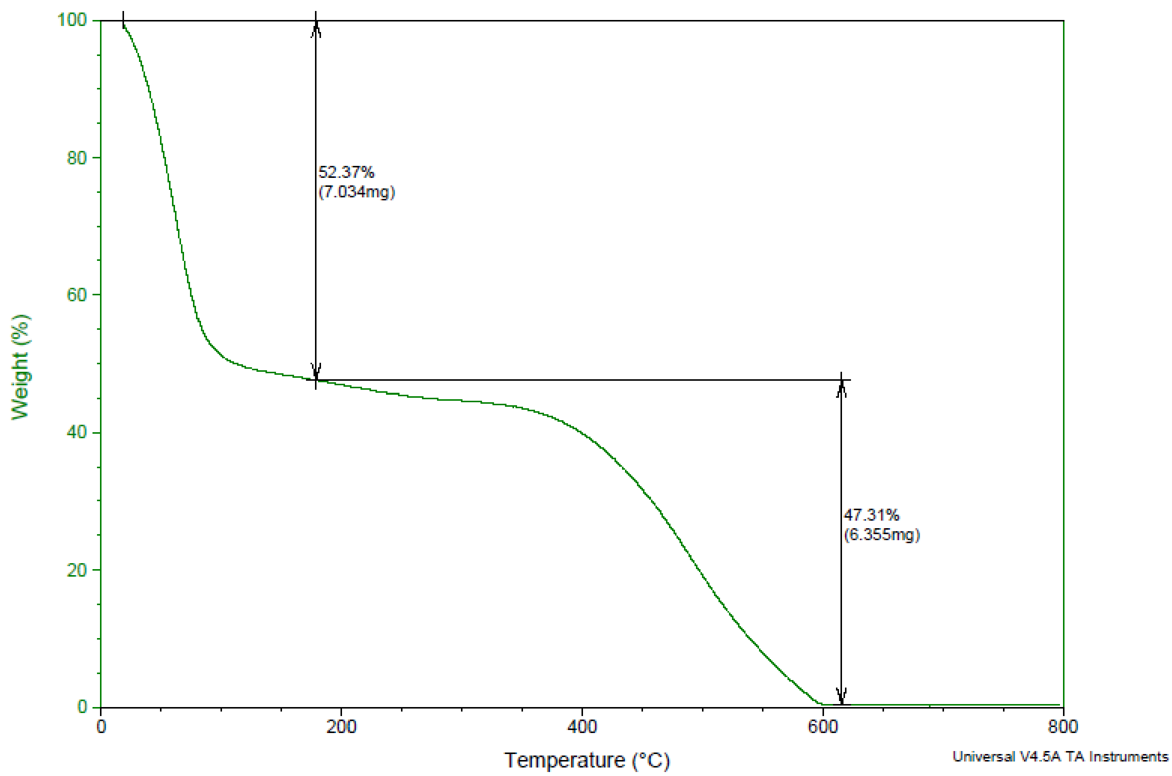

Figure 3.21: Overlay TGA of 7.5% WS_2- PANI at 10 ^{o}C/min.

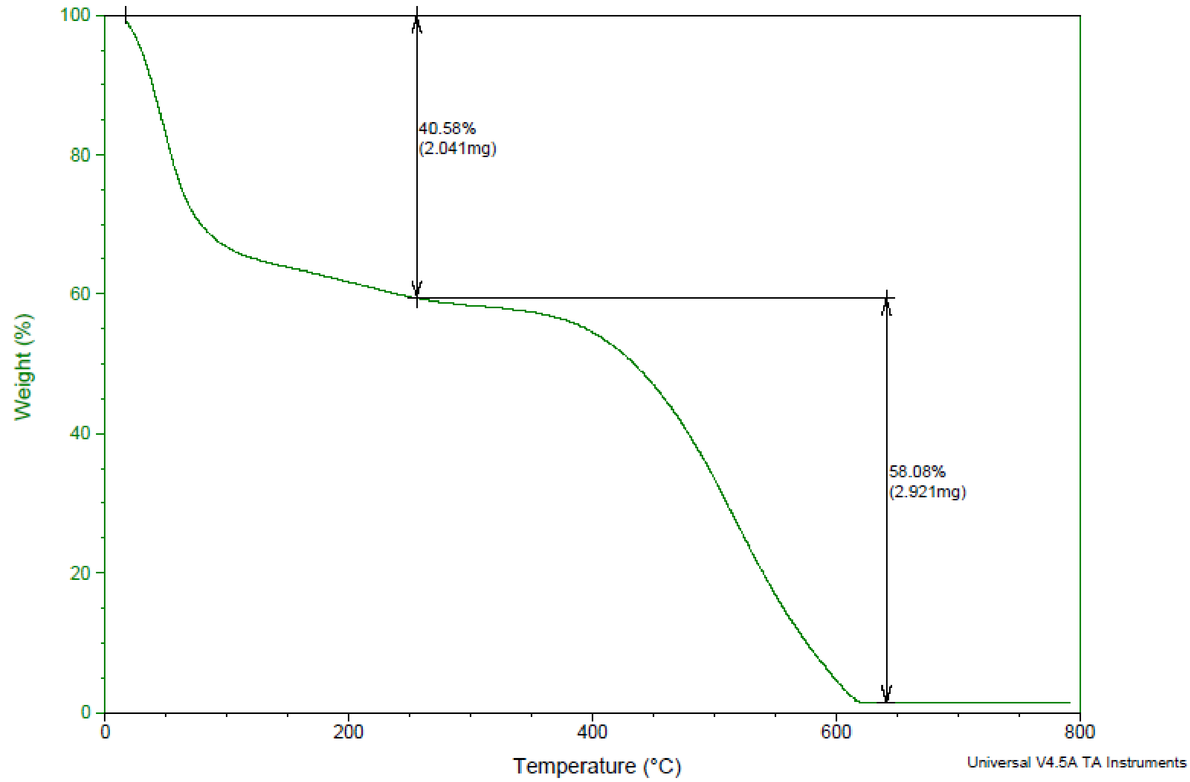

Figure 3.22: Overlay TGA of 7.5% WS_2-PANI at 20 ^{o}C/min.

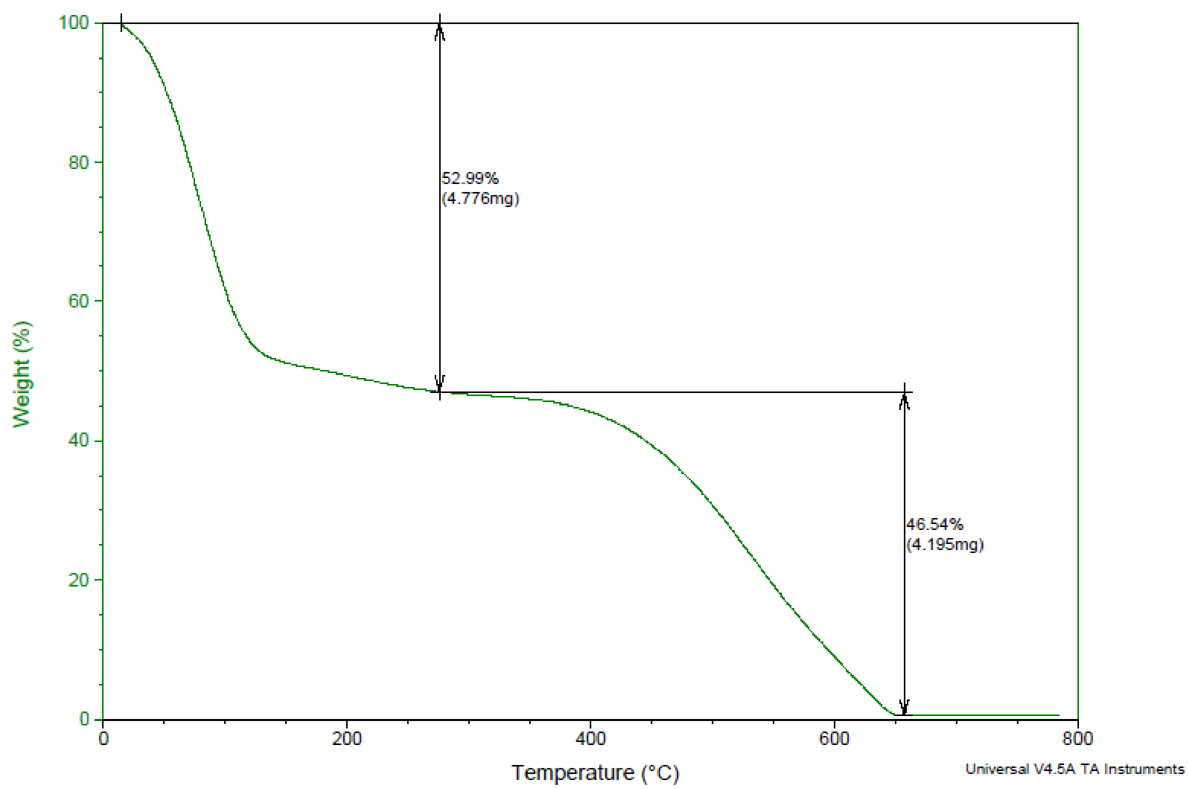

Figure 3.23: Overlay TGA of 7.5% WS_2- PANI at 40 ^{o}C/min.

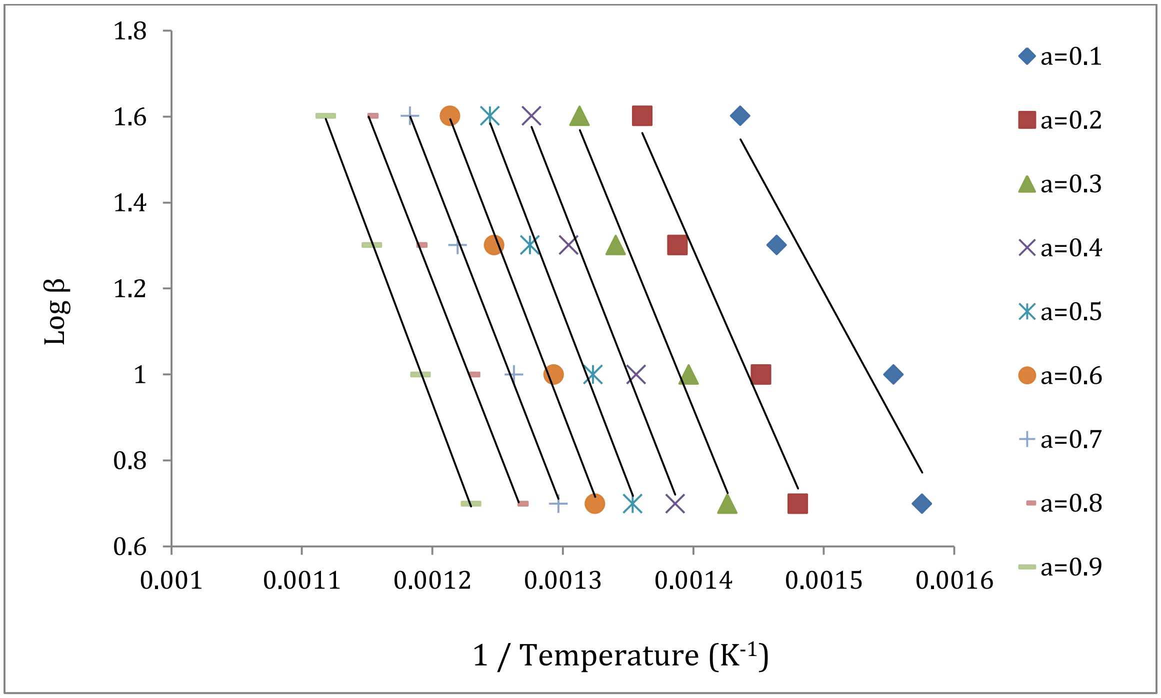

Figure 3.24: The regression lines to conversion α of 0.1 -0.9 based on the Ozawa's method for 7.5 % WS_2-PANI.

Table 3.6: The correlation coefficient (R) and the activation energy (Ea) obtained using Ozawa's method for 7.5 % WS_2-PANI.

Sample	Conversion α	R	Ea (kJ/mol)
7.5 % WS_2 by weight	0.1	0.9383	101.2
	0.2	0.9716	126.2
	0.3	0.9810	135.8
	0.4	0.9864	141.3
	0.5	0.9953	143.9
	0.6	0.9982	142.4
	0.7	0.9997	142.5
	0.8	0.9996	142.0
	0.9	07927	147.4
Average			147.7

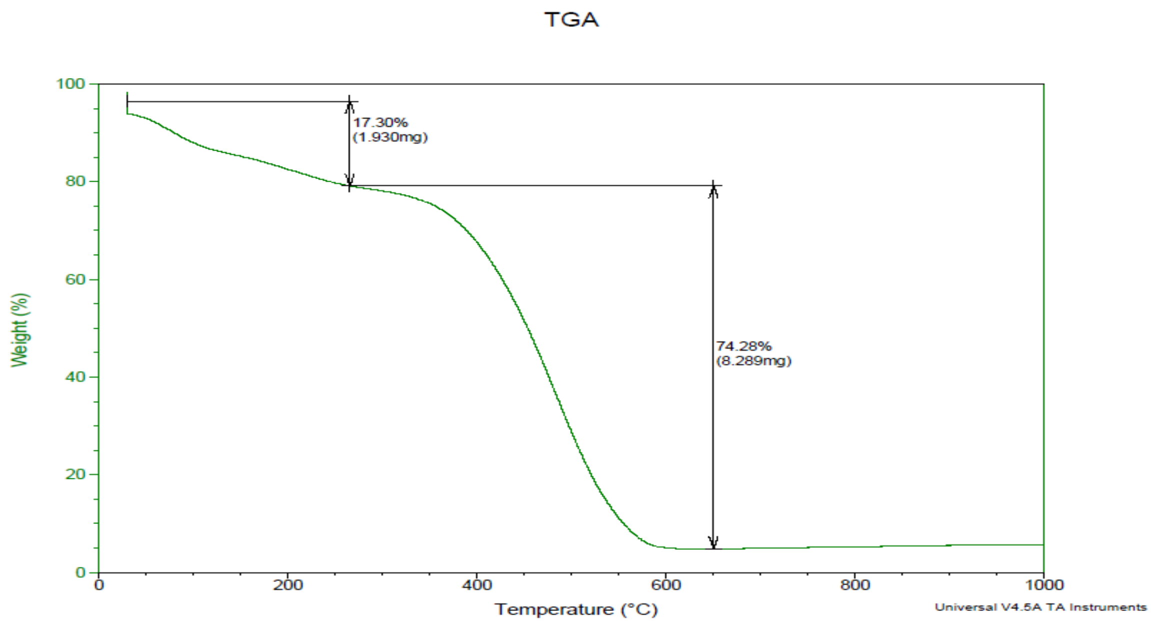

Figure 3.25: Overlay TGA of 10% WS_2- PANI at 5^{o}C/min.

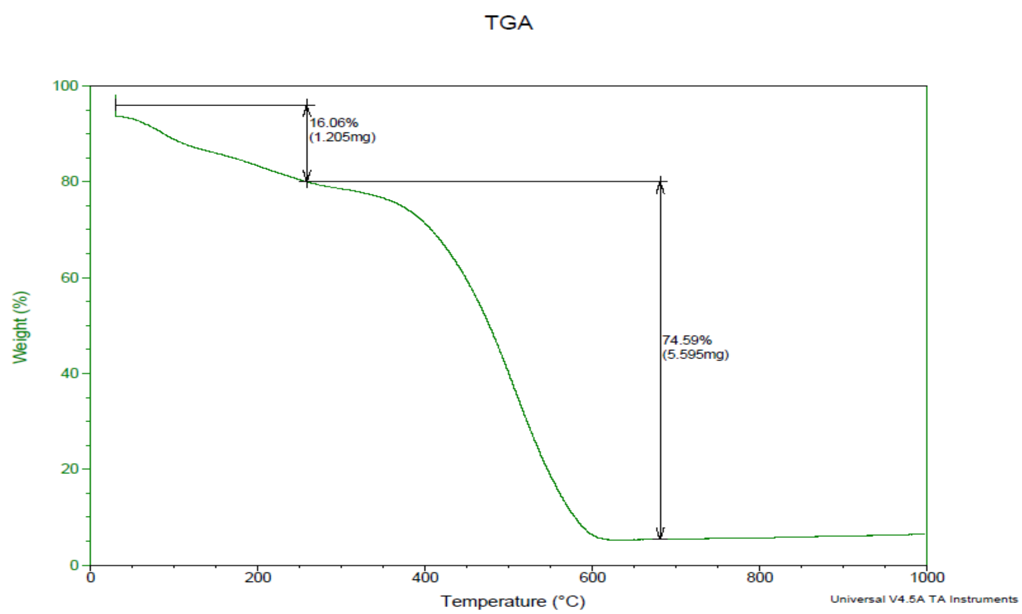

Figure 3.26: Overlay TGA of 10% WS_2- PANI at 10 ^{o}C/min.

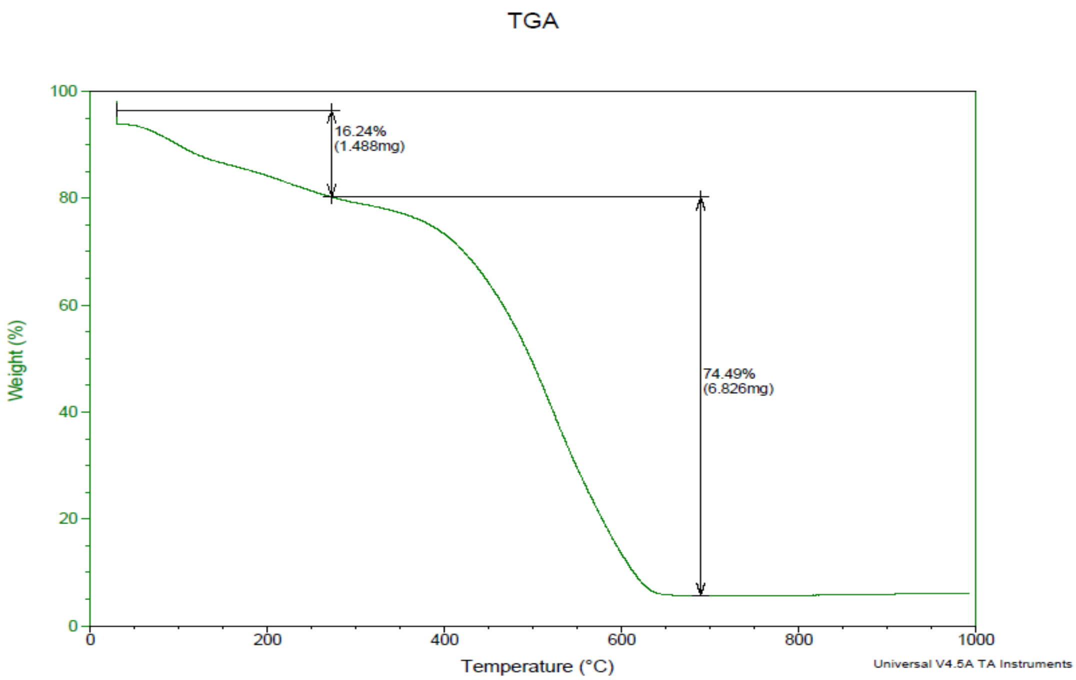

Figure 3.27: Overlay TGA of 10% WS_2- PANI at 20°C/min.

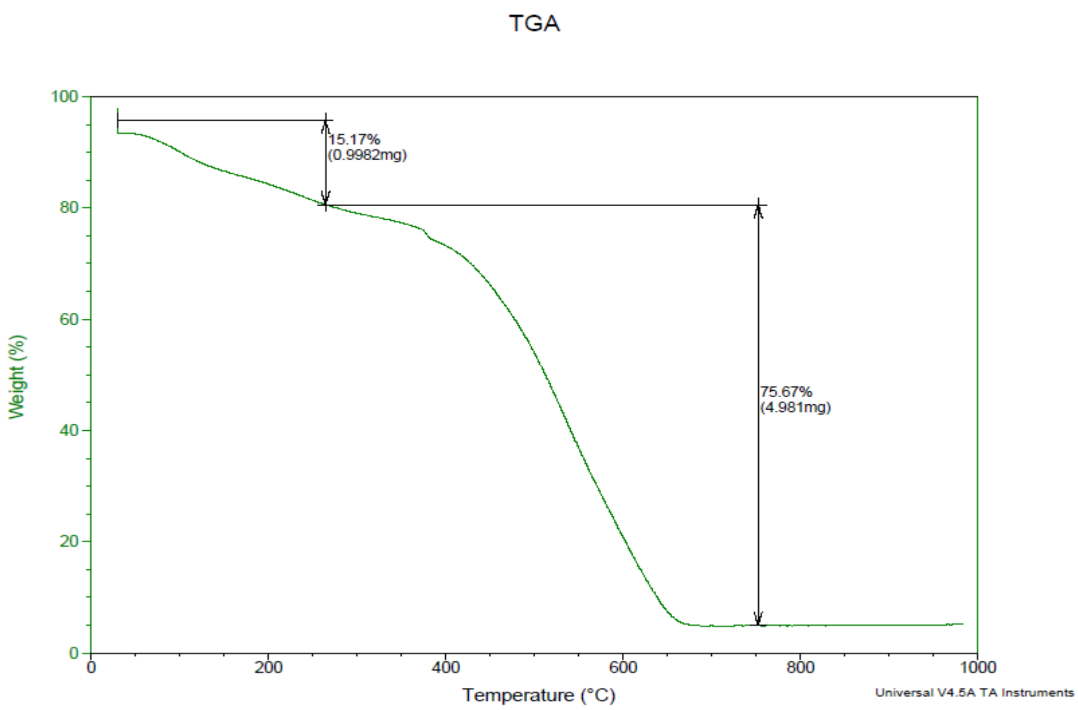

Figure 3.28: Overlay TGA of 10% WS_2- PANI at 40°C/min.

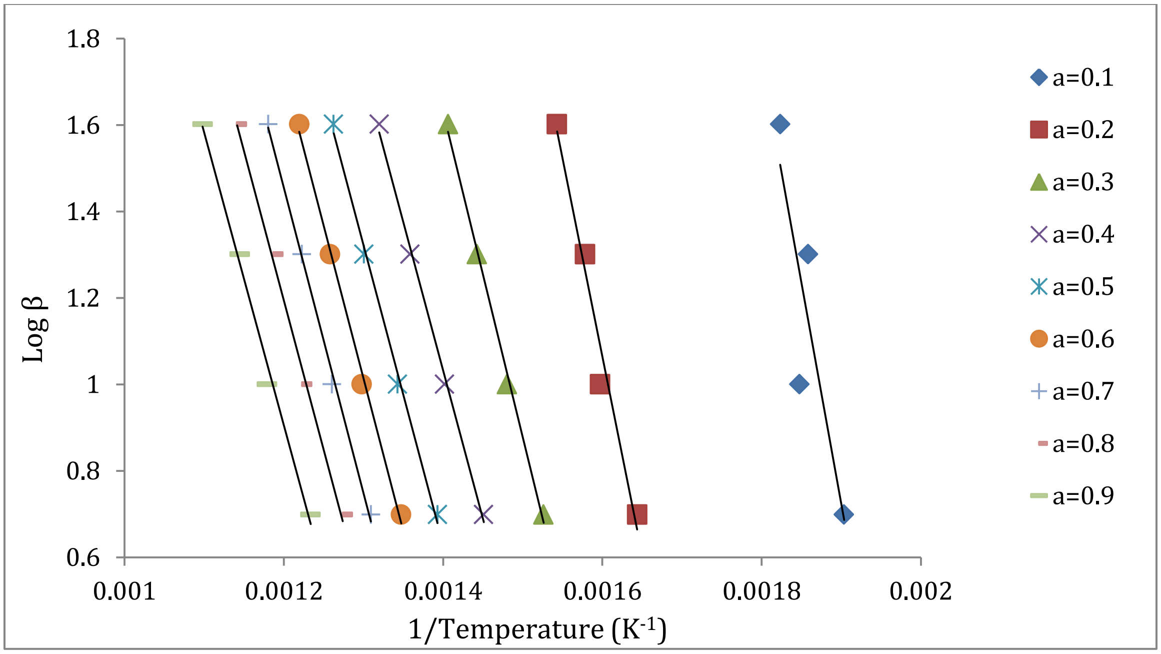

Figure 3.29: The regression lines to conversion α of 0.1 -0.9 based on the Ozawa's method for 10 % WS_2-PANI.

Table 3.7: The correlation coefficient (R) and the activation energy (Ea) obtained using Ozawa's method for 10 % WS_2-PANI.

Sample	Conversion α	R	Ea (kJ/mol)
10 % WS_2 by weight	0.1	0.9383	146.3
	0.2	0.9716	154.9
	0.3	0.9810	156.6
	0.4	0.9864	156.8
	0.5	0.9953	157.8
	0.6	0.9982	152.8
	0.7	0.9997	154.7
	0.8	0.9996	149.4
	0.9	07927	149.7
Average			153.3

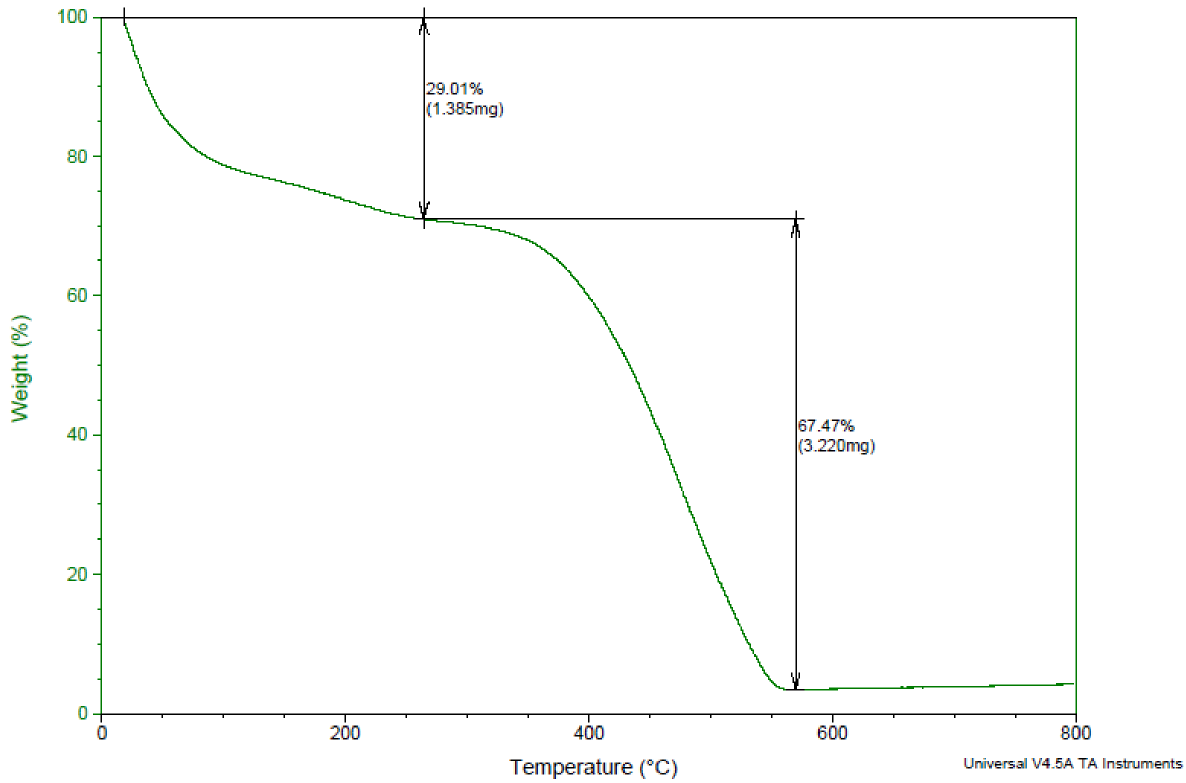

Figure 3.30: Overlay TGA of 12.5% WS_2-PANI at 5 ^oC/min

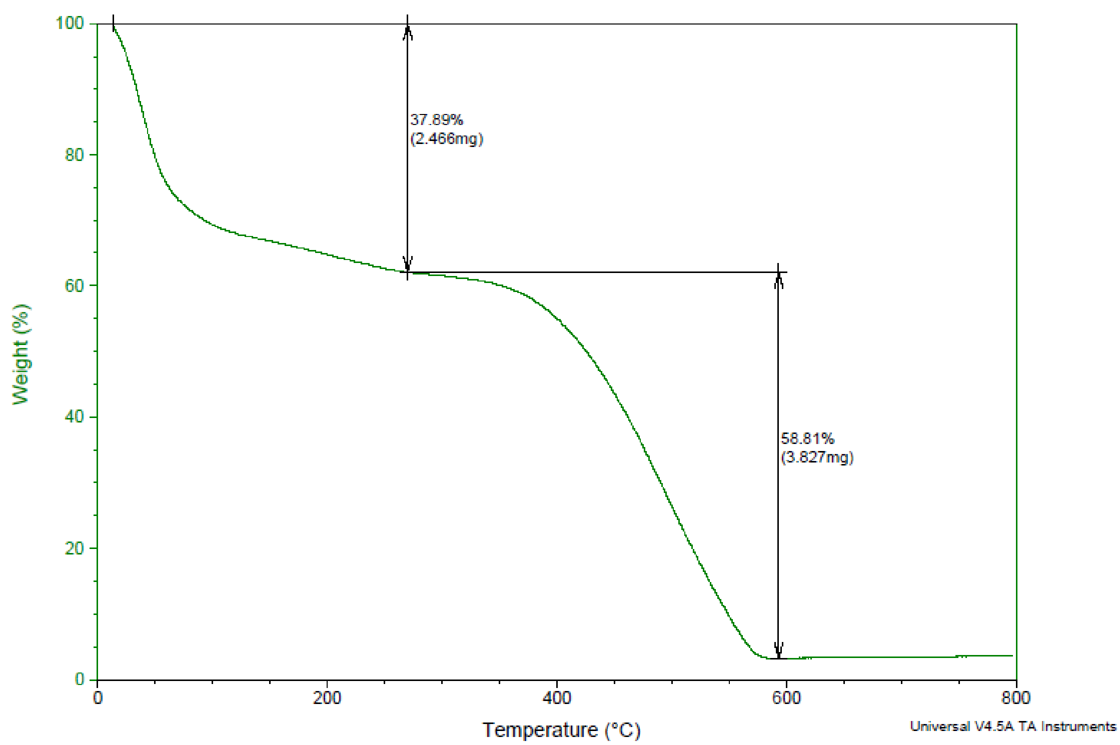

Figure 3.31: Overlay TGA of 12.5% WS_2-PANI at 10 ^oC/min

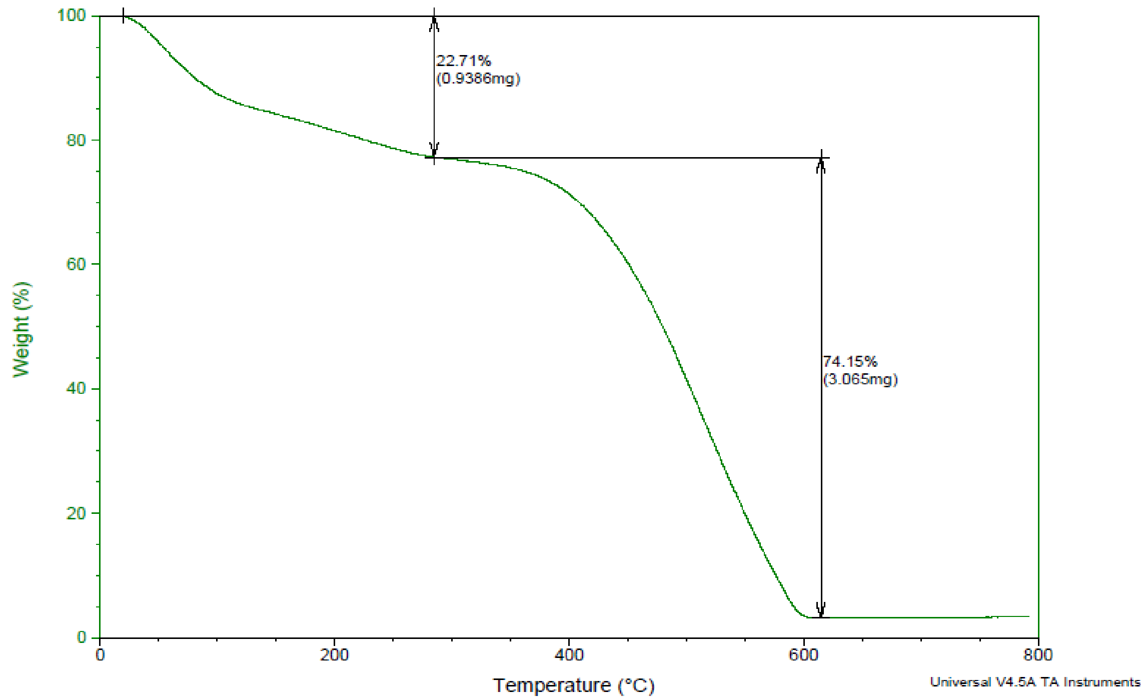

Figure 3.32: Overlay TGA of 12.5% WS_2-PANI at 20 ^oC/min

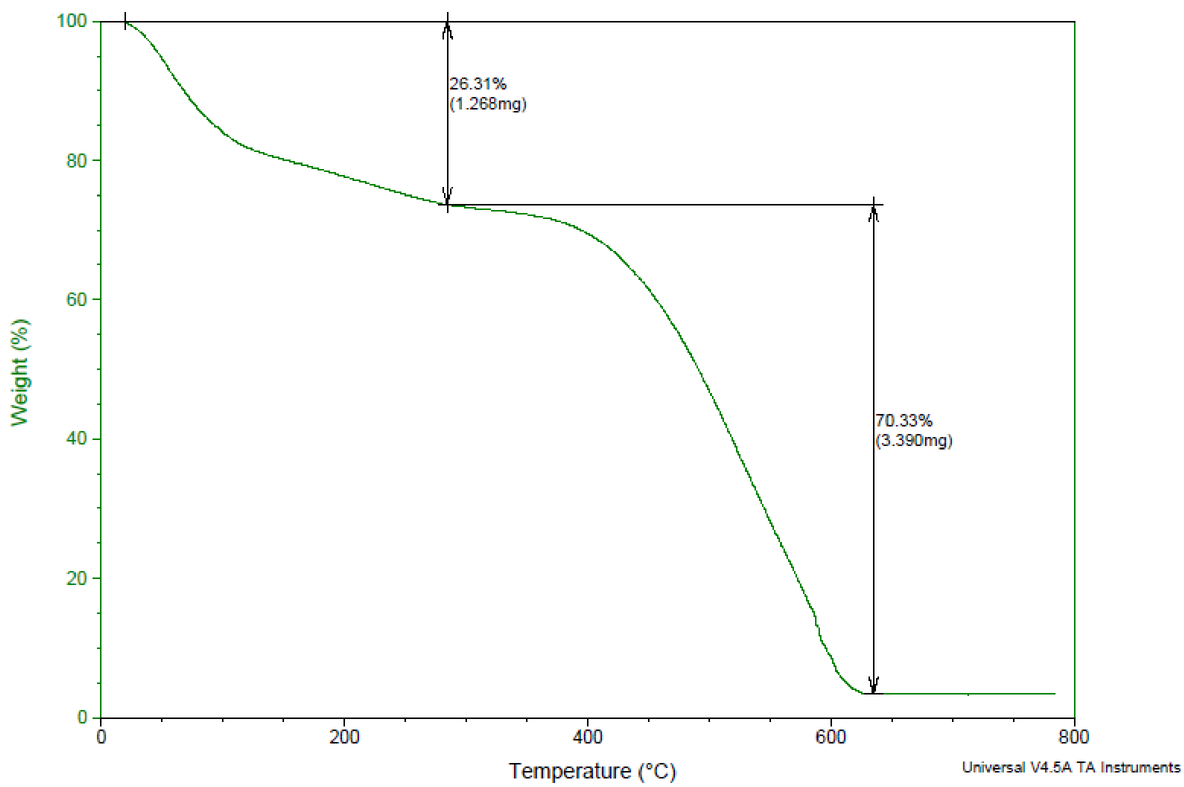

Figure 3.33: Overlay TGA of 12.5% WS_2- PANI at 40 ^oC/min

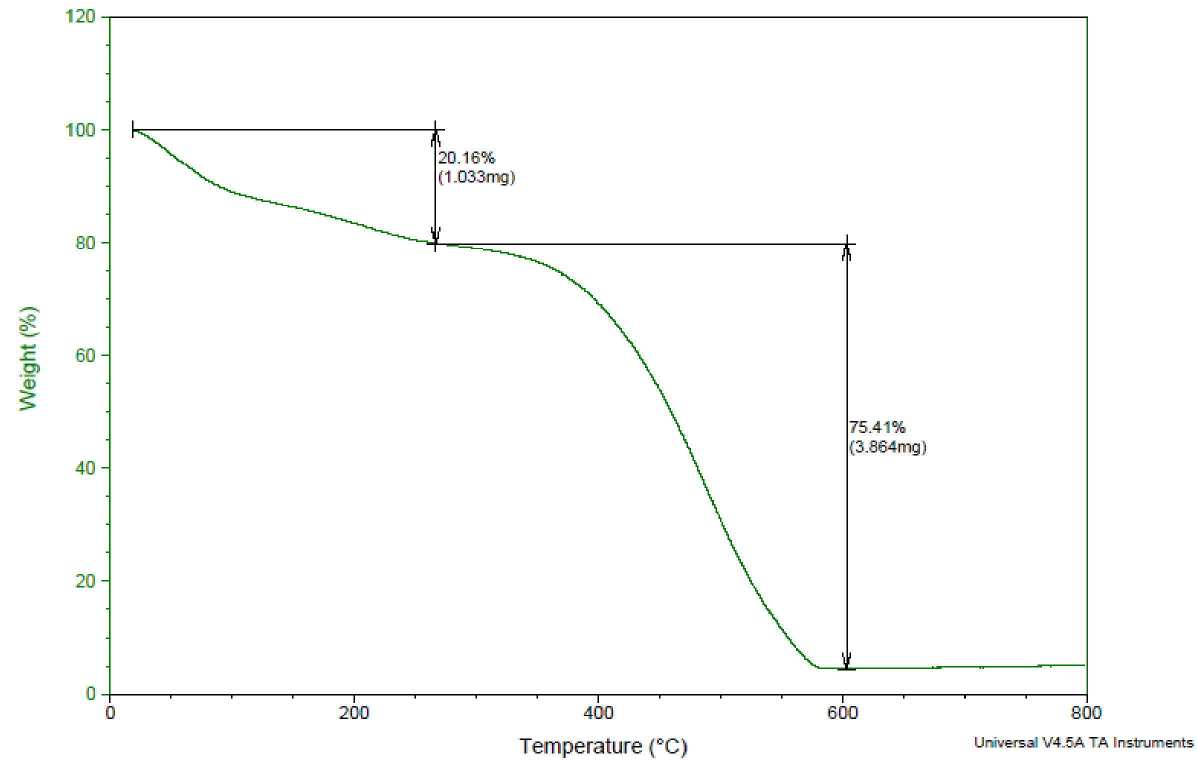

Figure 3.34: Overlay TGA of 15% WS_2-PANI at 5 °C/min

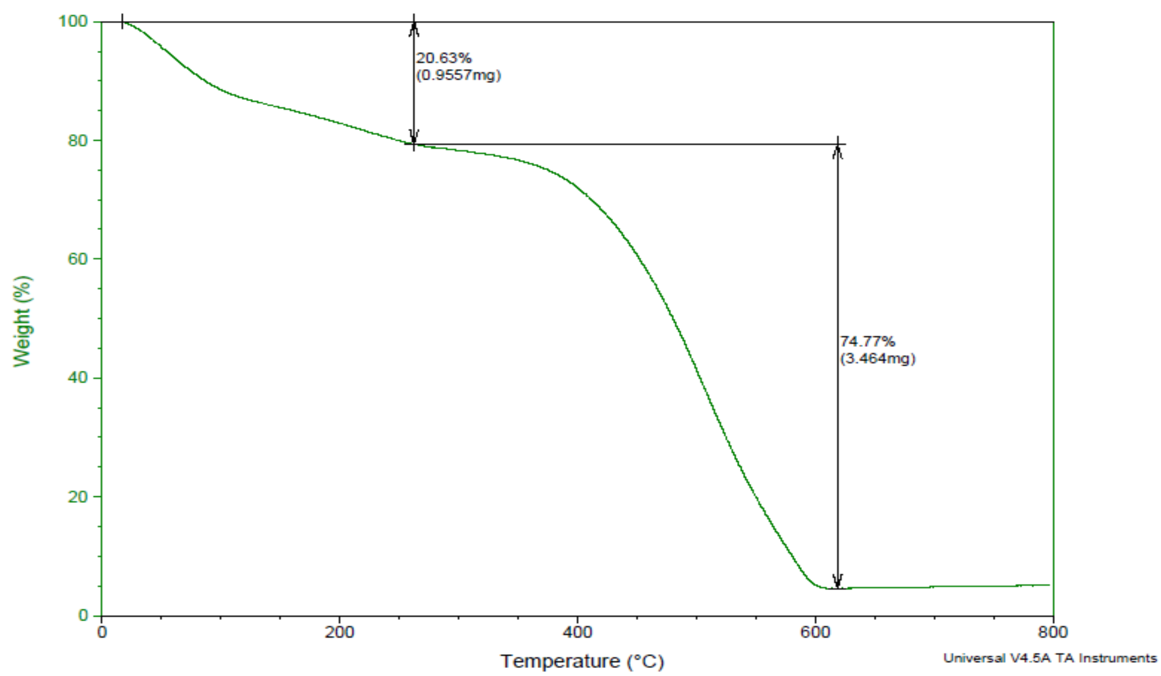

Figure 3.35: Overlay TGA of 15% WS_2-PANI at 10 °C/min

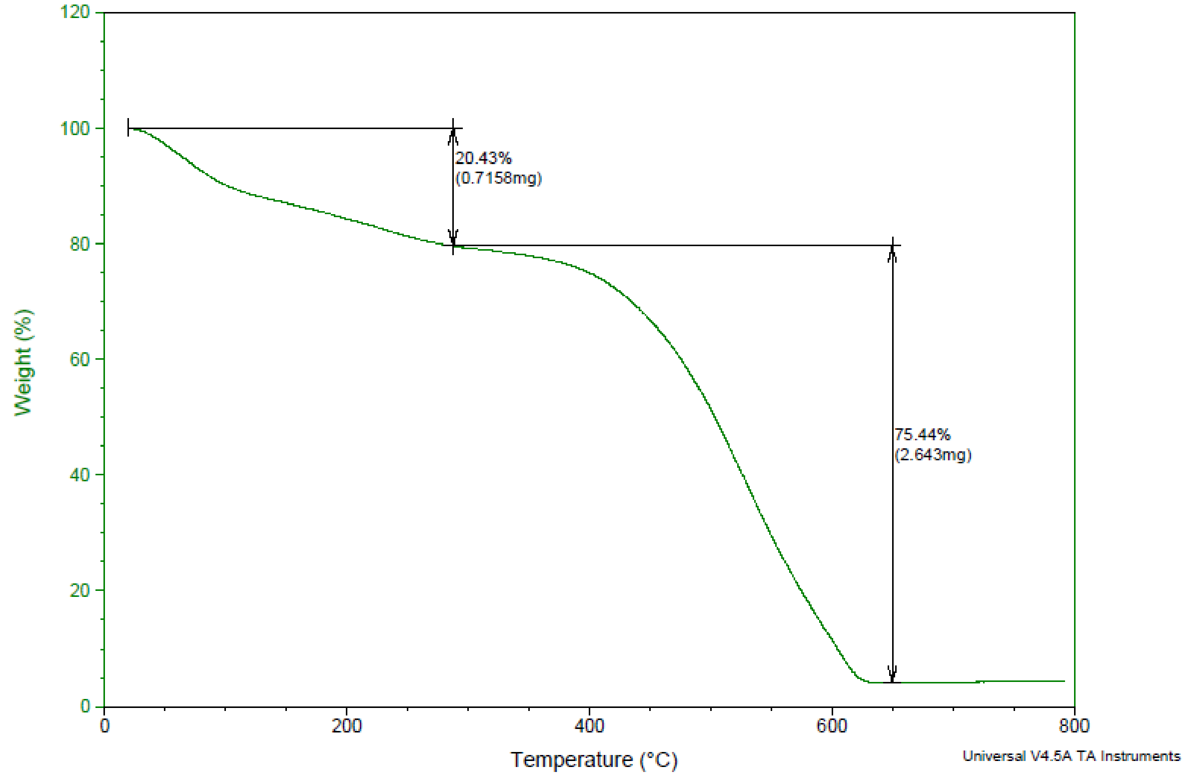

Figure 3.36: Overlay TGA of 15% WS_2-PANI at 20 ^oC/min

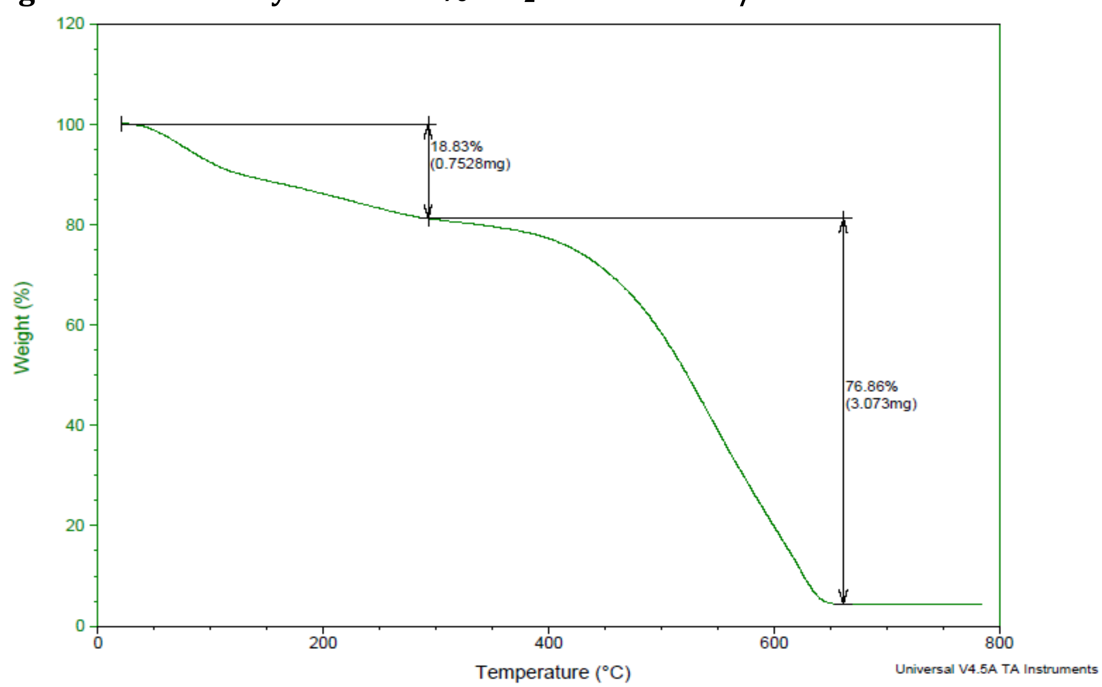

Figure 3.37: Overlay TGA of 15% WS_2-PANI at 40 ^oC/min

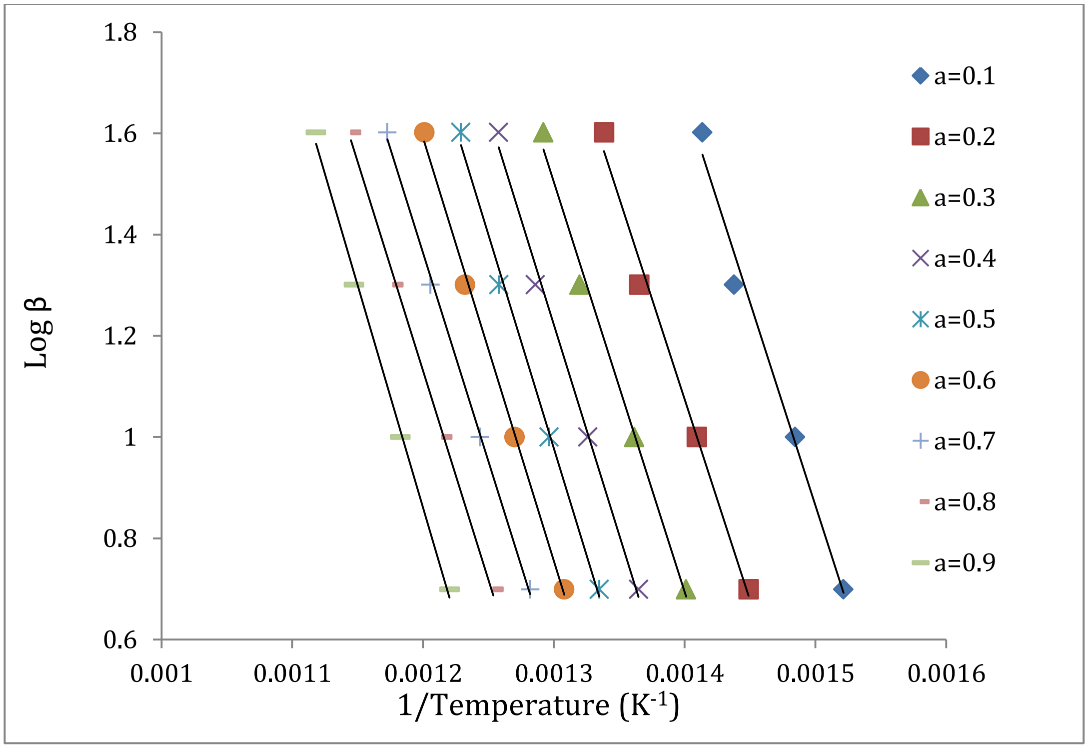

Figure 3.38: The regression lines for conversion α of 0.1 -0.9 based on the Ozawa's method for 15 % WS_2- PANI.

Table 3.8: The correlation coefficient (R) and the activation energy (Ea) obtained using Ozawa's method for 15 % WS_2- PANI.

Sample	**Conversion α**	**R**	**Ea (kJ/mol)**
15 % WS_2 by weight	0.1	0.9866	145.7
	0.2	0.9914	144.5
	0.3	0.9914	147.2
	0.4	0.9944	150.8
	0.5	09959	153.3
	0.6	0.9979	152.2
	0.7	0.9987	149.6
	0.8	0.9983	150.2
	0.9	0.9966	159.7
Average			150.3

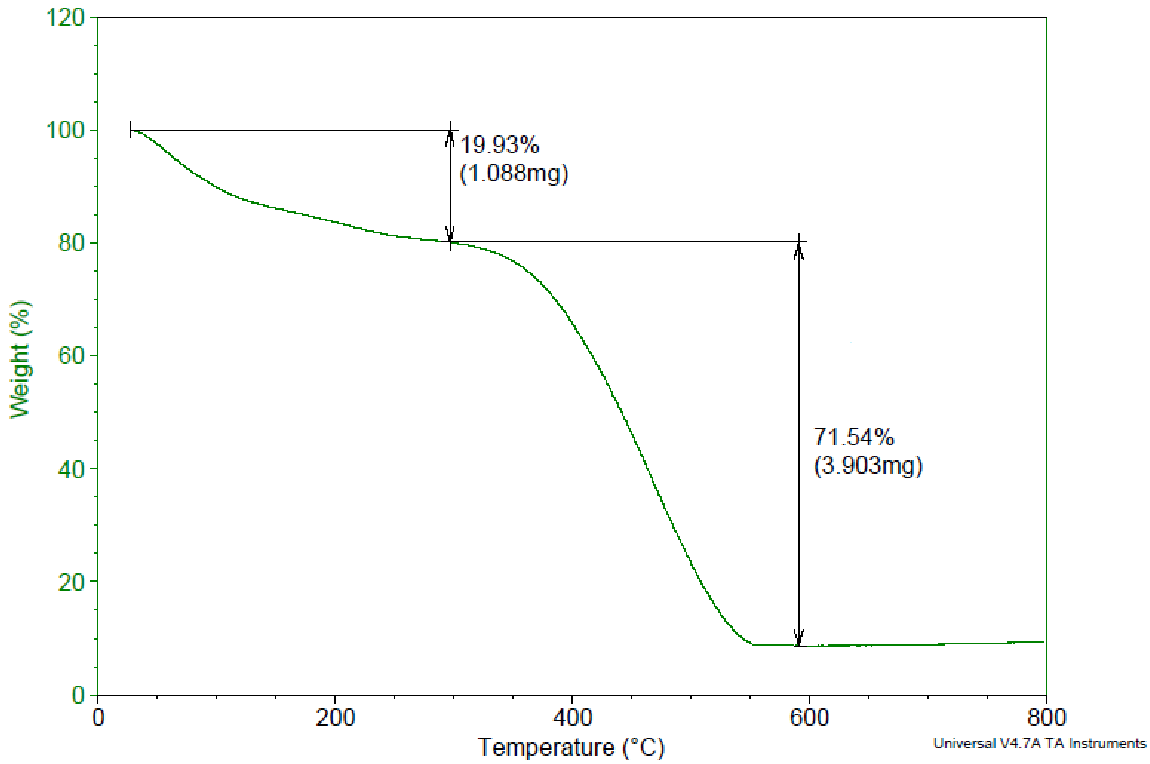

Figure 3.39: Overlay TGA of 20% WS_2- PANI at 5 ^{o}C/min.

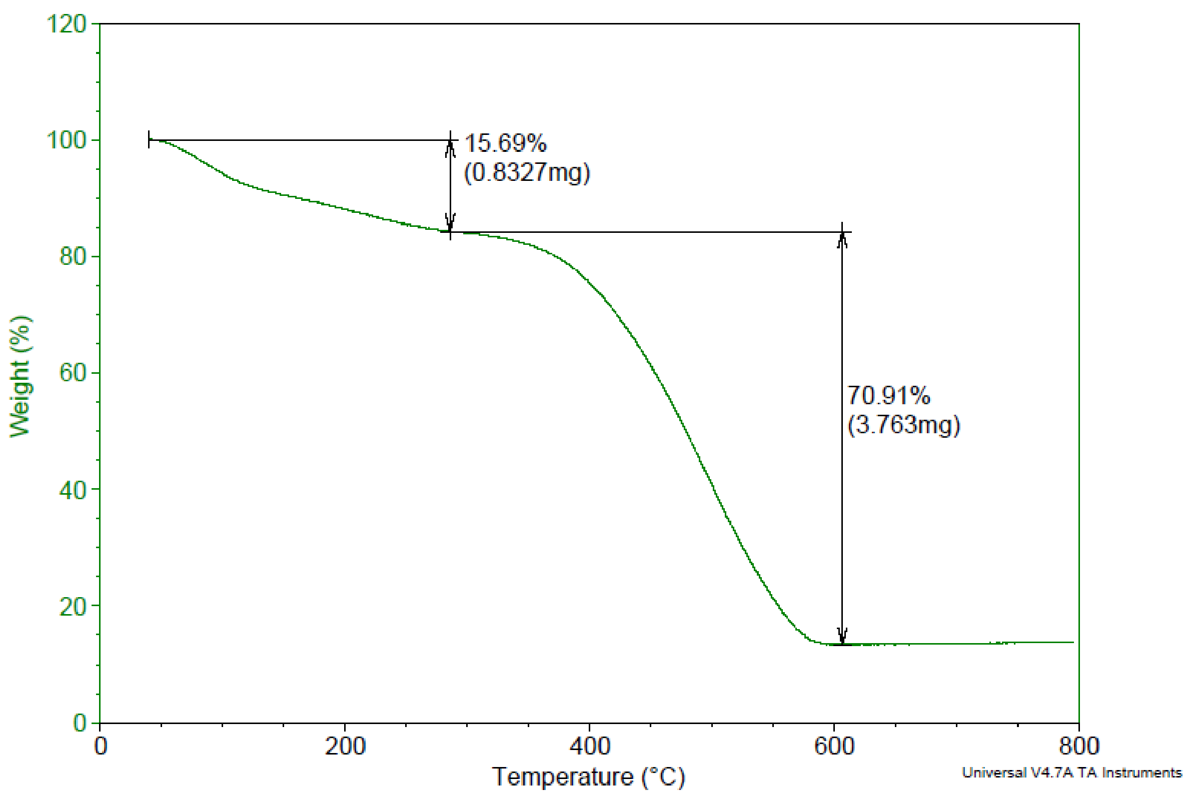

Figure 3.40: Overlay TGA of 20% WS_2-PANI at 10^{o}C/min.

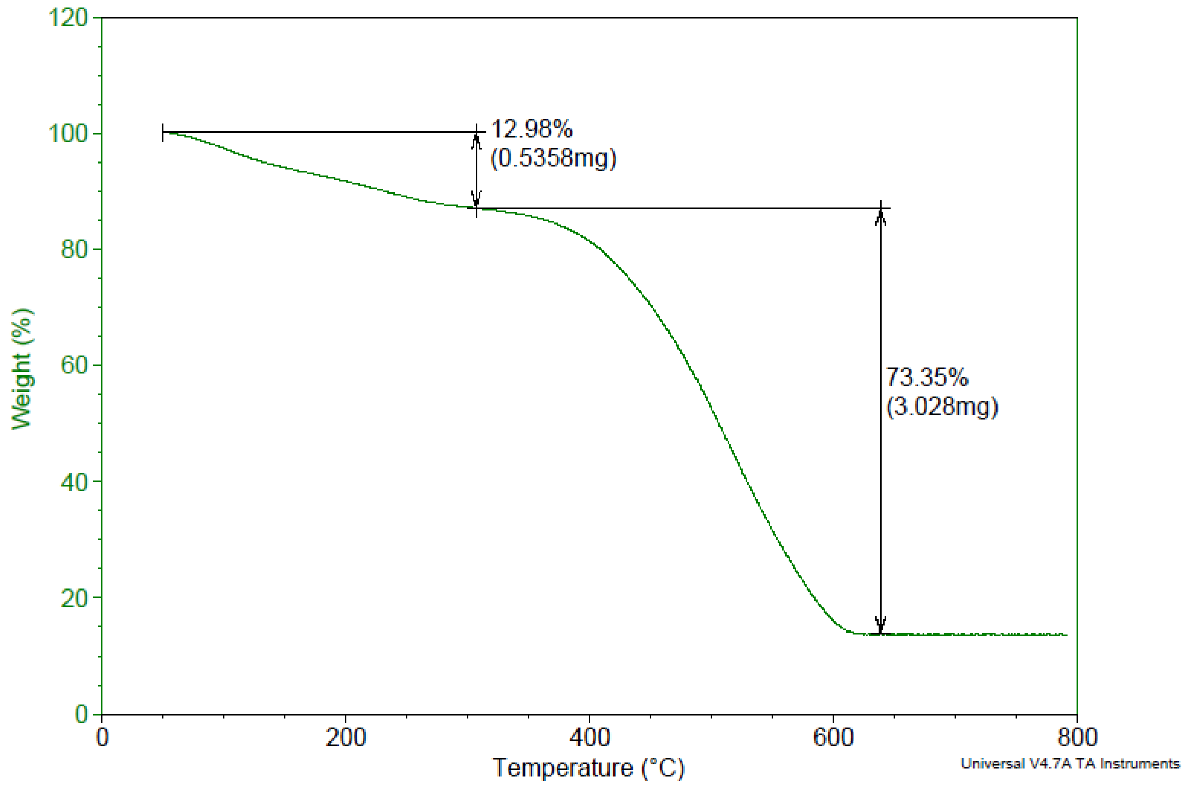

Figure 3.41: Overlay TGA of 20% WS_2-PANI at 20 ^oC/min.

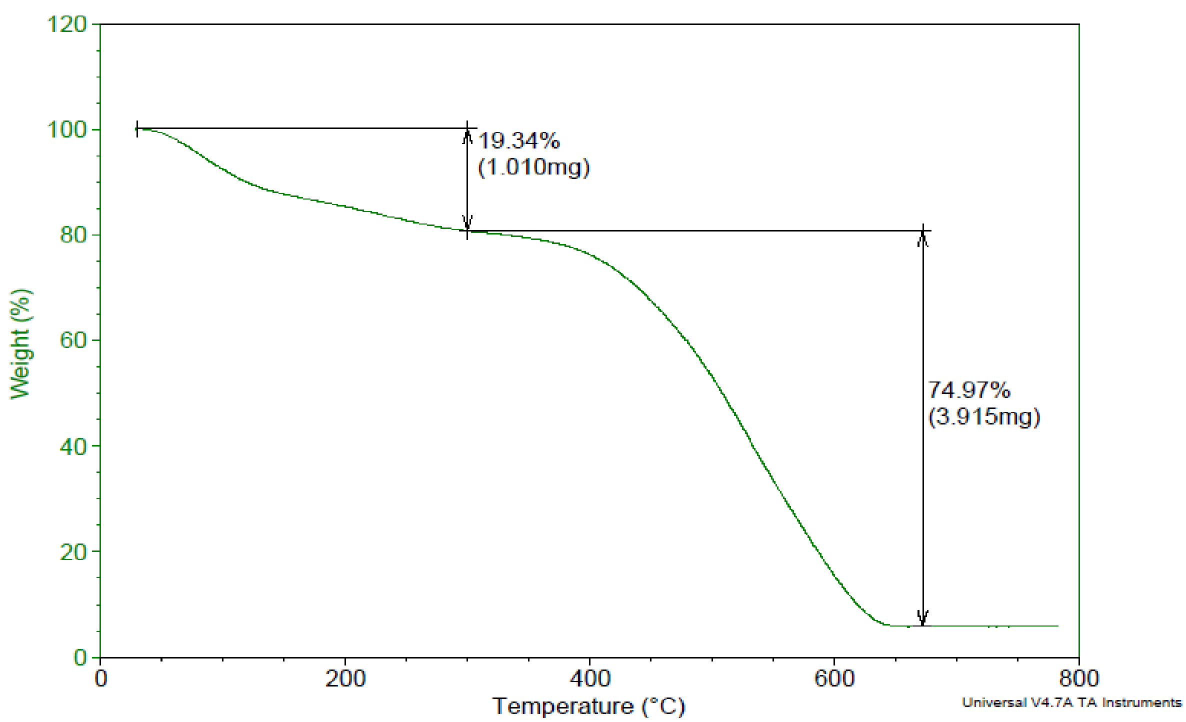

Figure 3.42: Overlay TGA of 20% WS_2-PANI at 40 ^oC/min.

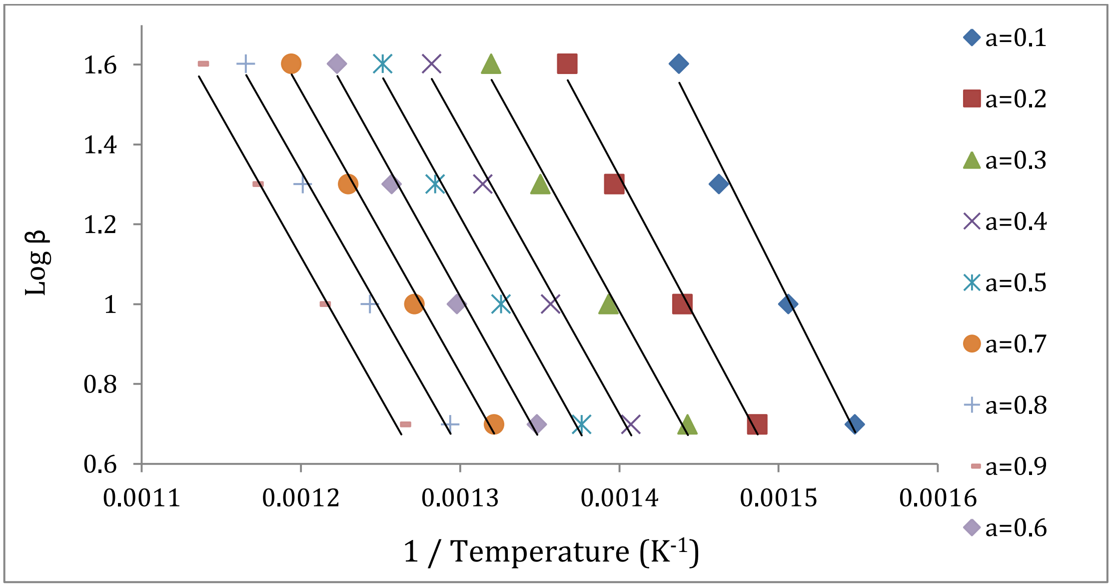

Figure 3.43: The regression lines to conversion of 0.1 -0.9 based on the Ozawa's method for 20 % WS_2-PANI.

Table 3.9: The correlation coefficient (R) and the activation energy (Ea) obtained using Ozawa's method for 20 % WS_2-PANI.

Sample	Conversion α	R	Ea KJ/mol
20 % WS_2 by weight	0.1	0.9873	144.2
	0.2	0.9899	135.3
	0.3	0.9897	131.3
	0.4	0.9905	129.8
	0.5	0.9910	130.5
	0.6	0.9928	130.2
	0.7	0.9944	128.6
	0.8	0.9941	127.4
	0.9	0.9928	128.4
Average			131.7

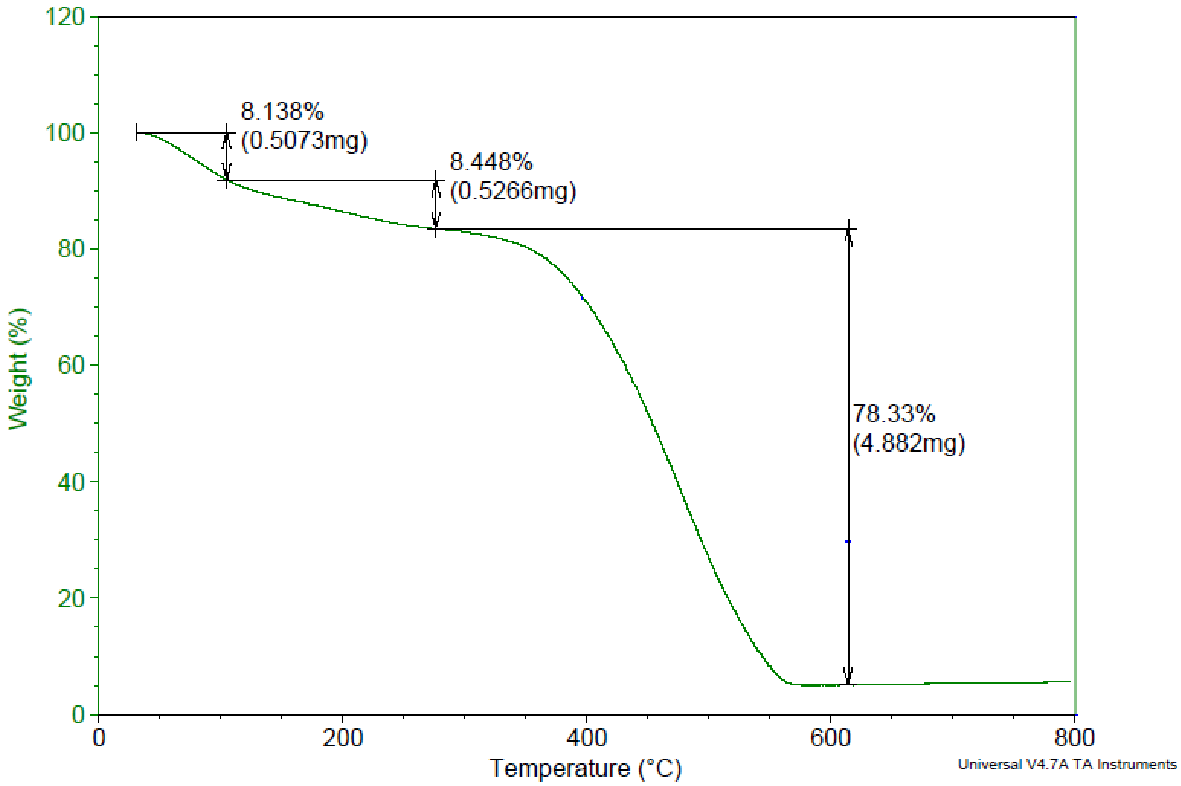

Figure 3.44: Overlay TGA of 37% WS_2-PANI at 5 ^oC/min

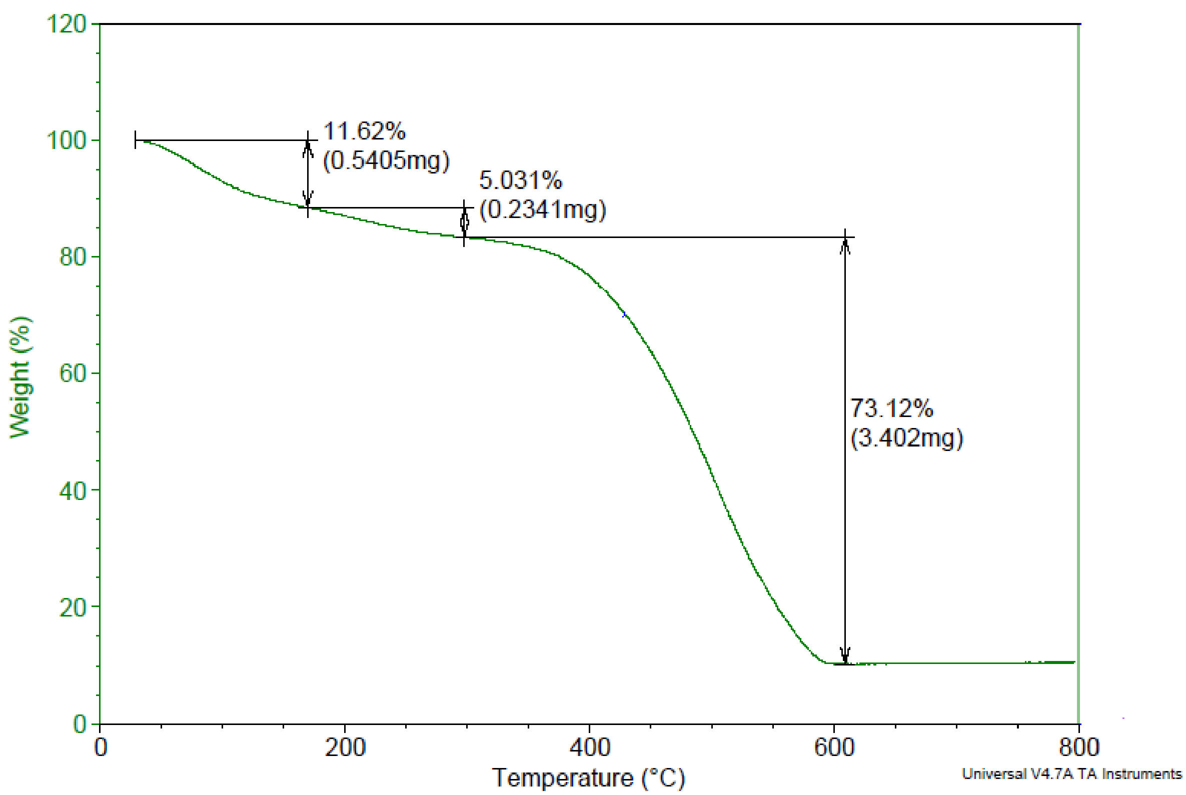

Figure 3.45: Overlay TGA of 37% WS_2- PANI at 10 ^oC/min

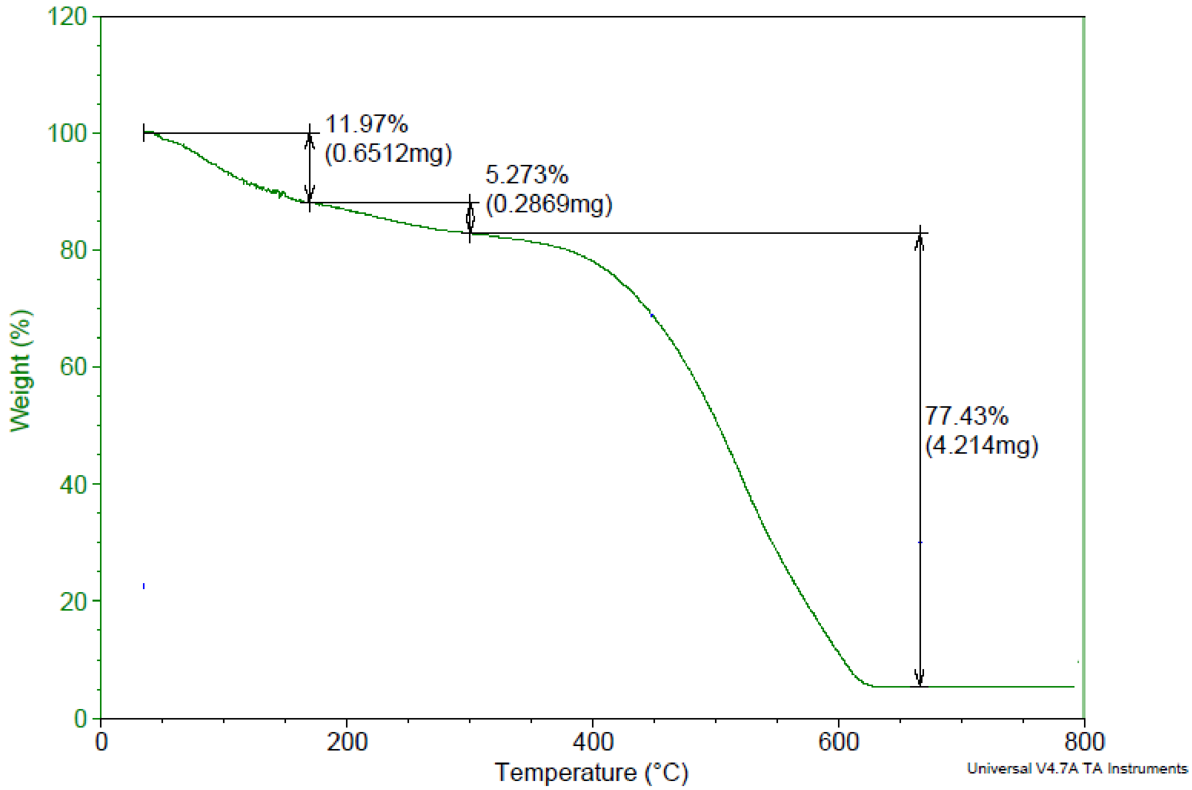

Figure 3.46: Overlay TGA of 37% WS_2-PANI at 20 ^oC/min

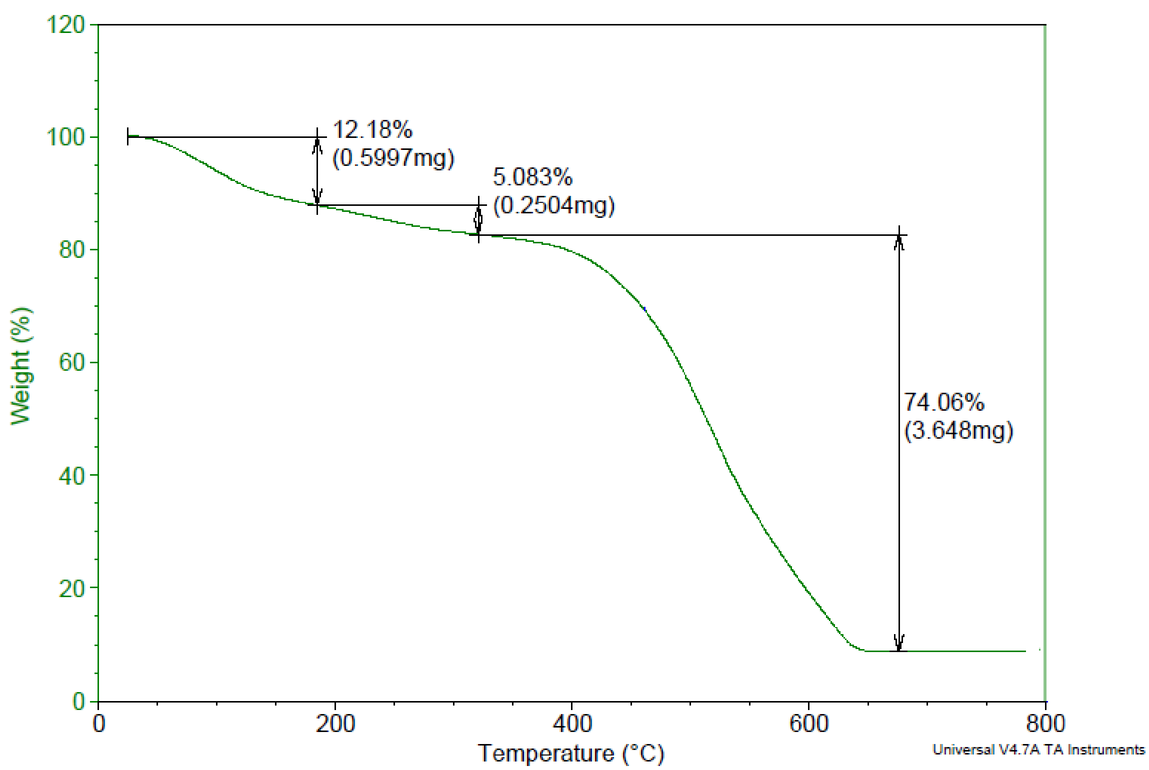

Figure 3.47: Overlay TGA of 37% WS_2-PANI at 40 ^oC/min

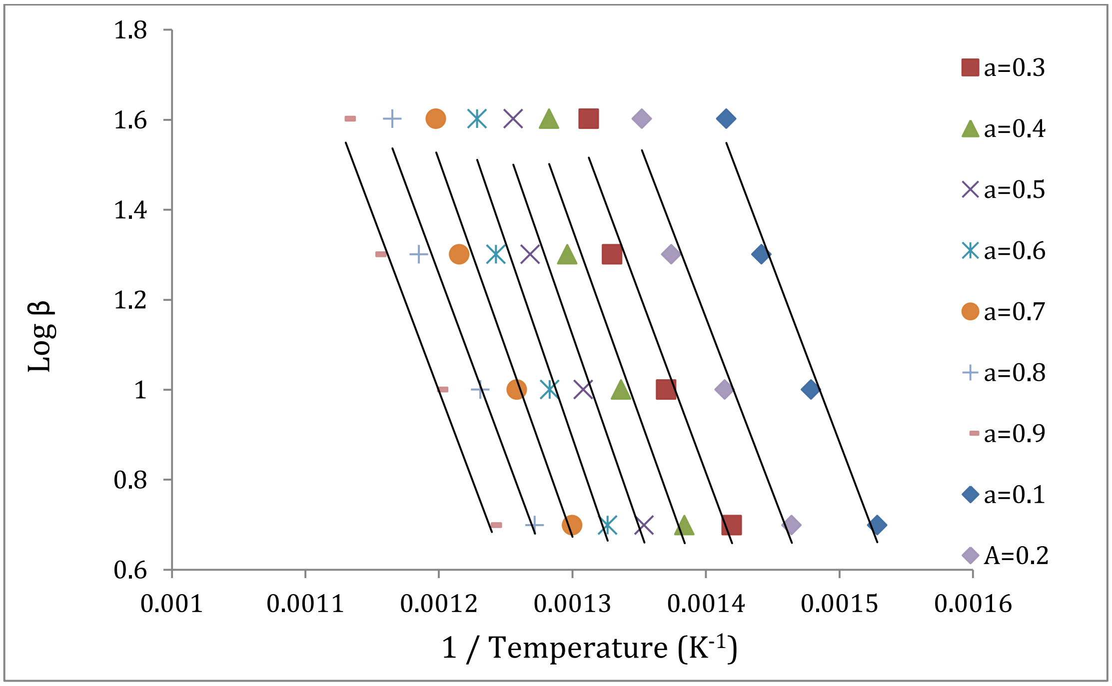

Figure 3.48: The regression lines to conversion of 0.1 -0.9 based on the Ozawa's method for 37 % WS2-PANI.

Table 3.10: The correlation coefficient (R) and the activation energy (Ea) obtained using Ozawa's method for 37 % WS_2-PANI.

Sample	Conversion α	R	Ea (kJ/mol)
37 % WS_2 by weight	0.1	0.9811	141.5
	0.2	0.9728	142.7
	0.3	0.9620	145.5
	0.4	0.9515	151.2
	0.5	0.9503	155.9
	0.6	0.9592	157.4
	0.7	0.9710	152.4
	0.8	0.9786	146.1
	0.9	0.9951	143.8
Average			148.5

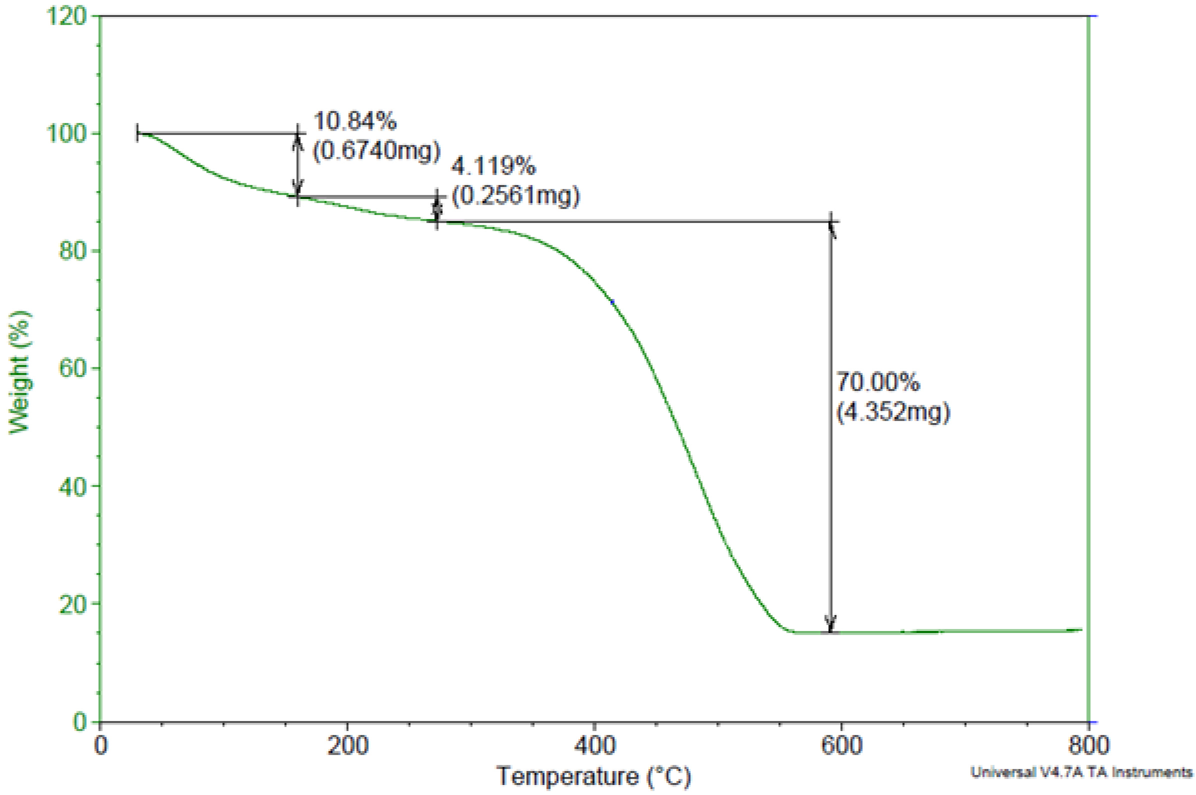

Figure 3.49: Overlay TGA of 64% WS_2-PANI at 5 ^oC/min

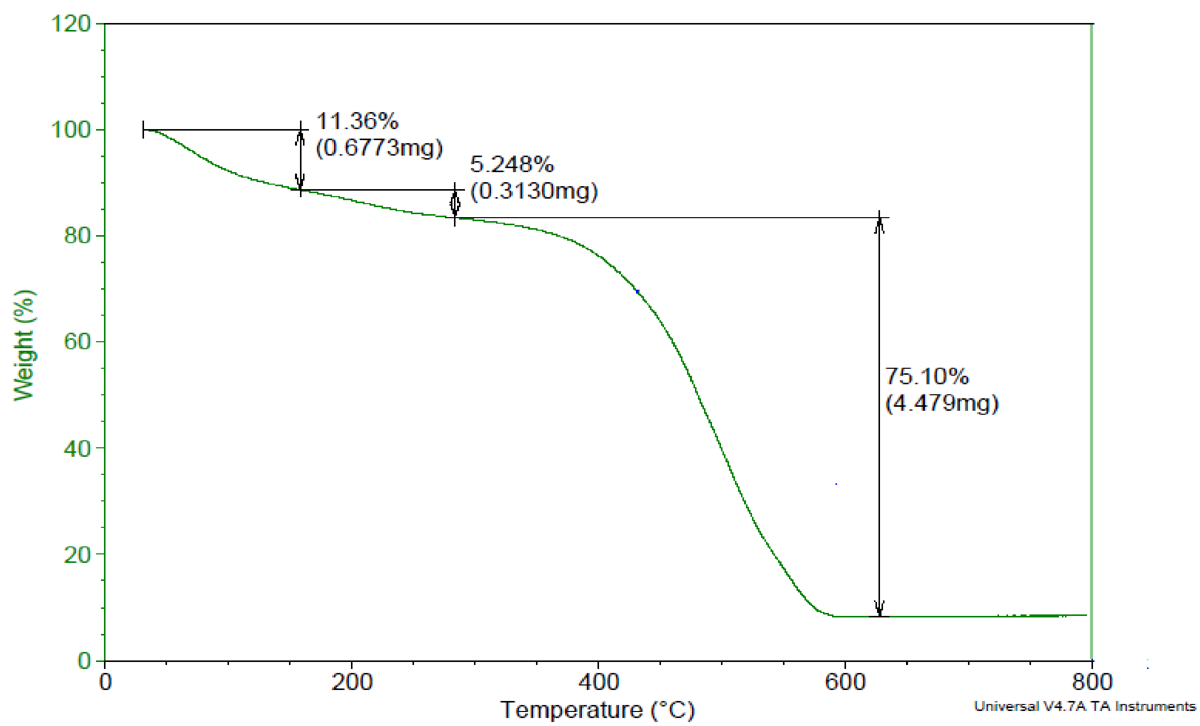

Figure 3.50: Overlay TGA of 64% WS_2-PANI at 10 ^oC/min

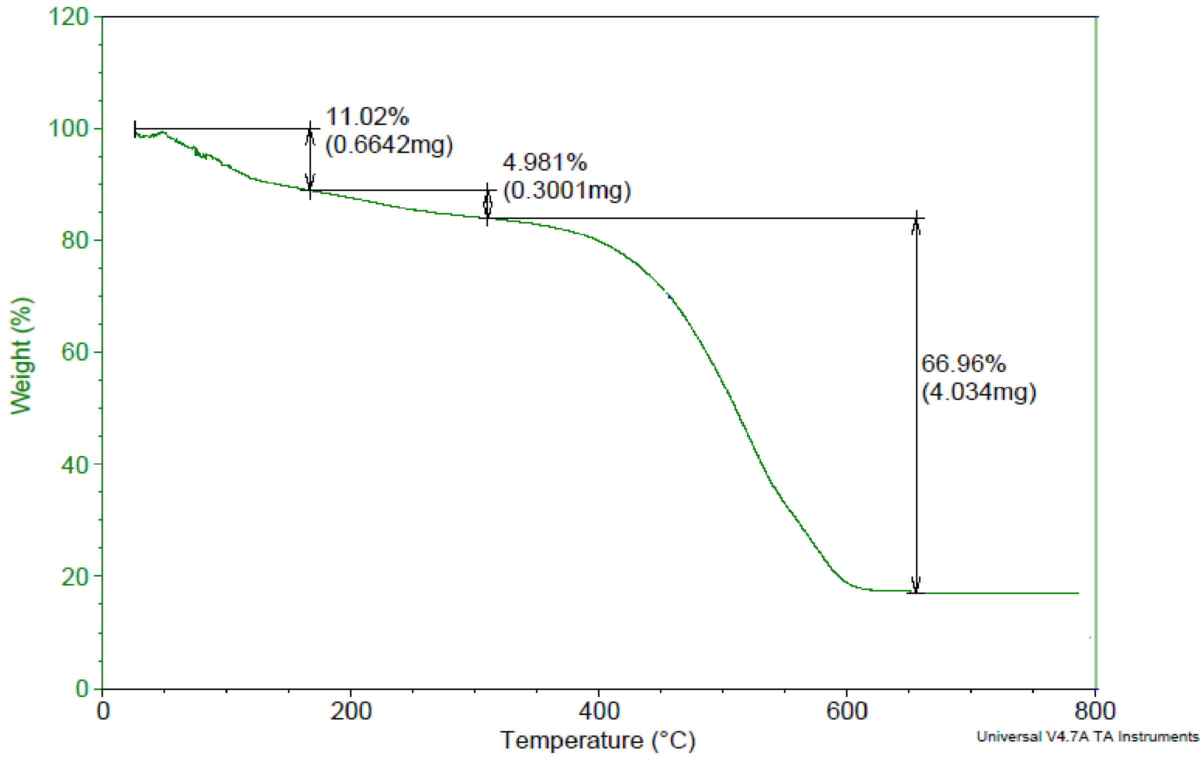

Figure 3.51: Overlay TGA of 64% WS_2-PANI at 20 °C/min

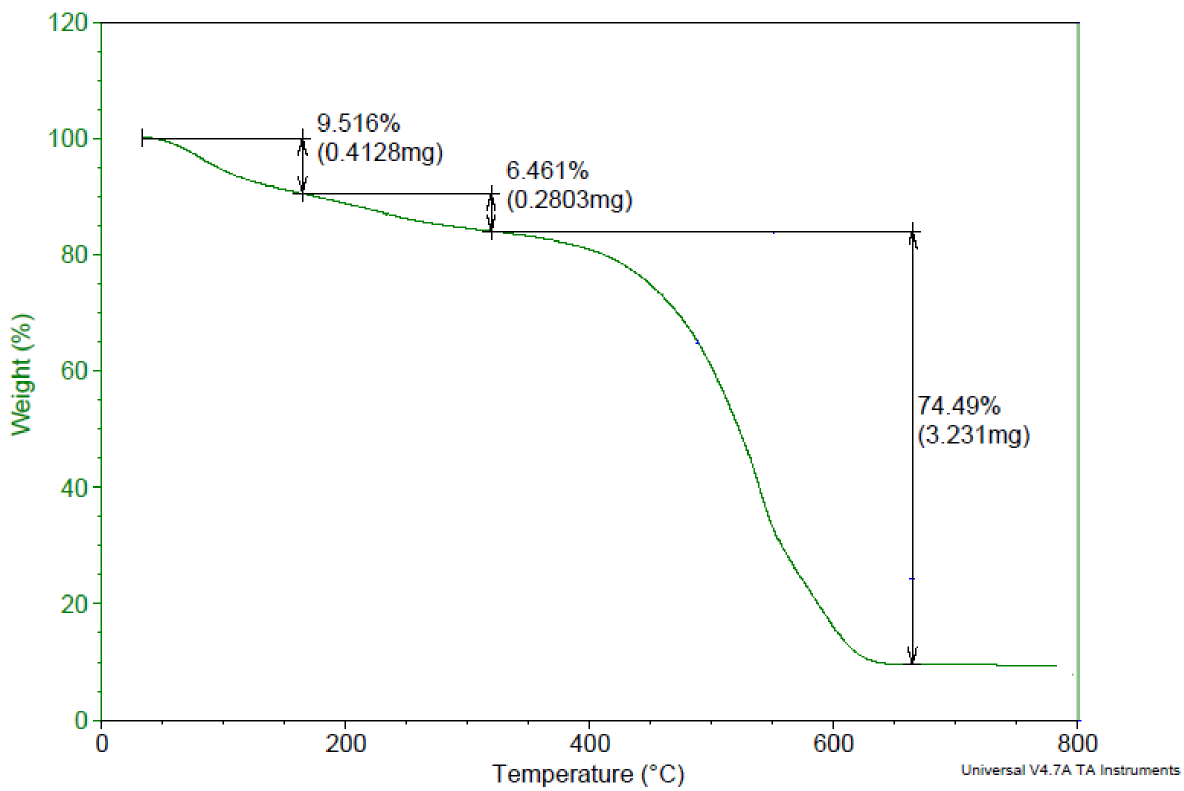

Figure 3.52: Overlay TGA of 64% WS_2-PANI at 40 °C/min

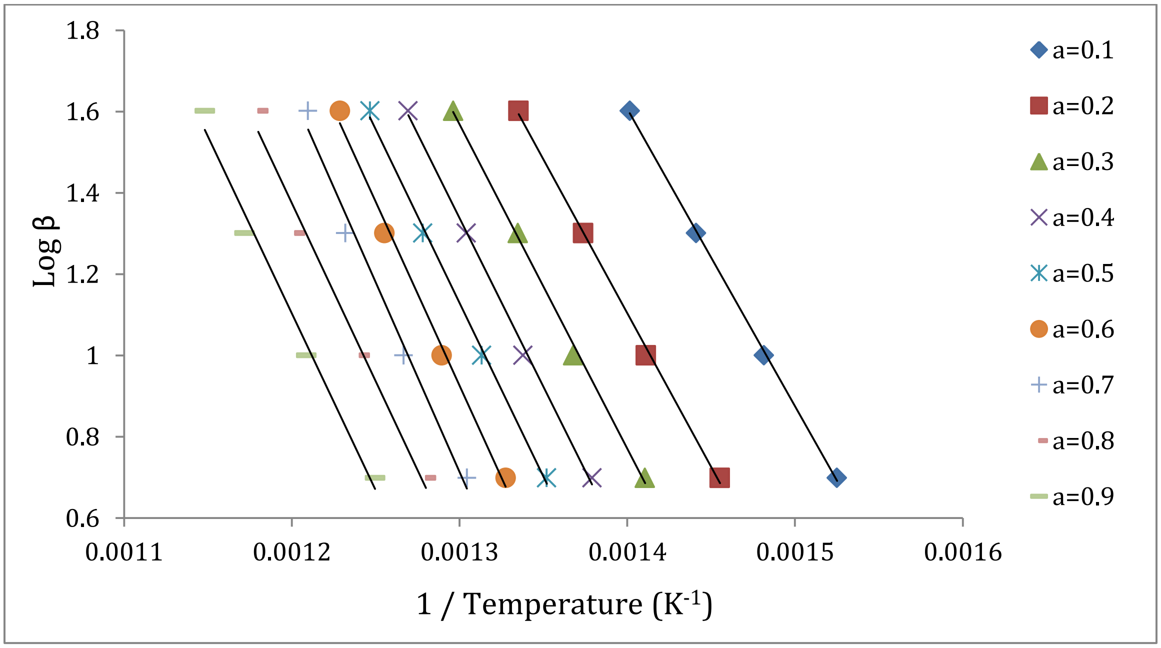

Figure 3.53: The regression lines for conversion α of 0.1 -0.9 based on the Ozawa's method for 64 % WS_2-PANI.

Table 3.11: The correlation coefficient (R) and the activation energy (Ea) obtained using Ozawa's method for 64 % WS_2-PANI.

Sample	Conversion α	R	Ea (kJ/mol)
64 % WS_2 by weight	0.1	0.9995	133.2
	0.2	0.9986	137.6
	0.3	0.9977	145.4
	0.4	0.9978	150.7
	0.5	0.9979	155.7
	0.6	0.9938	164.8
	0.7	0.9974	169.5
	0.8	0.9949	159.3
	0.9	0.9969	158.3
Average			152.7